Université de Lille

**Ecole doctorale EG Ecole Graduée ENGSYS-632**

**Unité de recherche L2EP EA2697**

# THÈSE

Présentée par : **Mhamad SHMAYSANI**

Soutenue le : 15 Décembre 2025

Pour obtenir le grade de : **Docteur de l'Université de Lille**

Discipline : **Sciences pour l'ingénieur**

Spécialité : **Génie électrique**

# Development of an energy supervision for DC railway smart grid – RACCOR-D

# « Développement d'une supervision énergétique pour le smart grid ferroviaire à courant continu - RACCOR-D »

| | |
|---|---|
| **THÈSE dirigée par :** | **M. Christophe SAUDEMONT** |
| | **M. Benoit ROBYNS** |
| **et co-encadrée par :** | **M. Khaled ALMAKSOUR** |

**Composition du jury**

| | | |
|---|---|---|
| **M. Marc PETIT** | Professeur des Universités, GeePs, Centrale Supélec | Rapporteur / Président |
| **M. Azeddine HOUARI** | Maître de conférences HDR, IREENA, Université de Nantes | Rapporteur |
| **Mme. Manuela SECHILARIU** | Professeure des Universités, AVENUES, UTC | Examinatrice |
| **M. Philippe LADOUX** | Professeur d'Université, Laplace, INPT | Examinateur |
| **M. Christophe SAUDEMONT** | Professeur, L2EP, JUNIA | Examinateur |
| **M. Khaled ALMAKSOUR** | Enseignant-chercheur, L2EP, JUNIA | Examinateur |
| **Benoît ROBYNS** | Professeur, L2EP, JUNIA | Invité |

THÈSE

# Acknowledgement

Pursuing a doctoral thesis is both an intellectually rigorous and deeply formative journey that extends well beyond the achievement of scientific outcomes. It involves sustained effort, moments of doubt, and a constant commitment to learning and growth. While the research process can at times feel solitary, this thesis is ultimately the result of collective support, guidance, and meaningful exchanges with many people. This acknowledgement is therefore a moment to express my gratitude to those whose contributions, encouragement, and presence were essential to the successful completion of this work.

First, I would like to express my deepest gratitude to my directors and supervisors, Christophe SAUDEMONT, Khaled ALMAKSOUR, and Benoît ROBYNS. Their guidance, expertise, and constant support have been invaluable to me, both professionally and personally. I am sincerely thankful for the time they dedicated to thoughtful discussions and the exploration of ideas, which significantly shaped my research and enriched my understanding throughout this doctoral journey. Their encouragement and constructive feedback not only helped me overcome challenges along the way but also strengthened my confidence and prepared me to successfully defend my work at its conclusion.

I would also like to express my sincere gratitude to the members of the jury for the honor of their participation and the careful attention they devoted to the evaluation of this work. I am particularly thankful to Professor Marc PETIT and Professor Azeddine HOUARI for serving as reviewers and for the time and effort they dedicated to thoroughly examining the manuscript and providing insightful and constructive feedback. I also wish to thank Professor Manuela SECHILARIU and Professor Philippe LADOUX for their valuable participation in the jury.

I would also like to warmly thank all the partners involved in the RACCOR-D project. In particular, I am grateful to our collaborators from SNCF Réseau, especially Tony LETROUVE and Hervé CARON, who accompanied us throughout the entire project. Their availability, valuable input, and continuous exchange of information were essential to the progress of this work, and our regular discussions greatly contributed to its advancement. I also wish to acknowledge our partners from SCLE, RTE, Laplace, CEA, and Railenium. It was a real pleasure to collaborate with all the individuals involved in this ambitious and rewarding project, and to share enriching discussions during our meetings and exchanges.

I would also like to express my sincere gratitude to my colleagues in JUNIA and L2EP for their support, collaboration, and the positive working environment they helped create throughout this thesis. Working alongside such motivated and generous individuals made the daily challenges of doctoral research more manageable and rewarding.

I would like to dedicate my deepest thanks to my heroes, my mother and my father. From the very first day, they have given me their unconditional support, even in the most challenging circumstances. They always placed my goals above everything else that mattered to them. This work is dedicated to them, as their kindness, selflessness, and devotion have shaped who I am today and taught me the values that guide me in both life and work.

To my sister and my brother-in-law, the two people closest to my heart, thank you for your constant support and care. Spending every holiday with you was the best therapy and a true source of comfort throughout this journey.

To my three brothers, Ali, Ahmad, and Hassan, you are the reason I keep moving forward. You make my life brighter every day, and watching you grow, learn, and face the different stages of life has been a continuous source of inspiration and motivation for me.

I extend my heartfelt gratitude to my family members in France, Toufic and Rashad, who stood by me at every step from the moment I arrived in France to begin this wonderful journey. Their constant presence, support, and care made my transition easier and this experience far more meaningful.

Last but certainly not least, I would like to thank my friends, who truly saved the best for last. Thank you for all the time we shared together, which made my life throughout this thesis both joyful and meaningful. The laughter, the long conversations, and the simple moments of escape helped balance the inevitable exhaustion that came with this journey.

# Abstract

With the continuous increase in railway traffic and energy costs, SNCF Réseau aims to enhance the performance of its traction substations while complying with European regulations on $CO_2$ emissions. While alternating current (AC) traction substations supply the main railway lines, direct current (DC) electrification still represents a significant part of the national railway network. However, this type of electrification suffers from relatively low voltage, high losses, and potentially limited traffic capacity. Through the RACCOR-D project, an essential step toward higher-voltage DC networks (above 1500 V), SNCF Réseau seeks to modernize its substations by transforming them into intelligent environments integrating photovoltaic (PV) and energy storage systems (ESS), in order to reduce dependency on the electricity transport network grid, lower operating costs, and minimize penalty charges.

The development of energy supervision tool in this context raises several scientific and technical challenges: it requires optimal coordination between the integrated PV and ESS systems within an environment strongly constrained by the variability of railway loads and forecasting uncertainties. The efficiency of an Energy Management System (EMS) thus depends on its ability to anticipate energy needs, plan storage usage intelligently, and react in real time to network fluctuations, while ensuring voltage stability and cost minimization. These requirements are particularly complex in DC railway networks, where the fast dynamics of trains and voltage limitations demand robust and adaptive supervision strategies.

The objective of this PhD thesis is to develop an energy supervision system dedicated to the DC railway network, aiming to optimize the management of the energy storage system (ESS) within the first architecture of the RACCOR-D project (PV and ESS connected at the substation via DC bus). The supervisor is designed to improve the energy and economic performance of the traction substation while satisfying the technical constraints specific to DC railway systems. It operates through a single mean of action: the reference power of the energy storage system. The supervisor is structured into two temporal complementary levels:

- The long-term level, corresponding to a day-ahead energy management system EMS based on nonlinear optimization, determines the optimal storage schedule for the following day using the traction substation's (TSS) power consumption forecasts and economic objectives, namely optimizing ESS usage according to the variability of the use of electricity transport network tariffs and reducing penalty costs related to subscribed power exceedance.

- The short-term level, based on real-time fuzzy logic supervision, dynamically adjusts the ESS reference power according to instantaneous measurements (DC bus voltage, ESS state of charge (SOC), grid power, etc.) and the day-ahead plan. This second level aims to correct deviations caused by forecast errors and uncertainties while ensuring compliance with technical constraints and economic objectives.

A second architecture is also investigated within the RACCOR-D project framework, integrating PV and ESS at the Parallel Poste (PMP: Point mise en parallel) between two substations. This configuration allows analyzing the potential to reduce voltage drops along the catenary and at the train's pantograph terminals, frequently observed in DC railway networks.

Real-time fuzzy logic-based supervision method is proposed to manage the ESS in order to limit these voltage drops at the midpoint between two substations and maintain them within acceptable limits. This architecture offers promising perspectives for DC railway networks in terms of traffic increase, voltage drop reduction, and optimization of substation spacing.

The proposed supervision framework was experimentally validated in a real-time simulation environment with data of TSS power consumption characterized by 1s time step. To enable its deployment in real installations, a SCADA-based industrial architecture has been developed, ensuring reliable communication between the supervisor and the smart grid components. This step establishes the foundation for the implementation of the supervisor on an industrial PC and its integration within the railway substation demonstrator, paving the way toward full industrial deployment of intelligent DC railway substations.

This project has been funded by the government as part of France 2030.

# Résumé

L'augmentation du trafic ferroviaire et des coûts de l'énergie, incitent SNCF Réseau à améliorer la performance de ses sous-stations (SST). Alors que les SST en courant alternatif (AC) couvrent les grandes lignes, les SST en courant continu (DC) représentent encore une part importante du réseau ferré national. En cas de fort trafic, leur tension relativement basse (1500V) peut être une limitation. Le projet RACCOR-D, étape vers des réseaux DC de tension supérieure, vise à moderniser les SST en intégrant des systèmes photovoltaïques (PV), de stockage d'énergie (ESS) et une supervision énergétique associée (EMS).

Le développement de cette supervision soulève plusieurs défis scientifiques et techniques, pour coordonner de façon optimale ESS et PV, dans un environnement contraint par la variabilité de la charge ferroviaire et les incertitudes de prévision. L'efficacité de l'EMS dépend ainsi de sa capacité à anticiper les besoins énergétiques, à planifier l'utilisation de l'ESS et à réagir en temps réel aux fluctuations de puissances, tout en garantissant le maintien de la tension DC et la minimisation des coûts. Ces exigences sont particulièrement complexes dans les réseaux ferroviaires DC, où les dynamiques rapides des trains et les limitations de tension nécessitent des stratégies de supervision robustes et adaptatives.

L'objectif de cette thèse est de développer un superviseur énergétique dédié au réseau ferroviaire DC, visant à optimiser la gestion de l'ESS dans la première architecture du projet RACCOR-D (PV et ESS connectés en SST au bus DC). Cette supervision énergétique vise à améliorer les performances énergétique et économique de la SST, tout en respectant les contraintes techniques propres au réseau ferroviaire DC. Elle agit sur un unique levier : la puissance de référence de l'ESS. Le superviseur énergétique est structuré en deux niveaux temporels :

- Long terme : EMS de type "J-1" basé sur une optimisation non linéaire, qui détermine la planification optimale de l'ESS pour le lendemain, en s'appuyant sur les prévisions de consommation de puissance de la SST et sur les objectifs économiques, notamment l'optimisation de l'utilisation de l'ESS (selon la variabilité du tarif d'utilisation du réseau de transport d'électricité, et la diminution des coûts des pénalités liés au dépassement de la puissance souscrite).
- Court terme : fondé sur une supervision en temps réel à base de logique floue (LF), qui ajuste dynamiquement la consigne de puissance de l'ESS, à partir de mesures instantanées (tension DC, état de charge de l'ESS, puissance réseau, etc.) et de la planification "J-1". Ce second niveau compense les écarts dus aux erreurs de prévision et aux aléas, en respectant les contraintes techniques et les objectifs économiques.

Une 2$^{de}$ architecture est ensuite étudiée, qui intègre le PV et l'ESS au Point de Mise en Parallèle (PMP) entre deux sous-stations. Cette partie aborde le problème de chute de tension au niveau de la catenaire et du train (pantographe), observée dans les réseaux ferroviaires DC. Une méthode de supervision en temps réel basée sur la LF est proposée pour superviser l'ESS, qui limite ces baisses de tension, et les maintient dans des limites opérationnelles. Cette architecture ouvre des perspectives pour le réseau ferroviaire DC, notamment en termes de réduction des chutes de tension, d'augmentation du trafic et d'optimisation de l'espacement entre les SST.

Le superviseur est validé expérimentalement en simulation temps réel, démontrant sa réactivité dans des conditions d'exploitation réalistes (consommation de puissance de la SST échantillonnée à 1s). Pour préparer son déploiement en conditions réelles, une architecture industrielle de type SCADA est développée, garantissant une communication fiable entre le

superviseur et les composants du réseau ferroviaire intelligent. Cette étape est le socle de l'implantation du superviseur sur PC industriel et de son intégration au démonstrateur de SST ferroviaire DC.

Ce projet a été financé par le gouvernement dans le cadre de France 2030.

# Table of Contents

# List of Figures

# List of Tables

# General Introduction

With the continuous increase in railway traffic and energy costs, the railway network operator in France SNCF réseau looks for solutions that improve the performance of its substations and respond to European regulation concerning CO2 emissions. While AC railway substations in France are characterized with high power and covering the main traffic of the large railway lines, the DC electrification still represents an important percentage in the railway lines coverage in France. This electrification still suffers from relatively low voltage, high losses, and limited traffic circulation.

The SNCF réseau through the RACCOR-D project aims to modernise the existing DC substations, transforming it into a smart grid environment that hosts photovoltaic (PV) and energy storage systems (ESS).  The idea behind this transformation is to depend less on the electricity transport network that supplies the DC substations and reduce the costs related to the use of the transport network and the penalties that are causing a major concern for the railway network operator. With a future vision to increase the voltage level of the DC traction substation, trying to match the performance of the AC railway networks. This thesis is a first step that consisting of developing the energy supervision for the railway smart grid.

The objective of this thesis is to develop a real time supervision tool to manage the ESS for the railway smart grid, when integrated with the PV system at the traction substation (TSS) in a defined 1$^{st}$ architecture of RACCOR-D. This supervision must meet the objectives and constraints for diverse railway smart grid elements, dealing with objectives with different nature, while acting only on one element which is the ESS. The mean of action is sending a power reference setpoint in real time to the ESS.

The proposed supervision tool is composed of two levels long and short term. The long term is a day ahead EMS that uses forecast of TSS power consumption and local PV electricity production to find the optimal schedule of the ESS for the upcoming day. The short-term is the real time supervision tool developed as a fuzzy logic supervisor. It relies on actual measurement in real time from the railway network (DC voltage, ESS State of Charge - SOC, power drawn from the grid…) in addition to the day ahead planning (day ahead EMS decision), to generate a reference setpoint in real time for the ESS. The real time supervision aims to deal with the shortcomings of day ahead EMS, and deal with the forecast errors and uncertainties. Trying to achieve and respond to the economic and technical objectives in real time while respecting the diverse constraints.

A 2$^{nd}$ architecture is considered, integrating the ESS and the PV at mid-point between two substations. This architecture aims to study the possibility of treating the problem of catenary voltage drop. A real time supervision method based on fuzzy logic is proposed of the ESS management. The supervision aims to solicit the ESS in a way that limits the voltage drop of the catenary that occurs at the middle point between two substations and keeps it within operational limits. This architecture offers an important perspective that impact the DC railway network in terms of traffic increase, voltage drop, and substation spacing.

The developed supervision system was experimentally validated through detailed simulations and real-time testing, confirming its robustness and adaptability under realistic railway operating conditions. To facilitate its industrial transfer, the supervisor has been designed for deployment beyond the research environment. The model initially implemented in MATLAB/Simulink is being translated into an industrially compatible Python-based application, ensuring interoperability with SNCF Réseau's existing infrastructure. The implementation on an industrial server will guarantee data availability, communication reliability, and operational robustness, paving the way for large-scale integration within future smart DC substations.

The problematic regarding the DC railway electrification and the challenges that the SNCF réseau faces is explained in Chapter 1 of the thesis. Along with the context of RACCOR-D project. The methodology behind the energy supervision tool proposed is explained in Chapter 2. Different approaches that can be used in railway energy management are benchmarked, and the methods used for the energy supervision strategy are then chosen in a way that suits RACCOR-D application. The development of the day ahead EMS (long term supervision) is presented in Chapter 3. Covering the optimization-based ESS planning and the necessary forecast models that provide necessary forecasted profile of TSS consumption to the optimization algorithm. Chapter 4 represents the design of the real time supervision tool, with results that compare the performance of the day ahead supervision with the proposed real time supervision strategy. Assessing the advantages and the impact of the real time supervision in terms of accuracy and efficiency. Also, this chapter covers the development of the supervision tool for the 2$^{nd}$ architecture that considers the perspectives of RACCOR-D. The experimental validation is presented in Chapter 5 alongside the industrial transfer phase. The objective behind this part of work is to prepare the proposed energy supervision tool to be implemented in a real demonstrator of a DC TSS.

# Chapter 1. Problematic

## 1.1 Introduction to railway electrification

Over the past century, railway networks worldwide have shifted from steam locomotives to predominantly electric power. Today, most rail systems run on electricity: over 85% of passenger rail travel worldwide, along with more than half of freight movement is powered by electricity [1] . In the European Union (EU) about 79% of rail energy consumption is electric (versus ~52% in 1990) [2] . Fig. 1.1 shows that electricity has consistently been the dominant energy source for EU rail transport from 1990 to 2022, while the use of gas oil and diesel has steadily declined and renewables and biofuels remain marginal, with minimal uptake over the same period. The electricity power is used to supply all kinds of railways applications from conventional intercity lines, tramways, metros, and regional express services, all of which increasingly rely on continuous and reliable electrification to guarantee their services. These lines support both passenger and freight transport, enabling efficient mobility of people and goods across national and regional networks.

As of 2022, the European Union accounts for over 200,000 km of railway lines, of which approximately 54% are electrified and 7,500 km are high-speed tracks, primarily concentrated in France, Germany, Spain, and Italy [3] [4] .

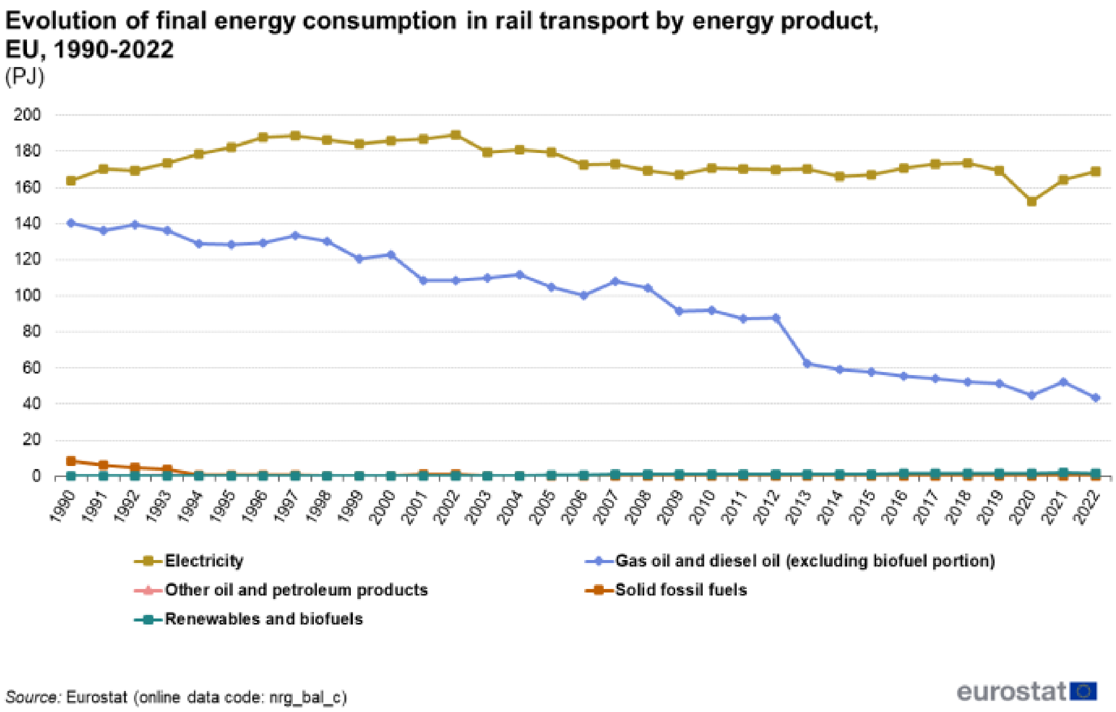


*Fig. 1.1 Energy consumption in rail transport by energy product [2]*

This widespread electrification, combined with continuous network expansion, has made rail transport increasingly vital in sustainable mobility strategies. Thanks to their ability to move large volumes of people and goods efficiently, with low emissions and high reliability. Their centralized and long-lived infrastructure makes them well-suited to support future transport systems that are resilient, efficient, and aligned with long-term climate goals. Globally, rail carries around 7% of all passenger-kilometres but contributes only ~1% of transport $CO_2$ emissions [1] . In the EU, rail likewise produces less than 1% of transport emissions while moving roughly 7.5% of passengers and 17.6% of freight traffic [5] . Recognizing this potential, the European Union's Green Deal and mobility strategy set ambitious targets – including doubling high-speed rail traffic by 2030 and tripling freight volumes by 2050 - as part of a plan to cut transport emissions by 90% by mid-century [6] .

This positions railways as a backbone for smart and sustainable mobility [7] . Railway networks are among the most spatially extensive and strategically important infrastructures in modern economies [8] . However, achieving the projected growth in railway traffic requires major modernization efforts. With existing networks, such an increase is not feasible without substantial upgrades to capacity, electrification, and digitalization [9] . Consequently, railway infrastructure managers across Europe are implementing strategic programs to enhance efficiency and sustainability in response to rising traffic demand and stricter $CO_2$ regulations [10] . The improvement of existing network has proven with research that various technics and options can be subjected to the railway network without the need of large changes in its infrastructure, which by the way can be costly and difficult to implement from scratch. This orientation toward modernization and sustainability is also consistent with recent European policies promoting sustainable mobility for all [11] .

## 1.2 Evolution of railway networks (AC DC electrification)

Since the early 20th century, railway networks around the world have gradually shifted from steam to electric traction, beginning with low-voltage direct current (DC) systems and later adopting higher-voltage alternating current (AC) systems. Early electrification projects commonly used DC at voltages of a few hundred to 1500 volts via third-rail or overhead wires, which worked for short routes but suffered from heavy voltage drop and power loss over long distances. Technological advances in the mid-1900s enabled the use of high-voltage AC (such as 15 kV 16.7 Hz or 25 kV 50 Hz), which allowed more efficient transmission of power across longer lines [12] . For this reason, many railways that were newly rectified uses AC standards, while countries with established DC networks often retained and expanded their legacy systems [12] . This history explains why multiple electrification schemes still coexist internationally – for example, Europe employs five main standards (750 V DC, 1.5 kV DC, 3 kV DC, 15 kV AC, and 25 kV AC) depending on the region [13] . Today, roughly one-third of the world's railway track length is electrified, and in Europe about 43% of all electrified routes still operate on DC (at 1.5 or 3 kV) despite the later dominance of AC elsewhere [12] . Table 1.1 Common electric railway traction systems in the world [14] . Table 1.1 summarizes the most common electric railway traction systems (TPS: traction power system) in the world.

*Table 1.1 Common electric railway traction systems in the world [14]*

| TPS | Voltage Level | Coverage (km) | Selected Countries |
|---|---|---|---|
| | 600 V and 750 V | 7 650 | UK |
| **DC** | 1.5 kV | 20 440 | Japan, France, The Netherlands |
| | 3 kV | 68 890 | Russia, Spain, South Africa |
| | 15 kV, 16 2/3 Hz | 32 940 | Germany, Switzerland, Norway |
| **MVAC (Single Phase)** | 25 kV, 50/60 Hz | 72 110 | Russia, France, China, South Africa |

| | | |
|---|---|---|
| 11–12 kV, 25 Hz and others | 3 000 | USA |

### 1.2.1 AC electrification

The 25 kV–50 Hz AC railway electrification system, widely adopted since its introduction in 1954, has become the standard for modern rail networks due to its technical and economic advantages. This system operates by supplying high-voltage alternating current, typically 25 kV, through overhead catenaries, which are powered by substations connected to the national high-voltage transmission grid. One of the key features of this architecture is the wide spacing between traction substations (TSS), generally ranging from 50 to 100 km, made possible by the reduced electrical losses and lower current intensities caused by the high voltage transmission. In this electrification, adjacent substations often supply overlapping catenary segments, allowing trains to be simultaneously powered from multiple sources [15] . Fig. 1.2 shows a simplified AC electrified railway substation and its different elements.

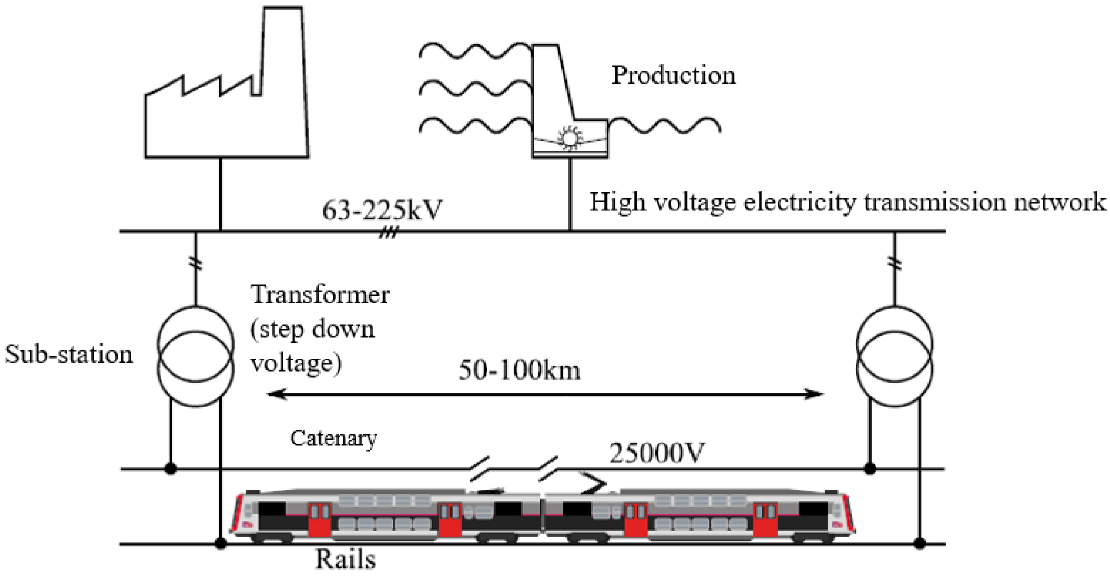


*Fig. 1.2 AC railway electrification [16]*

These substations serve as the critical interface between the national power grid and the railway infrastructure. The main components and characteristics of the electrification system are:

- High-voltage connection: Substations draw power from the national grid, typically at voltage levels between 63 kV and 225 kV.
- Step-down transformers: Installed within substations to reduce transmission voltage down to 25 kV, suitable for railway catenary systems.
- Catenary system: Overhead lines supply 25 kV AC to the train’s pantograph for traction.
- Onboard electrical systems: Trains require onboard transformers to step down 25 kV and rectifiers or inverters to convert AC to DC when using DC traction motors.
- Phase separation and neutral sections: Neighbouring substations are connected to different electrical phases to balance the national grid load and avoid phase mismatches. To prevent electrical conflicts at phase boundaries, neutral sections serving as electrically isolated segments of track are introduced. Trains must open their circuit breakers when passing through these sections, momentarily cutting power. Although brief, this interruption can affect traction and requires careful control [17] .

This design improves redundancy and voltage stability. While this system supports high-power operation and long distances between substations, it also requires onboard transformers and rectifiers to adapt the high-voltage AC supply to DC traction motors. Additionally, the high voltage presents insulation challenges, especially in tunnels and confined infrastructure.

### 1.2.2 DC electrification

The 1500 V DC railway electrification system, historically established in France during the early 20th century, remains in service across nearly half of the country's electrified rail lines. In this architecture, energy is supplied by a series of substations spaced at relatively short intervals typically every 5 to 15 km due to the inherent voltage limitations and significant current levels. Each substation includes a step-down transformer and an AC/DC converter, usually diode-based, which together deliver direct current to the overhead catenary [15] .

The low voltage level allows for direct traction motor supply without requiring onboard transformation or rectification stages, particularly suitable for DC motor-based propulsion chains. However, this convenience comes at the cost of network complexity: the short range between substations demands a dense and costly infrastructure, and the high current flow necessitates the use of thick, heavy catenary conductors to reduce voltage drops. The intense current also causes thermal losses at the contact point between pantograph and wire, limiting overall efficiency and power transfer capability. While the system's low voltage simplifies insulation and facilitates deployment in constrained environments such as urban tunnels, its scalability is hindered, especially for high-power applications or long-distance lines. The DC electrification architecture is illustrated in Fig. 1.3.

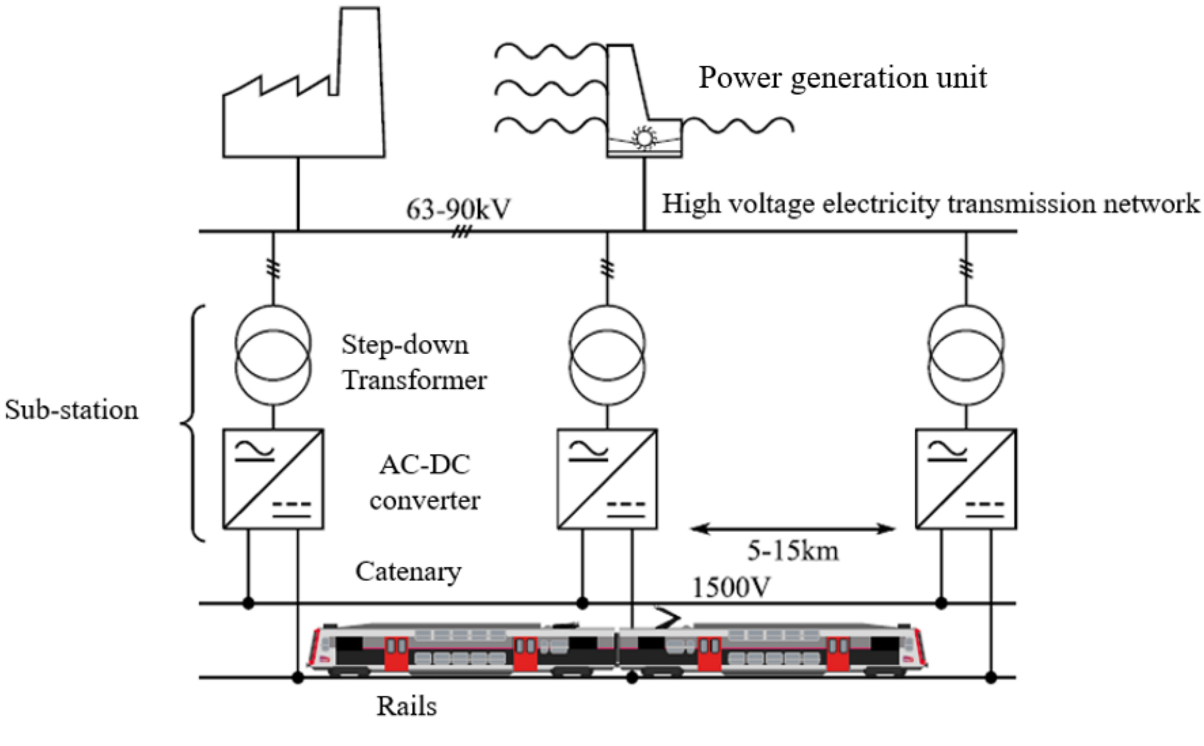


*Fig. 1.3 DC railway electrification [16]*

### 1.2.3 Comparative analysis of AC & DC electrification

Direct current (DC) electrification was used in the earliest electric railways and became standard for urban transit systems (e.g. trams and subways), while alternating current (AC) electrification was later adopted for high capacity mainlines. In modern practice, AC systems operate at much higher voltages (typically 15–25 kV, 50/60 Hz, with some up to 50 kV) whereas DC systems are usually limited to 600–3000 V [18]. The high voltage of AC overhead lines allows them to transmit more power with lower current, reducing resistive losses and requiring fewer substations along a route [19] [20] .

Accordingly, AC electrification has been favoured for high-speed intercity and heavy-haul railways that demand efficient long-distance power delivery. By contrast, lower-voltage DC networks (whether third-rail or overhead) suit urban and suburban lines with short distances and frequent stops, albeit at the cost of more frequent substations and higher current draw for the same power [21] [22] .

Modern AC-driven locomotives employ onboard transformers and inverters to achieve large traction power and effective regenerative braking, enabling high performance and energy efficiency [19] . DC rolling stock historically featured simpler traction equipment (and earlier DC motors offered excellent speed control), but conventional DC infrastructure faced challenges such as complex voltage conversion and an inability to return braking energy to the grid. In fact, traditional DC substations could not feed regenerative braking power back to the utility, so excess braking energy was often dissipated as heat, wasting energy [23] .

Recent advances have narrowed these gaps: both AC and DC systems now incorporate regenerative braking (though DC lines often require technologies like reversible substations or wayside energy storage to capture braking energy [23] ). Researchers are even exploring medium-voltage DC schemes to combine the strengths of each approach – for example, using ~25 kV DC traction power to enable wider substation spacing and eliminate phase-balancing issues, while still delivering high power over long distances [19] .

In summary, AC electrification provides superior scalability and transmission efficiency for long-distance and high-speed rail applications, whereas DC electrification offers practical advantages in dense urban transit contexts; importantly, ongoing innovations continue to improve energy efficiency and interoperability across both systems.

### 1.2.4 DC electrification in France (actual situation)

France exemplifies this dual legacy: it adopted 1.5 kV DC electrification on major lines in the 1920s, then introduced 25 kV AC after the 1950s for newer lines, resulting in a network split between the two systems. Fig. 1.4 shows the AC and DC electrified railway lines in France. The DC electrified lines are more dominant in the south of France region [24] .

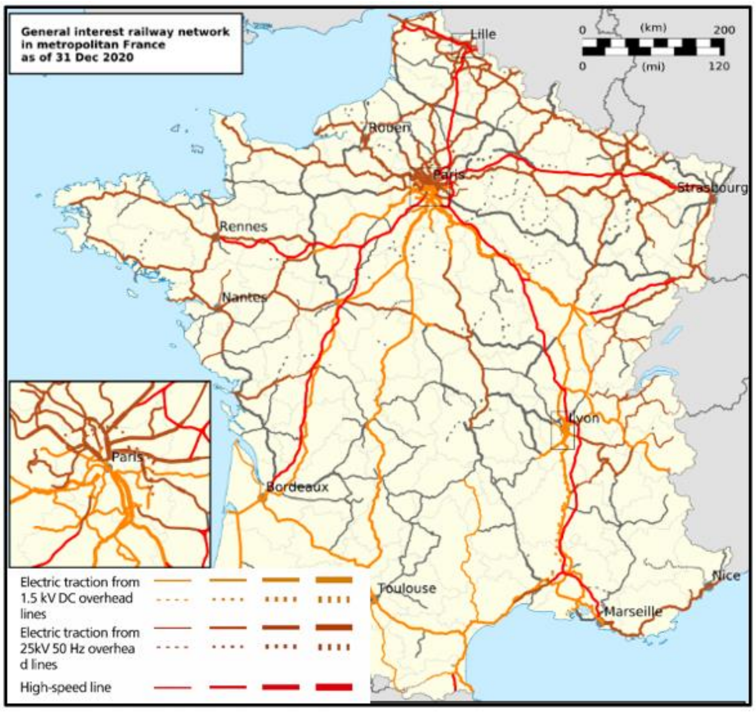


*Fig. 1.4 Railway map of France [24]*

The French national railway network includes approximately 15,000 km of electrified lines, of which 40% are powered by 1.5 kV DC. This infrastructure is supported by over 350 DC substations, which face numerous technical limitations due to low voltage levels. These limitations include restricted power delivery capacity for locomotives and elevated line losses caused by high current levels in catenaries. As a result, large copper sections (up to 1000 mm²) are needed in high-traffic areas to reduce resistive losses, leading to high infrastructure costs [36] .

A typical 1.5 kV DC railway electrification system consists of overhead contact lines (catenaries), feeder cables, return rails, and DC traction substations (TSS). At the substation level, three-phase AC power from the utility grid is first transformed to a lower AC voltage, then rectified using silicon-based rectifiers to supply 1.5 kV DC to the overhead lines. Trains draw power directly from these lines via pantographs. The overall network is organized with substations spaced at regular intervals. Typically, 3 to 5 km in dense urban environments, and up to 10 to 20 km for intercity lines. To manage voltage stability and current return paths, paralleling stations (PMP) are installed between substations, helping to equalize rail potentials and reduce resistance in the return circuit [25] [26]  While this configuration has historically enabled reliable service, its low-voltage/high-current nature imposes operational limits, particularly as traffic demand and energy efficiency targets continue to rise. Fig. 1.5 shows a simplified schematic of the DC network electrification with public network that usually refers to the high voltage electricity transmission network. The transformer rectifier unit, and the PMP connections between three consecutive substations.

The SNCF Réseau occupies the TSS elements from transformer, rectifier, and catenary overhead. It is connected to the electricity transport operator RTE, that manages the AC side of the railway grid.

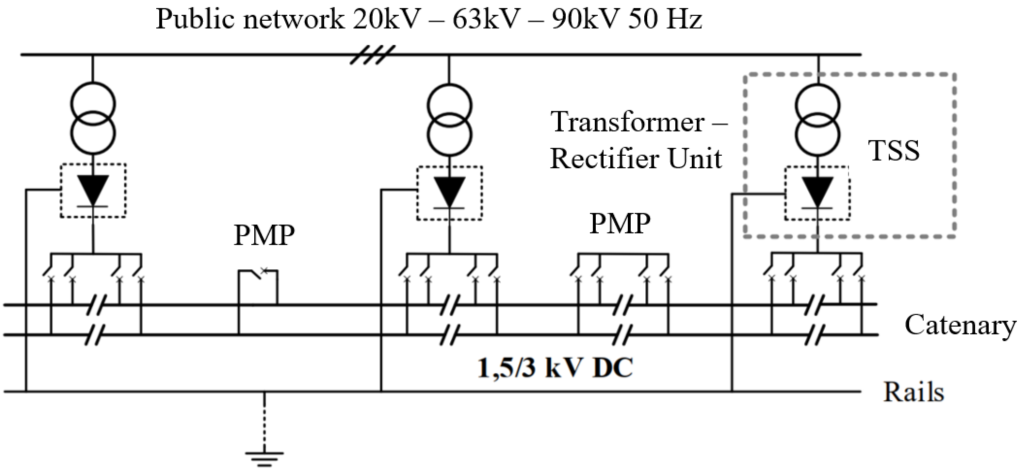


*Fig. 1.5 Simplified schematic of DC TSS [36]*

## 1.2.5 Electricity market for the railway network operators

### 1.2.5.1 Financial flows

At present, nearly 90% of SNCF's passenger transport services operate on electrified railway lines. As a railway operator, SNCF procures electricity directly from suppliers in a similar manner to other network users like RTE (Réseau de Transport d'Électricité) and formerly RFF (Réseau Ferré de France). The cost of transmitting this electricity through the public grid is billed to SNCF Réseau by the electricity transport network RTE [72].

The overall energy bill considered in this study is composed of the following components:

1. The acquisition of electricity, either through market-based contracts or under the ARENH (Accès Régulé à l'Électricité Nucléaire Historique) scheme (which provides regulated access to legacy nuclear electricity at a fixed price €/MWh).
2. Charges for using the transmission network, calculated in accordance with the TURPE (Tarif d'Utilisation des Réseaux Publics d'Électricité) framework [28] .

These billing structures are grounded in the broader liberalization of the French and European electricity markets, initiated by the EU Directive 96/92/EC [70] . This regulatory shift mandated a separation between the generation, transmission, and distribution of electricity to ensure transparency and competition [71] .

Fig. 1.6 Tariffication scheme illustrates:

- The energy flow path: from electricity suppliers → RTE (transport) → SNCF Réseau;
- The financial flow: payments from SNCF to electricity provider (RTE) based on ARENH allocations + payments from SNCF to transport network operator RTE via TURPE 6 regulation
- The Railway undertakings: payments from railway companies supplied by SNCF réseau for their electricity consumption [27] .

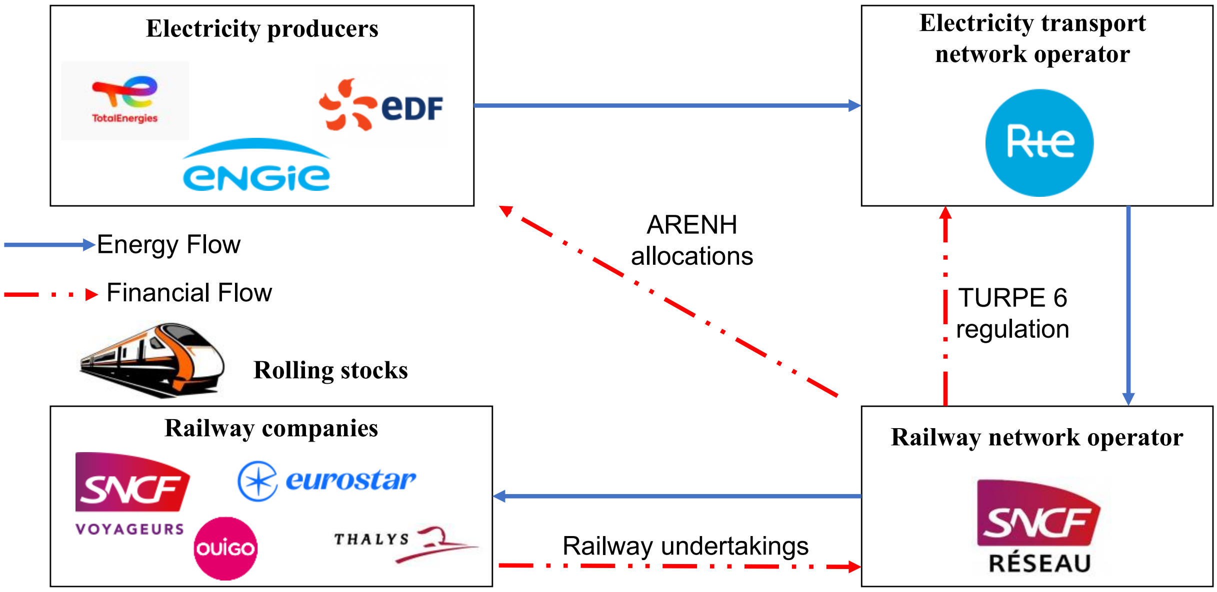


*Fig. 1.6 Tariffication scheme*

### 1.2.5.2 Cost of use of public grid (TURPE)

The TURPE 6 tariff is established through a regulated framework between RTE and the consumer, which is the railway network operator, under the supervision of CRE (Commission de Régulation de l'Énergie) [71] . With the TURPE 6 HTB framework, the SNCF Réseau is billed by RTE the use of the national electricity transmission network, through a structured set of tariff components designed to reflect both the power capacity reserved and the energy actually withdrawn across its railway traction substations [28] . As a high-voltage consumer (primarily HTB1 and HTB2), SNCF Réseau billing includes a fixed component related to subscribed power ("part puissance") and a variable component based on the actual energy consumed ("part énergie"), both modulated by seasonal and hourly coefficients defined by the seasonal-hourly differentiation defined by French electricity tariffs (*horosaisonnalité*) principle. This approach differentiates between peak, off-peak, and seasonal periods, applying specific pricing multipliers to each slot [28] .

The different TURPE components are shown in Fig. 1.7. The TURPE tariff is structured around several components that apply differently to consumers, producers, and distributors, each reflecting a specific aspect of network usage. These include the annual management (CG) and metering (CC) components, which cover administrative and measurement costs; the annual delivery (CS) component, which accounts for the withdrawal of electricity from the grid; and additional terms such as the monthly subscribed power overrun (CMDPS), reactive power (CER), backup supply (CACS), and scheduled overrun (CDPP) components. Producers are also subject to the annual injection component (CI), reflecting the cost of feeding energy into the grid. Together, these elements ensure a fair allocation of network operation and maintenance costs among all stakeholders.

In the present work, particular attention is given to the "Composante de Soutirage" (CS), as it represents the primary cost driver for SNCF Réseau and directly influences the energy management and optimization strategies discussed in the following sections.

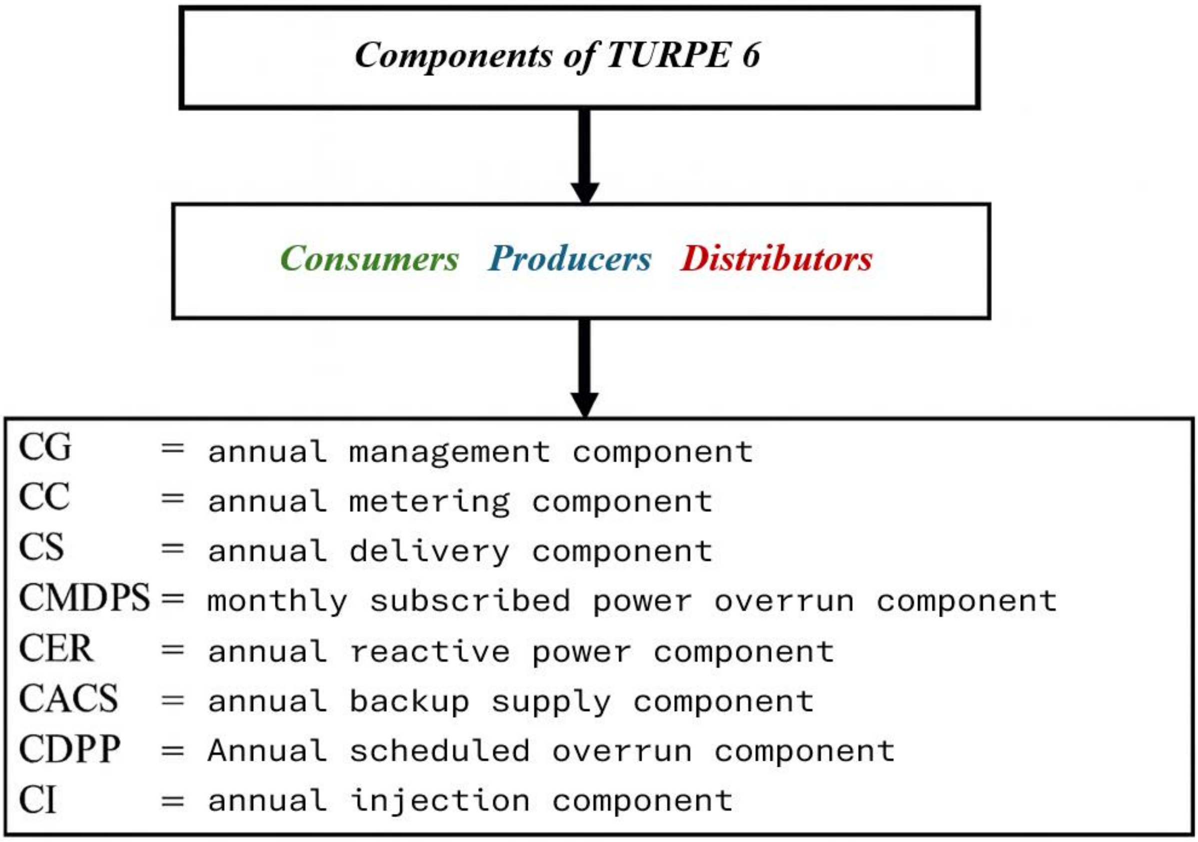


*Fig. 1.7 TURPE components for the producers, distributors, and consumers*

The annual withdrawal component "Composante de Soutirage (CS)" is calculated from the sum of power subscribed over five predefined time slots and the amount of energy withdrawn, with weightings that reflect time-of-use priorities. In cases where actual consumption exceeds the subscribed power, the CMDPS (Monthly Subscribed Power Overrun Component) is triggered, significantly increasing the bill through a penalty formula that applies a coefficient of 0.04 to the square of the difference as written in Equation (1.1).

$$\begin{aligned} CS = b_1 \times PS_1 + \sum_{i=1}^{5} b_i \times (PS_i - PS_{i-1}) + \sum_{i=1}^{5} c_i \times E_i \\ + \sum_{12 \text{ mois}} \sum_{i=1}^{5} 0.04 \times b_i \times \sqrt{\sum_j \left(P_j - PS_i\right)^2} \end{aligned} \tag{1.1}$$

$PS_i$ is the subscribed power for time band $i$ (peak, full high-season, off-peak high-season, full low-season, off-peak low-season), with corresponding coefficients $b_i$ (€/kW/year). The second term accounts for the fixed cost of subscribed power, while the third term adds the variable cost linked to the consumed energy $E_i$, weighted by coefficients $c_i$ (c€/kWh). The last term corresponds to the monthly penalties for exceeding the subscribed power (CMDPS), where $P_j$ denotes the actual 10-minute average power in excess of $PS_i$, and 0.04 is the regulatory weighting factor defined by TURPE6.

To manage these costs, SNCF Réseau selects among three contractual usage profiles (short, medium, or long duration) per substation, based on the ratio of annual energy consumption to peak subscribed power. This choice influences the balance between fixed and variable charges. Adjustments to subscribed power throughout the year are subject to specific conditions, including financial penalties if capacity reductions are reversed.

### 1.2.6 Challenges in existing DC railway networks

This section presents the main problems that the DC TSS suffer from today. These problems have the form of technical, economic, and environment problems. It introduces the problematic that RACCOR-D project must treat and therefore the thesis problematic.

#### 1.2.6.1 Infrastructure aging and technical limitations

Despite their extensive deployment and historical importance, DC railway electrification systems, particularly those operating at 1.5 kV, are increasingly constrained by the physical and technical limitations of their aging infrastructure [10]. Due to the relatively low supply voltage, high current levels are required to meet traction power demands, which results in substantial resistive losses along the overhead lines and rails. To mitigate these losses, large copper conductors up to 1000 mm² in cross-sectional area are employed in high-density traffic zones, significantly increasing material and installation costs [21].

Additionally, substations must be located at short intervals to maintain voltage levels within acceptable limits. As the traffic load grows, this configuration becomes unsustainable, particularly on lines where expansion or densification is required. These limitations not only affect energy efficiency but also restrict the ability of locomotives to operate at their full rated capacity, thereby compromising timetable reliability and service quality.

#### 1.2.6.2 Energy inefficiency

Low-voltage DC systems inherently suffer from high electrical losses due to the elevated currents required to deliver sufficient power. These losses manifest as heat in the overhead contact lines, rails, and internal resistance of rectifiers, and can account for more than 10–12% of the total energy consumed by the railway system. Studies show that the feeding losses in a 1.5 kV DC system are inversely proportional to the square of the voltage—meaning that doubling the voltage (e.g., to 3 kV) can reduce these losses by a factor of four, assuming constant power delivery.

Simulation analyses from [30] reveal that while higher-voltage conventional systems (e.g., 3 kV DC) offer substantial loss reductions, intermediate solutions using DC-to-DC converters can further optimize efficiency during transition phases. The energy inefficiency of legacy systems becomes particularly problematic when considered alongside modern railway electrification goals, such as SNCF's target of improving energy performance by 20% by 2025. According to SNCF's 2024 Financial Report, the company has already achieved significant energy savings over 80€ million between 2020 and 2024 and continues to modernize its traction substations and rolling stock to enhance energy recovery and reduce losses. These efforts form part of a broader decarbonization pathway extending to 2050, which includes increased renewable electricity procurement and digital supervision tools for optimized power demand [73] .

#### 1.2.6.3 Operational constraints under growing demand

With increasing traffic density and the rise of high-frequency rail services, the current 1.5 kV DC system struggles to meet the dynamic operational demands of modern networks. Voltage drops under high-load conditions lead to reduced pantograph voltages, often requiring traction units to operate in power-limited modes to avoid overcurrent faults. This affects not only energy efficiency but also adherence to scheduling and acceleration profiles. Moreover, the integration of renewable energy sources and bidirectional power is crucial for decarbonization and smart grid compatibility. Although it is difficult to achieve within DC railway TSS with diode rectifiers due to the lack of bidirectional substation infrastructure and the limitations of mechanical circuit breakers. These challenges are compounded by the lack of flexibility in current substation and line configurations, which makes adaptation to new traffic patterns or energy sources both technically complex and economically burdensome.

#### 1.2.6.4 Economic problems

The rising cost of electricity in France, coupled with the restructuring of grid tariff mechanisms, particularly the transition from TURPE 6 to TURPE 7, has introduced significant financial pressure on railway operators like SNCF Réseau. TURPE (Tarif d'Utilisation des Réseaux Publics d'Électricité), regulated by the French Energy Regulatory Commission (CRE), defines the access charges paid to RTE for using the public electricity transmission network [31] .

Since the beginning of TURPE 6 in 2021, one of the key financial burdens has been the steady increase in the power weighting coefficient, used to calculate penalties for exceeding subscribed power. As illustrated in Fig. 1.8, this coefficient has surged by over 140% between 2021–2022 and 2024–2025, rising from values as low as 2.9 €/kW/year to over 10 €/kW/year depending on the time slot. This evolution indicates a policy aimed at limiting peak demand, leading to higher sensitivity of SNCF's operations to power exceedances.

The most recent TURPE 7 framework introduces stricter penalties for peak demand and reactive power consumption, leading to higher overall costs compared to previous agreements between RTE and SNCF Réseau [31] . Nevertheless, the analysis conducted in this work relies on historical data recorded under the TURPE 6 tariff structure, as the implementation of TURPE 7 is planned for the coming years. Within the TURPE 6 period, the power weighting coefficients evolved annually, as depicted in Fig. 1.8, illustrating a consistent upward trend that reflects the gradual reinforcement of tariff constraints over time. This pricing evolution poses serious economic challenges, particularly for legacy DC systems that are inherently less efficient and harder to modernize.

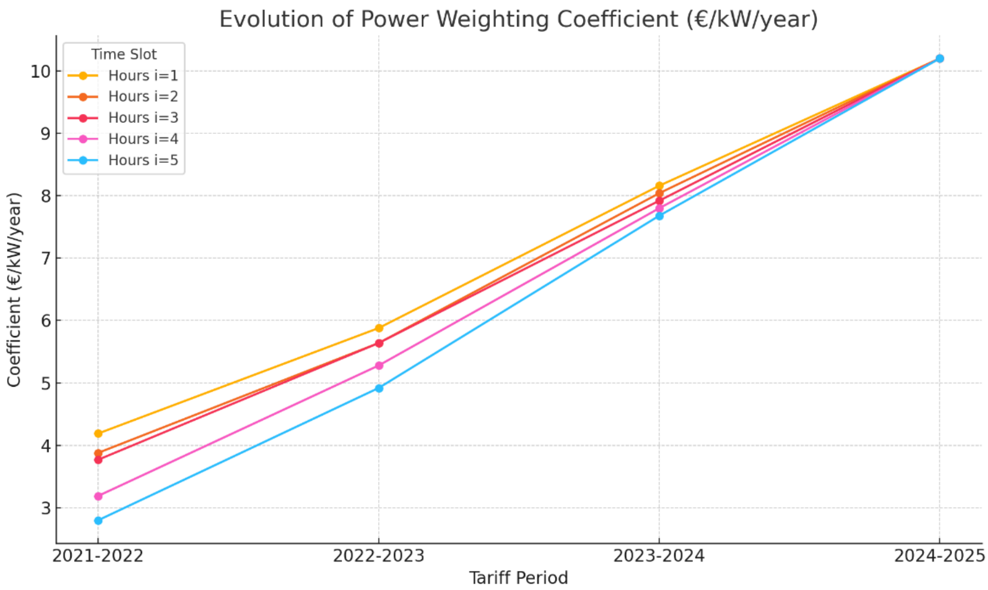


*Fig. 1.8 Yearly evolution of price penalty price coefficient throughout TURPE6 tariff*

#### 1.2.6.5 Environmental impact

The energy inefficiency of legacy 1.5 kV DC railway systems contributes not only to higher operational costs but also to indirect environmental impacts, especially in contexts where the electricity grid is not fully decarbonized. Due to significant resistive losses estimated at 10–12% in rectifier-based DC TSS, additional energy must be produced to meet actual traction demand, effectively increasing upstream $CO_2$ emissions even for electrified trains [32] . While rail is often promoted as a low-carbon mode of transport, such inefficiencies diminish its environmental advantages when the marginal electricity still contains fossil inputs. This undermines progress toward key decarbonization targets such as the European Green Deal's goal of reducing transport-sector emissions by 90% by 2050 [33] , as well as France's *Stratégie Nationale Bas-Carbone* aiming for carbon neutrality within the same timeframe [34] . Improving the electrical efficiency of the railway network is therefore not just a technical issue, it is a prerequisite for aligning rail operations with national and EU climate commitments.

## 1.3 Review of proposed technical solutions for enhancing DC railways

### 1.3.1 Medium voltage DC (MVDC) electrification

In response to the growing operational limitations and inefficiencies that characterize traditional 1.5 kV and 3 kV DC railway systems, recent research conducted with "SNCF réseau" has increasingly focused on the transition toward Medium Voltage DC (MVDC) electrification, with 9 kV DC emerging as a technically and economically balanced solution. The proposed new voltage electrification argues that 9 kV DC strikes a compelling compromise by offering significant performance gains while maintaining compatibility with existing electrification and traction system paradigms [29] [36] .

The MVDC approach yields several key benefits. First, it enables greater spacing between TSSs, reducing infrastructure density and associated maintenance costs. Second, by reducing the current required to deliver equivalent traction power, it permits a substantial reduction in the cross-section of overhead conductors from 850–1000 mm² in 1.5 kV DC systems down to approximately 230 mm² in the MVDC configuration. This not only lowers capital costs but also simplifies the mechanical structure of the catenary system [29] .

More critically, simulation studies confirm that energy efficiency is significantly improved. Losses in traditional 1.5 kV systems driven by high Joule heating in conductors and rails can reach up to 12% of the energy supplied. In contrast, the adoption of a 9 kV DC system reduces these losses to below 4%, even when factoring in thinner conductors and fewer substations [29] . These findings, corroborated by case studies on the French railway network, underscore MVDC's viability as a long-term solution aligned with the dual objectives of infrastructure rationalization and carbon-neutral electrification.

Fig. 1.9 and Fig. 1.10 illustrate the permissible combinations of overhead-line cross-sectional area and substation spacing for different DC voltage levels in railway electrification, distinguishing between classic and high-speed tracks. Each coloured region represents a voltage level, bounded by thermal limits (horizontal boundaries) and rail-to-ground voltage limits (vertical boundaries). The upper bound of 600 mm² for conductor size reflects an economic constraint, as larger sections would significantly increase the cost of support structures. For classic tracks, a 6 kV system offers an efficient solution, enabling substation spacing beyond 30 km with manageable conductor sizes. In contrast, high-speed tracks, which impose greater power demands (reflected by higher conductance $G = 0.75$ S/km), require higher voltage levels, typically above 7.5 kV, to allow substation spacing of over 40 km, aligning with common AC electrification practices.

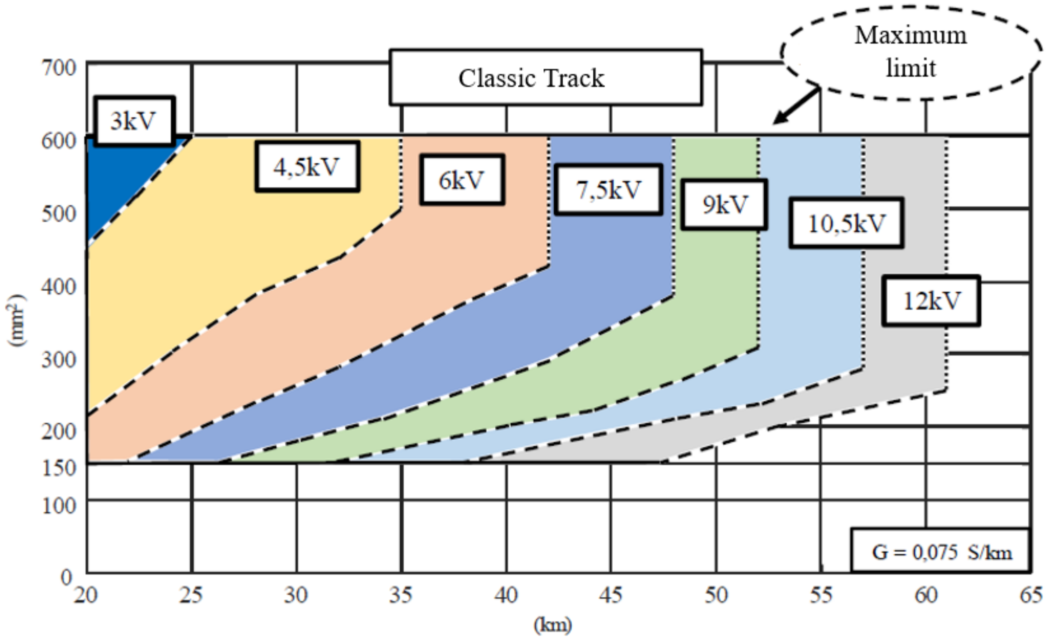


*Fig. 1.9 Overhead-line cross-sectional area versus substation spacing for a rail-to-ground conductance of 0075 S/km. Suburban transport (classic track) [36]*

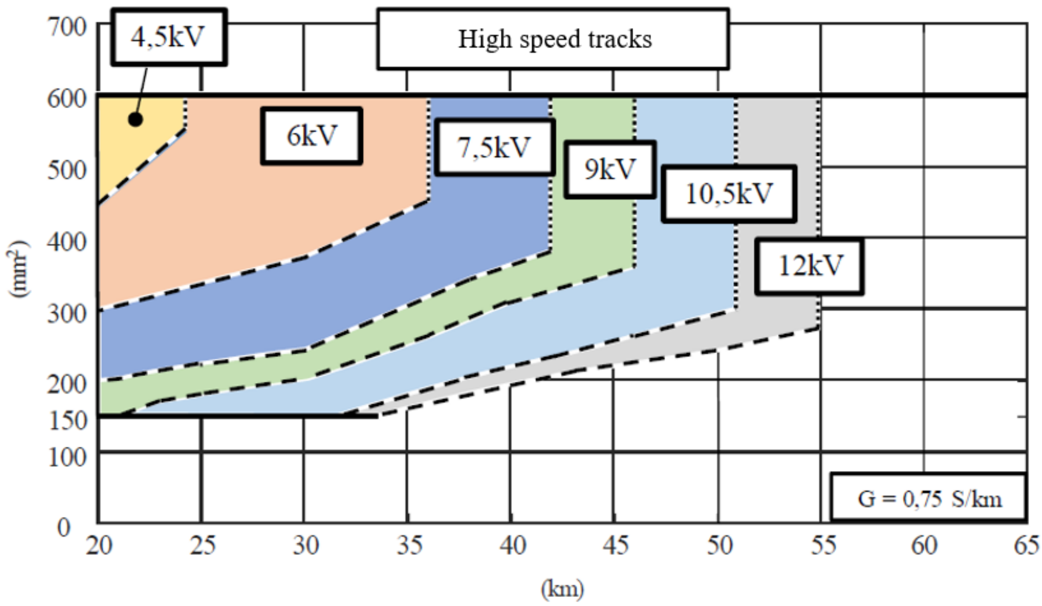


*Fig. 1.10 Overhead-line cross-sectional area versus substation spacing for a rail-to-ground conductance of 0075 S/km. High speed tracks [36]*

### 1.3.2 Hybrid and transitional architectures

The transition from conventional 1.5 kV or 3 kV DC railway systems to Medium Voltage DC (MVDC) architectures offers clear benefits, including improved energy efficiency, reduced substation density, and enhanced integration of renewable energy sources. However, a complete and immediate infrastructure overhaul remains economically and operationally challenging. In response, the literature has proposed several hybrid and stepwise strategies designed to enable a gradual, cost-effective modernization of existing rail networks.

A progressive migration strategy in which a 9 kV DC feed-wire is installed alongside the existing 1.5 kV overhead line is proposed in [35] . During the transition phase, power electronic transformers (PETs) located either at substations or onboard rolling stock manage real-time voltage conversion, allowing continued operation of legacy trains. Over time, conventional 1.5 kV substations are replaced by modular 9 kV units, resulting in lower energy losses and a significant reduction in substation count [35] . A case study conducted with the “SNCF réseau” on the Bordeaux–Hendaye corridor confirms the feasibility of this hybrid configuration, demonstrating stable pantograph voltages and improved system performance. Once the fleet is upgraded for native 9 kV operation, the infrastructure can be fully converted, completing the transition.

Fig. 1.11 illustrates the transitional process of upgrading the DC railway grid to a 9 kV system. As shown in Fig. 1.11 (a), certain intermediate substations will be entirely decommissioned and replaced by DC-DC step-down Power Electronic Transformers (PETs) to continue supplying the existing 1.5 kV overhead line. The final stage in this electrification evolution involves directly feeding the overhead line with 9 kV DC, as shown in Fig. 1.11 (b). Consequently, all remaining 1.5 kV transformer-rectifier units, along with the previously installed DC-DC PETs, will be removed. Simultaneously, the overhead line infrastructure will undergo a complete renewal. The newly installed catenary system will feature reduced copper cross-sections and lighter support structures, resulting in substantial cost savings for the overall infrastructure.

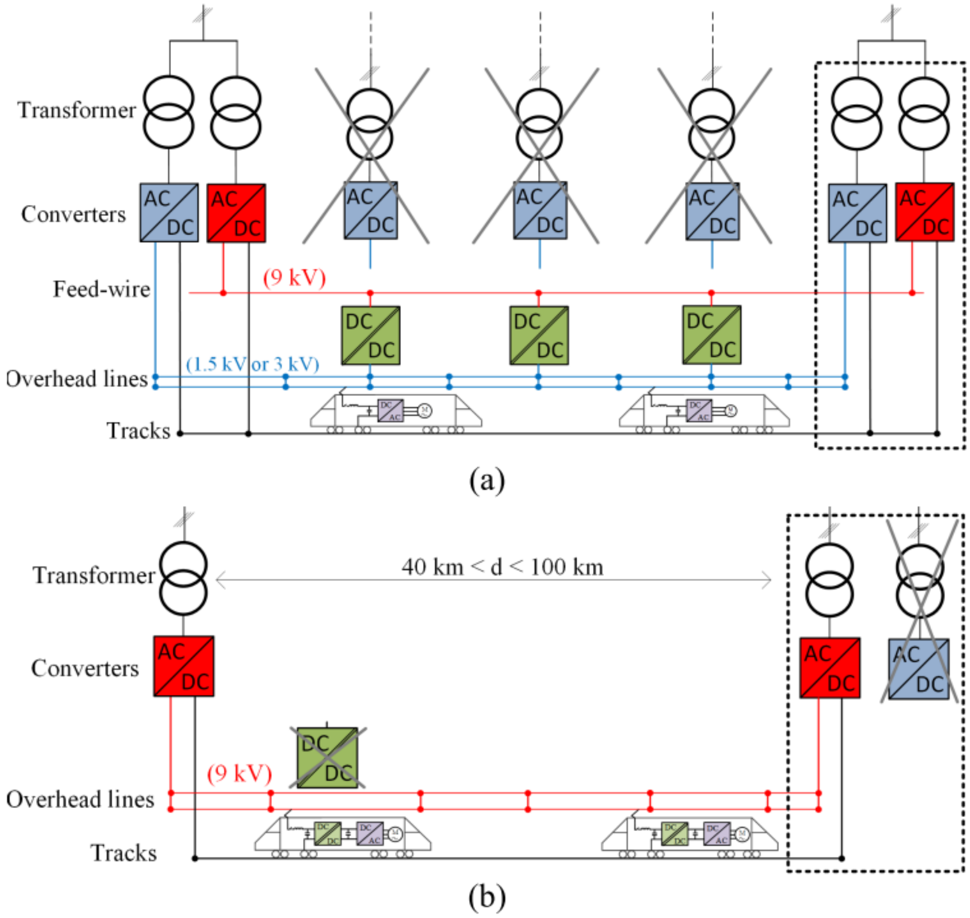


*Fig. 1.11 Intermediate electrification system: three-wire supply system with a 9-kV feed wire. (b) Final stage: 9-kV dc electrification system [37]*

A more comprehensive approach is proposed in [38] , who introduces a 24 kV MVDC grid supported by modular voltage source converters (VSCs). This architecture enables bidirectional power flow, supports both urban and high-speed networks, and allows dual voltage rolling stock to operate seamlessly across legacy and modern segments. Their case study on the Madrid–

Barcelona corridor illustrates a 50% reduction in installed transformer capacity, extended substation spacing up to 120 km, all without compromising voltage stability or operational performance. The proposed VSC MVDC-based railway system as a new traction power system framework offers great potential compared to conventional MVAC systems. Fig. 1.12 (a) illustrates the core of the traction substation in the proposed paradigm. It is composed of a three-phase modular multilevel VSC connected to the power system through a step-down transformer. Fig. 1.12 (b) shows the bidirectional, isolated dc–dc converter used. On the 24-kV side, a multilevel inverter for the high speed track and on the 3 kV side for DC metropolitan network.

Through a comprehensive review of MVDC railway systems, research in [21] emphasizing the importance of gradual transition mechanisms such as modular power-electronic converters and dual-voltage compatibility. The work highlights MVDC's suitability for smart grid integration, enhanced energy recovery, and the accommodation of distributed generation, while also pointing to the regulatory and standardization needs that must accompany technical progress.

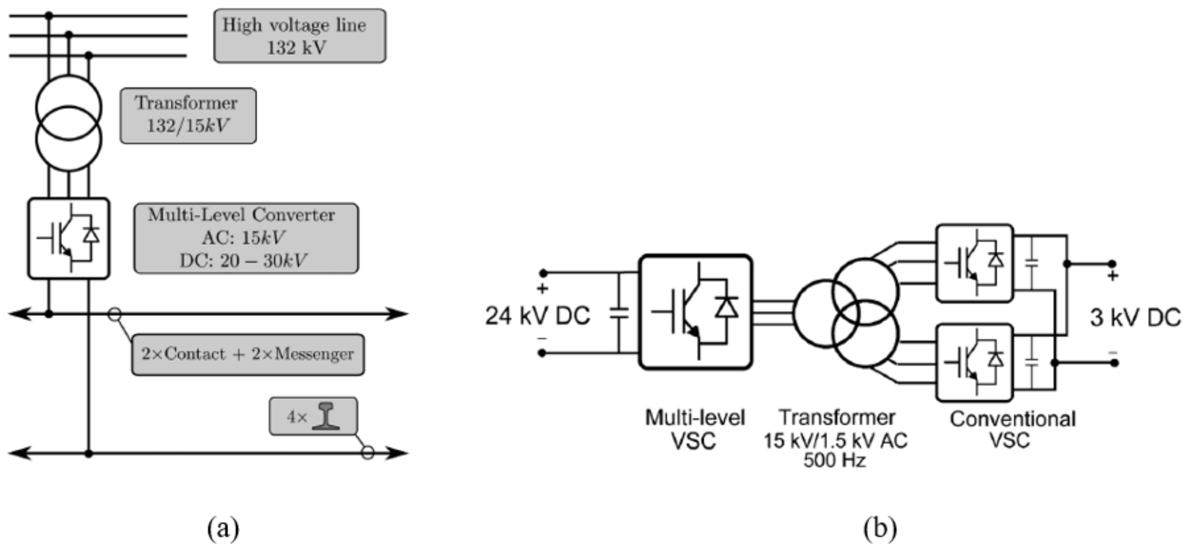


*Fig. 1.12 (a) Transformer and multilevel VSC for the 24-kV dc electrification system. (b) VSC-based interconnection of high-speed (24 kV) and metropolitan (3 kV) railways*

The shift toward MVDC and hybrid DC architectures necessitates a re-evaluation of the underlying converter and protection infrastructure. Traditional transformer-rectifier groups and electromechanical breakers are insufficient for high-performance, and medium-voltage operation. To this end, a new generation of Power Electronic Traction Transformers (PETTs) has been introduced, capable of handling high-voltage DC levels with galvanic isolation and modularity. These PETTs typically integrate multilevel DC-DC converter topologies and Silicon Carbide (SiC)-based semiconductor switches, offering high power density, low switching losses, and improved thermal performance key requirements for both wayside and onboard integration [39] .

### 1.3.3 Reversible substations and energy management

A critical limitation of legacy DC railway systems lies in their inability to effectively make use of regenerative braking energy. In conventional configurations, braking energy is often dissipated as heat through onboard resistors or is ineffectively reinjected into the grid due to unidirectional power flow constraints. Converter technology can replace the rectifier leading for a possible bidirectional power flow as shown in Fig. 1.13. The recuperation of regenerative braking energy can now be achieved through new electrification systems that support [40] . such reversibility [40] [121] .

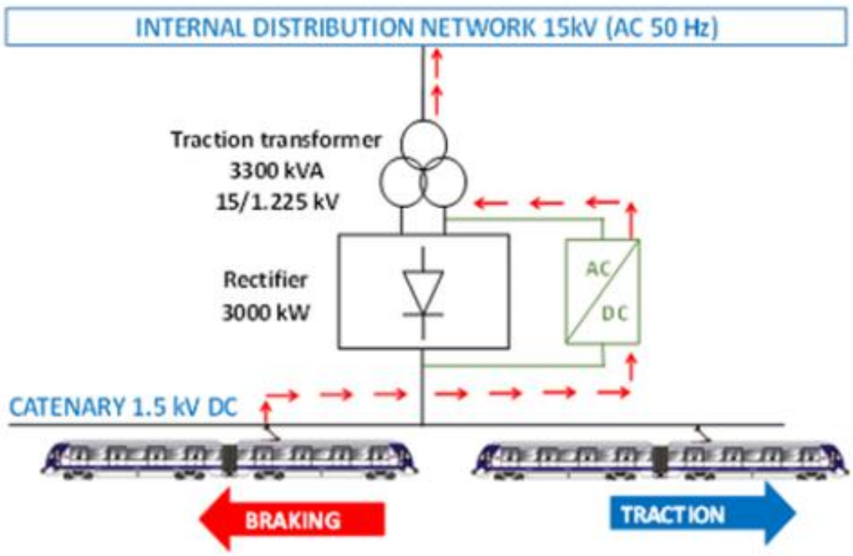


*Fig. 1.13 Reversible substation working method [40]*

The reversible substations offer a bidirectional power exchange between the traction system and the upstream electrical grid. These substations employ voltage source converters or reversible thyristor-controlled rectifiers (RTCRs) to manage power flows during deceleration phases, thereby allowing for the recuperation of otherwise wasted braking energy. The implementation of RTCRs, as highlighted in [41] , not only facilitates energy recovery but also improves voltage regulation and reduces infrastructure costs by enabling wider substation spacing and reduced rail losses. Field-tested systems on reversible DC substations have been developed and commercialized under platforms such as the Enviline™ ESS developed by ABB. In which the wayside ESS is designed for DC railway transportation networks. Its primary purpose is to capture and reuse regenerative braking energy, thereby reducing traction energy consumption by up to 30% and mitigating peak power demand on the grid [42] . The INGEBER system is an energy recovery solution tailored for DC railway networks, designed to capture surplus regenerative braking energy and feed it back into the AC grid [43] . Siemens offers the Sitras RCC (rail charging converter), a powerful flexible solution for the efficient charging of battery-electric trains. And a self-commutated IGBT inverter Sitras® PCI that plays a pivotal role in the electrification of infrastructure, setting a benchmark for sustainable mobility. This innovative product enables the transmission of a train's braking energy into the superordinated medium-voltage network, thereby reducing energy costs [44] [45] .

Complementing these hardware innovations, [46] proposed a medium-voltage DC (MVDC) railway electrification scheme based on modular multilevel converters (MMC-FB), demonstrating through simulation that such substations can both feed traction loads and inject surplus regenerative or photovoltaic energy back into the AC grid with high power quality and near-unity power factor. Their work confirms that advanced converter-based substations inherently support reversibility and enable flexible integration of renewable energy sources into the traction network.

In parallel, research in [47] introduced a novel power-based coupling methodology to assess the technical impact of injecting regenerative braking energy into surrounding AC distribution grids. Applied to Panama Metro Line 1, their methodology models the DC railway system and AC grid independently and links them via a lumped inverter model, enabling efficient assessment of voltage fluctuations and grid strength without requiring detailed converter simulations.

The rise of microgrid concept and the entrance of multiple actors in the railway grids such as auxiliary loads and EV charging stations pushed researcher to develop optimization-based energy management strategies are being explored to further enhance efficiency. Providing arrangement of power exchange between different actors (grid, RES, ESS, EV, etc...) to maximize the use of local renewable energy production and for efficient use of ESS**.** In this context, a Model Predictive Control (MPC) framework for a smart railway station integrating PV generation, battery and supercapacitor storage, and regenerative braking as shown in Fig. 1.14. The MPC controller allocates energy flows across storage and loads while maintaining voltage stability within the microgrid [48] , using a Mixed-Integer Quadratic Programming (MIQP) formulation to manage complex operational constraints of the different smart grid actors.

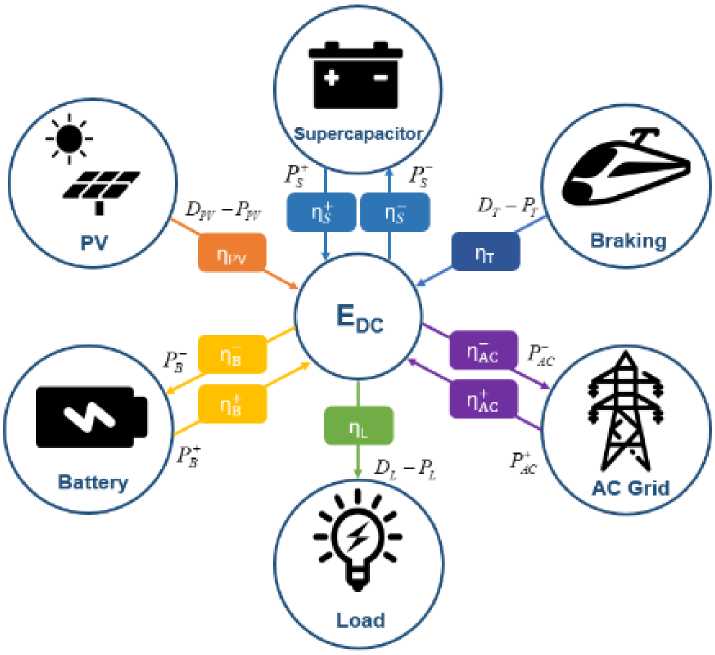


*Fig. 1.14 Representation of smart microgrid with different actors [48]*

## 1.3.4 Summary of the recent solutions

Recent progress in DC railway electrification shows a clear move from traditional, one-way, and energy-intensive systems toward smarter and more flexible ones. Medium Voltage DC (MVDC) solutions, especially around 9 kV, have proven to reduce energy losses, allow greater distance between substations, and lower infrastructure costs, while remaining compatible with existing trains and equipment. Hybrid and step-by-step approaches make it possible to modernize the network gradually by using modular converters and power electronic transformers. At the same time, reversible substations and new converter technologies have made it possible to recover braking energy that was previously lost, improving overall efficiency and sustainability.

Together, these innovations form the foundation of the next generation of railway electrification. They increase efficiency, make control systems smarter, and improve compatibility with renewable and decentralized energy sources. They also create the right conditions for integrating renewable generation and encourage the use of energy storage systems (ESS) to reuse electricity that was previously wasted. In addition, they help maintain system stability, especially in networks with frequent train operations. These advances open the way to smart railway energy systems, where different energy sources such as PV systems, ESS, and EV charging stations can work together under intelligent energy management systems.

## 1.4 Smart grids (systems with multiple sources)

Given the rising traffic density and energy demand across the French railway network, the traditional 1.5 kV DC traction system is reaching its technical and operational limits in supporting high-frequency services. To address these challenges, SNCF Réseau has launched several modernization initiatives aligned with its national objective of improving overall energy efficiency by 20% between 2015 and 2025. These initiatives are part of a broader decarbonization strategy aimed at reducing electricity costs during peak hours and limiting the network's carbon footprint. Projects such as RACCOR-D, led by SNCF Réseau, are testing the deployment of smart grid technologies integrating batteries, photovoltaic (PV) systems, and intelligent control to enhance local energy autonomy and network flexibility. In parallel, SNCF is pursuing large-scale photovoltaic development—targeting 1 GWp of installed solar capacity by 2030—and conducting pilot projects like Solveig, which explores PV integration directly on railway infrastructure [74] [75] .

Together, these efforts mark SNCF's transition toward smart, decentralized energy management, reducing dependency on the public grid and promoting cleaner, cost-efficient, and more resilient railway operations.

### 1.4.1 Integration of renewable energy sources to the railway networks

The integration of renewable energy sources (RES) into railway power systems has emerged as a promising strategy to address the limitations of conventional DC railway networks in terms of supply reliability, voltage regulation, and environmental sustainability. Photovoltaic (PV) systems, in particular, have shown significant potential when deployed on station rooftops, depots, and adjacent unused land to support local loads and improve the overall energy balance by reducing electricity drawn from the grid and associated transmission losses [49] .

More broadly, the development of stationary hybrid renewable energy systems (HRES) combining PV, wind turbines, and energy storage offers a flexible and scalable solution to power both electrified railways and isolated sections of the grid, enhancing supply reliability while lowering operational costs and fossil fuel dependence [50] . These systems, often configured in grid-connected or stand-alone architectures, can support auxiliary loads, TSSs, or even enable partial railway microgrid operation.

Such integration is further enhanced by the application of smart grid principles, which enable the dynamic coordination of distributed generation, energy storage systems (ESS), and demand-side management through integrated communication and power electronics technologies [49] . In this context, railway-adapted smart microgrids have been proposed to incorporate distributed energy resources, bidirectional converters, and intelligent control strategies capable of optimizing energy flows, recovering regenerative braking energy, and improving system resilience [51] .

Real-world deployments have illustrated the effectiveness of combining PV generation with demand response strategies to reduce peak loads and operational energy consumption across stations and auxiliary buildings [49] . Moreover, the deployment of ESS on a wayside connection has shown significant benefits in capturing regenerative braking energy, stabilizing catenary voltage, and mitigating stray currents, especially in MVDC configurations where mid-line support is critical [52] [53] [54] .

The MVDC railway architecture mentioned earlier [21] further enhances these capabilities by enabling direct PV coupling to the traction power supply, where renewable generation units can feed the MVDC feeder without intermediate AC conversion. This architecture also enables stable interaction with the upstream AC grid through controlled power-electronic converters, ensuring balanced power exchange and voltage regulation under variable renewable and traction load conditions. Such bidirectional and controllable energy flows demonstrate that MVDC systems can serve as the backbone of renewable-powered railway microgrids [46] . These advancements collectively position RES, hybrid systems, and smart grid technologies as key enablers of the transition toward more efficient, and intelligent railway infrastructure.

### 1.4.2 Services of ESS in railway network

As energy efficiency, grid stability, and operational flexibility become central pillars of smart railway electrification, ESS have emerged as multi-functional assets capable of delivering diverse technical services. Rather than functioning solely as regenerative energy buffers, modern ESS architectures provide a suite of grid-integrated, intelligent, and service-driven functionalities. This section dissects the primary services enabled by ESS in electrified railways.

#### 1.4.2.1 Regenerative braking energy recovery

Regenerative braking allows trains to convert kinetic energy into electrical energy during deceleration. However, in the absence of Energy Storage Systems (ESS), this energy is often dissipated as heat through braking resistors due to limited catenary receptivity or the absence of concurrently accelerating trains. ESS mitigate this by enabling the systematic capture and reuse of regenerative braking energy (RBE), thus reducing the net traction energy drawn from the grid and improving overall system efficiency.

Modern solutions including hybrid ESS configurations that combine supercapacitors and lithium-ion batteries are designed to absorb high-intensity braking events and discharge energy during acceleration phases, supporting smoother power profiles and network stability [55] [56] . Practical implementation in controlled systems using DC/DC converters has demonstrated that ESS can significantly reduce energy losses and peak power draw [57] .

Fig. 1.15 shows the basic principle of capturing regenerative braking energy. In DC railway systems, the decision to either dissipate braking energy on board or feed it back into the grid is defined during the design and commissioning of the line. If the substation and network are designed to be receptive (1), braking vehicles can reinject part of their energy into the grid. Otherwise, the energy is dissipated through onboard braking resistors (2). When several vehicles brake simultaneously, the network may become saturated, forcing excess energy to be dissipated. To prevent this, one or more ESS can be installed along the track providing a path for the energy. The additional consumer increases the grid receptivity and is able to store braking energy (3) and release it again if required in acceleration (4), thus relieving the substations. A key challenge, however, lies in enabling trains to dynamically assess network conditions through intelligent power management and communication mechanisms, allowing regenerative energy to be utilized more effectively in real time.

Promising perspectives are arising from the development of Lithium Titanate Oxide (LTO) cells that allow direct connection to the DC network, eliminating the need for power converters while maintaining high charge/discharge efficiency and cycle life [58] . However, this solution still require voltage matching and a robust battery management system suitable for this kind of direct connections.

These configurations make ESS deployment more flexible and cost-effective, especially in dense urban rail environments.

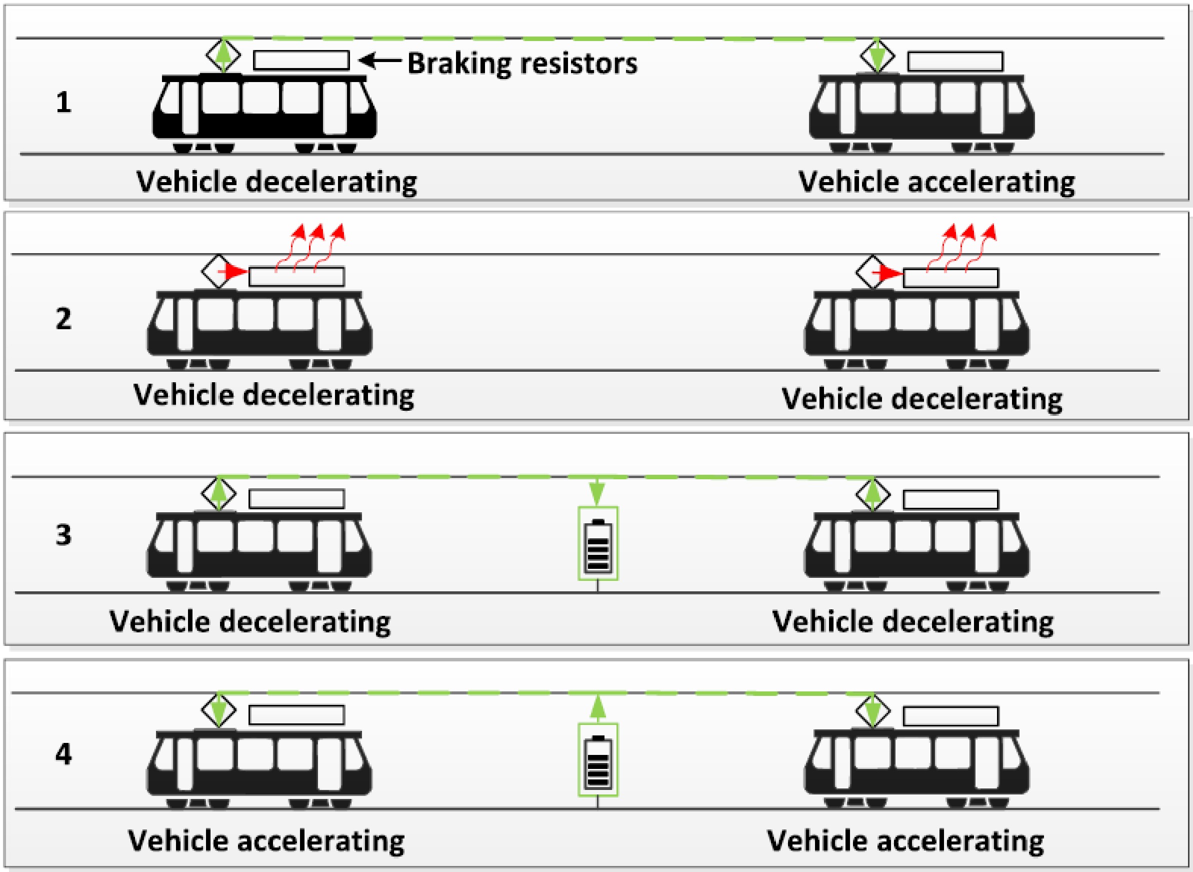


*Fig. 1.15 Braking and accelerating in a grid with and without ESS [48]*

#### 1.4.2.2 Maintain voltage level and power quality support

Voltage drops are a major limitation in long DC railway sections and during dense train traffic. Energy Storage Systems (ESS) help maintain the pantograph voltage above critical thresholds to ensure continuous traction. For instance, research in [59] proposes a smart microgrid-based electric railway system integrating ESS, regenerative braking, and renewable sources. Their control strategy ensures dynamic voltage regulation through coordinated operation of ESS and Railway Power Conditioners (RPCs), which act as energy hubs and power-quality compensators. Simulations demonstrate how their system maintains DC bus voltage stability under fluctuating traction and regenerative loads, reducing stress on the grid and enhancing reliability.

The SNCF contribution in this field appears in the development of a Modular Battery Energy Storage Systems (MBESS) that operates in voltage-source or current-source modes depending on grid conditions, to reinforcing network resilience including the issue of voltage drops [12] .

Another study conducted on VSC based TSS, showed that the integration of PV system and ESS at mid-section of the railway track achieve the highest catenary voltage stabilization. At mid-section, the catenary voltage drop will be at its maximum since it's the point where the catenary linear resistance will be at its maximum [52] . The resistance of the catenary depends on the position of the train; its linear resistance is expressed in Ω/km. The furthest the train is from the substation the higher the resistance. Fig. 1.16 illustrates the integration of PV and ESS (connected to the catenary) at mid-section between two TSS.

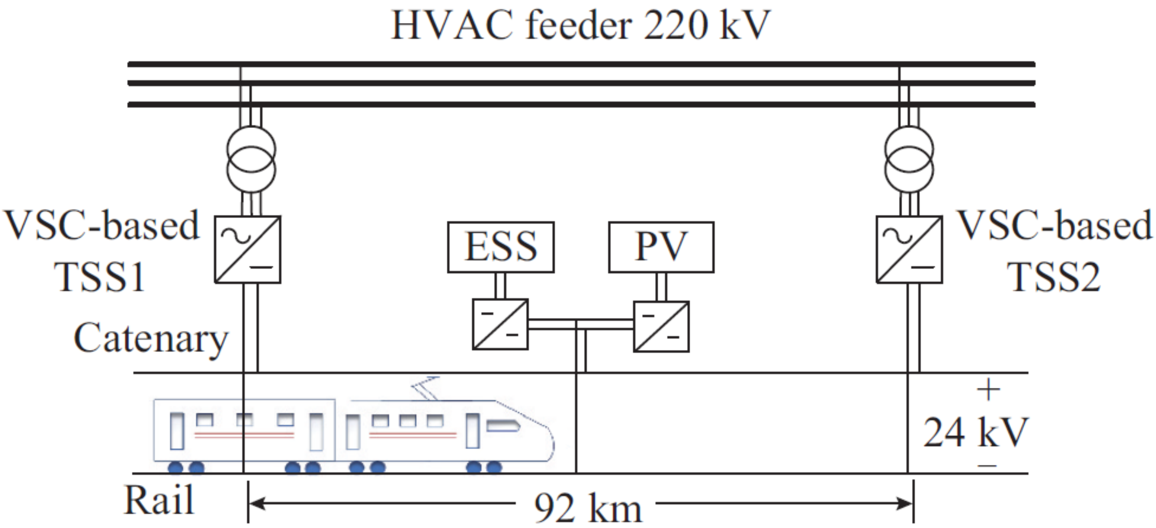


*Fig. 1.16 VSC based TSS with PV and ESS at mid-section [43]*

#### 1.4.2.3 Peak shaving and substation relief

Energy Storage Systems (ESS) offer critical peak shaving and substation relief services for railway grids by strategically discharging during high-demand periods (trains acceleration and high traffic scenarios) and charging during low-demand intervals. This smoothing of the power profile reduces peak loads by over 30%, as validated by platform-based simulations and real-world implementations, such as a high-power ESS installation in Poland's 3 kV DC traction network [60] . By reducing peak demand, the ESS eases the load on substation equipment, helping to delay expensive infrastructure upgrades and lower the extra costs that occur during high-tariff periods [61] . Furthermore, ESS supports dynamic substation load management through predictive control strategies. The study proposes a wayside ESS integrated with a Railway Power Conditioner (RPC) to address peak demand and grid instability in electrified railways. The ESS-RPC system, connected to the DC bus of traction substations, employs Li-ion batteries to actively regulate maximum demand through short-term load forecasting using a hybrid Auto Regressive Integrated Moving Average (ARIMA) neural network model. This approach reduces substation peak loads by 12.7% [62] . Another study reviews the integration of ESS in electrified railways, highlighting their role in peak shaving and grid stress reduction through a dynamic control methodology presented in [63] . These capabilities not only enhance grid stability but also lower maximum demand charges of railway electricity costs.

#### 1.4.2.4 Back up services

ESS in railways are deployed as either onboard (OESS) or wayside (WESS) solutions, each addressing distinct operational needs. The Beijing Metro Study demonstrates how coordinated OESS and WESS can optimize regenerative braking recovery while performing peak shaving, with OESS enabling immediate energy reuse during acceleration and WESS stabilizing grid-level demand [64] . Meanwhile, the Warsaw University Study highlights WESS applications in substation relief and emergency power for catenary-free sections, while OESS ensures train mobility during outages critical for evacuation or bridging short power gaps. Together, these studies underscore that onboard systems prioritize localized energy autonomy (e.g., emergency traction), whereas wayside systems excel at grid-scale resilience (peak load reduction and EV charging support) [65] .

#### 1.4.2.5 Smart grid integration and energy management

As part of modernization of DC railway substations, railway network operators are integrating renewable energy sources for multiple reasons as explained earlier. As railway systems evolve into smarter, decentralized infrastructures, energy storage systems are increasingly integrated into smart grid architectures where they interact dynamically with the available renewable energy sources, the public grid, and other actors that may be present in the network. Within this framework, ESS are no longer passive storage elements but become actively managed assets, coordinated by intelligent Energy Management Systems (EMS). These systems perform multi-objective optimizations that balance cost, energy efficiency, grid stability, and component health. There are plenty of methods used to develop EMS, the choice of the method depends on the system specification and the type of application. Modern EMS approaches leverage advanced control algorithms, such as fuzzy logic, rule-based, and mixed-integer linear programming (MILP), to manage ESS operation under variable railway traffic, PV generation, and TSS load consumption.

For example, an optimization-based EMS is developed with MILP for an interconnected railway stations equipped with PV, and ESS. With an objective to coordinate the ESS in a way that reduces the dependency of the grid and enhances self-consumption of PV systems under uncertainty in SOC and solar irradiance. Leading to an evident reduction in energy costs [66] [67] .

Also, a fuzzy logic control scheme that adjusts power flow in a railway based on real-time voltage conditions and battery SOC, successfully reducing battery degradation while maximizing energy recovery is developed in [68] .

To support long-term viability, ESS integration must also consider battery aging mechanisms and their impact on lifecycle cost. As explained in [69] , incorporating aging models into the EMS allows for smarter sizing and dispatch decisions, ultimately increasing the return on investment while maintaining system reliability.

Together, these strategies of EMS applied to railway smart grids elevate the importance of ESS that create a path for excess of renewable energy production and regenerative braking energy. Which has a direct impact on maximising the self-consumption of renewable energy sources and minimizing the dependency on the grid that led to economical savings in terms of energy costs.

## 1.5 Context of project RACCOR-D

Funded by France 2030, the RACCOR-D project, developed in collaboration with SNCF Réseau, RTE, JUNIA-L2EP, SCLE, Railenium, INPT-Laplace, and CEA present a strategic ambition to modernize legacy DC traction substations by progressively transitioning them into smart, medium-voltage DC (MVDC) substations. This initiative responds directly to the well-documented limitations of the 1.5 kV DC system represented in high resistive losses, dense substation spacing, and constrained traffic scalability. By addressing these issues, RACCOR-D positions DC electrification back into perspective alongside AC systems, particularly in terms of cost efficiency, operational performance, and energy optimization. The longer-term vision, informed by previous technical studies conducted by SNCF Réseau, involves upgrading the line to an MVDC configuration. In such a scenario, the DC TSS itself could potentially be decommissioned and fully replaced by the RACCOR-D system, which would function as a self-sufficient smart energy node composed of only PV and ESS. This would not only reduce infrastructure complexity but also contribute to the strategic goal of increasing the spacing between substations without compromising energy availability or grid stability.

One of the central motivations behind RACCOR-D is the integration of smart grid functionalities into the existing railway infrastructure. Recent advancements in converter topologies, power electronics, and energy storage technologies, alongside the development of the smart grid concept allow DC substations to evolve into active energy hubs. Fig. 1.17 represents the potential future of the DC TSS, where the traction unit (diode rectifier + transformer) is replaced with MVDC converter. With a potential bidirectional power flow from and to the electricity transmission network RTE. The research behind this transformation is conducted by Laplace laboratory and RTE, with the contribution of the railway network operator SNCF réseau. This future vision also hosts PV designed by CEA, and ESS technology. Connected to the railway network through DC-DC converters that falls under SCLE responsibilities. The energy management work falls under the L2EP that forms the problematic of this thesis.

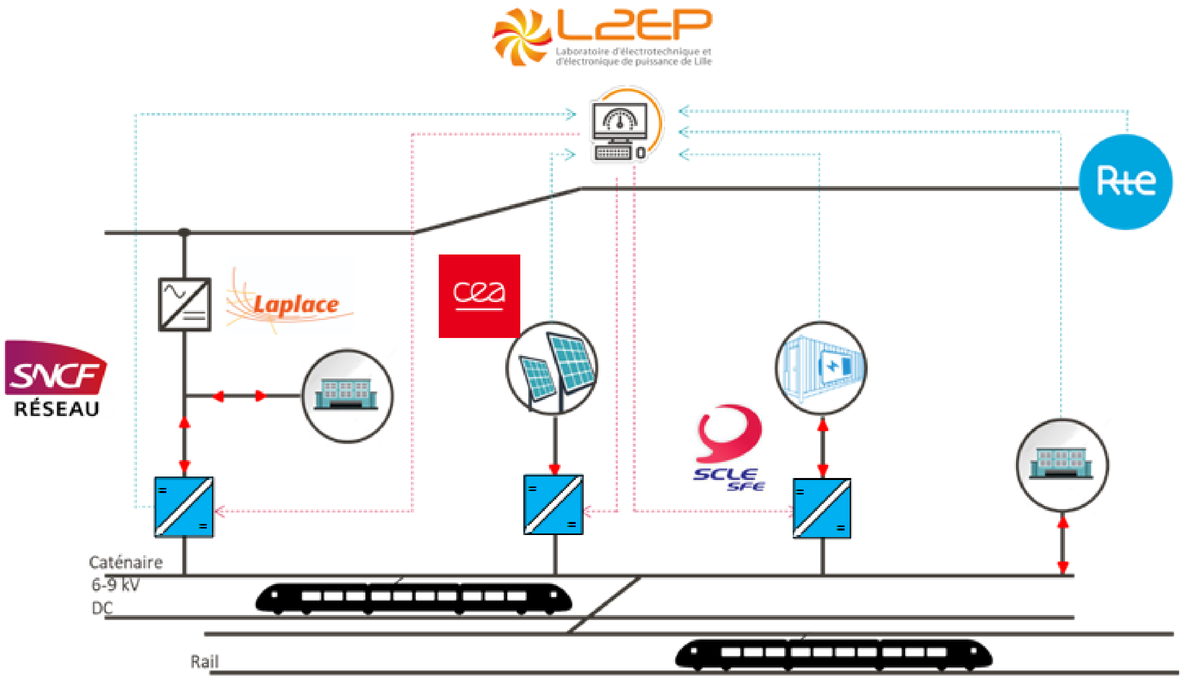


*Fig. 1.17 Future architecture of the DC railway TSS with RACCOR-D system*

Fig. 1.18 summarizes the role of every RACCOR-D project partner. The work is divided into 5 main groups, where the fifth one covering the energy management is the one concerned by this thesis. The research done in this area uses the first vision of RACCOR-D project in terms of PV, ESS capacity, and DC-DC converters rated power. The study considers available rectifier based TSS without tackling the future perspectives in terms of medium voltage and bidirectionality. The energy management must be evaluated and tested with existent data; future vision of RACCOR-D is not implemented and cannot be investigated under the proposed energy management work since it offers additional objectives and constraints caused by the modification of the substation nature.

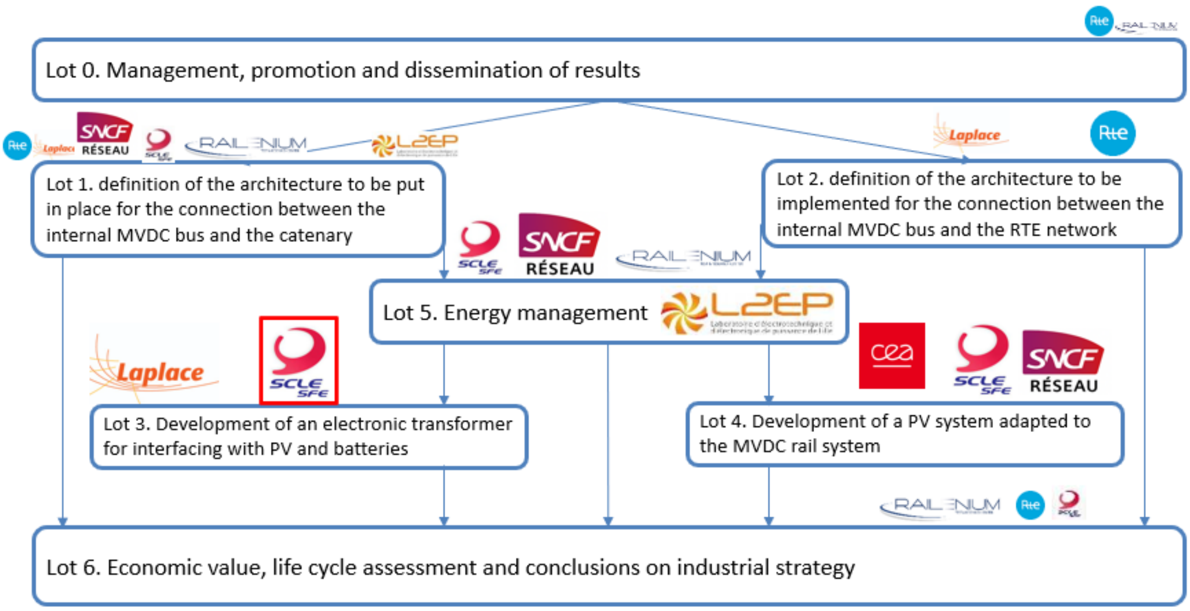


*Fig. 1.18 Mission of every RACCOR-D project collaborator*

To this end, a DC TSS, located in southern France, has been selected as a pilot site for experimental deployment. This TSS serves as a good example of the challenges facing the broader French railway network: it operates under low-voltage constraints that limit power supplied to the TSS load and the ability to support increased rail traffic. Integrating on-site PV production and battery energy storage offers a solid solution to respond to the economic problems explained earlier.

In light of this future perspective, an alternative RACCOR-D architecture is envisaged, in which the system is installed at the mid-section between two substations. Such positioning would allow it to act as a decentralized power buffer and voltage support node, bridging the electrical gap created by the removal of one traditional TSS. This novel architecture, made possible through MVDC technology and advanced supervision tools, would maximize the value of local renewable energy while ensuring the continuity and quality of railway service.

RACCOR-D, therefore, not only represents a technical demonstration of smart grid integration in a railway context but also sets the stage for developing new supervisory frameworks that can optimize the interaction between controllable (ESS, PV) and non-controllable (AC/DC converters, railway traction load) elements. The project responds to both national goals for railway modernization and broader European directives targeting energy efficiency and carbon neutrality.

## 1.6 Thesis problematic and research positioning

The transformation of legacy DC traction substations into smart grid nodes equipped with photovoltaic (PV) production and energy storage systems (ESS) introduces a new operational paradigm. These substations, which historically functioned as passive infrastructure elements, are now expected to host dynamic, bidirectional, and multiple energy interactions. In this context, the optimal operation of ESS requires not only an adequate energy management system (EMS) but also real-time supervision tool capable of responding to the uncertainties inherent in both railway load demand and renewable generation.

A critical obstacle is the absence of real-time measurement of traction substation (TSS) load. In general, the TSS load covers the load of the circulating trains, the losses of the TSS equipment, auxiliary loads (EV charging stations for example). Unlike industrial or residential microgrids where flexible loads can be modulated to support energy objectives, railway systems are rigid in their consumption patterns. The energy management framework must therefore operate under asymmetric controllability, where the load is fixed and only the ESS can be actively manipulated. Consequently, the proposed energy management solution must be adaptive of the nature of the railway network, balancing between the multiple objectives with different nature from the multiple elements and actors of the railway smart grid.

While the scientific literature provides valuable contributions to energy management in railway-integrated smart grids, real-time supervision remains largely underexplored. Most existing works prioritize offline or predictive optimization strategies (MPC, MILP), assuming either perfect foresight or full measurability of system states. However, these assumptions break down in operational railway environments where ESS must react instantaneously to uncertain and unmeasured phenomena. This thesis addresses that gap by developing a real-time supervision tool, grounded in fuzzy logic and designed to handle imprecise or missing measurements while maintaining computational tractability and fast decision cycles. Also, a classic optimisation-based EMS is developed to be compared with the proposed real time supervision tool. The day ahead EMS that relies on forecast information regarding the PV production and the TSS load consumption can be limited in term of uncertainty that highly exists in the TSS load variation and PV generation that depends on the weather fluctuation.

This elevates the challenge of developing an adequate forecast model suitable for the TSS load nature and dynamics. Improving the forecast leads to higher accuracy for the day ahead EMS that serves as a long-term supervision in terms of ESS scheduling and achievement of the objectives set. The real time supervision is designed as a short-term supervision level; it comes after the day ahead planning and operates in real time to deal with the uncertainties and guarantee the achievement of the objectives while respecting the necessary constraints of the railway smart grid elements.

Another layer of complexity arises from the multi-agent nature of smart railway grids, where different actors such as PV system, ESS, public grid (electricity transport network), pursue distinct and sometimes conflicting objectives. These include energy cost minimization, renewable energy self-consumption, peak shaving, voltage stability, and compliance with operational constraints imposed by the train timetable. Designing a unified supervision tool that can balance these heterogeneous objectives under uncertainty, in real time, forms the core scientific challenge of this research.

To structure the investigation, the following research questions are posed:

1. How can a unified energy supervision tool be designed to manage ESS with limited load observability and high uncertainty and variation of railway load?
2. What are the most suitable energy management and supervision methods that can achieve the objectives and the real time supervision under multiple objectives to be treated with different nature with limited means of action?
3. How does the integration of real-time supervision affect the operational efficiency, energy cost, and respect ESS constraints of a DC railway substation enhanced with PV and ESS?

This work contributes a novel real-time supervision framework that considers the day ahead planning in its decision making process. The real time supervision is developed to guarantee the treatment of the limitation of the day ahead developed EMS. The performance of the day ahead EMS is evaluated and compared with the developed complete real time supervision tool. In addition, a study on the improvement of the forecast of the TSS load is established to deal with the unique nature and pattern of TSS consumption, characterized with peak consumptions that occur for short durations.

All of the above are mainly concerned about the integration of PV and ESS in the $1^{st}$ architecture of RACCOR-D. Where the integration is done at the TSS level. A suitable real time supervision tool that achieves the objectives behind this architecture must be develop considering its proper characteristics. In addition to the first architecture, a $2^{nd}$ architecture of RACCOR-D is established as a perspective, where the PV and ESS are connected between two adjacent substations. A real time supervision tool must be developed in a way that treats the different objectives that arrive with this different architecture.

## 1.7 Conclusion

This chapter has provided a comprehensive overview of the current state, limitations, and transformation pathways of DC railway traction substations, with a particular focus on the challenges faced by legacy 1.5 kV DC systems in France.

In response, recent research and industrial initiatives RACCOR-D project have explored the integration of smart grid principles into railway systems through the deployment of photovoltaic (PV) generation and energy storage systems (ESS). These technologies, supported by advances in power electronics and converter architectures, offer promising solutions to enhance substation performance, increase energy autonomy, and reduce reliance on the public electricity grid. The potential shift toward Medium Voltage DC (MVDC) electrification represents a long-term vision that could overcome the structural limitations of low-voltage networks, enabling wider substation spacing and improved network efficiency.

The RACCORD project exemplifies this vision, positioning an actual DC TSS as a demonstrator site for integrating renewable energy and storage technologies into railway operations. Looking forward, RACCOR-D opens the possibility of replacing conventional substations altogether, with ESS and PV operating autonomously at mid-sections of the line in a decentralized smart grid configuration.

However, these transformations introduce new operational complexities. The presence of multiple actors with differing objectives (PV, ESS, railway load, railway network, public electricity transmission network) requires the development of advanced energy management and real-time supervision systems. These systems must be capable of handling uncertainties in both TSS load and PV production, under conditions where not all system states such as TSS load are directly observable. The energy management is what coordinates the smart grid elements such as ESS to extract the maximum benefits behind the smart grid transformation of DC railway network.

This chapter has set the stage for the main research question of this thesis: how can we design an intelligent, energy supervision framework specifically adapted to smart railway substations in the context of RACCOR-D project. One capable of optimizing energy flows despite uncertainty, limited controllability, and multiple objectives. The next chapters build upon this foundation, first by examining energy flow dynamics and forecasting methods in detail, using the forecast to develop a day ahead energy supervision, and then by moving toward real-time supervision strategies that complete the day ahead. The thesis investigates two possible architectures for RACCOR-D and a developed supervision method for each architecture.

# Chapter 2. Methodology of energy management and supervision for different architectures of RACCOR-D

## 2.1 Introduction

This chapter provides a comprehensive benchmark and literature review of existing methods for energy supervision and management within smart grids, with a particular focus on railway systems. By examining current strategies and technologies, this review aims to build a solid foundation of knowledge and offers a critical analysis of their principles, capabilities, and limitations. This methodological overview supports the rationale behind the approaches developed in RACCOR-D project to address the challenges outlined in Chapter 1. Through this analysis, we aim to identify the most suitable techniques and justify the integration of a hybrid solution combining day-ahead energy management with real-time supervision.

In addition to the methodological benchmark, this chapter presents the different architectures of the RACCOR-D system, where photovoltaic (PV) and energy storage system (ESS) are integrated either directly at the traction substation or at the middle of the distance between two substations at the level of a parallel post called PMP (poste de mise en parallèle). Each integration strategy is tailored to specific operational objectives and technical constraints. The developed models representing these architectures are introduced and explained in detail. For each architecture, a dedicated MATLAB/Simulink model was developed to reproduce the operation of the railway traction substation. These models simulate the system's dynamic performance and supply the real-time measurements required by the supervision tool during simulation.

## 2.2 Problematic of energy management in a railway smart grid

The implementation of Energy Management Systems (EMS) in railway smart grids is a complex task that involves coordinating controllable assets such as energy storage systems (ESS) and photovoltaic (PV) generation while dealing with the strong variability and limited controllability of traction loads. Unlike tertiary or industrial power systems, where the load profile changes gradually and can be relatively well forecasted, the demand profile of a traction substation (TSS) is characterized by sudden peaks, strong variability, and the absence of real-time observability of train-induced consumption. These characteristics make the accurate scheduling and operation of ESS particularly challenging.

Although EMS developed for day-ahead planning based on forecasts as mentioned in Chapter 1 ensures an initial schedule for ESS operation, prediction errors in PV production or TSS load can significantly deviate the proposed ESS schedule away from the optimal schedule. The mismatch between predicted and actual operating conditions may result in constraint violations, such as subscribed power overruns, inefficient ESS cycling, or missed opportunities for PV self-consumption.

For this reason, real-time supervision must be an integral part of the global energy management framework. Real-time supervision provides the necessary corrections needed to manage uncertainties, adapts continuously to deviations from forecasted profiles, and remains robust under the unpredictable dynamics of railway operation. This supervision layer plays a key role in maintaining a balance between technical and economic objectives, such as minimizing energy costs, improving the use of photovoltaic generation, and ensuring grid constraint satisfaction, while keeping the system reliable in the presence of uncontrollable and non-observable traction loads in real time.

In this context, the central challenge is not only to design efficient scheduling tools but also to identify appropriate supervision strategies that can operate with limited measurements, adapt to rapid variations of TSS load, and remain computationally feasible for real-time deployment in railway smart grids, providing decision in seconds time interval.

In summary, the complexity of this supervision strategy raises multiple scientific and technical challenges, leading to the following research questions:

- How can energy management strategies in railway smart grids be adapted to handle the high variability and difficult to predict traction load?
- What forms of real-time supervision are most suitable for improving the robustness of ESS and PV operation under forecast errors and absence of real time measurement of the TSS load?
- To what extent do deviations between predicted and actual PV production or TSS consumption impact the effectiveness of energy management, and how can supervision strategies mitigate these effects?
- How can supervision methods balance economic objectives (minimizing subscribed power penalties and energy costs) with technical requirements (maintaining voltage levels, storage constraints) in dynamic railway environments?

The benchmark of energy management and supervision methods is a key into the development of the energy management strategy. The essential evaluation of the methods permits to structure the energy supervision tool to be compatible with nature of DC railway networks, using proper methods of energy management and for energy supervision.

## 2.3 Benchmark of energy management and supervision methods for railway smart grids

Having detailed the architectures under consideration, this section now reviews the existing methods found in the literature for energy management and supervision in smart railway grids integrating renewable generation and energy storage systems. The benchmark focuses on how energy management systems are designed and implemented across different contexts, highlighting their underlying optimization techniques, levels of complexity, and adaptability to uncertainties. The review also distinguishes between long-term energy scheduling (typically performed via optimization methods) and short-term supervision (including heuristic or AI-based corrections).

The discussion begins with the optimization methods most frequently employed in the design of EMS, including both linear and nonlinear approaches. These methods are evaluated in terms of their accuracy, computational efficiency, and suitability for addressing railway-specific constraints. Subsequently, the analysis shifts to other classes techniques that could be adaptive strategies to the energy management of railway smart grid, such as Multi-Agent Systems (MAS), Artificial Neural Networks (ANN), and rule-based methods. Each category is examined with respect to its performance, level of required information, and capacity to respond to system uncertainties and real-time operational variations.

Fig. 2.1 illustrates the main families of methods that have been explored in the literature for EMS applications. These approaches can be broadly categorized into rule-based methods, optimization-based methods, and AI-based methods, with hybrid strategies often emerging at the intersections of these families. Rule-based approaches, whether deterministic or fuzzy, remain widely used for their simplicity and fast implementation, although they often lack adaptability under uncertain or dynamic conditions. Optimization methods, ranging from classical mathematical programming to advanced model predictive control (MPC), provide systematic ways to generate long-term schedules and ensure constraint satisfaction, but their performance is strongly dependent on the accuracy of forecasts and the computational resources available. AI-based methods, such as machine learning (ML), deep learning (including Convolutional Neural Networks CNN, Recurrent Neural Networks RNN and Long Short-Term Memory LSTM), and multi-agent systems (MAS), introduce flexibility and data-driven intelligence, making them particularly suitable for handling variability and partial observability.

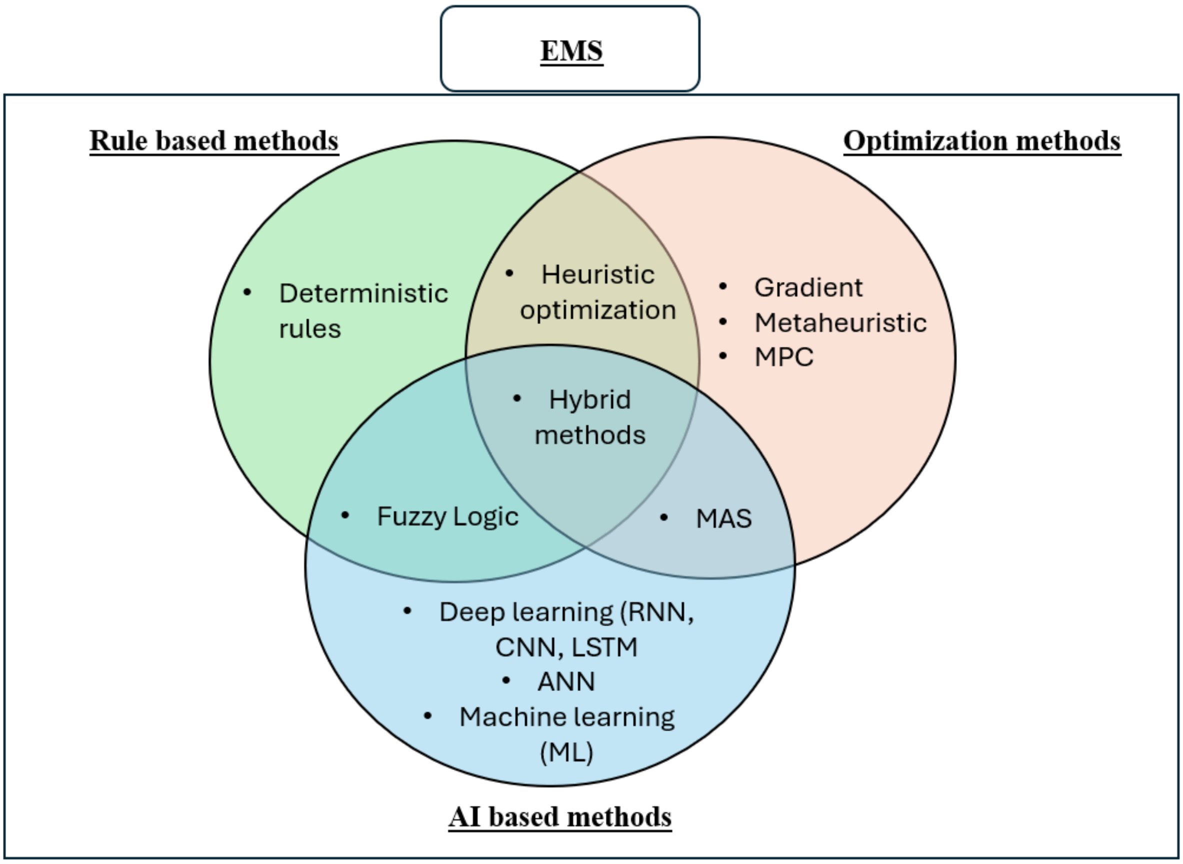


*Fig. 2.1 Families of methods for energy management and supervision in smart grids.*

In practice, many recent contributions highlight the increasing importance of hybrid frameworks, which combine the strengths of these families to overcome their individual limitations. For example, AI-based forecasting tools are often integrated with optimization algorithms to enhance scheduling accuracy, while fuzzy or rule-based supervision can be employed in real time to correct deviations from planned trajectories. The following sections examine these methods in more detail, focusing on how each class has been applied in railway smart grids, and setting the ground for a critical evaluation later in the chapter.

### 2.3.1 Optimization-based energy management systems

Optimization techniques applied to energy management systems can be broadly classified based on the linearity of the model and the availability of gradients. Fig. 2.2 classifies the optimization methods between linear and nonlinear, while listing the common solvers used in each method separating between gradient based solvers and non-gradient solvers [16] .

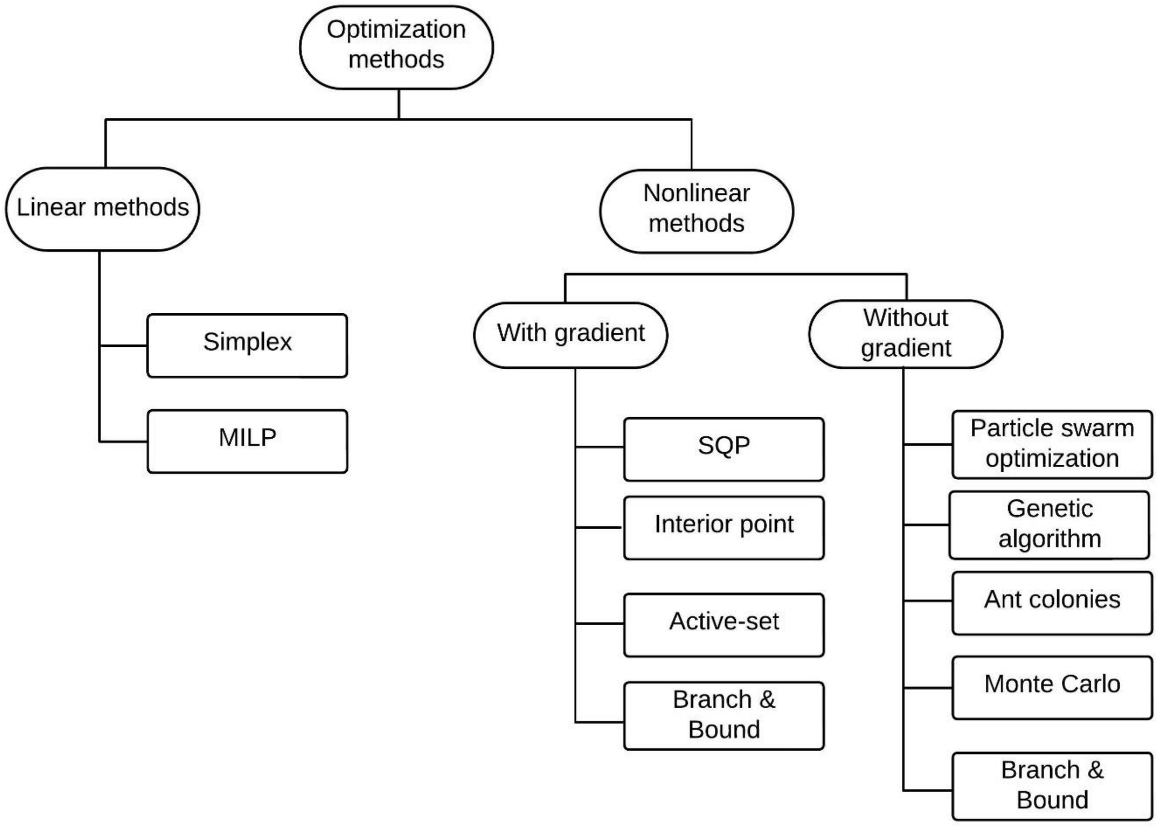


*Fig. 2.2 Classification of optimization methods*

Linear programming (LP) methods, such as the Simplex algorithm, are effective when both the objective function and the constraints are linear. However, purely linear models often lack the capacity to capture nonlinear aspects of real-world EMS problems (for example, battery cycling limits, nonlinear penalty costs, or renewable generation uncertainty) [76] . In practice, many energy systems exhibit such nonlinearities in their technical constraints and cost functions, which linear programs cannot represent without simplifications or approximations.

The mixed integer linear programming (MILP) is an effective method for handling linear problems with a mix of continuous and discrete variables. For instance, developed MILP-based strategies that schedule ESS operations and the purchased power from the grid in railway stations, aiming to minimize grid energy consumption and enhance the use of PV and regenerative braking energy (RBE) [66] [67] . MILP framework allows the integration of continuous and binary variables, which makes it suitable for problems that simultaneously determine system sizing decisions (such as ESS capacity) and control actions (such as power dispatch schedules). As a result, MILP can efficiently compute the optimal solution while handling both types of variables within the same optimization problem [77] .

By contrast, nonlinear optimization methods are better suited for EMS applications with complex system dynamics or nonlinear cost terms. Gradient-based algorithms such as Sequential Quadratic Programming (SQP), interior-point, and active-set methods are particularly effective when the optimization variables and constraints vary continuously and the cost function changes smoothly, allowing the use of gradients to guide the search for the optimal solution [78] .

SQP in particular has proven well-suited for day-ahead EMS applications (smart grid optimization), effectively handling nonlinear constraints such as battery state-of-charge evolution and cycling limits [79] . However, its main limitation lies in the computational burden when dealing with high-dimensional problems involving multiple energy storage systems with diverse behaviours resulting in a large number of decision variables and constraints. In such cases, MILP formulations are often preferred not because they outperform SQP in capturing nonlinear dynamics, but because they approximate and linearize these nonlinearities to achieve faster computation and tractable problem sizes [80] .

In hybrid railway networks that combine PV, wind, and energy storage, a nonlinear optimization can schedule the power exchanged among the grid, renewables, and storage to lower operating costs of the railway network [81] . By reducing the problem size by aggregating time periods and using a scenario tree to represent RES uncertainties, a specific solver is then adapted to the optimization problem. These measures ensured tractability of the large-scale nonlinear programming (NLP), which involved hundreds of thousands of variables and constraints, and allowed the solver to converge to an optimal solution [81] .

On the other hand, non-gradient (heuristic or metaheuristic) methods – such as Particle Swarm Optimization, Genetic Algorithms (GA), Ant Colony Optimization – are often employed for highly complex or non-differentiable EMS problems with many discrete decisions or multiple local minima [82] . These techniques can explore a wide solution space and are useful when derivative information such as the mathematical gradients of the objective or constraint functions is unavailable or difficult to compute. However, their convergence is typically slower, and they offer no guarantee of finding a globally optimal or even feasible solution under strict constraints, in contrast to mathematical programming methods [83] . These limitations make purely heuristic approaches less attractive for critical infrastructure like railway grids, where reliability and optimality of the solution are paramount [84] .

Optimization methods are used for long term or medium-term energy management, where the power profiles are already known or at least predicted. The randomness of renewable energy production due to weather fluctuations and the high dynamics of railway traction load pattern causes a difficulty in the application of optimization algorithm to work with the appropriate production and consumption power profiles. Real time fluctuation will cause problems such as power imbalance, curtailment of RES production, and sub-optimal operation due to the lack of real time correction.

To overcome this problem, these models consider uncertainties in PV production and electricity prices through scenario generation and reduction techniques [85] . In this approach, a large number of possible future conditions (scenarios) are first generated using probabilistic models of weather forecasts and price variations. Then, similar scenarios are grouped and reduced to a smaller representative set, allowing the optimization problem to remain computationally tractable while still capturing the main sources of uncertainty. Similarly, a MILP-based energy management model for a smart railway station using a stochastic approach, explicitly integrating PV generation and regenerative braking energy with ESS operation [86] . This contribution introduced comprehensive PV/RBE integration via scenario-based uncertainty modelling, but it relies on scenario generation and lacks real-time correction, limiting its adaptability to sudden changes in operating conditions.

### 2.3.2 Multi-timescale control

The impact of optimization methods on the energy management of electric networks with multiple sources and storage systems is highlighted by their ability to determine the optimal operation of controllable grid elements. EMS based on optimization have proven effective in achieving economic gains and reducing energy costs. However, unexpected variations in renewable energy production and the high dynamics of the TSS load consumption in real time can cause actual operations to deviate from optimal schedules.

To maintain optimality, the predicted production and consumption profiles used as inputs to the optimization must match real-time values. In the context of railway systems, this is difficult to guarantee due to the variability of renewable generation and the rigid nature of train traction loads, which, unlike in other energy systems, cannot be shifted or curtailed in response to control actions. To address this challenge, multi-time scale control strategies have been proposed, which distinguish between day-ahead scheduling and intra-day corrections. For instance, authors in [87] introduce a two-stage framework combining day-ahead planning and intra-day rolling optimization to adapt energy and reserve dispatch based on updated renewable forecasts.

This concept is implemented through rolling optimization, where newly available forecast data are used to adjust the ESS schedule derived from day-ahead optimization. Two main approaches can be distinguished. The first relies on a fixed rolling interval, in which the ESS dispatch is periodically corrected (every 15–30 minutes) over a short prediction horizon using the same optimization model with refreshed inputs. This enhances responsiveness to forecast changes compared to static scheduling but remains limited by its fixed and non-adaptive update interval, which does not adjust dynamically to sudden variations.

Alternatively, Model Predictive Control (MPC) frameworks provide a more adaptive solution by continuously re-optimizing over a shifting prediction horizon. This flexibility makes MPC more responsive to fast fluctuations in PV generation and train loads. However, its deployment is limited by computational burden and the need for reliable, real-time measurements. These aspects are discussed and demonstrated in [88] , who apply MPC for the multi-time scale dispatch of a traction system with hybrid storage, and [89] , who implement a two-level control strategy where a low-level controller corrects deviations from a high-level MILP-based plan. The challenge of designing optimal references for local controllers in real time, while satisfying nonlinear and discrete constraints, is also addressed in [90] using a mixed-integer MPC formulation.

To summarize the core principles of MPC-based intra-day control:

- The MPC runs in shorter intervals, collect updated measurements, formulate a short-horizon optimization problem.
- Minimize the deviation from the day ahead plan
- ESS constraints respected after the intraday adjustments
- Maintain the minimization of the real time operational cost

While both rolling optimization and MPC improve adaptability to real-time conditions, their deployment in railway systems must balance computational complexity, forecast availability, and real-time performance. In this context, alternative methods such as rule-based or fuzzy supervision may be more suitable for ultra-fast adjustments due to their low computational requirements and independence from updated forecasts.

### 2.3.3 Multi agent systems (MAS)

Multi-Agent Systems (MAS) have emerged as a promising approach to energy management in smart grids thanks to their flexibility and adaptability. Unlike traditional centralized optimization-based EMS, MAS architectures distribute decision-making among autonomous agents, allowing the system to coordinate diverse objectives while adapting to uncertainties [91] This makes MAS particularly suitable for environments with high variability or decentralized ownership, such as community microgrids where different energy actors may pursue competing preferences.

A MAS is composed of autonomous entities, called agents, which can be physical or virtual [92] [93] . Each agent perceives and interprets its environment, communicates with others, and takes actions that influence the system [93] .

Fig. 2.3 Generic agent–environment interaction (left) and its application to a railway smart grid through a MAS-based EMS (right). Fig. 2.3 illustrates the fundamental concept of agent behaviour and its application to railway smart grids. On the left, the generic agent–environment interaction is shown: each agent perceives the state of its environment, processes the information, and decides on actions that influence the environment in return. On the right, this principle is applied to the context of a railway smart grid. Different subsystems such as the ESS, PV, public grid, and auxiliary load are represented as autonomous agents interacting with the railway load agent (train consumption) under the coordination of a multi-agent EMS. Through continuous interaction, they negotiate and collaborate under the coordination of a multi-agent EMS [94] . In this way, local objectives such as SOC management, PV utilization, or grid constraint compliance can be coordinated at the system level to achieve global energy management goals.

MAS are particularly effective in distributed energy systems with multiple controllable components, such as ESS, flexible loads, or generators, where each agent manages its own local objective while coordinating with others to achieve a global optimum [95] [96] . As demonstrated in [97] , hierarchical MAS architectures extend this concept by enabling flexible energy dispatch, real-time responsiveness, and system-level optimization under communication constraints and dynamic operating conditions.

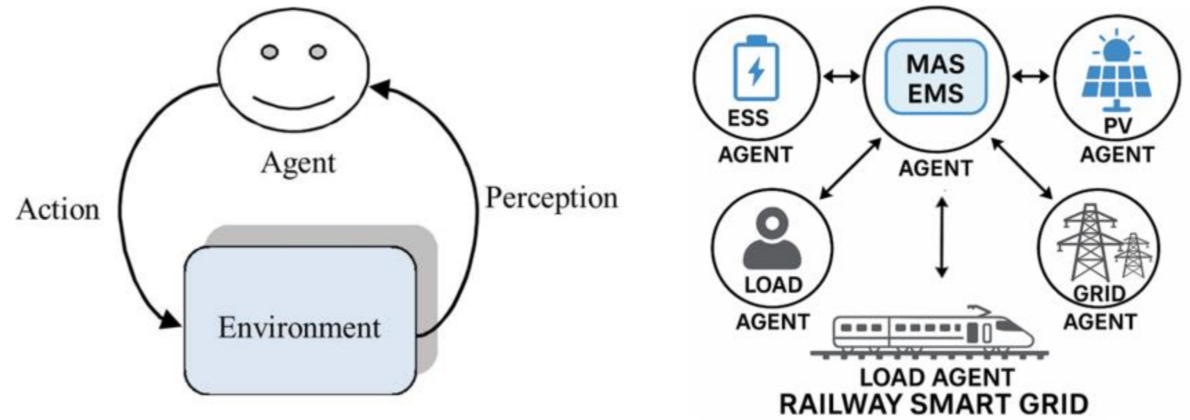


*Fig. 2.3 Generic agent–environment interaction (left) and its application to a railway smart grid through a MAS-based EMS (right).*

While MAS offer strong potential for distributed energy management, their direct application to the railway sector faces important constraints. Railway traction loads are highly dynamic, stochastic, and strictly schedule-driven, which limits the effectiveness of agent-based demand shifting or flexible load management. Furthermore, the communication infrastructure needed to support distributed agent coordination is often difficult to justify in such a centralized and safety-critical environment.

In practice, each agent in a MAS can embed its own decision-making algorithm, which may range from simple heuristic rules to advanced optimization solvers such as MILP, nonlinear programming, or metaheuristics. This structure allows agents to autonomously optimize their local objectives while maintaining coordination with others through negotiation or communication protocols. As such, MAS can be regarded as a decentralized AI approach, where distributed intelligence and embedded optimization combine to achieve system-wide objectives in a flexible and adaptive manner.

Despite these constraints, MAS can still be valuable in specific railway contexts notably in the control of auxiliary loads connected to the railway network and flexible in terms of control like EV charging stations [98] , as well as for the management of station-based ESS or PV systems. MAS can also be used in hybrid architectures that combine centralized optimization with local agent-based adjustments. In such hybrid frameworks, MAS can therefore complement centralized EMS by providing local autonomy and fast real-time adjustments, enhancing the system's adaptability to dynamic operating conditions [99] .

In the specific case of the RACCOR-D architecture, the applicability of MAS is strongly limited. The main constraints can be summarized as follows:

- Limited controllable assets: the only element available for supervision is the ESS.
- Lack of flexibility in traction loads: train circulation follows fixed schedules, and their power demand cannot be reduced or shifted.
- Absence of real-time measurement: without continuous monitoring of electrical parameters especially the train consumption, agent-based decision-making becomes ineffective.
- Communication overhead: implementing a distributed MAS framework requires extensive communication infrastructure, which is difficult to justify in such a centralized and safety-critical environment.

### 2.3.4 Rule based EMS

Another strand of research investigates rule-based and event-driven control strategies for microgrids. These systems are simpler and faster but typically suboptimal and inflexible in handling competing objectives or uncertainty [100] Supervisory control strategies that combine PV, battery, and other distributed sources have also been explored in railway DC microgrids with energy recovery systems relying on a rule-based EMS [59] . Showing potential for railway smart grid environments in terms of computational burden and fast reaction to fluctuations. Besides, the implementation simplicity of rule-based methods, it doesn't require extensive data forecasting, scenario generation like optimization-based methods, or complicated communication like MAS methods.

However, the developed rules cannot guarantee optimal performance like optimization-based methods. Also, rule-based methods can be inflexible handling high dynamics and operating conditions change, the rules are typically static and may struggle with complex decision-making.

To address these shortcomings, fuzzy logic-based supervisors have gained attention as an effective real-time control approach. Unlike optimization methods, fuzzy systems allow reasoning under uncertainty and imprecision, which is essential in railway substations where real-time measurements of load or PV are often incomplete or noisy. Fuzzy systems can handle multiple objectives such as maintaining SOC limits, ensuring voltage stability, and maximizing self-consumption through heuristic rules embedded in the inference system [101] .

Fuzzy logic models are constructed with a set of rules in their inference engine, however the defuzzification method is considered an intelligent mathematical computation that the trade-off between multiple objectives. In the defuzzification stage the aggregation of rule is done while mathematically estimating the weight of each rule of the inference. The development of fuzzy logic systems depends on expert knowledge of system as shown in Fig. 2.4.

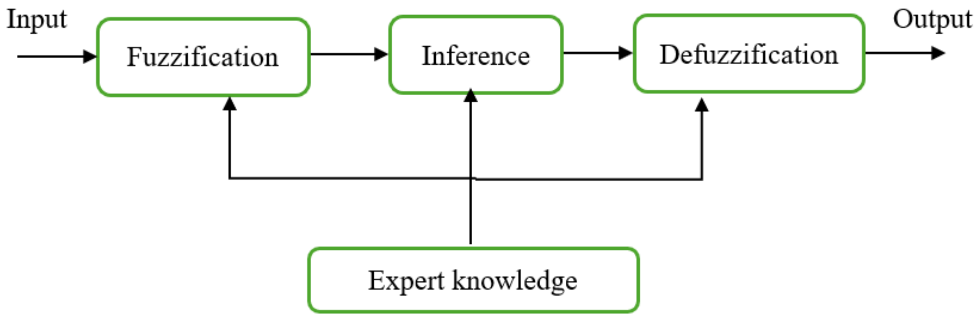


*Fig. 2.4 Fuzzy logic method principle*

### 2.3.5 AI-based methods

Artificial Intelligence (AI) techniques are increasingly applied in energy management systems for their capacity to learn from data, capture nonlinear behaviours, and adapt to uncertain operating conditions. Within this broad field, machine learning (ML) methods such as support vector machines, decision trees, and clustering algorithms have been widely explored for tasks like load forecasting, anomaly detection, and stability assessment in smart grids [102] . More recently, deep learning (DL) architectures, including recurrent neural networks (RNNs), long short-term memory (LSTM), and convolutional neural networks (CNNs), have demonstrated superior performance in handling complex time-dependent patterns in energy data, making them suitable for PV production prediction, demand forecasting, and real-time fault detection [103] [104] . Reinforcement learning (RL) has also been integrated into EMS frameworks to provide adaptive decision-making under uncertainty, particularly for dynamic pricing and demand-side management [102] .

Among these families, Artificial Neural Networks (ANNs) remain the most widely employed, forming the foundation of both ML and DL approaches [105] . ANNs are especially valuable in smart grid applications due to their ability to approximate nonlinear functions and capture complex dynamic behaviours [106] . Their "black-box" nature allows them to model input–output relationships without requiring explicit physical formulations, making them well-suited for environments where system dynamics are poorly understood or highly variable, such as those involving PV generation and battery storage [107] .

The main advantages of ANN-based methods are their ability to handle nonlinearity and adapt to high-frequency variations [102] , a property highly relevant in DC railway substations where load profiles are subject to abrupt, high-magnitude fluctuations. Over time, ANN models can learn from historical data and improve predictive accuracy, supporting robust and informed EMS decisions. However, their practical deployment in railway applications faces several challenges:

- High computational complexity, particularly for deep learning models

- Significant requirements for data collection, preprocessing, and synchronization with train timetables
- Limited explainability and trust in safety-critical environments

Real-world railway environments often suffer from limited data availability, fragmented measurements, or low temporal resolution, all of which reduce the effectiveness of ANN training and generalization. Furthermore, the black-box nature of neural networks poses challenges for explainability and trust, which are critical in safety-sensitive sectors like rail transport [108] .

For these reasons, ANNs are most effectively used in railway EMS as support tools for forecasting or estimation rather than for full supervisory control [105] . When coupled with optimization-based EMS, AI-driven forecasts can significantly enhance awareness, provide reliable input profiles, and improve the robustness of decision-making [109] . Hybrid frameworks, combining ANN forecasts with deterministic scheduling, thus represent a pragmatic compromise, leveraging the predictive strength of data-driven models while maintaining interpretability and operational stability. It is also worth noting that previously discussed methods, namely fuzzy logic and Multi-Agent Systems (MAS), are classified under the AI-based category. Fuzzy logic belongs to the family of soft computing approaches, where linguistic rules and membership functions provide human-like reasoning in uncertain environments, while MAS represent a branch of distributed artificial intelligence, enabling autonomous agents to coordinate decisions and adapt to dynamic operating conditions.

Artificial intelligence methods, and in particular ANN-based models, can be highly beneficial in preparing reliable input data for optimization-based EMS. Their forecasting capability and accuracy in predicting both load demand and PV production provide a solid input profile for the optimization algorithm. In turn, this allows the optimizer to compute more accurate and cost-effective schedules, regardless of the application, whether ESS scheduling, PV curtailment, or resource allocation. In this way, AI-driven forecasting strengthens the overall performance of optimization-based strategies, reinforcing the rationale for hybrid EMS architectures that combine data-driven prediction with deterministic scheduling.

### 2.3.6 Summary of the existing methods

In the context of the RACCOR-D project and within the energy management work of the railway smart grid, the real time supervision is a concept that must be applied. The objectives behind this real time supervision are related to the economic profits and the guarantee of the constraints respect for the different elements of the railway smart grid.

Where fast fluctuations in load and PV production must be addressed without high computational overhead, fuzzy logic supervision offers a superior alternative. It enables robust and interpretable real-time decisions based on partial state information such as DC bus voltage deviation and ESS state of charge.

Compared to predictive optimization, fuzzy logic provides lightweight control and better adaptability in uncertain environments, which aligns perfectly with the requirements of railway smart grid applications.

Overall, existing methods provide strong optimization frameworks for energy management in railway smart grids, notably through MILP and MPC-based strategies. However, they exhibit limitations in handling real-time uncertainties and dynamic changes in operational conditions. In RACCOR-D project, two-stage energy management strategy is distinguished: a day-ahead scheduling phase based on forecasted profiles and a real-time supervision phase capable of correcting deviations from the forecast, ensuring a more resilient, economical, and technically robust operation of the railway smart grid. The detailed methodology of the real-time supervision system is presented in the following sections.

The EMS approaches reviewed in the benchmark are summarized in Table 2.1, which highlights the scope, strengths, and limitations of each method. Linear Programming (LP), Mixed-Integer Linear Programming (MILP), and Nonlinear Programming (NLP) are widely used for day-ahead ESS scheduling due to their ability to generate economically optimal solutions under technical constraints. These methods are suitable for medium- or long-term planning where accurate forecasts are available. Rolling MPC strategies enhance these day-ahead solutions by providing a predictive window for intra-day corrections, improving robustness in dynamic environments. However, they rely on frequent forecast updates, demand high computational resources, and may be difficult to deploy in real-time settings such as traction power systems.

*Table 2.1 Summary table of the literature methods*

| Approach | Scope | Strengths | Limitations |
|---|---|---|---|
| **LP** | Day-ahead EMS | Fast, globally optimal for linear problems | Needs strong simplifications; misses nonlinear losses/aging/penalties |
| **MILP** | Day ahead EMS | Handles large optimization problems | Linearization reduces physical fidelity; size/solve time grow quickly |
| **NLP** | Day-ahead high-fidelity scheduling | Captures SOC dynamics, efficiencies, coupled constraints; high-quality plans | Heavier modelling/compute; needs well-scaled differentiable models |
| **Rolling MPC** | Intraday rolling correction (minutes) | Tracks reference; enforces future constraints; principled | Requires maintained predictive model and solver; compute can be tight |
| **Fuzzy Logic** | Real-time supervision (seconds) | Very fast, robust to noise/uncertainty. Explainable; easy safety rules No need for a complex physical/mathematical model | No formal optimality: performance depends on rule/membership design |
| **Rule based** | Real-time or intraday | Very fast, robust to noise/uncertainty; explainable; easy safety rules | Brittle under variability; weak multi-objective trade-offs |
| **MAS** | Various scales | Decentralized, scalable; handles heterogeneity | Limited impact when traction demand isn't deferrable; comms/safety overhead |
| **ANN** | Forecasting/estimation support | Learns nonlinear patterns; boosts awareness | Data/compute heavy; black box; not ideal for primary supervision alone |

In contrast, real-time supervision requires low-latency, low-complexity solutions that can operate with partial state information and in the presence of uncertainty. Rule-based methods offer a fast and simple framework for this, but they often fail to generalize in complex, multi-objective scenarios. Fuzzy logic bridges this gap by combining the simplicity and interpretability of rule-based systems with the ability to perform multi-criteria decision-making through expert-defined inference rules. It is particularly well-suited for applications where mathematical modelling is intractable, such as in smart railway grids characterized by a diversity of loads, renewable generation, and energy storage systems. ANN, while powerful for forecasting and pattern recognition, are generally unsuitable as primary real-time supervisors due to their data requirements, lack of interpretability, and computational cost. Similarly, Multi-Agent Systems (MAS) offer flexibility and scalability in distributed control, but their application in railway contexts is limited by the non-controllability of core loads such as trains. Based on these considerations, fuzzy logic has been selected as the real-time supervision approach for the RACCOR-D project, offering an optimal balance between responsiveness, simplicity, and decision-making intelligence.

## 2.4 Global supervision strategy

Building on the benchmark analysis and the rationale developed in the previous section, this part presents the global supervision strategy adopted in the RACCOR-D project. As established, no single EMS method alone satisfies both the long-term optimality and the real-time adaptability required by a smart railway grid. Therefore, a hybrid architecture is implemented, wherein a day-ahead optimization module computes an optimal schedule for ESS operation based on forecasted load and PV production profiles. This day-ahead schedule is then provided as an input to a fuzzy logic-based real-time supervisor, which also receives real-time measurements (PV power, TSS load, DC bus voltage, and ESS State of Charge - SOC). Rather than directly correcting the day-ahead plan, the fuzzy supervisor evaluates current operating conditions and generates a new reference setpoint that ensures constraint satisfaction and improved responsiveness to dynamic events. The following section details the structure, data flow, and interaction between these two supervision layers.

This architecture is illustrated in Fig. 2.5. Forecasting algorithms process historical TSS consumption and train timetable data to predict the TSS consumption profile. The PV forecast is done externally by Steadysun, a specialized solar-forecasting service. Steadysun uses a combination of numerical weather prediction models, satellite imagery, sky imaging, and AI/ML techniques to estimate the photovoltaic generation for future periods (from minutes up to several days ahead) for a given installation [110] .

These PV forecasts are calibrated to the specific characteristics of the PV system (panel type, orientation, location, local weather patterns) and delivered via an API [111] . These predicted consumption and PV profiles, together with tariff structures and TSS system parameters (TSS subscribed power limits, ESS capacity), are fed into the day-ahead optimization block to compute the ESS schedule. In real time, the fuzzy logic supervisor takes this day ahead planned schedule plus the current system state (actual PV output, actual power drawn from the grid, actual ESS SOC and others) and issues adaptive supervision signals to handle disturbances that couldn’t be foreseen in the scheduling stage.

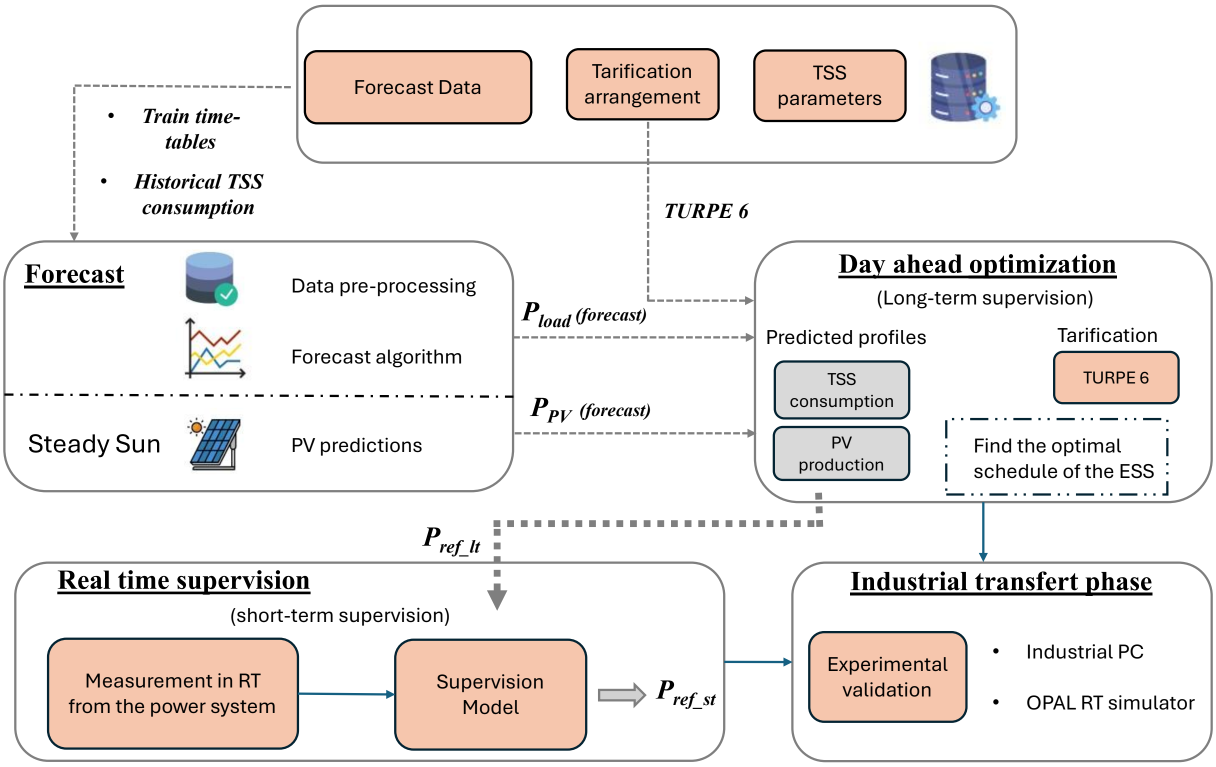


*Fig. 2.5 Global supervision architecture combining day-ahead optimization and real-time supervision*

## 2.5 Methodology of the development of the day-ahead EMS

The day ahead level in the proposed supervision strategy requires a forecast of the power consumption of the substation and the PV power production. With the help of AI based methods for forecast and data prediction, it is possible to prepare a trained model capable of providing acceptable predicted profile of TSS consumption to be used in the day ahead optimization process.

### 2.5.1 Forecast method for TSS power consumption

In the literature, ANN and machine learning (ML) techniques have shown improvement and high capabilities in the prediction and forecast domain. These approaches have been widely applied to residential, commercial, and industrial loads, where consumption patterns are relatively regular and well-instrumented. However, their application to railway traction substations (TSS) remains limited due to the specific nature of railway loads, characterized by strong intermittency, sharp power peaks, and partial observability.

Beyond the choice of the forecasting algorithm itself, the development of a reliable forecasting framework requires a structured methodology that transforms raw historical measurements into accurate and usable predictions of TSS power consumption. In this work, the forecasting process is organized into three main phases: data preprocessing, model selection and training, and model validation and testing.

The choice of an appropriate forecasting method largely depends on the availability and quality of historical data, as well as the intrinsic characteristics of the load to be predicted. In the case of traction substations, consumption is strongly influenced by train circulation, which introduces irregular patterns and sharp variations. For this reason, the data preprocessing step must first align the available train timetable information with the corresponding power consumption records, ensuring proper synchronization between events and their electrical impact. This alignment allows the forecasting model to capture correlations between train operations and substation demand more accurately.

The training phase of the model depends directly on the volume and resolution of the available dataset. Larger datasets with high temporal granularity generally enable the use of more complex models, such as recurrent neural networks (LSTM for example), which are particularly effective in capturing sequential dependencies. Conversely, when data is scarce or of limited resolution, simpler models or hybrid approaches may be more reliable to avoid overfitting. However, when data are limited or of low resolution, simpler or hybrid models may be preferable to reduce the risk of overfitting. Although overfitting can be mitigated in LSTM networks through regularization techniques such as dropout, early stopping, or cross-validation, achieving robust generalization still largely depends on the quality and diversity of the training data.

Finally, validation and testing ensure that the chosen model generalizes well to unseen operating conditions. This step is particularly important in railway applications, where uncertainties in train delays, traffic density, or weather-related PV fluctuations can lead to significant deviations from nominal patterns. Robust evaluation through appropriate error metrics, such as the Mean Absolute Error (MAE), Root Mean Square Error (RMSE), and Mean Absolute Percentage Error (MAPE) are employed. These indicators quantify the deviation between predicted and actual load values, providing an essential measure of the model's accuracy and its ability to capture variations in real consumption patterns.

### 2.5.2 Optimisation problem formulation

The choice of an optimisation method and its solver depend on the nature of the objective function and the constraints involved. In general, the development of an optimisation problem follows these main steps:

- Definition of the inputs and outputs of the optimisation process.
- Mathematical formulation of the objective function to be optimised.
- Mathematical modelling of the constraints (both equality and inequality).
- Definition of the boundaries or permissible ranges for the decision variables.

The problem can be expressed mathematically as:

$$\text{Find } x \text{ such that: } \begin{cases} min f(x) \\ x \in X, \\ g(x) \leq 0, \\ h(x) = 0 \end{cases}$$

Here, $f(x)$ is the objective function to be minimised (or maximised, depending on the problem), $g(x) \leq 0$ represents the inequality constraints, and $h(x) = 0$ represents the equality constraints. The set $X$ defines the feasible space, which may include variable bounds and other structural limits.

The goal of the optimisation process is to determine the values of the decision variables $x$ that minimise the objective function $f(x)$ while satisfying all the constraints. Inequality constraints define permissible limits for variables, while equality constraints enforce exact values or relationships that must be maintained throughout the process.

In this work, the optimisation problem involves nonlinear relationships between variables in both the objective function and the constraints. Therefore, nonlinear programming (NLP) techniques will be employed, as they are well suited to handling complex, real-world energy optimisation problems where linear approximations are insufficient.

The optimization method is furtherly explained in Chapter 3, where the optimization problem formulation and the necessary constraints are explained for the 1st architecture of RACCOR-D project.

## 2.6 Methodology of the development of the real time supervision

The development of supervision strategies for complex systems, particularly those involving uncertainties or ill-defined dynamics, often benefits from methodologies that can encapsulate expert knowledge and manage imprecise information. Fuzzy logic provides a robust framework for this purpose. This section outlines the conceptual development of a fuzzy logic model, emphasizing the role of understanding system functionalities (often representable through functional and operational graphs), the definition of membership functions, and the resulting operational structure of the fuzzy supervisor [112] .

### 2.6.1 System specification

This step in the development of the methodology came to respond to the following points:

- The objectives of the real time supervision and its convenient operation time horizon
- The constraints of the railway smart grid elements such as the ESS and the DC bus, that the supervisor must respect
- The available means of control provided by the system, for which the supervisor defines the corresponding reference to meet the defined objectives.

The definition of the system specification must justify the use of the proposed supervision method. Explaining the difference between the objectives set for the day ahead EMS level and the objectives set for the real time supervision. With the necessary means of actions that achieve these objectives in real time considering the constraints imposed by every actor in the railway smart grid.

### 2.6.2 Supervisor structure

In a DC railway smart grid, the interaction of multiple interconnected components increases the complexity of operating and coordinating the railway power network. These actors include the electricity transmission network (transmission system operator: TSO), PV system, energy storage system, and the TSS railway loads (trains and station auxiliaries). First, not all DC substations are equipped with necessary devices for measurement and data acquisition to transfer information in real time to the supervision tool. The main challenge is to make use of available measurement to compensate for the absence of real-time data on TSS load consumption while achieving the objectives of the real time supervision. At the same time, it is not feasible to control all the actors within the smart grid, so the supervision must concentrate on the elements that can be effectively managed.

Defining the supervisor structure clarifies the necessary inputs and outputs required for its operation. Each input variable corresponds to a specific objective or constraint of the system such as minimizing grid power overrun, maximizing the use of the PV production, or respecting storage limits, while the output correspond to the main means of action, represented in RACCOR-D by the energy storage system. The ESS thus acts as the single controllable element through which several objectives are pursued simultaneously. This situation naturally introduces trade-offs between competing goals, highlighting the relevance of using fuzzy logic to manage compromises in real-time operation.

### 2.6.3 Graphical representation of supervisor functionality based on the system knowledge

The functional graph provides a clear way to describe the different functional configurations and transitions that the supervised system can exhibit. It shows how the system evolves from one mode to another depending on the conditions of the state variables. The supervisor then interprets these transitions to decide which functional mode should be activated according to the current situation [112] ]. Fig. 2.6 illustrates an example of a transition between two modes, moving from N1 to N2 based on the condition of the corresponding state variable.

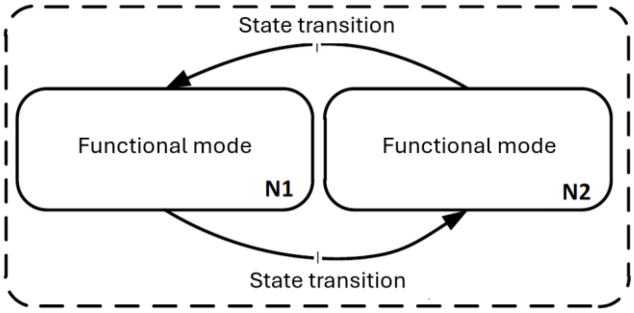


*Fig. 2.6 Graphical representation of functional modes of the FL supervisor [120]*

### 2.6.4 Development of membership functions

The translation of system input and output variables into fuzzy variables is an essential step in the development of the supervisor. This stage, called fuzzification (Fig. 2.4), may be preceded by a normalization phase of the variables. This step covers the defining of the membership functions associated with the input and output variables of the fuzzy supervisor.

Unlike a boolean set, which is defined by a characteristic function that takes only the discrete values 0 or 1, a fuzzy set is characterized by a membership function that can take any value within the interval $[0,1]$ or $[-1,1]$ [101] [100] . In the example shown in Fig. 2.7 the set of possible state-of-charge (SOC) values of the storage system defines the operating range of the variable SOC. The terms “Small”, “Medium”, “Big” then represent the linguistic values of this variable. For instance, when the state of charge is 30%, it belongs to the fuzzy set “Small” with a degree of membership equal to 0.5; simultaneously, it may also belong to the fuzzy set “Medium” with the same degree of 0.5.

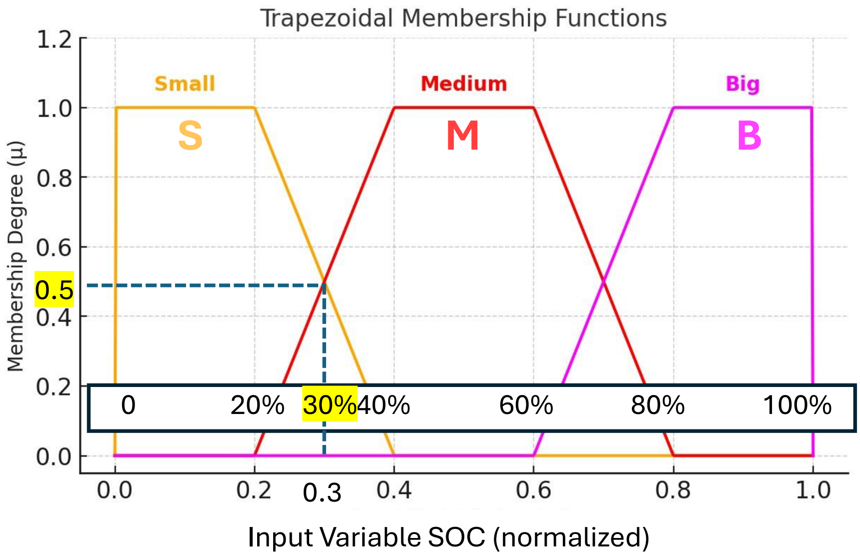


*Fig. 2.7 Example of trapezoidal membership function for an input variable*

This definition illustrates how fuzzy sets allow the representation of gradual transitions between states, rather than abrupt thresholds, thereby improving the supervisor's ability to manage uncertainties and nonlinearities in the system's operation. The corresponding membership functions are generally of trapezoidal or triangular form, chosen to balance simplicity of implementation and adequacy of representation for the studied physical variables.

The following terms are used to define the main stages of a fuzzy reasoning process:

- Fuzzification: this operation converts real-valued input variables into fuzzy quantities. It determines the degree of membership of a given value within a fuzzy set.
- Inference: the logical operation by which a proposition is accepted based on its relationship with other propositions assumed to be true. This mechanism first employs logical operators' *min* to determine the activation level of each rule and its appropriate conclusion. Then, by aggregating the conclusions of all activated rules (using, for example, the *max* operator), the fuzzy output set of the output variable is obtained.
- Defuzzification: this final stage converts the fuzzy output set resulting from the inference process into a real, measurable quantity. Among the most commonly used methods for this purpose is the centroid (centre of gravity) method.

These stages may be preceded by a preprocessing phase for shaping the input variables, referred to as normalization, and followed by a phase for rescaling the output quantities to their real physical values, known as denormalization. Through the normalization process, the physical quantities lose their units and are expressed in per unit (p.u.) form. Additional information on the construction of a supervisor based on fuzzy logic can be found in [113] . The number of fuzzy rules depends on the number of membership functions defined for the variables. To simplify the definition of these rules, the symmetry of the fuzzy sets can be taken into account.

### 2.6.5 Graphical representation of the operation modes

To naturally extract fuzzy rules for energy supervision, the next step consists in translating the functional graphs into a graphical representation of fuzzy operating modes. This representation outlines the different operational modes of the system. The transitions between these modes are defined based on the membership functions of the input variables, previously established, and on the actions corresponding to each operational mode, represented by the fuzzy sets of the output variables. Fig. *2.8* illustrates the principle of the operational graph for the example of the storage system's state of charge. In this case, the output variable corresponds to the short-term reference power of the storage system $P_{ref\_st}$. The fuzzy sets associated with this variable are, for instance, Z (Zero), NM (Negative Medium, trapezoidal shape) and PM (Positive Medium), when SOC is S (Small, trapezoidal shape), M (Medium, trapezoidal shape) and B (Big, trapezoidal shape) respectively.

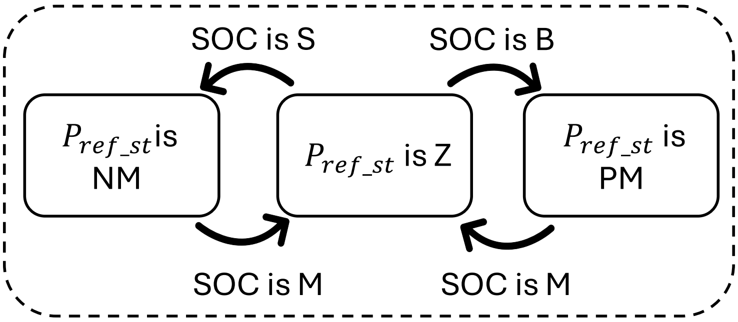


*Fig. 2.8 Graphical representation of the operation modes of the FL supervisor*

### 2.6.6 Fuzzy rules

Once the input and output variables have been defined with their respective linguistic terms and membership functions, the operational graphs (which depict the desired supervisor logic, including different states/modes and the conditions for transitioning between them) are used to formulate the fuzzy rule base. Each distinct state or mode within the operational graph, along with the specific input conditions that lead to it or define it, translates directly into one or more IF-THEN fuzzy rules.

For instance, if an operational graph shows that when "Input A is Low" and "Input B is Medium," the system should enter "Operational Mode X" which corresponds to "Output Z being High," this directly forms a fuzzy rule:

IF (Input A IS Low) AND (Input B IS Medium) THEN (Output Z is High). The transitions between modes in the operational graph, triggered by changes in input variable states, also guide the formulation of rules that ensure the supervisor behaves according to the intended expert logic. This systematic translation ensures that the collective behaviour of the fuzzy rules mirrors the decision-making pathways detailed in the operational graphs.

### 2.6.7 Definition of performance indicators

An essential step to evaluate the performance of the proposed supervision scheme is to define key performance indicators that validates the achievement of the objectives of the real time supervision. These indicators can relate to the different elements of the smart grid (SNCF network, ESS, PV…). The indicators help in analysing the performance of the supervision strategy and tell whether the problematic and the objectives are achieved or no.

These indicators are also designed to enable a comparative analysis between different supervision cases:

- Long term supervision (LT), representing day-ahead supervision only with the developed EMS,
- Real time or short-term supervision (LT+ST), corresponding to the developed real time supervision tool combining the day ahead EMS with the real time fuzzy logic supervisor.

- The reference case without RACCOR-D, reflecting conventional operation of the traction substation.

## 2.7 Architectures and modelling methodology

To address the energy efficiency and operational limitations of conventional railway electrification, RACCOR-D project explores two distinct architectures for integrating PV and ESS into the smart railway grid. This section presents a study of these two architectures in terms of concept and modelling method, each designed to meet specific technical and economic objectives under different integration scenarios. The developed model for each architecture serves as a test bench simulation for the developed energy supervision tool with its two levels of supervision.

In the first architecture, the ESS and PV are connected directly to the TSS, forming a DC bus that links the local load, renewable generation, storage, and the upstream grid. This configuration leverages historical consumption data to optimize energy costs and minimize peak demand penalties.

The 2$^{nd}$ architecture positions the ESS and PV at a mid-point, referred to as the parallel post (PMP) between two substations. The PV and ESS feed the railway load directly through the catenary. For this reason, the modelling of the catenary is essential unlike in architecture 1 where the model represents a traditional microgrid considering the total consumption of the TSS load. In architecture 2 the load is represented with train circulation among the tracks that connect two consecutive TSS. And the voltage drop of the catenary can be caused by the variation of the catenary resistance that depends on the train position at the track. Dynamic modelling of train circulation is developed to simulate system behaviour and to highlight the voltage drop. Two consecutive TSS are considered with assumption that the modelled train movement causes the TSS power consumption without relying on the historical data.

The first architecture is considered as test bench for testing the proposed supervision method; it can lead to accurate results due to the availability of historical data and the capabilities of predict the profile of the TSS power consumption through forecast. The developed supervision tool can be integrated with its two levels, profiting from the day ahead and real time supervision that extract the maximum objectives of the integration of PV and ESS.

Similarly, the 2$^{nd}$ architecture and its equivalent model allow the test of a specific supervision strategy that considers only the real time level. The day-ahead EMS cannot be applied for the 2$^{nd}$ architecture because it is not possible to predict power consumption for two consecutive TSS with a dynamic trains circulation without making big assumptions.

### 2.7.1 Architecture 1: ESS and PV integrated at the substation

The first architecture corresponds to a configuration that can be realistically implemented in the context of the RACCOR-D project. By directly integrating renewable energy sources (RES) and ESS at the traction substation via a DC bus, this setup provides a practical framework for testing the proposed energy management and supervision methods under conditions close to real operation. The following subsection details its concept and objectives.

#### 2.7.1.1 Architecture 1 concept and objectives

The architecture depicted in Fig. 2.9 corresponds to the first architecture of RACCOR-D system, which integrates PV system and ESS directly at the level of DC railway traction substation via DC bus. This configuration interfaces with the electricity transmission network RTE (operating at 63 kV) through traction unit (transformer + diode rectifier), delivering energy to a DC bus at 1.5 kV that supplies the catenary powering electric trains. Similar to the concept of a traditional DC microgrid, where the power is exchanged through a DC bus, and all smart grid elements are directly connected to this bus.

In this setup, the PV system injects power $P_{PV}$ locally into the DC bus, reducing dependence on the upstream grid $P_{grid}$ while the ESS can either discharge energy $P_{sto}$ to support the traction load or absorb excess energy when available, such as during low-load periods or peak PV production.

The TSS power consumption is the denoted $P_{load}$ and it represents the overall consumption of the substation. For simplicity, the only actor that contributes to $P_{load}$ is the power drawn by the circulating trains. Historical data are available for the TSS consumption which permit to use actual power consumption as the necessary load profile to be used for testing the energy management and supervision method.

The economic benefits of this architecture are quantified through the energetic bill of the TSS, which depends on the power drawn from the grid $P_{grid}$.

In the first architecture, the interaction with adjacent substation is neglected. Train circulation dynamics are not explicitly modelled; instead, the load $P_{load}$ is taken directly from historical consumption data.

The integration of ESS in this architecture serves multiple operational and economic objectives. First, it enables peak shaving, thereby reducing overruns of the subscribed power, a critical metric in railway operations subject to high penalties when demand exceeds contractual limits. Second, the ESS allows the system to strategically shift energy usage, effectively reducing time-of-use electricity costs by charging during low-tariff periods or from surplus PV and discharging during peak-tariff periods. Third, the combined operation of ESS and PV facilitates the maximization of local renewable energy consumption, reducing the carbon footprint of rail operations and enhancing energy autonomy. This configuration is particularly well-suited for smart grid-enabled railways, as it provides increased flexibility, grid relief, and improved economic efficiency without compromising service reliability.

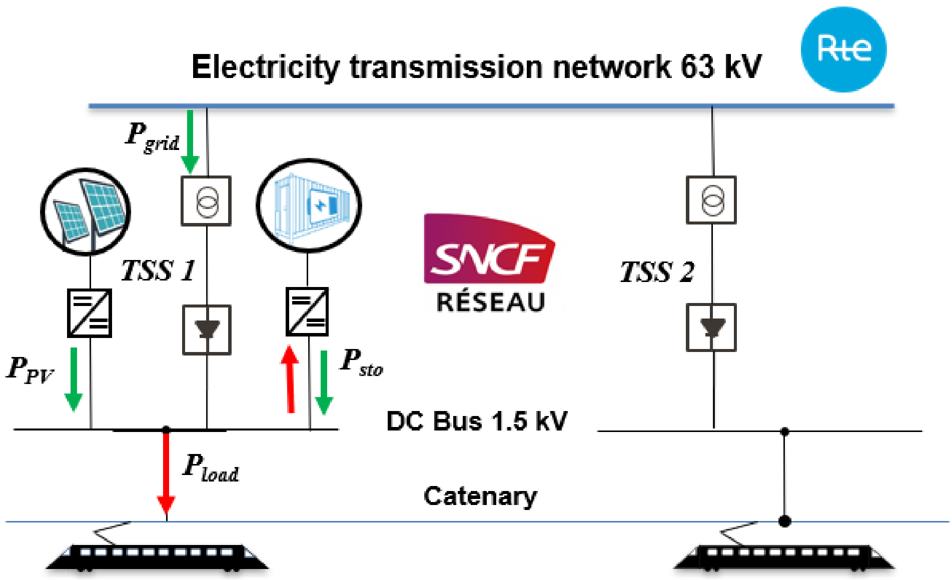


*Fig. 2.9 Architecture 1 for the integration of PV and ESS at TSS via DC bus*

In this study, a positive power value denotes an injection into the DC bus, while a negative value indicates power absorption. Accordingly, $P_{PV}$ and $P_{sto}$ are positive when the PV system or ESS deliver energy to the DC bus and negative when they consume it (for instance, during ESS charging). The grid power $P_{grid}$ is considered positive when energy is drawn from the upstream AC network and negative when energy is injected back into it. This convention is consistently applied throughout the equivalent circuit model and all subsequent formulations.

The objectives behind the real time supervision can be therefore summarized as follow:

- Ensure an ESS schedule in real time that responds to the economic objectives.
- Reduce the peak consumption that causes subscribed power overrun by soliciting the ESS in discharge for peak shaving.
- Maximize the use of PV production avoiding curtailment, by charging the ESS during excess of production periods.

#### 2.7.1.2 Equivalent electric model for architecture1

To evaluate the behaviour of Architecture 1 under different operating conditions and to test the proposed supervision strategies, an equivalent electrical model was developed in MATLAB/Simulink. This model provides a simplified but sufficiently accurate representation of the traction substation and its interactions with the PV system, ESS, and railway TSS load. The simplification focuses on assessing the supervisor's performance rather than the detailed modelling of converter interfaces between the ESS, PV systems, and the railway network. Accordingly, the ESS and PV are represented as direct current sources corresponding to their final output after power conversion.

The equivalent model of the 1st architecture of RACCOR-D is represented by voltage and current sources as shown in Fig. 2.10. The upstream traction substation is modelled as a DC voltage source $E_{TSS}$ in series with an equivalent resistance $R_{eq}$, which represents the voltage drop at the output of the diode rectifier when it is conducting current. For the real-time supervision, the railway load is represented by a controlled current source, denoted TSS Load, obtained from historical power consumption data. Similarly, the PV profile is modelled as a controlled current source $I_{PV}$, driven by forecast or real-time PV generation data. The ESS is controlled by a reference setpoint provided by the developed real-time supervision tool (Fig. 2.5). This setpoint is applied to a battery model whose output is represented as a controlled current source $I_{sto}$. Finally, the transformation from power to current is performed by dividing by the instantaneous DC bus voltage, which is measured in real time.

The economic objectives influenced by the reduction of the power drawn from the grid can be assessed through the necessary calculation for the energetic bill of the TSS relying on the power drawn from the grid $P_{grid}$. With the equivalent circuit model, $P_{grid}$ is calculated through simulation while the ESS schedule is optimized - using the developed supervision tool - with respect to the time of use costs along with the penalties paid for overrunning the substation subscribed power. Using the equivalent circuit model of the railway architecture, $P_{grid}$ is derived in simulation, impacted by the ESS schedule (obtained using the developed supervision tool) optimized with respect to time-of-use tariffs and penalties for subscribed power overruns.

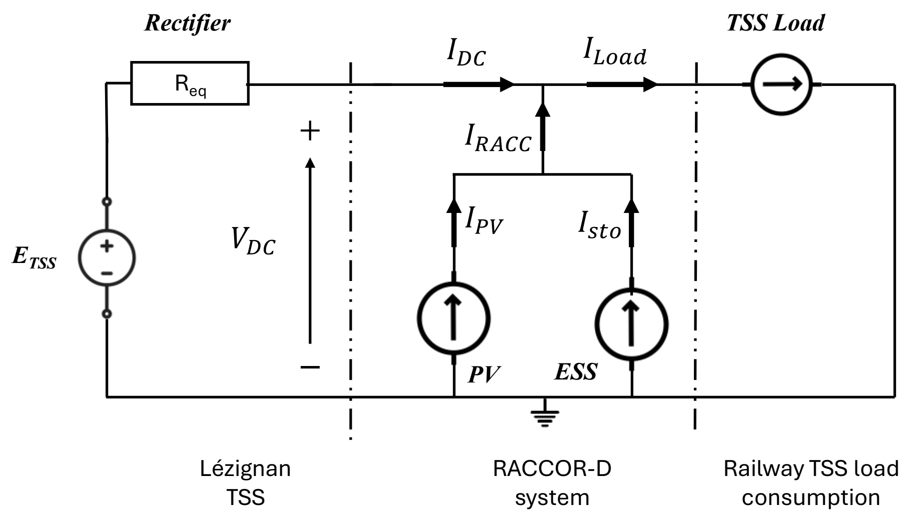


*Fig. 2.10 Electrical representation of equivalent circuit model of architecture 1*

The equivalent circuit can thus be formalized by the following relations. The power balance equation calculates the power drawn from the grid essential for economic objectives evaluation. At the DC bus, it is expressed as:

$$P_{grid}(t) = P_{load} - P_{PV} - P_{sto} + R_{eq} I_{dc}^2 \tag{2.1}$$

And the current at the output of the traction unit is:

$$I_{dc}(t) = I_{load} - I_{PV}(t) - I_{sto}(t) \tag{2.2}$$

Each element is modelled as a current source defined by:

$$I_x(t) = \frac{P_x(t)}{V_{dc}(t)} \quad , \; x \in \{load, PV, storage\} \tag{2.3}$$

$P_{load}$ and $P_{PV}$ are derived from dataset containing the values of PV power and TSS power consumption. $P_{sto}$ is the output power of the ESS model supervised by the real time supervision tool that provides necessary power reference setpoints $P_{ref\_st}$. Assuming a perfect control of the ESS without any losses and with perfect response to the reference setpoints.

### 2.7.2 Architecture 2: ESS and PV integrated at parallel post between two substations

The second architecture corresponds to a configuration where RES and ESS are integrated at the midpoint between two traction substations, at the level of a parallel post (PMP). This setup represents an alternative scenario for the RACCOR-D project, designed to address the issue of voltage drops that typically occur at mid-span in DC railway lines. By positioning the ESS and PV at the PMP, this architecture provides a framework for testing supervision methods aimed at regulating the catenary voltage within safe operational bounds, while respecting ESS technical constraints. The following subsection details its concept and objectives.

#### 2.7.2.1 Architecture 2 concept and objectives

Chapter 1 revealed the services of the ESS in railway networks. One of the services is to maintain the voltage level of the catenary. In DC electrification, the lowest catenary voltage occurs in the section located at midpoint between two substations. Such low voltage requires a higher current drawn from the substation to supply the circulating train needs. As a consequence of these high currents, the voltage drop increases significantly. Therefore, when the catenary voltage becomes too low, it is necessary to limit the train current, which in turn limits the train power and consequently reduces its speed.

At mid-point, the train is at the farthest point between the two substations that supply the track, so the catenary resistance depends on the train's position. The greater the distance, the higher the resistance. Drawing more current from the TSS therefore results in a larger voltage drop along the line, due to the increased III flowing through the line resistance RRR. This also increases the return current, known as stray current. While insulation techniques mitigate stray currents and rail potential issues, the catenary voltage drop remains critical. Previous studies in [52] [114] have shown that reducing voltage drop with the integration of RES and ESS between two TSS also contributes to lowering stray current and rail potential.

The circulating trains supplied by the catenary linking two consecutive substations might be forced to reduce their consumption by reducing their speed when the voltage is within critical low values. This can impact the train schedules causing delays and problems for railway companies.

The main objective in this architecture is to regulate catenary voltage level within safe operational bounds, while respecting ESS technical constraints.

In this configuration, illustrated in Fig. 2.11, the two traction substations TSS1 and TSS2 each supply the catenary through transformer–rectifier units delivering 1.5 kV DC. The trains draw power from the line, denoted $P_{train1}$ and $P_{train2}$, while the substations inject power $P_{TSS1}$ and $P_{TSS2}$ to meet the demand. At the midpoint between the substations, a PMP hosts the RACCOR-D integration of PV system ($P_{PV}$) and the storage system ($P_{sto}$). The PMP injects or absorbs active power into the catenary, denoted $P_{RACC}$, with the dual role of supplying trains and compensating for voltage drops along the line. The positioning of the ESS and PV at this location enables targeted support of the weakest point of the DC network, thereby improving the overall voltage profile and reducing the current drawn from the substations.

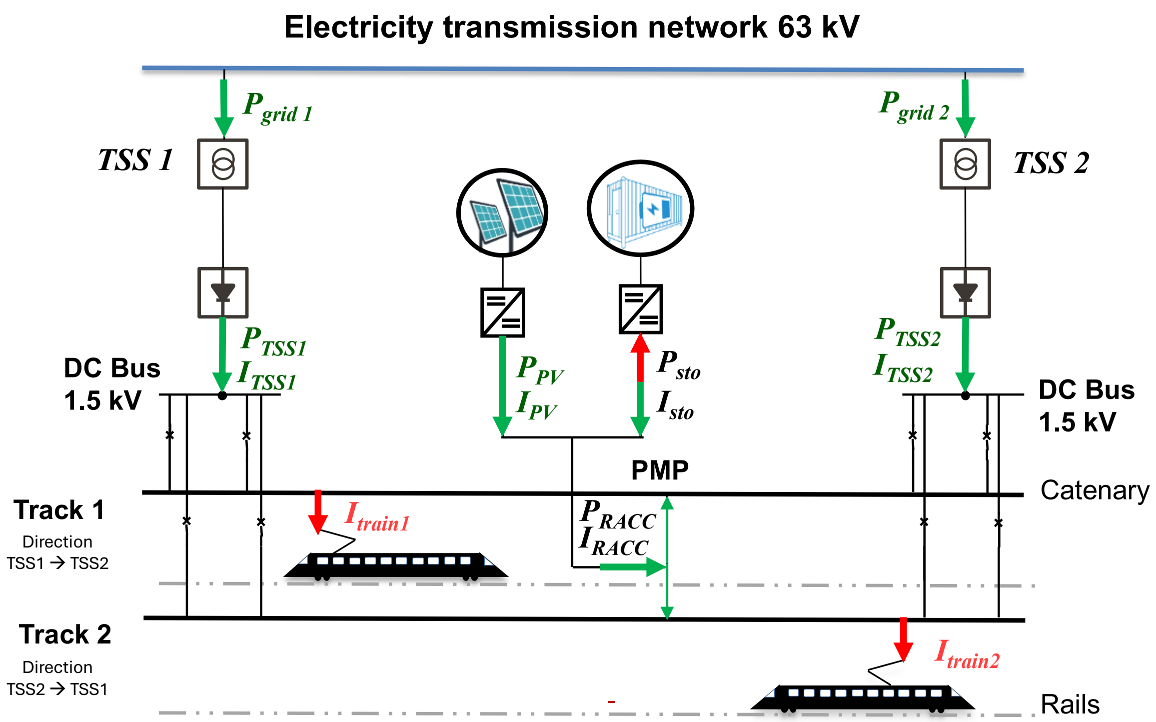


*Fig. 2.11 RACCORD architecture 2: ESS and PV connected at PMP between two TSS*

This architecture permits to test a developed supervision tool for the ESS. The ESS must be supervised in a way that treats different objectives from the ones specific for architecture 1. Mainly the catenary voltage drop that was not targeted in the first architecture.

The absence of power consumption of two substations with an accurate train timetable make it difficult to obtain the exact power consumption of two consecutive TSS resulted by specific train dynamics. Also, it is not possible to rely on historical power consumption of each TSS, since the overall consumption of each substation depends on its proper connected tracks.

Assumptions are therefore necessary in this architecture study:

- The speed can be considered constant along the track connecting the two substations
- The rated current of the circulating train is supposed to be known at a reference speed value
- Only considering the tracks that connect the two substations, assuming that when train leaves the track it stops drawing current from the nearest TSS

Because of these assumptions and the lack of accurate substation consumption data, it is not possible to evaluate the economic indicators of this architecture in the same manner as for Architecture 1. In this case, the load is dynamically modelled from train timetables rather than taken from measured TSS profiles, meaning that no precise correspondence can be established between the power drawn by TSS1 and TSS2 and the actual operation of specific trains on the connecting track. Consequently, the analysis of this architecture focuses primarily on the electrical behaviour of the system, particularly the maintaining of catenary voltage and reducing the voltage drop, rather than on direct economic assessment.

#### 2.7.2.2 Equivalent electrical model of architecture 2

To capture the operation of Architecture 2, the physical configuration described in the previous subsection is translated into an equivalent electrical circuit, shown in Fig. 2.12. The model represents TSS1 and TSS2 as ideal DC voltage sources $V_{DC_0}$ with equivalent resistance that models the voltage drop at the output of the diode rectifier $R_{eq}$, the PMP as the integration point of PV and ESS, and the catenary as two resistive portions whose values vary dynamically with train position. enabling the simulation of voltage profiles, losses, and the effect of midpoint injection on catenary support. The trains are modelled as controlled current sources. The train current is derived from a reference operating point assuming the knowledge of $P_{train}$ that is constant due to the constant speed.

$$I_{train}(t) = \frac{P_{train}}{v_{pant}} \tag{2.4}$$

Where $P_{train}$ is the train power consumption and $v_{pant}$ is the pantograph voltage of the train.

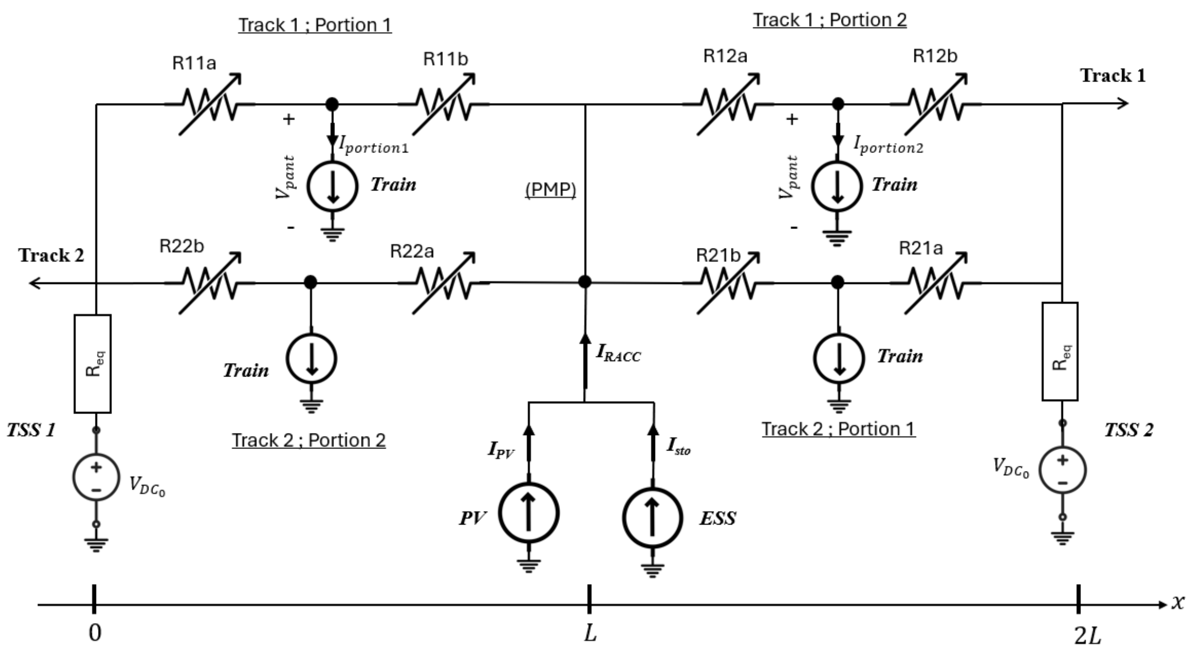


*Fig. 2.12 Electrical representation of equivalent circuit model of architecture 2*

The equivalent electrical circuit of Architecture 2, shown in Fig. 2.12, is designed to represent the midpoint integration of PV and ESS between two DC traction substations. It is composed of the following elements:

- Traction substations (TSS1 and TSS2): modelled as ideal DC voltage sources with equivalent resistance $R_{eq}$, each delivering 1.5 kV to the catenary. These supply the trains circulating on their respective sections of track.
- Midpoint systems (PMP): the PV installation and the ESS are represented as controlled current sources connected at the midpoint. They can inject or absorb power depending on PV production and ESS state of charge, thereby supporting the catenary voltage and reducing current drawn from the substations.
- Catenary and track resistance: the line between the two substations is divided into two portions: portion 1 from TSS1 to the midpoint (PMP), portion 2 from the midpoint to TSS2.
- Trains: represented as controlled current sources that activate when a train is present on the corresponding portion of the track. The current drawn is proportional to the train's speed and switches from portion 1 to portion 2 as the train moves across the midpoint.

Each portion of the track includes two symmetrical resistive branches per track: for track 1 for example $R_{11a}$, $R_{11b}$ for Portion 1 and $R_{12a}$, $R_{12b}$ for portion 2. These resistances represent the distributed electrical resistance of the catenary and vary dynamically with the train's kilometric position (KP).

The activation of the controlled current source for each train depends on its position along the track named $x$. While the effective resistive path from the supplying source (TSS1, TSS2, or the midpoint) changes dynamically with location. The track is modelled as 20 km in total, divided into two portions:

- In portion 1 ($x \in [0,10]$ km): the train draws power via a current source associated with Portion 1 $I_{por1}$.
- In portion 2 ($x \in [10,20]$ km): the first current source disactivates and the second activates, corresponding to the second portion of the track $I_{por2}$.

The catenary is represented by distributed resistances that vary with the train's KP. As a train moves along the line, the electrical distance between the train and the supplying source changes, modifying the effective resistance of the path through which current flows. This effect is critical in DC railways, where the midpoint between substations typically experiences the highest resistive voltage drops.

To capture this phenomenon, the catenary resistances are updated dynamically as a function of train position $x$ and the linear resistance $R_L$ ($R_{\Omega/km}$). While $L$ is the total distance between a TSS and the PMP.

For a train moving from TSS1 to PMP (track 1):

$$R_{11a}(x) = R_{\Omega/km} \cdot x \tag{2.5}$$

$$R_{11b}(x) = R_{\Omega/km} \cdot ( L - x ) \tag{2.6}$$

For a train moving from PMP to TSS2:

$$R_{12a}(x) = R_{\Omega/km} \cdot (x - L) \tag{2.7}$$

$$R_{12b}(x) = R_{\Omega/km} \cdot ( 2L - x ) \tag{2.8}$$

Where:

- $R_{\Omega/km}$ is the linear catenary resistance per segment,
- L = 10 km is the length of each portion,
- $x(t)$ is the train's position at time $t$.

This variable-resistance approach allows the model to reproduce the gradual increase of voltage drop as trains move away from the substations and approach the midpoint, reflecting real-world DC railway behaviour.

At this midpoint, the integrated PV system and ESS are represented as controlled current sources that can inject or absorb power depending on operating conditions. Their combined contribution is expressed as:

$$I_{RACC}(t) = I_{PV}(t) + I_{sto}(t) \tag{2.9}$$

The operation of the midpoint sources can follow different strategies, for example:

- injecting forecasted PV generation,
- charging or discharging the ESS based on its state of charge (SOC),
- or responding to local voltage deviations as a corrective action.

In this way, the PMP helps relieve TSS1 and TSS2, reduces current flow along the catenary, and maintain catenary voltage during high-demand periods.

While the substations supply currents given by:

$$I_{TSS1}(t) = f(R_{11a}, R_{11b}, I_{\text{portion1}}), \tag{2.10}$$
$$I_{TSS2}(t) = f(R_{12a}, R_{12b}, I_{\text{portion2}}). \tag{2.11}$$

With $I_{\text{portion1}}$ and $I_{\text{portion2}}$ representing the train currents when the train is circulating in portion 1 and portion 2 of the track, respectively (Fig. 2.12).

This modelling approach allows the PMP to supply part of the train demand, thereby reducing the burden on TSS1 and TSS2 and maintaining the catenary voltage, particularly during high-load conditions near the midpoint.

By combining the spatial dynamics of the catenary with the temporal dynamics of train movement, the equivalent circuit enables detailed simulations of voltage profiles, power flows, and load sharing. This provides a basis for evaluating how midpoint-located PV and ESS affect voltage stability, stray current mitigation, and the overall energy efficiency of DC railway grids.

For a real time supervision, the ESS is connected to a real time supervisor that send power reference setpoints. The PV controlled current source has actual measurement of PV generation,

## 2.8 Conclusion

This chapter provided a comprehensive benchmarking of the principal families of Energy Management and Supervision (EMS) methods applied to smart grids, with a particular focus on their applicability to DC railway traction systems. The comparative analysis encompassed optimization-based techniques (LP, MILP, NLP, and MPC/rolling optimization), rule-based and fuzzy logic strategies, artificial intelligence approaches (machine learning, artificial neural networks, and deep learning), and multi-agent systems. Each category was critically evaluated in terms of its dependence on forecast accuracy, computational complexity, interpretability, and capacity for real-time adaptation under unmeasurable and rapidly fluctuating traction loads.

The findings demonstrate that no single EMS approach can simultaneously guarantee long-horizon economic optimality and short-horizon robustness under uncertainty. This limitation motivates the development of hybrid EMS frameworks that integrate day-ahead optimization for strategic scheduling with real-time supervision capable of addressing the operational objectives of the railway network operator. The developed real-time supervisory tool is designed to enhance the fulfilment of these objectives ensuring economic gains during real-time operation, improving responsiveness to system dynamics, and providing the adaptability required for deployment within a real demonstrator environment.

In this context, the RACCOR-D project brings significant added value through the development of dynamic electrical models for two representative DC railway architectures, designed to emulate realistic operating conditions. The first architecture integrates photovoltaic generation and energy storage systems directly at the DC bus of the traction substation, while the second explores an inter-substation configuration enabling energy exchange between adjacent stations. Together, these models establish a comprehensive simulation environment that reproduces the dynamic behaviour of a DC railway network, thereby enabling in-depth investigation of how the proposed supervision tool operates within a smart railway grid and interacts with substation dynamics.

# Chapter 3. Day ahead supervision (EMS)

## 3.1 Introduction

The day ahead energy supervision strategy is based on the forecast of the TSS power consumption and PV production. The optimal ESS schedule for the upcoming day requires a solid forecast method that serves the final objective of the optimization. The forecast must provide a consumption profile close to reality and suitable for the objective of the optimization phase that will propose the optimal ESS schedule. However, the dynamic nature of the TSS load make it difficult for existing forecast algorithm to deal with it.

This chapter presents the complete day ahead EMS, explaining the developed forecast strategies and the optimization problem formulation. The available historical data are explained and two approach with different time step are compared. The first method relies on linear regression that finds the correlation between several training input parameters related to circulating trains dynamics. The 2$^{nd}$ method used is the time series forecast with Recurrent Neural Network (RNN) using Long Short Term Memory (LSTM) approach. This method only relies on the historical TSS electrical consumption without the need for more information about the circulating trains.

The optimization algorithm relies on the input data provided from the TSS forecast and the PV production forecast. In this context, having a proper forecast that prepares a realistic TSS load consumption profile for optimization is more suitable than relying solely on stochastic approaches or scenario generation, which often require extensive computational resources and may not capture the specific operational dynamics of railway substations. The impact of the forecast strategy on the optimization is evaluated with performance indicators that validate the choice of the forecast strategy. The 1$^{st}$ architecture of RACCOR-D is considered for the day ahead EMS. The ESS and the PV connected at the substation allows a formulation of the optimization problem that will be the core of the EMS.

This chapter is constructed as follow, first the available historical data is explained to give and idea on what it is possible to work with and in which architecture. Then the forecast approaches used to predict TSS power consumption. The results of the forecast are presented next with metric evaluation to assess the forecast methods. After the explanation of the results of the forecast, the optimization method is explained in detail completing the developed day-ahead EMS. The results of the optimization are presented with different case studies, comparing optimized solution or schedule with a baseline schedule of the ESS. Also, the result section covers the assessment and analysis of the impact of the forecast method on the optimization outcome. Finishing with a conclusion on the proposed methods developed in the sake of building the day ahead EMS.

## 3.2 Available historical data for TSS consumption forecast

### 3.2.1 Historical TSS power consumption

The TSS load consumption is developed with the help of the historical data that measures the power drawn from the grid. The historical data worked on is for the years of 2015, 2016, and 2017. This data is saved as average of 10 minutes.

For year 2017, the dataset consists of 52,416 entries, with power consumption measurements recorded at 10-minute intervals throughout 2017. The recorded power values range from 0 kW to 8370 kW, with an average consumption of 1298.77 kW. The big difference between the average power compared to the peak values put difficulties to the forecast models to capture accurately the power consumption peaks. Fig. 3.1, compared to the 10 minutes power consumption shown in Fig. 3.2, the average of one hour cannot precisely capture the dynamics of the power consumption peaks that occur for relatively short periods of time.

The outlier analysis of Fig. 3.2 identifies extreme peaks and dips in power consumption, which could be caused by unusual events such as failures, maintenance activities, or system overloads. Top 1% high outliers likely correspond to railway traffic surges or special events, while bottom 1% low outliers are possibly due to power shutdowns, maintenance operations, or anomalies.

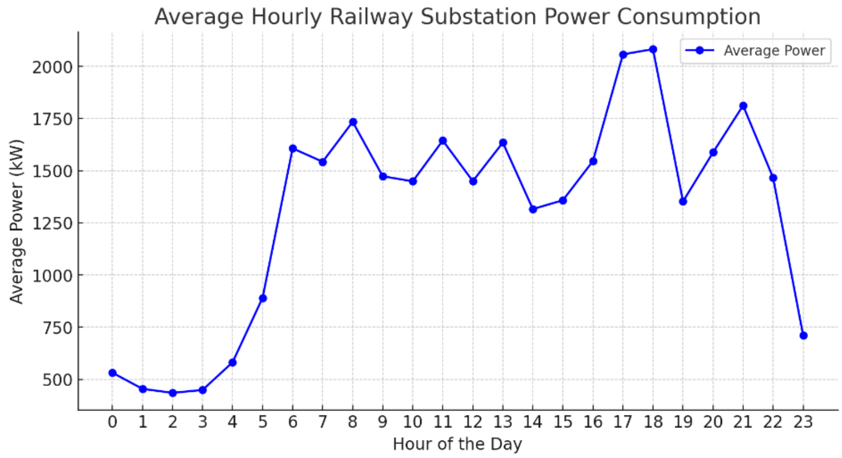


*Fig. 3.1 TSS power consumption with 1h average*

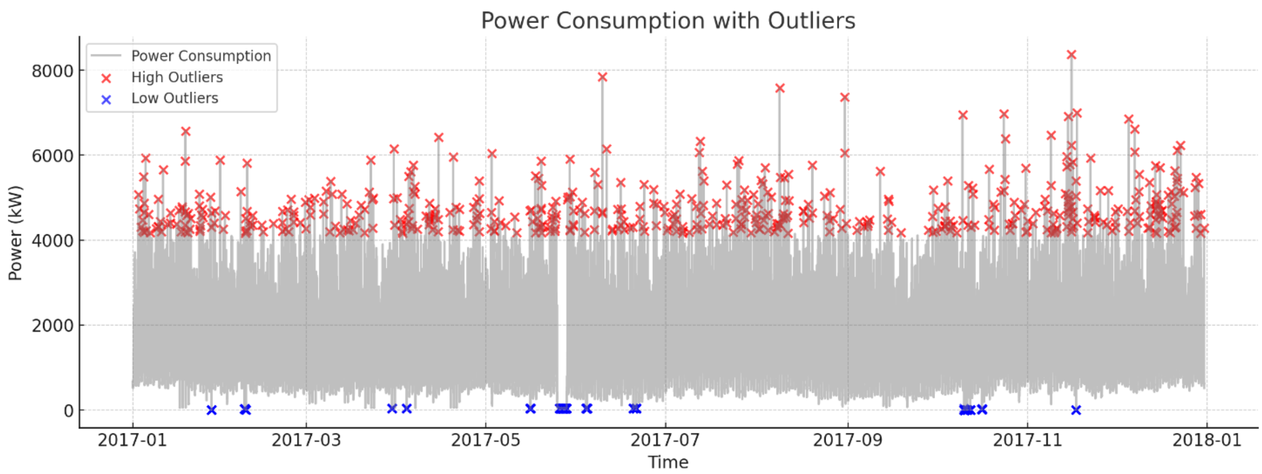


*Fig. 3.2 Historical TSS power consumption with outliers*

The outliers create challenges for forecast and prediction algorithms. They cause model instability, making it hard for deep learning models like LSTM to generalize patterns. Skewed predictions arise when high outliers (e.g., railway traffic surges) and low outliers (e.g., power shutdowns) distort training, leading to overfitting or underfitting. This results in a loss of forecasting accuracy, with models either underestimating or overestimating demand. Additionally, extreme values can mask real trends, making it harder to identify seasonal or daily consumption patterns essential for long-term forecasting.

The large gap between the average consumption (1298 kW) and the peak demand (8370 kW) highlights this variance, making it difficult for models to capture rare but critical peaks. Such underestimation can lead to power shortages, inefficient use of resources, and mistakes in capacity planning, while also making it harder to see the underlying daily or seasonal trends. In the end, because extreme events occur so rarely in the dataset, the models become less reliable, and their forecasting accuracy is reduced.

### 3.2.2 Provisional trains information

Available train timetables offer provisional circulating trains information. This information can describe train dynamics at the connected tracks of the TSS. The departure, arrival, or passage time of the trains at TSS1 and the neighbouring substations from both sides are sorted in raw data files in addition to the train types. So, it is possible to calculate the total travel duration performed by all trains in every specific hour of the day at the 4 tracks connected to the TSS. Also, it is possible to sort the train types whether it is for passengers or for cargo. Along with the status that describe trains behaviour at the considered TSS from departure, arrival, or passage.

The trains information used in this study comes from the historical database provided by SNCF, which contains the official theoretical timetables of the railway network. These timetables specify the planned departure and arrival times of trains, the type of service (passenger or freight), and the expected duration of travel on each track section. They represent an idealized schedule for railway operations, assuming punctual circulation under normal conditions. In practice, however, actual train movements may deviate from these theoretical timetables due to delays, operational constraints, or disturbances on the line. Consequently, the theoretical database reflects the planned railway operation but does not necessarily correspond to the real circulation observed at the TSS.

For this study, two months of timetable data were obtained from SNCF. An extraction algorithm was developed to transform the raw data into input variables suitable for forecasting. As illustrated in Fig. 3.3, the algorithm sorts the following criteria for each hour of the day:

- The accumulated travel time of the trains circulating on tracks 1,2,3,4 ‘total duration’.
- The number of trains passing the substation ‘P’.
- The number of arrivals (trains that performed a stop at the substation) ‘A’.
- The number of trains that performed a departure from the substation ‘D’.
- The types of the train’s ‘cargo’ or ‘passenger’.

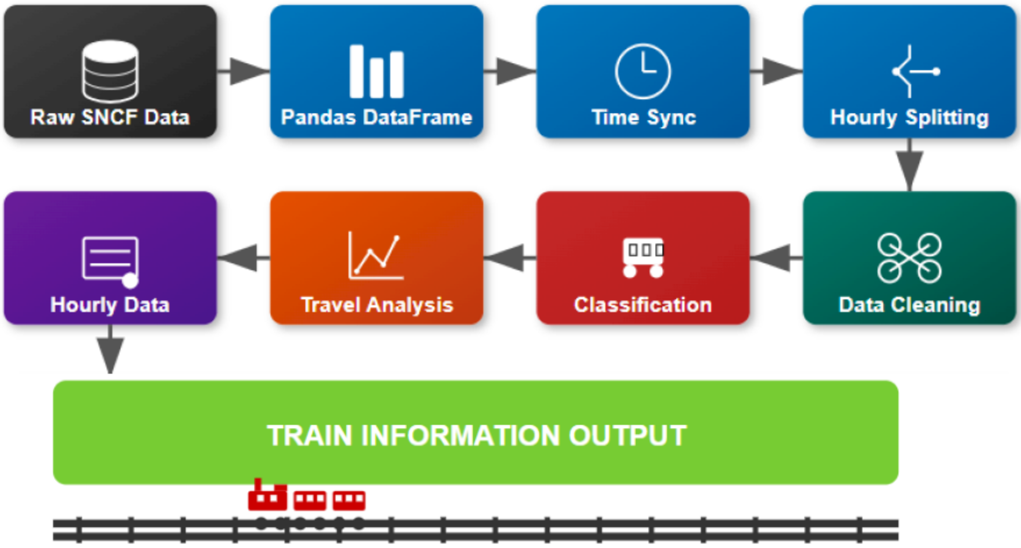


*Fig. 3.3 Data preprocessing from HOUAT extraction*

### 3.2.3 Correlation study between input and output of the forecast

Before developing forecasting models, it is essential to evaluate whether variables derived from train timetables are actually related to the substation's power consumption. For this reason, a correlation analysis was performed to measure the strength of the relationships between different train operation indicators and the TSS load.

The analysis shows that the total travel time of trains on all four tracks has the strongest correlation with substation power consumption, with a coefficient of 0.82 (Fig. 3.4 (a)). This means that longer cumulative travel durations generally coincide with higher TSS demand. Passenger-related variables also show strong relationships: the number of passenger trains correlates with a coefficient of 0.76, and the number of passages ("P") with 0.77. By contrast, departures ("D") and cargo trains exhibit weaker correlations of 0.65 and 0.61, respectively. This suggests that passenger circulation, being more frequent and regular, contributes more consistently to substation demand than freight operations, which are less predictable and less frequent. The other important correlations between inputs and output power are the number of passengers trains 'Passengers' and 'P' that represents the status of trains (passage). For the number of departures 'D' and the number of cargo trains have less correlation factor with the output with 0.65 and 0.61 respectively. This suggests that passenger circulation, being more frequent and regular, contributes more consistently to substation demand than freight operations. In addition, some cargo trains are not electrified, which introduces further complexity: since the dataset does not specify which freight trains are diesel-powered and which are electric, their contribution to TSS load cannot be precisely determined. This uncertainty reduces the apparent correlation of cargo variables with substation energy consumption.

As shown in Fig. 3.4 (b), applying the correlation analysis for 10 minutes step time data didn't show strong correlation between input parameters and output. With a sampling time of one hour, deviations in the train timetable have little impact: as long as trains circulate within the hour, the correspondence between timetable-based inputs and the hourly average power consumption remains strong. At a finer resolution of 10 minutes, however, even small delays (5–10 minutes) break this alignment, leading to poor correlations between input variables and measured TSS load.

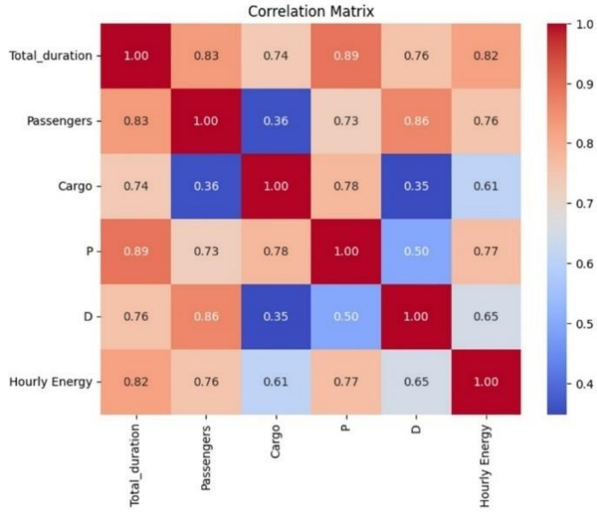


*(a) 1 hour time step*

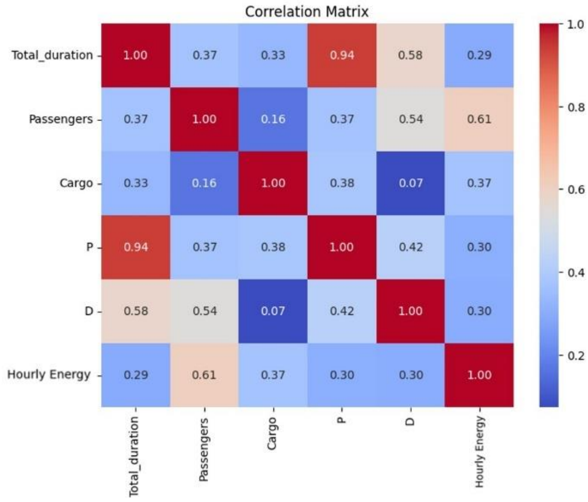


*(b) 10 minutes time step*

*Fig. 3.4 Correlation matrix*

To obtain reliable forecasts at such resolutions, data would need to be registered in real time and synchronized with the actual TSS consumption, which was not possible at the demonstration site. As a result, the available dataset was reduced and less representative, making high-resolution forecasting impractical.

Given these constraints, the forecasting step was carried out at an hourly resolution. Linear regression was selected because it offers a straightforward and interpretable framework for testing whether timetable-derived variables can explain variations in TSS power consumption. The limited size and resolution of the dataset make advanced machine learning or deep learning approaches unsuitable at this stage. Linear regression thus provides a practical first step to evaluate the predictive potential of train timetable and dynamic variables before moving toward more advanced models in subsequent sections.

## 3.3 Linear regression forecast model

Linear regression is a fundamental statistical and machine learning technique used to model the relationship between a dependent variable and one or more independent variables [72] . In the proposed forecast method, the linear regression provides a simple baseline approach to model the relationship between substation power consumption and input variables derived from train timetables of Equation (3.1).

$$y = \beta_0 + \beta_1 x_1 + \beta_2 x_2 + \cdots + \beta_n x_n + \epsilon \tag{3.1}$$

Where $y$ is the dependent variable and represent the TSS power consumption is expressed as a linear combination of predictors $x_n$ with coefficients $\beta_n$ representing their weights plus an error term $\epsilon$.

In this study, the predictors are derived from train timetable variables. Based on the correlation analysis, total travel duration showed the highest predictive power, while other inputs such as the number of cargo trains were weakly correlated. To avoid degrading performance, the regression model therefore relies mainly on the most relevant predictors. The dataset was divided into 80% for training and 20% for testing (Fig. 3.5), ensuring that the model was evaluated on data not used during training.

Fig. 3.5 illustrates the resulting forecast. Despite its simplicity, linear regression provides a useful benchmark for evaluating whether timetable-based variables can improve forecasting accuracy, especially given the limited and partly theoretical dataset available in this study.

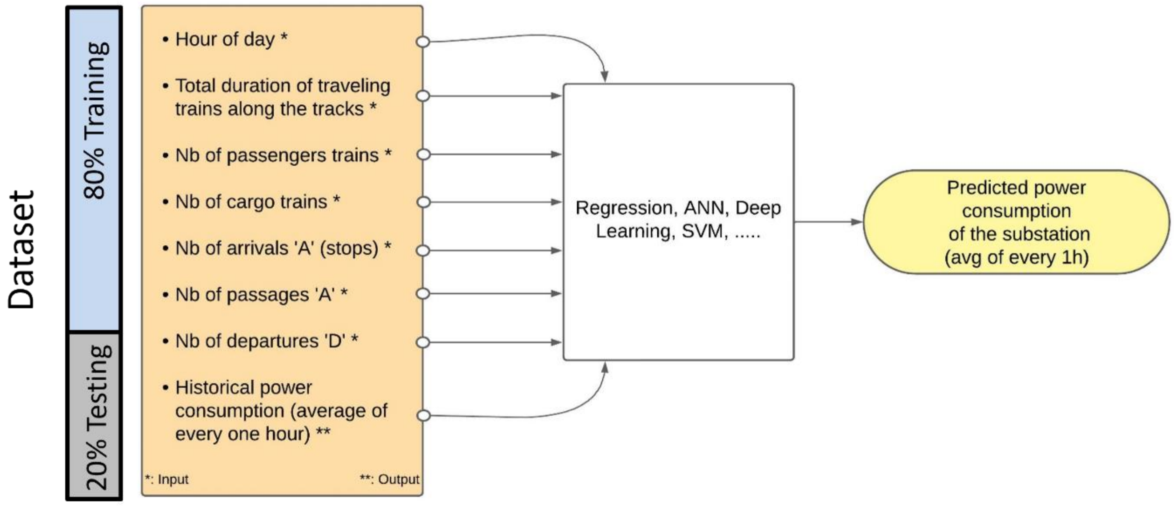


*Fig. 3.5 Forecast with linear regression*

## 3.4 LSTM for time series forecast

While linear regression provides a simple and interpretable benchmark for forecasting TSS consumption, its capacity to capture nonlinear dynamics and short-duration peaks is limited. In addition, regression models require synchronized timetable information together with power consumption data and multiple input variables, which is difficult to guarantee in practice due to the lack of real-time synchronization between train schedules and substation measurements. To address both of these limitations, more advanced time-series forecasting methods are required.

Among such methods, recurrent neural networks (RNNs) have proven particularly effective, as they rely solely on historical power consumption to predict future trends and profiles. This makes them more practical for railway energy forecasting, where historical load data is available and reliable, while synchronized timetable information is not.

Recurrent neural networks, however, suffer from vanishing gradients when modelling long-term dependencies. Long Short-Term Memory (LSTM) networks, a specialized type of RNN, overcome this limitation through memory cells that can capture both short-term variations and long-term patterns [115] . This makes them especially relevant for forecasting TSS power consumption, which exhibits recurring daily cycles combined with abrupt peaks caused by train circulation.

LSTM models analyse the nature of historical profiles, identifying underlying trends, patterns, and dynamics to generate accurate power consumption forecasts. The effectiveness of LSTM in predicting load consumption for both household and area-wide scales was demonstrated in [116] , where significant improvements over traditional methods were noted in terms of accuracy and reliability. LSTMs are particularly adept in scenarios where historical substation power consumption data serve as the primary input variable [117] .

Building an LSTM-based forecast model for predicting substation power consumption involves a structured workflow, summarized in Fig. 3.6 Structured workflow for building the LSTM forecasting model.. The process begins with data preparation, where historical consumption profiles are normalized, divided into training and testing subsets, and one representative time series is selected for training. In the model training stage, the network architecture is configured with LSTM, dense, and dropout layers, and trained using the Adam optimizer, activation function, a defined number of epochs and batch size, and a mean squared error (MSE) loss function. Finally, in the test set evaluation stage, the trained model is applied to the unseen test data, and the predictions are unnormalized and assessed using quantitative metrics (RMSE: root mean squared error, MAE: mean average error, and Pearson correlation coefficient), complemented by visual inspection to ensure that the temporal patterns of the forecasts align with actual consumption. This pipeline ensures that the model not only fits the training data but also generalizes effectively to new profiles, thereby capturing both the long-term cyclic patterns and the short-term dynamics critical for reliable TSS power forecasting.

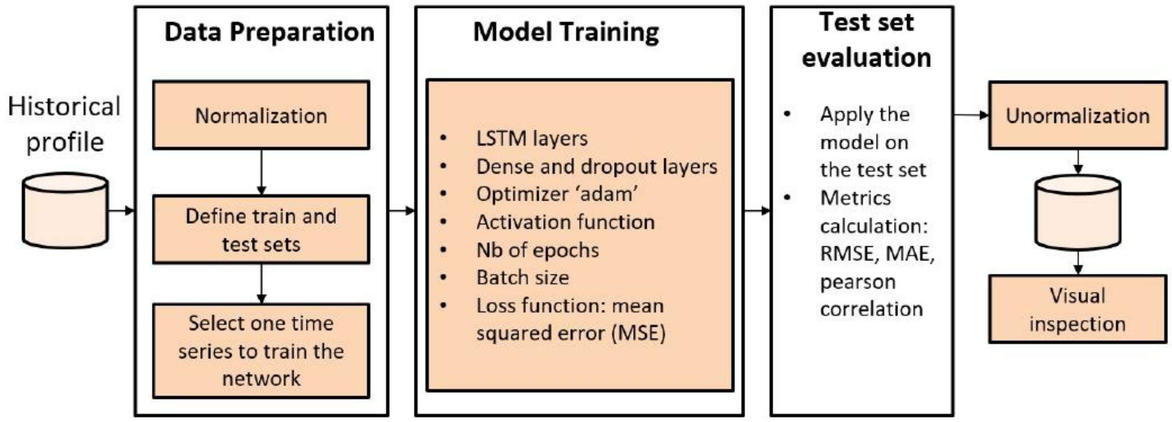


*Fig. 3.6 Structured workflow for building the LSTM forecasting model.*

### 3.4.1 Simple LSTM model (LSTM1)

In this study, a neural network architecture is employed specifically for forecasting power consumption at railway substations using historical TSS power consumption data. The foundation of the model is a LSTM layer, which is instrumental in processing sequential data and capturing both short term and long-term dependencies inherent in electricity consumption patterns. Within the LSTM layer, mechanisms such as forget, input, and output gates are used to manage the flow of information, enabling the retention or discarding of information based on its relevance to the prediction task as seen in Fig. 3.7 Architecture of the weighted LSTM forecast model (LSTM1).

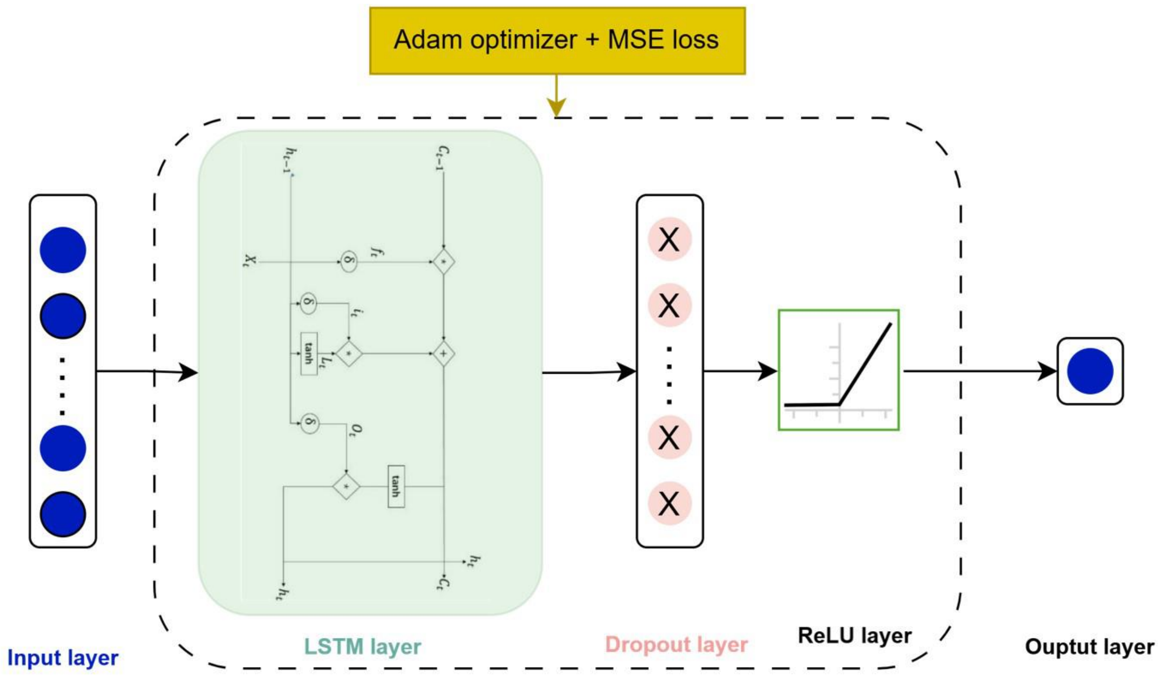


*Fig. 3.7 Architecture of the weighted LSTM forecast model (LSTM1)*

Following the LSTM layer, a dropout layer is incorporated to mitigate the risk of over fitting, a common challenge in deep learning models. This layer functions by randomly deactivating a subset of neurons during the training process, which prevents the model from learning noise and irrelevant details, thus enhancing its ability to generalize on unseen data. After the dropout layer, a Rectified Linear Unit (ReLU) activation layer is included. The ReLU activation function introduces non-linearity, allowing the model to learn complex and non-linear relationships in the dataset. This activation function is particularly effective due to its computational simplicity and its capability to maintain the gradient flow during back propagation, thereby reducing the likelihood of the vanishing gradient problem [119] .

The final stage of the model involves an output layer where the forecast of future power consumption is generated. A linear activation function is utilized in this layer to produce a continuous output that corresponds to the predicted power values. Throughout the training process, the Adam optimizer, coupled with a Mean Squared Error (MSE) loss function, is employed. The Adam optimizer is chosen for its adaptive learning rate capabilities, which enhance the speed of convergence, while the MSE loss function quantifies the prediction error, providing a clear objective for the model to minimize during training. This sophisticated configuration allows the neural network not only to capture the intricate dependencies within the power consumption data but also to generalize effectively to new data, thereby yielding reliable and accurate forecasts essential for operational and strategic planning in railway infrastructure management.

### 3.4.2 Weighted LSTM forecast model (LSTM2)

To improve the behaviour of the LSTM and for better peak detection. A new LSTM layer is added followed with an additional dense layer and a dropout layer. With a customized loss function that incorporates weights to the highest predictions errors illustrated by Fig. 3.8.

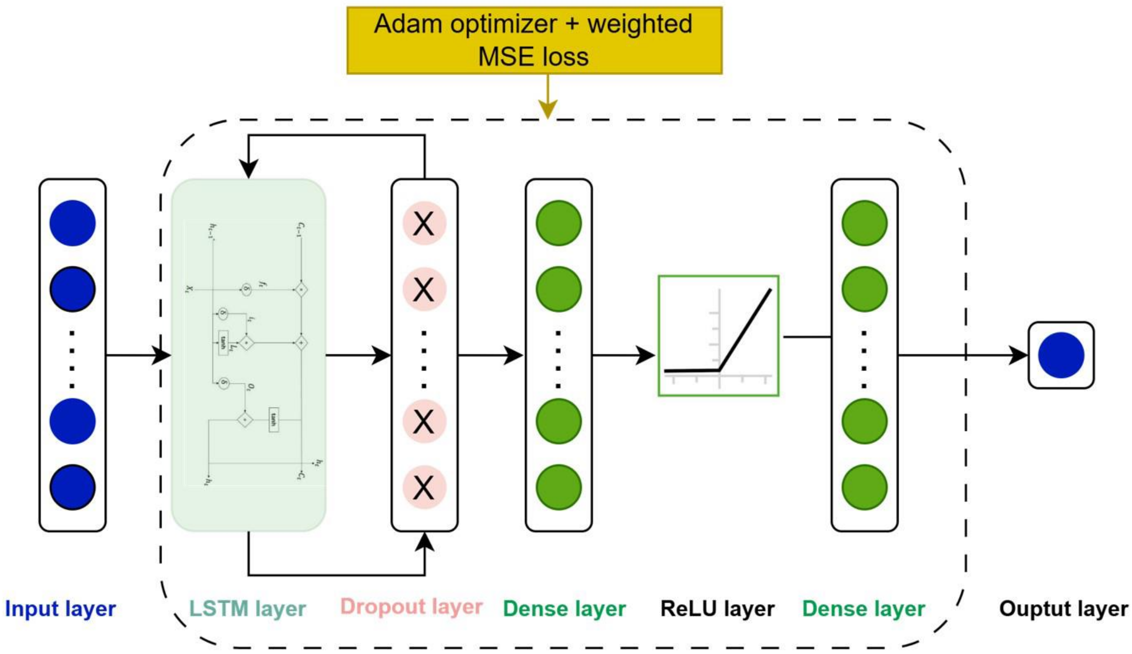


*Fig. 3.8 Architecture of the weighted LSTM forecast model (LSTM2)*

The custom loss function, weighted MSE loss, enhances the standard Mean Squared Error (MSE) loss by incorporating a dynamic weighting mechanism to prioritize high-value predictions. In this approach, a threshold is defined as the mean plus two standard deviations of the true values, effectively identifying critical high-consumption scenarios or peaks. Errors in this case are assigned a significantly larger weight, while errors for regular values are weighted normally.

To formalize this approach, the weighted root mean squared error (wMSE) can be expressed as:

$$\mathrm{wMSE} = \frac{\sum_{i=1}^{N} w_i \ (y_i - \hat{y}_i)^2}{\sum_{i=1}^{N} w_i} \tag{3.2}$$

With

$$w_i \begin{cases} \alpha, & if\ y_i \geq \mu + 2\sigma \\ 1, & otherwise \end{cases}$$

Where:

- $y_i$ = the actual value at time $i$
- $\hat{y}_i$ = the predicted value at time $i$
- $w_i$ is the weight assigned to each sample,
- $\mu$ and $\sigma$ are respectively the mean and standard deviation of the actual dataset
- $\alpha$ is a scaling factor that penalizes large errors occurring in peak consumption periods.

This formulation ensures that deviations during critical high-load events contribute more heavily to the overall error metric, thereby improving the model's sensitivity to peaks.

By applying this weighting scheme, the loss function penalizes deviations more heavily for high-consumption predictions, ensuring that the model focuses on accurately capturing these critical patterns. This modification addresses a common limitation of standard MSE, which treats all errors equally, often leading to suboptimal performance in scenarios where peak values carry higher operational or economic importance.

As a result, the weighted MSE loss function improves the model's sensitivity to extreme cases, aligning the learning objective with domain-specific requirements, such as energy forecasting, where accurate prediction of peaks is essential for effective resource management and cost optimization. This approach contributes to the robustness and practical relevance of the forecasting model by emphasizing high-value regions, which are critical in many real-world applications.

## 3.5 Error metrics and performance indicators

The effectiveness of the forecast models is assessed by evaluating the difference between actual and predicted values. The mean absolute error (MAE) and the root mean squared error (RMSE) are calculated. The MAE (3.3) represents the average absolute difference between actual and predicted values. While RMSE (3.4) squares the differences before averaging and takes the square root of the result to give more weight for larger errors than MAE, making it more sensitive to outliers or larger deviations. Also, the mean relative error (MRE) is also calculated in (3.5), it measures how far the predictions values are from their actual values in relative terms. It is important to assess the prediction accuracy [122] **.**

$$MAE = \frac{1}{n}\sum_{i=1}^{n}|y_i - \widehat{y_i}| \tag{3.3}$$

$$RMSE = \sqrt{\frac{1}{n}\sum_{i=1}^{n}(y_i - \widehat{y_i})^2} \tag{3.4}$$

$$MRE = \frac{1}{n}\sum_{i=1}^{n}\frac{|y_i - \widehat{y_i}|}{y_i} \tag{3.5}$$

Where: $n$ is the number of data points, $y_i$ is the actual value, and $\hat{y}_i$ is the predicted value for the $i^{th}$ data point.

The Pearson correlation coefficient (3.6), often denoted as $r$, is a statistical measure that quantifies the strength and direction of the linear relationship between predicted and actual variables. All that was also calculated, were evaluated to examine the amount of the error happening in the forecast output in order to test the performance of the models and see whether it can be used in the EMS as inputs to the optimization algorithm.

$$r = \frac{\sum_{i=1}^{n}(x_i - \bar{x})(y_i - \bar{y})}{\sqrt{\sum_{i=1}^{n}(x_i - \bar{x})^2}\sqrt{\sum_{i=1}^{n}(y_i - \bar{y})^2}} \tag{3.6}$$

Where: $\bar{x}$ is the mean value of the testing dataset values, $x_i$ is the actual value in X_test, $\bar{y}$ is the mean value of the y_test values, and $yi$ is the predicted value in y_test. The combined actual and predicted testing data are evaluated using these metrics. All reported values are normalized with respect to the range of the dataset.

## 3.6 Forecast evaluation and results analysis

In this section the results of the different forecasts are evaluated. Knowing that the linear regression approach has a unique dataset because of the available processed historical train dynamics. Although, it is important to highlight its perspective and the importance of performing solid work on data collection and synchronization between trains information and TSS power consumption.

### 3.6.1 Comparison between linear regression and LSTM (1h time step)

The forecast done covers two months long of TSS power consumption data, with a point every 10 minutes resampled into a one-hour average. With 80% training size and 20% testing, the testing data set is a new profile that the forecast model did not see before. The same dataset was used for the LSTM and regression model. In the latter, more inputs were used related to trains information. Both models were able to learn the pattern and predict the shape of the power consumption. However, it was clear that both models struggled to predict high power peaks that occur which can be critical as shown in Fig. 3.9.

The hourly energy doesn't suit well the nature of the TSS load, peak consumptions exist for short periods of time during the day (a matter of minutes) when taking the average it is difficult to detect the peak consumption, The optimization will deal with a TSS power profile that doesn't show the penalties that will be calculated on average of 10 minutes for overrunning the subscribed power $P_{sub}$. This put more difficulties in terms of minimizing penalty costs.

The metrics were calculated from the errors between actual values of the test set and the prediction values. The values of MAE and RMSE are normalized and expressed as percentages in Table 3.1

Both methods show comparable values for MAE, reflecting similar levels of average error. However, the higher RMSE obtained from the regression model indicates that the regression method has larger deviations in some of its predictions, leading to more pronounced errors compared to the LSTM. When comparing MRE, the LSTM model demonstrates superior performance in predicting a power profile, as its predictions are, on average, closer to the actual profile than those of the regression method. The Pearson correlation coefficient $(r)$ for both methods indicate a strong positive linear relationship between predicted and actual values, as the values are close to 1. Nevertheless, it is worth noting that the regression model could potentially benefit from integrating additional inputs and a larger synchronized dataset, such as detailed train-related information, which might lead to improved accuracy if there is a strong correlation between the input and output variables.

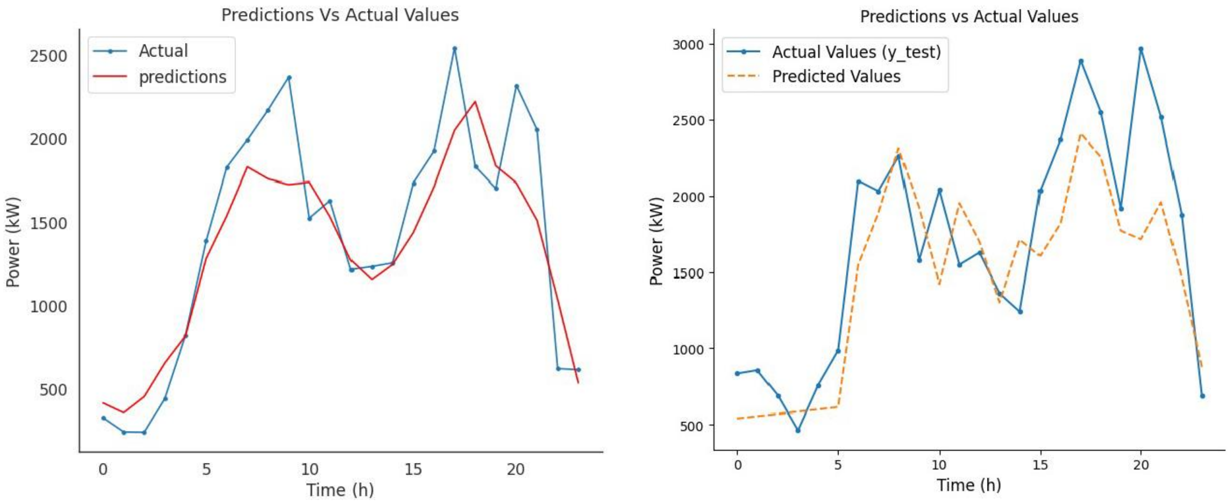

(a) *LSTM model* (b) *Regression model*

*Fig. 3.9 Predicted and actual values of TSS power consumption using LSTM and linear regression – 24 hours power profile.*

*Table 3.1 Forecast models metrics*

| Method | **MRE** | **MAE** | **RMSE** | ***r*** |
|---|---|---|---|---|
| LSTM | 18.77% | 9.19% | 12.24% | 0.844 |
| Regression | 21.96% | 13.96 | 17.29 | 0.853 |

### 3.6.2 Forecast with 10 minutes time step using LSTM

The choice of the 10 minutes times step serves better the objective of the forecast. The penalties paid by the SNCF network are calculated for exceeding the subscribed power on an average of 10 minutes. Also, the 10 minutes time step better captures the train dynamics of TSS consumption with peaks.

The graph of Fig. 3.10 shows a TSS consumption profile of 24h period. It is taken from the testing dataset where $P_{act}$ is the actual historical data, $P_{forecast}$ LSTM1 is the TSS predicted power consumption using the simple LSTM method, and $P_{forecast}$ LSTM2 is the predicted consumption using the weighted LSTM forecast method. The visual inspection of Fig. 3.10 Profile of 24-hour actual TSS consumption and the predicted TSS consumption using LSTM1 and LSTM2 models. shows that the simple LSTM model (LSTM1) is limited in terms of detecting the power values around the subscribed power ($P_{\text{sub}} = 3500\ kW$). The comparison of two LSTM models based on their performance metrics applied to a testing dataset reveals significant insights into their predictive capabilities and characteristics. The performance metrics are listed in Table 3.2. The first model, LSTM1, which is a simpler model, exhibits a Normalized Mean Absolute Error (NMAE) of 5.43% and a Normalized Root Mean Squared Error (NRMSE) of 8.03%. These metrics suggest that LSTM1 maintains a relatively low level of prediction error and variability, confirming its efficiency in forecasting with minimal deviation from actual values. On the other hand, the second model, LSTM2, which is more complex, shows higher error metrics with an NMAE of 7.29% and an NRMSE of 10.18%. The increased error rates may be indicative of the model's overfitting or its sensitivity to the noise and complexity within the dataset. Notably, LSTM2 also has a higher Mean Relative Error (MRE) at 39.87%, compared to 29.62% for LSTM1, suggesting that the complex model may not be as effective at handling or generalizing the underlying patterns in the data as the simpler model. Despite the higher error rates, LSTM2 demonstrates a slightly better Pearson Correlation Coefficient of 0.7135, compared to 0.7056 for LSTM1.

This metric indicates a marginally stronger linear relationship between the predicted and actual values, suggesting that while LSTM2 may capture the directionality of the data trends slightly better, it does so with less accuracy and higher variability. In summary, while LSTM2 may potentially capture complex patterns slightly more effectively as indicated by the Pearson coefficient, LSTM1's lower error metrics across NMAE, NRMSE, and MRE suggest it might be the more reliable and efficient choice for practical applications, particularly where the trade-off between complexity and performance needs to be carefully managed.

Overall, LSTM1 is better suited for applications that prioritize smooth predictions and overall accuracy. In contrast, LSTM2 is ideal for scenarios that require precise detection of peak consumption, although this may come with higher overall errors, especially during the periods of low consumption, the predictions of LSTM2 tend to be higher than the actual values which causes high error percentages.

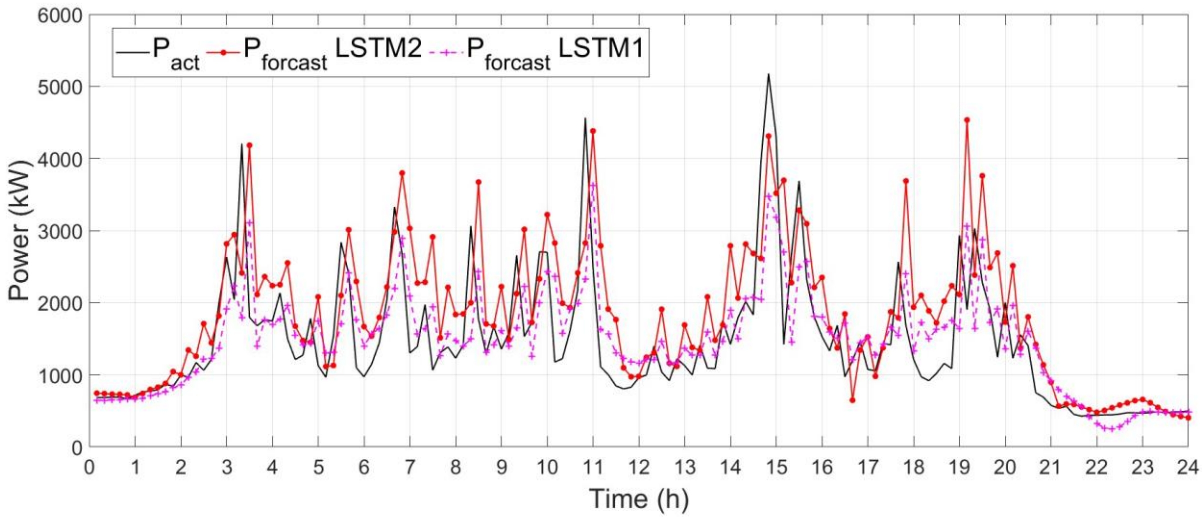


*Fig. 3.10 Profile of 24-hour actual TSS consumption and the predicted TSS consumption using LSTM1 and LSTM2 models.*

*Table 3.2 Metrics comparison between LSTM models*

| Metric | LSTM1 (Simpler Model) | LSTM2 (More Complex Model) |
|---|---|---|
| Normalized Mean Absolute Error (NMAE) | 5.43% | 7.29% |
| Normalized Root Mean Squared Error (NRMSE) | 8.03% | 10.18% |
| Mean Relative Error (MRE) | 29.62% | 39.78% |
| Pearson Correlation Coefficient | 0.7056 | 0.7135 |

### 3.6.3 Summary of the tested forecast methods

To obtain a load profile suitable for optimization, the forecast must be performed with a 10-minute time step, as penalties for subscribed power overruns are calculated on this basis. The LSTM models, trained only on historical TSS consumption data, proved more consistent and practical under current conditions, since they avoid the need for synchronized timetable information and extensive data preprocessing. Linear regression, on the other hand, opens a prospective avenue: if large, clean, and synchronized datasets combining train timetables with substation consumption were available, additional input variables could be exploited to improve forecasting accuracy. At present, the limited size and quality of the dataset prevent this approach from being fully effective, but with improved data collection infrastructures, more advanced machine learning methods beyond linear regression could be investigated to enhance accuracy and robustness of the forecast.

## 3.7 Optimization problem formulation

The day ahead EMS is applied to the first architecture of RACCORD described in Chapter 2. Fig. 3.11 gives a reminder for the architecture worked on with the different symbols and the power flows in the railway network. Also, it shows the connected tracks where train information is extracted from train timetables for the development of the linear regression forecast model. Assuming that the TSS power consumption $P_{load}$ is influenced by train circulation at the 4 tracks. And neglecting the losses of the transformer and rectifier for simplicity in the optimization problem formulation.

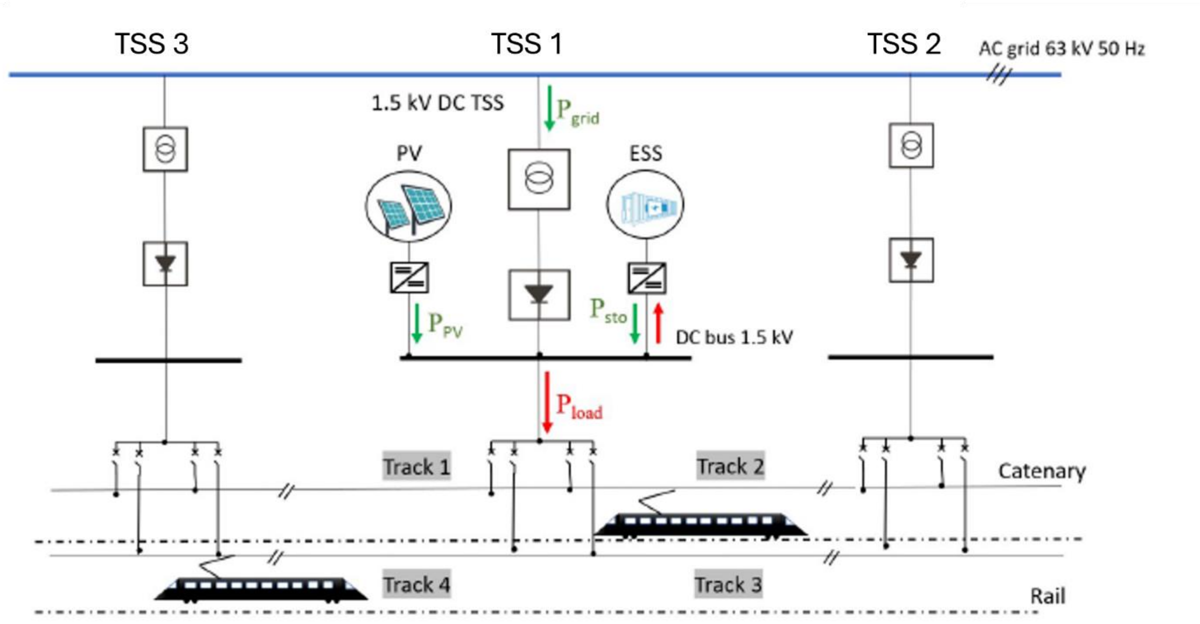


*Fig. 3.11 Architecture 1 of RACCORD*

The power discharged from the energy storage system (ESS) is considered positive, whereas charging power is associated with a negative power flow. Consequently, when discharging, the ESS injects power into the network with a positive sign, similarly to the photovoltaic (PV) system. Conversely, during charging, the ESS absorbs power from the network and is therefore considered as a load. the maximum discharge power of the ESS denoted $P_{disch-max}$ represents the maximum power limit in the discharge. Finally, the subscribed power has a constant value throughout the day. Table 3.3 summarizes the different specification and rated values of some elements in the system.

*Table 3.3 Electrical parameters and variables of the railway architecture*

| | | |
|---|---|---|
| Maximum allowable power of ESS | $P_{sto-max}$ | 1200 kW |
| Maximum charge power | $P_{ch-max}$ | -600 kW |
| Maximum discharge power | $P_{disch-max}$ | 1200 kW |
| Maximum PV power | $P_{PV-max}$ | 600 kW |
| Total ESS capacity | $E_{sto}$ | 1800 kWh |

| | | |
|---|---|---|
| Subscribed power | $P_{sub}$ | 3500 kW |

These specifications are fixed in order to test the day ahead EMS based on optimization. It might not reflect the actual or precise dimension of the railway smart grids elements. But it first in the first place to validate the proposed EMS.

### 3.7.1 Optimization objective function

The considered pricing scheme for the TSS depends on the time of use of electricity transportation network (TURPE) that results by negotiation between railway network operator and the electricity transport network (RTE) as explained earlier in Chapter 1 [28] .

From the energy costs, the SNCF réseau pays for the use of the public grid included within the electricity transport and delivery costs, and penalties for overrunning the subscribed power (CMDPS). Equation (3.7) recalls the CS part of the TURPE6 agreement. In this formulation, $CS$ represents the total annual withdrawal cost (composant de soutirage).

The variable cost is the cost of use the public electricity transport grid and has a variable coefficient $c_i$. The penalty costs that have a variable coefficient $b_i$ that changes depending on the season and the hour of the day.

Through the installation of PV and ESS in RACCOR-D project, the SNCF aims to reduce the dependency on the conventional grid during high tariffication cost of use of the public grid and reduce the penalties caused by overrunning the subscribed power. Fig. 3.12 shows the variation of the coefficient $c_i$ during the day. It is possible to identify three periods, peak hours (highest cost), off-peak hours (lowest cost) and plane hours (average cost).

$$
\begin{aligned}
CS = b_1 \times PS_1 + \sum_{i=1}^{5} b_i \times (PS_i - PS_{i-1}) + \sum_{i=1}^{5} c_i \times E_i \\
+ \sum_{12\ \text{mois}} \sum_{i=1}^{5} 0.04 \times b_i \times \sqrt{\sum_j \left(P_j - PS_i\right)^2}
\end{aligned}
\tag{3.7}
$$

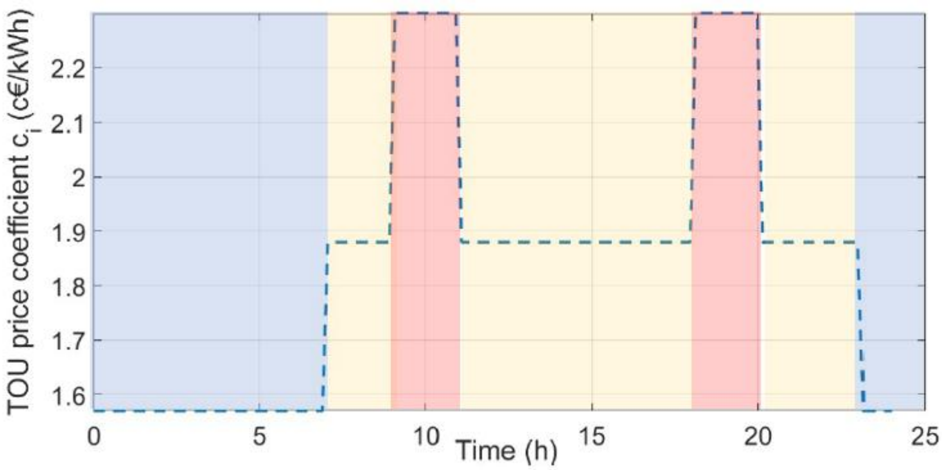


*Fig. 3.12 Daily variation of the TOU coefficient '$c_i$' (dotted line) in the high season tariff example.*

Day-ahead supervision was developed using a nonlinear optimization approach. A Sequential Quadratic Programming (SQP) algorithm is a suitable method for determining the optimal economic schedule for the ESS in a day-ahead scheduling, based on variable price profiles of penalties and use of public grid. The optimization minimizes a developed cost objective function, represented by Equation (3.10), which cover these main cost components:

- The costs of the energy consumed by the TSS demand over specific time intervals (covering demand of rolling stocks supplied by the TSS, auxiliary load, losses, and other possible consumers).
- The penalties for power demand overruns relative to the subscribed power.
- Use of the electricity transmission network (RTE) cost and it is denoted time of use cost (TOU) for simplicity.

The cost of electricity is fixed within a day to 0.2 €/kWh, the railway companies that use the TSS of the SNCF réseau are billed through an arrangement to compensate for the electricity used from the TSS. It is added to the objective function since the optimization is a day ahead EMS and a daily function of costs must be developed.

The cost function combines both the energy usage cost and the penalties for exceeding subscribed power limits: The objective function to be minimized is proposed to consider the variable part of the CS in addition to the cost of electricity consumed. The optimization algorithm will work on minimizing the total costs that adds the three components based on Equation (3.11). The optimization will consider one day so the seasonal variation of the weighting variables is not considered, and the sampling time is suited for the time step of the historical data which is 10 minutes. So, the components of the objective function are presented in Equations (3.8) (3.9) (3.10).

$$TOU = \sum_{t=1}^{144} \frac{1}{6} \times c_i \times P_{\mathrm{grid}}(t) \tag{3.8}$$

$$CMDPS = \sum_{t=1}^{144} 0.04 \times b_i \times \sqrt{\left(P_{\mathrm{grid}}(t) - P_{\mathrm{sub}}\right)^2} \quad for \quad P_{grid} > P_{sub} \tag{3.9}$$

$$Electricity\_cost = \sum_{t=1}^{144} \frac{1}{6} \times C_{\mathrm{elec}} \times P_{\mathrm{grid}}(t) \tag{3.10}$$

Where TOU is considered the time of use of public grid costs, CMDPS is the penalty costs for overrunning the subscribed power, and $Electricity\_cost$ represent the electricity cost for the consumed power of the TSS, it has a fixed coefficient throughout the day so it won't affect the optimization. The division by 6 in Equation (3.7) and (3.9) is to calculate the values in the 10 minutes average instead of 1 hour average of the price coefficients $C_{\mathrm{elec}}$ and $c_i$. Railway companies supplied by the TSS are responsible for paying SNCF network the electricity costs through tariffication agreements between SNCF réseau and the railway companies. The objective function denoted $f$ to be minimized is therefore:

$$f = min(TOU + CMDPS + Electricity\_cost) \tag{3.11}$$

### 3.7.2 Constraints modelling

Starting from the physicality of the system and the requirement of each of the smart grid elements, the main constraint is related to the uni-directionality of the power grid that block the possibility to sell excess power to the grid. In addition, the power balance must be satisfied at every time step t, along with constraints on the number of ESS charge/discharge cycles. The benefit behind setting a defined number of cycles per day is the prolongation of the ESS lifespan and limiting the SOC within defined values is to prevent the saturation of the batteries at high and low levels.

- To following constraints are modelled as follow to respond to the different limits and requirements imposed to the optimization process :State of charge (SOC) Limits: Equation (3.12) enforces the SOC of the ESS to stay within a defined range, specifically between $SOC_{min}$ and $SOC_{max}$, which are set at 0.2 and 0.8, respectively. This ensures that the battery's charge level remains within safe operational limits.

$$SOC_{\text{min}} \leq SOC(t) \leq SOC_{\text{max}} \quad (3.12)$$

- Power balance: At every time step $t$, the power balance equation must hold:

$$P_{\text{grid}}(t) = P_{\text{load}}(t) - P_{\text{PV}}(t) - P_{\text{sto}}(t) \quad (3.13)$$

This equation ensures that the power drawn from the grid accounts for the load demand after considering the contributions from PV generation and the ESS.

- End-of-day SOC: Equation (3.14) specifies that the SOC at the end of the day (at time step 144) should be 0.5. This condition is imposed to prepare the ESS for the next day's operation, balancing the stored energy at a midway point. The SOC calculation performed at every time step is represented in Equation (3.15).

$$SOC(144) \ = \ 0.5 \quad (3.14)$$

$$SOC(t) \ = \ SOC_0 \ - \ \frac{1}{E_{sto}} \sum_{t=1}^{144} \frac{P_{sto}(t)}{6} \quad (3.15)$$

Where $SOC_0$ is the initial state of charge at the beginning of the day, $E_{sto}$ is the ESS rated capacity, and $P_{sto}(t)$ is the battery charging or discharging power at each time step.

- Grid power non-negativity: Equation (3.16) ensures that the power drawn from the grid $P_{grid}$ is non-negative, as unidirectional power flow is considered. This implies that energy can only be drawn from the grid, not supplied back.

$$P_{grid}(t) \ \geq \ 0 \quad (3.16)$$

- Cycle limits for charging and discharging: Equations (3.17) and (3.18) limit the number of full charging and discharging cycles of the ESS to two cycles per day. These constraints involve summing the power flow over time (from $t \ = \ 1$ to $t \ = \ 144$) and scaling by 6, keeping the total energy exchanged within twice the capacity $E_{sto}$of the battery. This limitation reduces battery wear and prolongs its lifespan.

$$\sum_{t=1}^{144} \frac{|P_{\text{sto, ch}}(t)|}{6} \leq 2 \times E_{\text{sto}} \times (SOC_{\text{max}} - SOC_{\text{min}}) \quad (3.17)$$

$$\sum_{t=1}^{144} \frac{P_{\text{sto, disch}}(t)}{6} \leq 2 \times E_{\text{sto}} \times (SOC_{\text{max}} - SOC_{\text{min}}) \quad (3.18)$$

### 3.7.3 Decision variable and limits

The day-ahead EMS consists of scheduling the ESS for the upcoming day. The optimization decision variable is a temporal variable represented by the reference power set-points on average of 10 minutes to be sent to the ESS $P_{sto}$. While respecting the maximum power that can be used during the charging and the discharging $P_{ch\_max}$ & $P_{disch\_max}$. At the end of the optimization, the algorithm provides 144 set-points each one represents the average power of 10-minutes. The choice of 10 minutes time step is ruled by the available historical information that are saved as average of 10 minutes (the same average used for calculating CMDPS costs). A SQP algorithm is used to deal with the nonlinearity of the constraints and the objective function as expressed in Equation (3.11) that integrates the penalty costs (CMDPS). The calculation of the SOC at each time step is also done through a nonlinear equation as expressed in Equation (3.15). The optimization is done in MATLAB using ***fmincon*** function [118] .

The flow chart of Fig. 3.13 explains the optimization stages and the necessary input profiles required for the day ahead EMS. The forecast of the TSS consumption is done through the explained forecast methods, the PV production profile is a theoretical profile that describe the capacity of the PV system from maximum power and the surface of the installed system. The pricing coefficient are taken from the pricing scheme explained earlier.

The optimization block includes the terms that will impact the decision of the optimization (TOU and CMDPS) as they contain variable pricing coefficient, unlike the electricity cost that has a constant price value per kWh during the day.

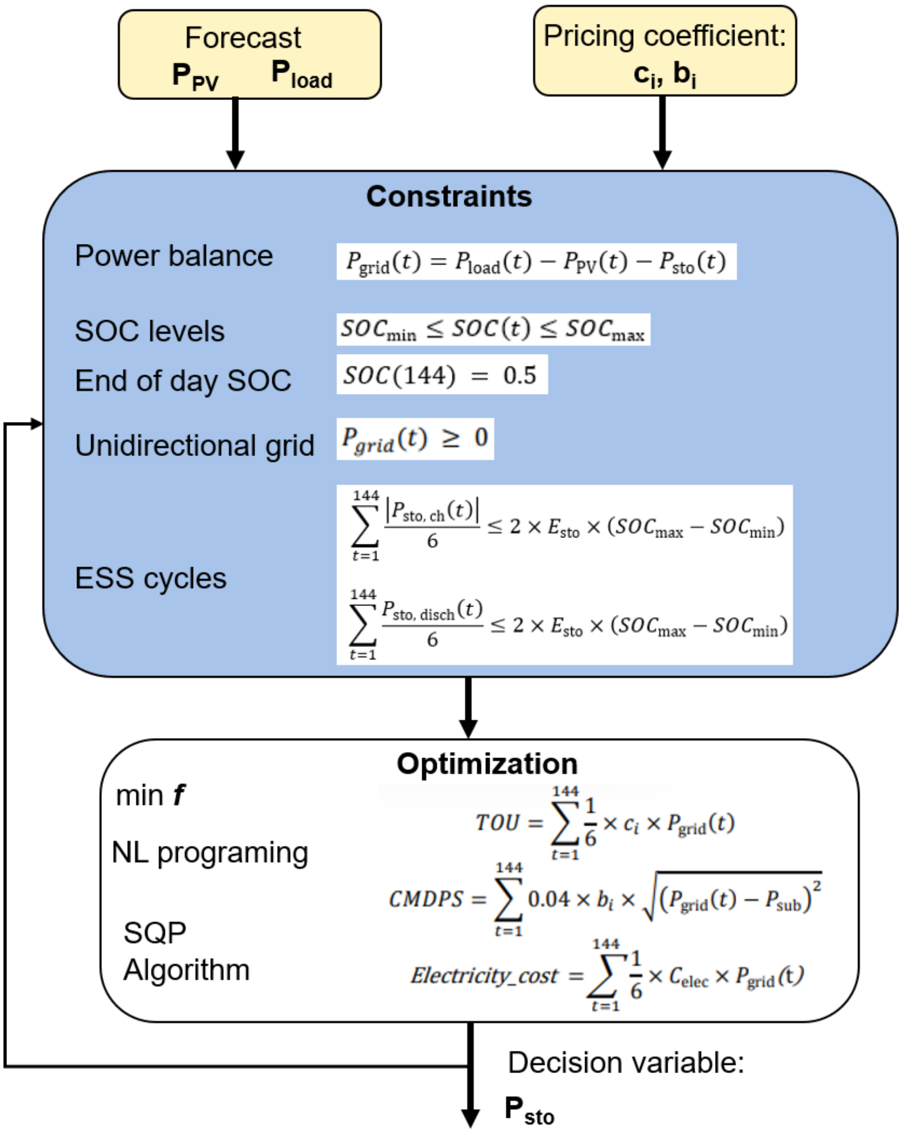


*Fig. 3.13 Flow chart explaining the optimization process*

## 3.8 Results and analysis

In this section, the outcomes of the day-ahead optimization are analysed and assessed. The impact of forecast quality on the EMS benefits is explored. The reference optimal ESS schedule is derived from the EMS using the actual historical TSS consumption. The schedules generated using the predicted consumption profiles from the LSTM methods are then compared to the reference. The deviation of these schedules from the reference will indicate the suitability of the forecasts for such applications.

Also, the key performance indicators are calculated. Namely the energy used by the ESS, and the amount of PV energy curtailment caused by the excess of PV production. Two typical days of TSS operation are considered. Day 1 with low penalty potential as the subscribed power is lightly over-passed. Day 2 where there are higher overruns of subscribed power. The aim of testing multiple days is to validate effectiveness of the nonlinear SQP optimization on finding a minimum of the objective function while respecting the constraints with multiple types of TSS load profiles.

The yearly average of weekdays and weekends are plotted in Fig. 3.14, showing that on average weekdays has higher consumption and higher peaks. It is assumed in the results that the typical weekday profile is the day characterized by higher traffic and higher TSS consumption therefore higher peak consumption than weekend profile.

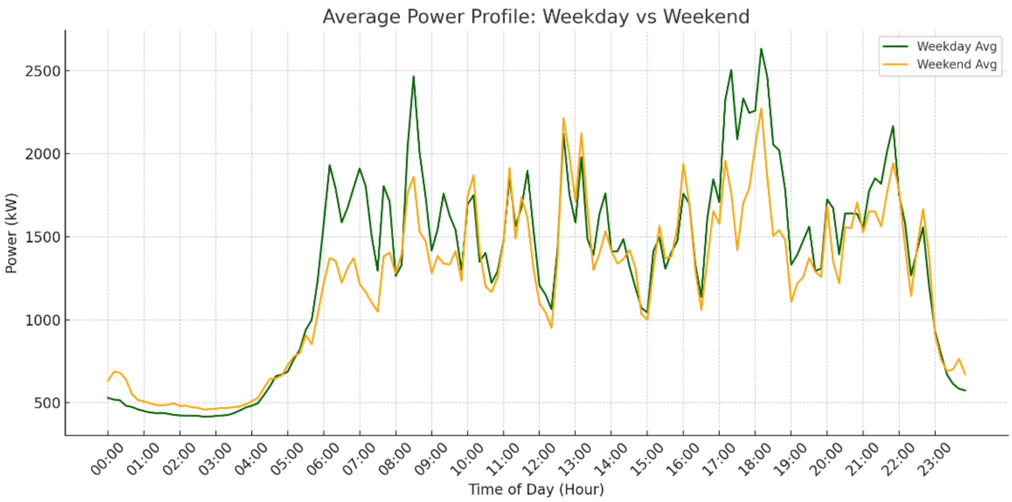


*Fig. 3.14 Average of TSS power consumption profiles of weekdays and weekends for the year 2017*

The economic benefit of using forecast-based optimization for day-ahead ESS scheduling is evaluated by comparison with a baseline schedule, in which the EMS charges the ESS during periods of low TSS consumption (early morning and night) and discharges it during the day.. The evaluation of the impact of the forecast method on the optimization outcome is done by comparing the results of the optimization when using the predictions of LSTM1 and LSTM2 separately with a reference case that neglect the errors of the forecast. A conclusion about LSTM method (simple or weighted) to be used for the day ahead energy management depending on the desired objective.

### 3.8.1 Reference case neglecting forecast errors

Having a reference case to start with is essential since the objective is to compare the impact of two forecast methods LSTM1 and LSTM2. The reference case reflects the ideal case where it will not be any difference between what is predicted and what is actually consumed. The reference case is the most optimal solution that can be obtained reflecting full knowledge of TSS consumption without any errors. The reference case serves as:

- Providing the most optimal solution to compare it with the solution obtained using forecast profiles as optimization inputs (from LSTM1 and LSTM2)
- Test in the first place the capabilities of the developed optimization method to find feasible solution.

The actual TSS power consumption from available historical data is used as an input to the optimization algorithm. The algorithm successfully found the optimal schedule of the ESS that respects the constraints and find the minimum cost described in (3.11).

Fig. 3.15 & Fig. 3.16 shows for the ESS schedule with the corresponding SOC; and the TSS load and the corresponding power drawn from the grid calculated from Equation (3.13) after the schedule of the ESS is proposed by the EMS optimization algorithm. These figures show the reference schedule that will perfectly schedule the ESS neglecting any uncertainties in the TSS power consumption forecast. The SOC level was maintained between its minimum and maximum limits 20 % & 80 %. Completing two cycles per day finishing with ESS half full at the end of the day similar to the beginning of the day (SOC = 0.5). The uni-directionality of the TSS is respected with the power balance scheme of Equation (3.13) preventing any negative grid power flow and maximizing the use of PV production. While providing a remarkable high discharge during overruns of the subscribed power, and during high time of use cost periods. The charging is scheduled to the beginning and the end of the day to profit from the low time of use cost described in Fig. 3.12.

The SQP nonlinear optimization was capable therefore of handling the constraints and the limits of the power system while finding an optimal solution that schedule the ESS for the upcoming day.

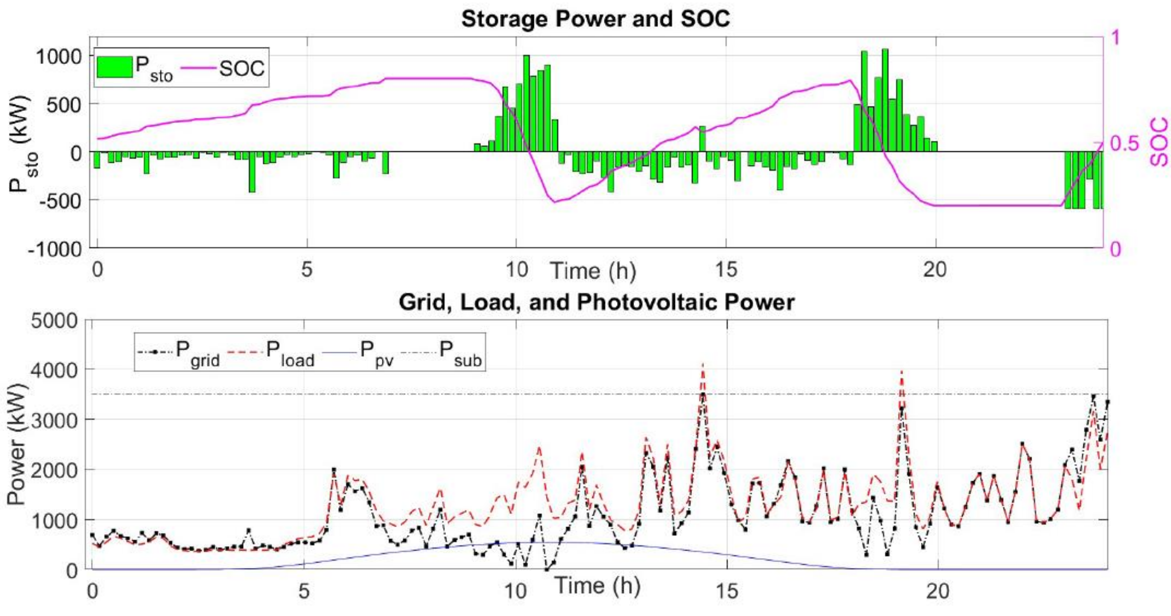


*Fig. 3.15 ESS schedule and power drawn from the grid in the reference case 'Day 1'.*

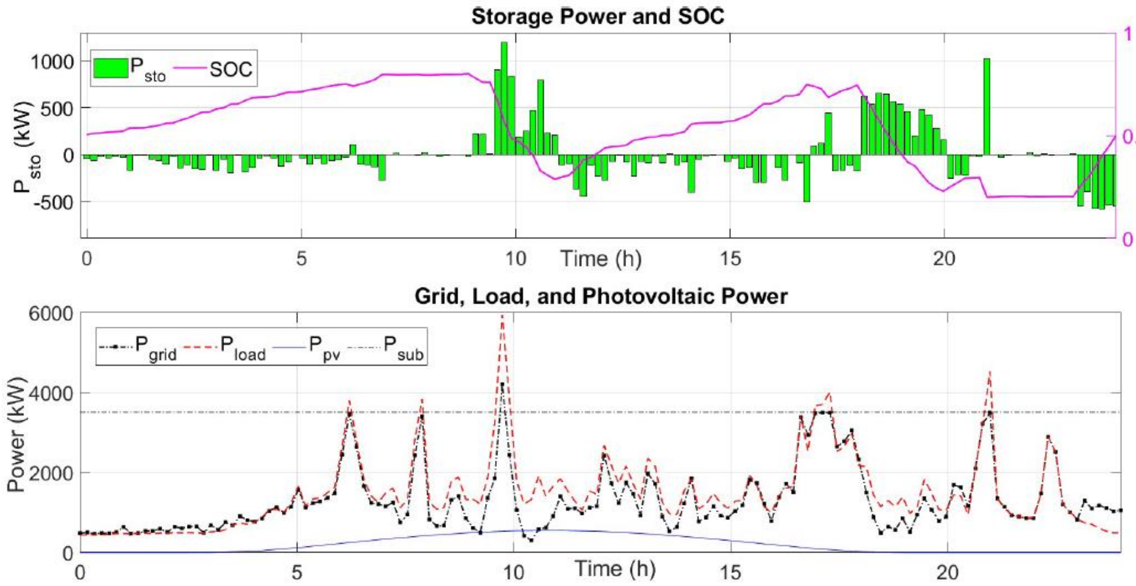


*Fig. 3.16 ESS schedule and power drawn from the grid in the reference case 'Day 2'.*

### 3.8.2 Case with the forecast TSS load profile used for the optimization process

The predicted profiles obtained through LSTM1 model and LSTM2 model are used as inputs to the optimization. The optimal ESS schedule is expected to vary from the reference schedule due to the uncertainties and forecast errors of the TSS. This schedule will be applied to the ESS when the actual TSS consumption occurs. It is expected to see unbalance in the power flow scheme and a potential PV curtailment. The maximization of the use of PV power might not be totally achieved. The influence of the forecast done can be therefore evaluated. The comparison between the LSTM models was done in the previous section (section 3.4) and quantified the advantages and the drawbacks of each model. In this section, their influence on the specific day ahead optimization application is analyzed.

For the evaluation and the analysis, two days were investigated to study the impact of the forecast: Day 1 represents a day with a medium overrun of subscribed power and Day 2 represents a day with high consumption and high overruns of the subscribed power. Each day has a reference case that represent the maximum optimality assuming that the predicted profile is exactly the actual TSS consumption profile. The solution obtained by using the actual TSS consumption as input is considered the best solution. The schedules obtained by using the forecast must be compared to the best solution, and how close they provide a schedule close to the best solution (reference case) is an indicator on how efficient the ESS day-ahead schedule is.

#### 3.8.2.1 Optimal ESS setpoints

The reference ESS schedule is compared with the ESS schedule obtained with the predictions of the simple LSTM and the predictions of the weighted LSTM. Although the error of the forecast could lead to noticeable errors, it is important to test the forecast outcome when used in the day ahead energy management application. The ESS schedule obtained after using the TSS consumption of the 2 days using LSTM1 and LSTM2 allows the calculation of the ESS energy used per day. In both cases, the SOC limits were respected, and the final SOC is equal to 0.5, and the energy used by the ESS is equal to 4.32 MWh for one day, which is equal to the two cycles limits. These results validate the effectiveness of the SQP on finding the minimum of the objective function while respecting the constraints with any type of predictions. In all cases, during the period of peak hour, the ESS is set to discharge during this period decreasing the dependency on the grid.

In Fig. 3.17 where the consumption of the TSS is average, both LSTM methods where not been able to detect the peak consumption occurring around 15h, the optimal schedule will therefore propose a small charging instead of discharge and keep the discharging of the ESS for peak hours only. The EMS therefore in such cases can reduce significantly the dependency on the grid during peak hours and reduces the peaks that occurs during the peak hours only.

Fig. 3.18 shows that the capabilities of the LSTM2 model to detect peak consumption points, forced the optimization to propose a relatively high discharge outside the peak hours between 20h and midnight. The ESS schedule in LSTM1 doesn't detect this peak consumption and therefore the EMS found no need to discharge during this point. This highlights the superiority of the weighted LSTM approach, which assigns greater importance to peak demand periods. In this case, the use of LSTM2 enables a more effective reduction of subscribed power overruns compared to LSTM1, thereby contributing more significantly to the objective of minimizing penalty costs.

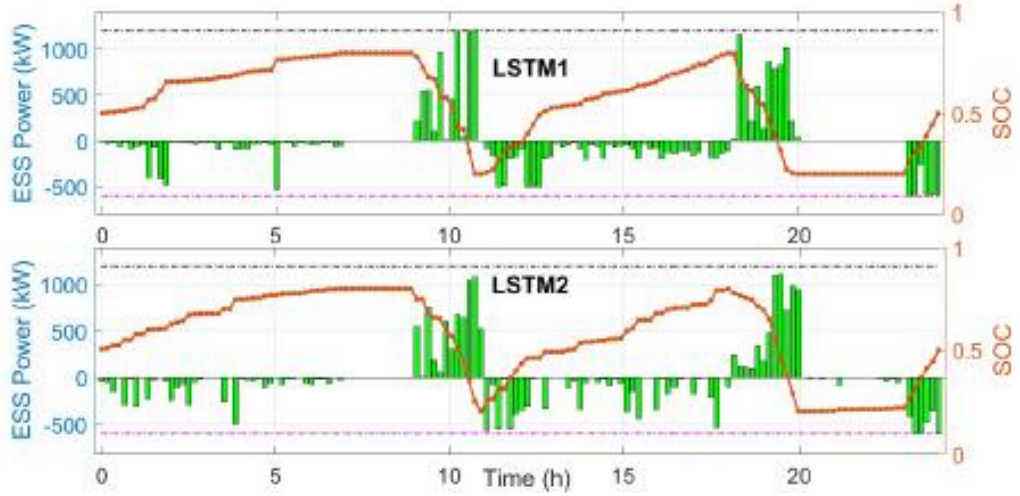


*Fig. 3.17 ESS schedule for both days obtained using both LSTM models for Day 1*

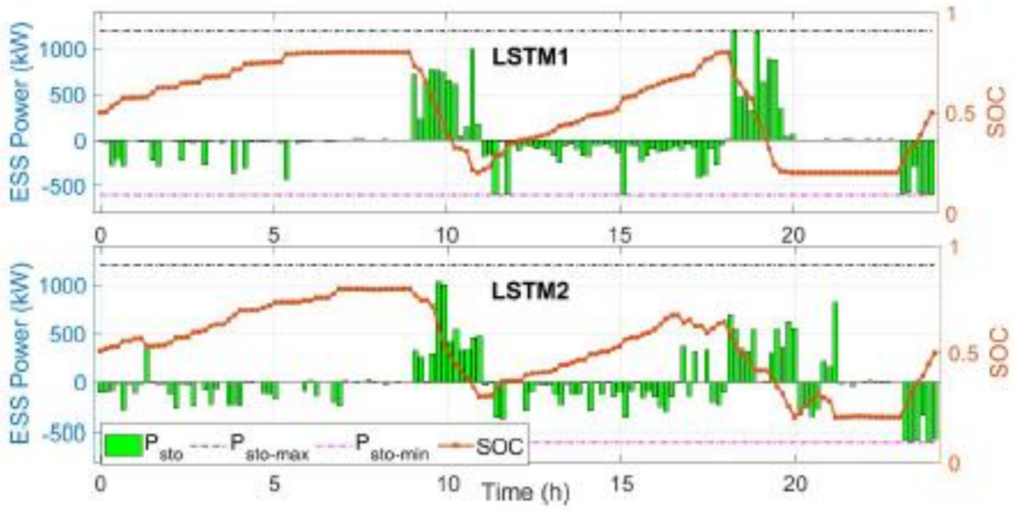


*Fig. 3.18 ESS schedule for both days obtained using both LSTM models for Day 2*

#### 3.8.2.2 Power drawn from the grid

The power drawn from the grid $P_{grid}$ in each of the cases is calculated based on the power balance equation (3.12). $P_{grid}$ permits to calculate the CMDPS by aggregating the amount of power that overpasses the subscribed power. Also, the negative values of $P_{grid}$ indicates an excess of PV production that must be curtailed to maintain the power balance scheme. The curtailed PV power harm the objective of maximizing the use of renewable energy but it might occur due to forecast errors. Any discharge of the batteries while PV production is high at a time where the actual TSS consumption is not as high as the predicted profile, the local production ($P_{PV}$ + $P_{sto}$) could exceed the TSS consumption $P_{load}$. The ESS is scheduled and fixed at day ahead, so the only solution is to curtail the excess of PV production to maintain power balance. This phenomenon occurred between 10h and 11h in Day 1 as shown in Fig. 3.19.

The overrun of the subscribed power in Day 1 occurring between 14h and 15h and occurring between 17h and 18h in Day 2 was reduced to its minimum in the reference case. The LSTM2 can decrease these peaks better than LSTM1 because of its better detection of the peak consumption points. This shows the superiority of LSTM2 forecast over LSTM1 forecast in terms of reducing the penalties caused by the overrun of the subscribed power.

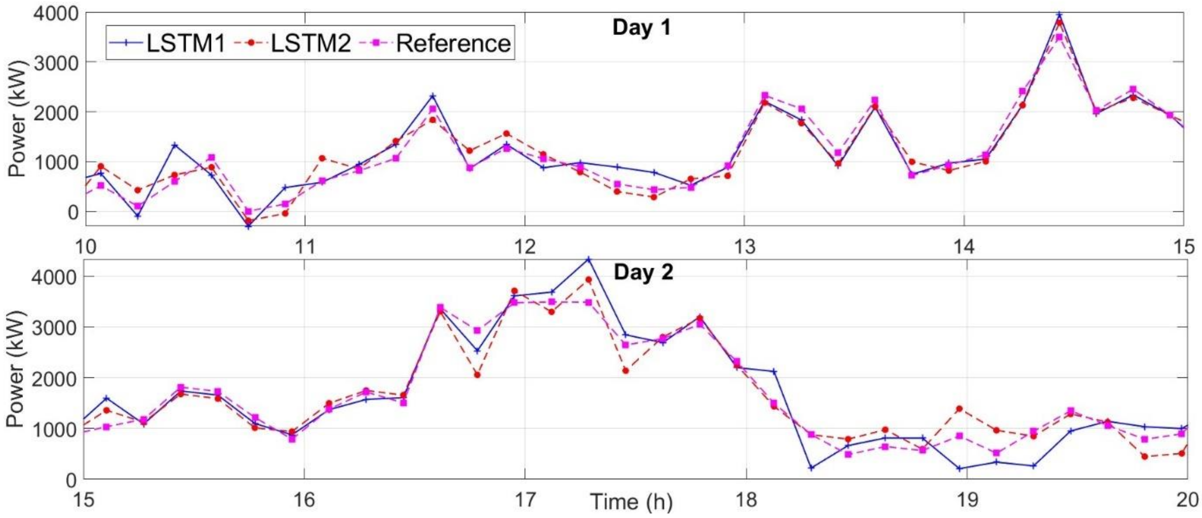


*Fig. 3.19 Power drawn from the grid on 'Day 1' and 'Day 2' in reference; LSTM1 and LSTM2 cases*

#### 3.8.2.3 LSTM1 and LSTM2 performance in the day-ahead schedule

The MRE and other metrics between the power drawn from the grid and the reference case compared to LSTM1 and LSTM2. The main key indicators that will validate the effectiveness of the optimization method used for the day ahead EMS are calculated from the power drawn from the grid $P_{grid}$. The most optimal $P_{grid}$ profile is obtained in the reference case in section 5.1 where the actual TSS power consumption is used as input to the optimization. This is the reason why all peak consumption points are detected and limited to its minimum (Fig. 3.15 and Fig. 3.16). The $P_{grid}$ profiles resulted from the use of LSTM forecasts (LSTM1 & LSTM2) is obtained and compared to the reference $P_{grid}$. The MRE and MAPE (Mean Absolute Percentage Error), measure the accuracy of values obtained using LSTM forecasts and the reference values. Both metrics indicate how far the $P_{grid}$ deviates from the reference. The effective of the forecast methods when used for the day ahead energy management is validated if there is no significant deviation from the reference case.

The MRE in the forecast between the actual and the predicted data is high. However, the MRE between the reference solution and the solutions provided by the optimization based on the forecast is 11% and 14% in ‘Day 1’ for LSTM1 and LSTM2 respectively as shown in Table 3.4. And between 10-11% in ‘Day 2’. This means that because of the uniqueness of the EMS application that focus on the penalty costs that was more evident than the reduction of TOU costs, the forecast algorithm offers a predicted TSS load profile that provide an ESS close by 85-90% to the optimal reference ESS schedule.

*Table 3.4 MRE and MAPE comparisons between LSTM models and reference for two days*

| | Model | MRE | MAPE |
|---|---|---|---|
| Day 1 | LSTM1 and Ref | 11% | 21.05% |
| | LSTM2 and Ref | 14.58% | 26.16% |
| Day 2 | LSTM1 and Ref | 10.07% | 16% |
| | LSTM2 and Ref | 10.96% | 12.73% |

### 3.8.3 Comparison with a baseline schedule

The economical gain translated in the reduction of penalty costs (CMDPS) is evaluated. The day ahead energy management with forecast must be compared with a baseline schedule.

The proposed baseline schedule aims to discharge the ESS during the periods of high TOU cost and charge the ESS during low-cost periods. To use more the ESS to compare with the results of the optimization, the ESS is forced to charge during the plane hours at the middle of the day profiting from possible high PV production. The SOC limits are respected in the baseline case. The baseline profile doesn’t profit from the maximum power of the ESS to maintain a discharge for the whole period of peak hours. This will impact negatively the reduction of peak consumption. Fig. 3.20 shows the ESS schedule proposed in the baseline case with its corresponding SOC. The energy used by the ESS exceeds the two cycles per day and it is equal at the end of the day to 4.62 MWh which is higher than the energy used by the batteries in the constrained optimization used along with the LSTM forecast.

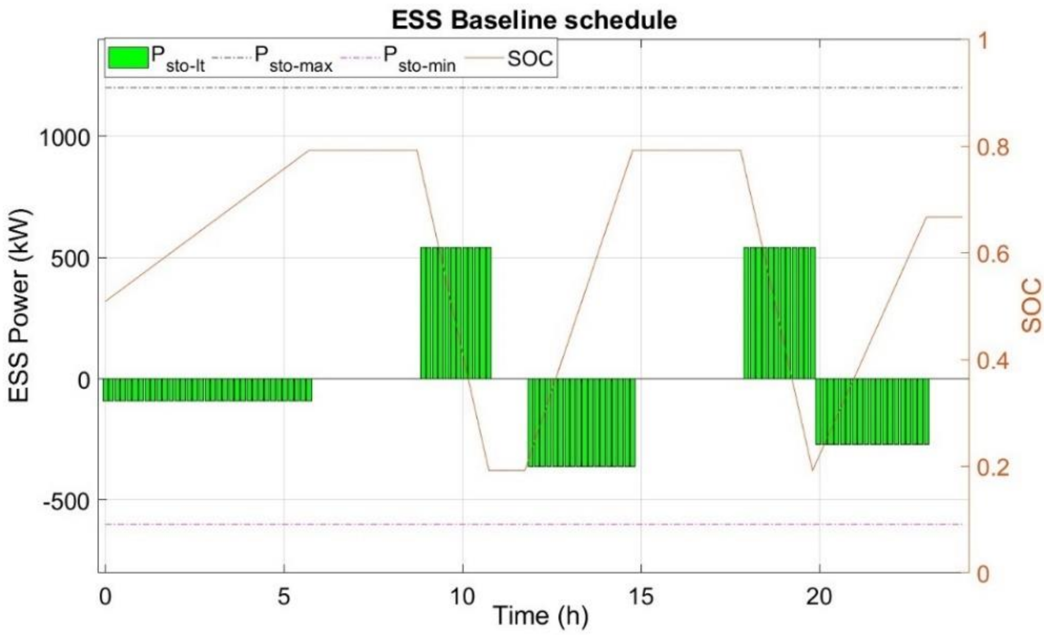


*Fig. 3.20 Proposed baseline schedule of the ESS.*

The histograms of Fig. 3.21 display the percentage decrease in CMDPS costs for two specific days using baseline schedule, LSTM1 with optimization schedule, and LSTM2 with optimization schedule with reference to the base to th case where there is no ESS and PV at the substation as shown in Equation (3.18). In Day 1, the LSTM2 followed by optimization provides the highest percentage decrease in the CMDPS (62%) compared to the percentage decrease caused by baseline schedule (44.4%) and the LSTM1 followed with optimization (36.9%).

$$\Delta CMDPS(\%) = \frac{CMDPS_{base} - CMDPS_{scenario}}{CMDPS_{base}} \times 100 \tag{3.18}$$

CMDPS scenario is the CMDPS calculated after subjecting the ESS to the baseline schedule in the first place, then the schedule proposed by the optimization that uses the forecast of LSTM1, and finally the schedule obtained through optimization using the forecast of LSTM2.

The incapability of detecting peak consumption in the LSTM1 has made the baseline more performative in reducing the penalties. This suggests that LSTM1's less accurate peak load forecasting results in suboptimal ESS scheduling, causing frequent excess of power limits. LSTM2, although exhibiting higher overall forecasting errors, achieves better peak demand detection, leading to a significant reduction in penalties. The optimization cases are always better in terms of respecting the ESS cycles per day and the ESS use less energy. This responds to the objective of prolongating the life span of the batteries.

In Day 2, the day with higher overruns of subscribed power, LSTM1 shows a 36.6% decrease in CMDPS costs while LSTM2 reduces penalties by 48.8%, demonstrating its improved peak prediction capabilities. Both LSTM models in this day were more adaptable to the objective of reducing the penalty costs than the baseline schedule, that reduced the penalties by 30%.

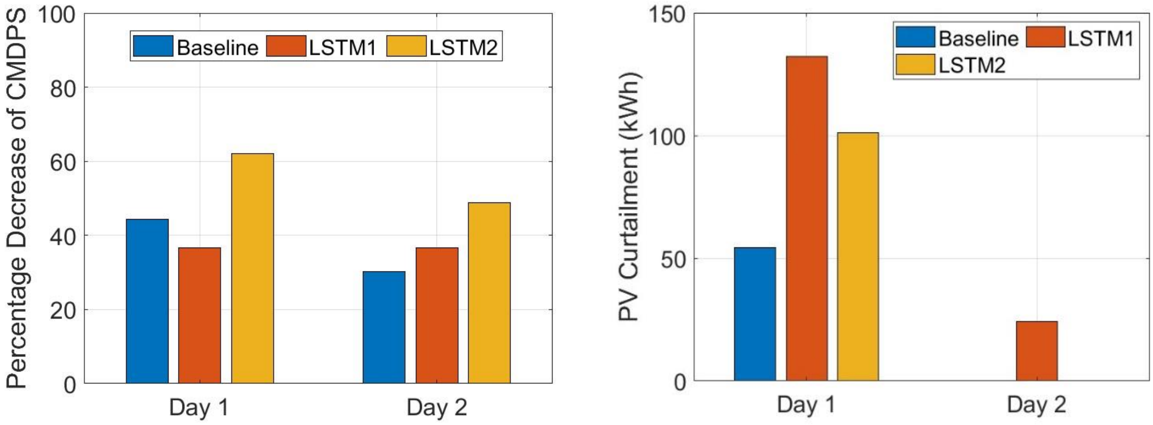


*(a) CMDPS gains* *(b) PV curtailment*

*Fig. 3.21 Percentage of decrease in CMDPS costs and amount of curtailed PV energy when transitioning from the case without ESS and PV to the baseline, LSTM1, and LSTM2.*

For the PV curtailment, the baseline schedule forced the charge of the ESS at mid-day where the PV production is at its highest, for this reason it is rare to find an excess of PV production considering the limited size of the PV system. In both days, the LSTM2 has less curtailed power than LSTM1, therefore it is the method that serves better the objective of maximizing the use of renewable production.

These results highlight the trade-offs between forecast accuracy and CMDPS penalties, with peak detection playing a crucial role in minimizing excessive charges and ensuring optimal ESS utilization. This makes the weighted LSTM method more suitable for the application, than the simple LSTM that has relatively lower errors than the weighted LSTM. The ability of detecting the peak consumption in the forecast is beneficial for the railway grid operator and offers a solution to limit the penalties when followed with a day ahead optimized schedule.

## 3.9 Conclusion

The proposed EMS was developed as a solution for the energy supervision of a wayside ESS connected at the DC bus of a railway traction substation. It relies on day-ahead forecasts of TSS electrical power consumption, combined with a nonlinear optimization algorithm that determines the optimal ESS schedule adapted to the predicted load profile. Two LSTM-based forecasting methods were implemented with a 10-minute time step, which better reflects the variability of TSS demand and aligns with the 10-minute resolution of subscribed power penalties. These methods require only historical consumption data and achieve small deviations from the reference case, which represents the most optimal solution. The nonlinear optimization framework effectively handled the system's nonlinear constraints and proved robust across multiple TSS load profiles, demonstrating adaptability to operational variations.

The improvement in forecasting accuracy significantly reduced CMDPS penalties compared to the baseline schedule, while also supporting the integration of renewable energy by minimizing PV curtailment more effectively than the simple LSTM model. Overall, this chapter highlighted the critical role of accurate TSS load forecasting in enhancing EMS performance within a smart grid environment. The proposed EMS achieved performance close to the optimal solution while offering a practical and robust strategy for managing ESS operation at DC substations.

# Chapter 4. Development of real time energy supervision for two architectures of RACCOR-D

## 4.1 Introduction

In the previous chapters, the hybrid energy management strategy of the RACCOR-D project was established. The supervision strategy explained in Chapter 2 covers two levels: day ahead EMS, where forecasts of traction substation (TSS) consumption and photovoltaic (PV) production were combined with a nonlinear optimization model to generate an optimal schedule for the energy storage system (ESS) for the next 24 hours. Followed with a real time supervision based on fuzzy logic method (FL) to provide real time reference setpoints to the ESS considering actual measurement from the railway network and the day ahead planning.

Chapter 2 benchmarked existing energy management and supervision methods and introduced the development of a fuzzy logic (FL) supervisor. For RACCOR-D, FL was chosen as the most suitable complement to the day-ahead EMS (Chapter 3) because it is robust, interpretable, computationally efficient, and able to adapt in real time to uncertainties without full system observability

This chapter therefore moves from the conceptual design of fuzzy logic supervision (Chapter 2) to its application for real-time supervision within the RACCOR-D architectures. The real-time supervisor dynamically sends reference setpoints to the ESS aiming to:

- Limit subscribed power overruns (CMDPS),
- Maximize PV self-consumption,
- Maintain battery state of charge (SOC) within safe limits,
- Achieve cost reduction of energy bill,
- Ensure acceptable DC bus voltage level.

The following sections present how the fuzzy logic supervisor is designed, describe the chosen input and output variables, and analyse its performance through simulations under different operating conditions (weekday vs. weekend profiles, sunny vs. cloudy PV production). In this way, Chapter 4 demonstrates the added value of fuzzy logic as the short-term supervisory layer that complements day-ahead optimization and enhances the overall resilience of the railway smart grid.

## 4.2 Design of the real time supervision tool in architecture 1 of RACCOR-D

In this section, the role of the real-time supervisor within the RACCOR-D project is introduced. The supervisor is designed to ensure that the ESS operates in coordination with PV generation and TSS consumption, while respecting technical and economic objectives. Its main functions are to limit subscribed power overruns, maximize the use of local renewable energy, maintain the SOC within safe limits, and maintain the DC bus voltage within limits. To fulfil these requirements under uncertain and variable operating conditions, the fuzzy logic concept introduced in Chapter 2 is now applied. After the general methodological description of fuzzy logic, this section details the design process of the real time supervision tool developed to serve the problematic of the first RACCOR-D architecture.

### 4.2.1 Reminder of Architecture 1: Positioning of the RACCOR-D system at the substation

The configuration of Architecture 1 has already been described in detail in Chapter 2. As a reminder, the ESS and PV are connected directly to the DC bus of the traction substation, in parallel with the grid supply. The DC bus 1.5 kV aggregates the electrical contributions from the transformer–rectifier unit, the PV generation, and the ESS, and distributes power to the railway tracks, where the load corresponds to train demand. For simplicity, $P_{load}$ is here represented as a single branch, although it encompasses the aggregate demand of all connected tracks of the TSS (total demand of the TSS).

This schematic reminder in Fig. 4.1 provides the basis for applying real-time supervision. The power balance is expressed with the same variables introduced earlier:

- $P_{grid}$ is the active power drawn from the grid $P_{grid} \geq 0$
- $P_{PV}$ is the power generated by the PV system $P_{PV} \geq 0$
- $P_{load}$ is the demand of the TSS caused by trains circulation at the connected tracks $P_{load} \leq 0$
- $P_{sto}$ is the storage system power with convention: $P_{sto} > 0$ while discharging (power injected into the DC bus). $P_{sto} < 0$ while charging (power absorbed by the storage).

The negative convention is assigned for the elements that absorb power, and the positive convention is for the sources that inject power to the DC bus.

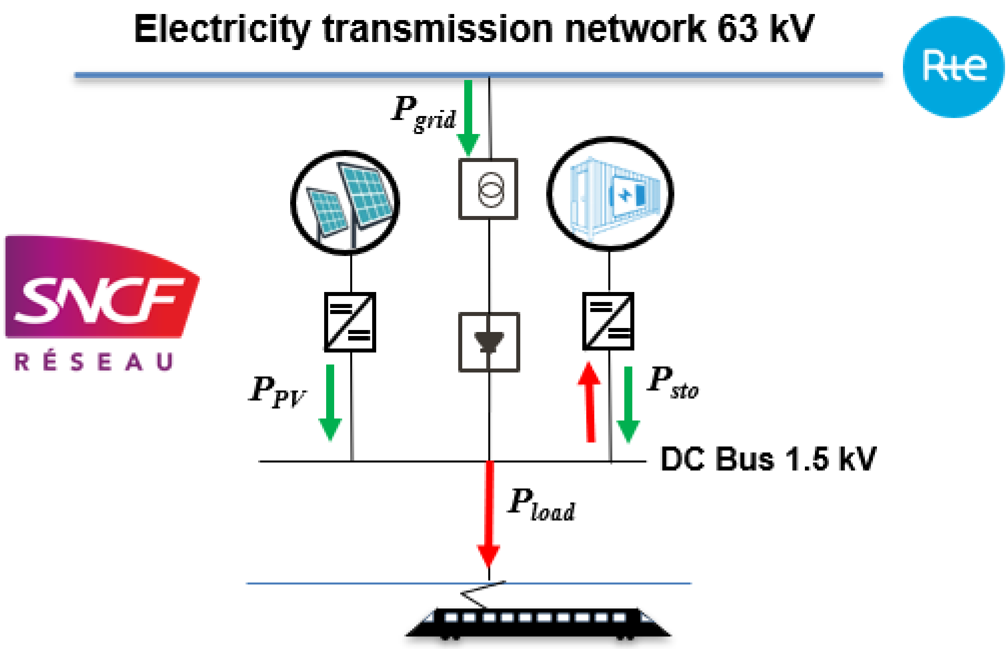


*Fig. 4.1 Simple representation of the 1st RACCOR-D architecture*

### 4.2.2 Development of the real time supervision

As detailed in Chapter 2, the supervision strategy in RACCOR-D relies on two temporal levels: a day-ahead EMS for optimal scheduling and a real-time supervisor to correct deviations caused by uncertainties and short-term variations. In the following sections, the different steps of the methodology for developing the real-time supervision are presented in the specific context of the RACCOR-D application, highlighting how the fuzzy logic concept is applied to meet both technical and economic objectives.

#### 4.2.2.1 System specifications

The French tariff structure TURPE 6 HTB1 [28] , defined by the "Commission de Régulation de l'Énergie (CRE)", governs the financial framework for high-voltage electricity consumers such as railway substations. This tariff includes both a fixed and a variable component. The fixed component is linked to the contracted subscribed power levels across seasonal and temporal periods, while the variable component covers energy usage costs and penalties for subscribed power overruns, referred to as *Composantes Mensuelles de Dépassement de Puissance Souscrite (CMDPS)*. These CMDPS are calculated with the average power drawn from the grid over 10-minute intervals exceeding the subscribed power, using a quadratic penalty formula [28] . In this study, consumption always refers to the TSS demand, derived from historical grid withdrawal data. The economic objective behind the developed supervision tool is therefore twofold: minimize the cost of energy drawn from the grid and reduce CMDPS-related penalties.

While the day-ahead supervision based on TSS consumption and PV production forecast optimizes a 24-hour battery schedule to achieve these objectives, it inherently suffers from limitations due to forecast errors, particularly underestimating short-duration peaks. In case of TSS demand, deviations between forecast and real consumption are often caused by train timetable shifts, and trains circulation delays. For PV production, meteorological uncertainties such as cloud cover, temperature, and irradiance fluctuations lead to differences between predicted and actual generation. As a result, real-time supervision becomes essential to dynamically respond to deviations in load profiles and PV consumption to maintain an economic objective in real time under the uncertainties.

The real time supervisor acts in this context by generating a new storage system's power setpoints in real time denoted $P_{ref\_st}$ to limit unforeseen consumption peaks and thus reduce CMDPS charges. Also, it must profit from the day ahead ESS schedule to minimize the use of public grid during high time of use of the electricity transmission network cost periods. The real time supervisor follows the day ahead schedule when no deviation between actual and predicted TSS power happen in real time and anticipate in case of necessity (e.g. peak consumption not predicted by the forecast and not seen by the day ahead supervision, or unplanned excess of PV production).

Another objective is to maximize the use of the PV production, which will lead to the maximum economic gain translated in minimizing the power drawn from the electricity transmission network and therefore minimizing the $Electricity\_cost$ term explained in Chapter 3. Similar to the day ahead, the real time supervisor aims to charge the ESS with the surplus of PV production instead of curtailing the excess power since the railway network TSS is unidirectional with transformer rectifier unit that doesn't allow any power to be injected to the grid side.

Unlike the economic objectives, which are already addressed in the day-ahead EMS and then adjusted in real time under uncertainty, maintaining the DC bus voltage within acceptable limits is not considered at the day-ahead stage. This technical objective is therefore handled exclusively by the real-time supervisor. Yet maintaining the voltage within its operational bounds, typically inside an acceptable margin of voltage variation not without overpassing the critical low and high voltage levels is crucial for ensuring the safe and efficient operation of the traction substation. This responsibility falls exclusively to the real-time supervisor, which adjusts the ESS charge/discharge behaviour based on voltage deviations.

The real time supervisor aims to treat the previous objectives while respecting several constraints for the ESS. In the day ahead supervision, the ESS constraints are related to:

- The maximum charge/discharge power of the ESS
- SOC level within minimum and maximum limits
- Number of ESS cycles per day

The real time supervision ensures that the same constraints are respected in real time. When the real time schedule deviates from the day-ahead schedule to deal with the uncertainties and in case of necessities as explained earlier, it must respect the ESS constraints throughout the day. Limiting the SOC of the battery between $SOC_{min}$ and $SOC_{max}$ (20% and 80%) is crucial to preserve the operational availability and longevity of the storage unit. The SOC limits values are imposed by the fabricant and provider of the ESS. In addition, the battery manufacturer recommends limiting the charge and discharge power to no more than half of the ESS capacity. For the considered DC TSS, with a storage capacity of 2.4 MWh, this corresponds to a maximum charging and discharging power of $P_{sto-max}$ to be 1.2 MW. These limits are also imposed by the size of DC-DC converter unit connecting the ESS to the DC bus, the power exchanged between ESS and DC bus must respect the rated power of the converter.

The number of daily cycles represents another critical constraint, as frequent cycling accelerates battery aging and reduces lifetime. The cycling constraint is not recommended by battery provider, instead it is chosen to be 2 cycles per day similar to the case of the day ahead supervision in Chapter 3. A cycle is defined as the cumulative energy required to fully charge the ESS from $SOC_{min}$ to $SOC_{max}$, followed by a full discharge from $SOC_{max}$ back to $SOC_{min}$.

In practice, a cycle can be calculated as:

$$N_{cycles} = \frac{E_{ch} + E_{disch}}{2 \cdot (E_{SOC-max} - E_{SOC-min})} \tag{4.1}$$

where:

- $E_{ch}$ is the total energy charged during the considered period,
- $E_{disch}$ is the total energy discharged,
- $E_{SOC-min}$ energy corresponding to the minimum SOC,
- $E_{SOC-max}$ energy corresponding to the maximum SOC,
- The usable capacity of the battery is therefore $E_{SOC-max} - E_{SOC-min}$.

Additional constraints are therefore considered in real time supervision related to the DC voltage, the voltage at the DC bus must stay in a range between two defined values:

- $V_0$ : represents the maximum voltage level that the DC bus cannot exceed
- $V_{crit}$ : represents the critical voltage level that the DC bus voltage cannot go below it.

Finally, the subscribed power $P_{sub}$, defined from the tariffication arrangement between SNCF réseau and RTE. $P_{sub}$ is the subscription power value that in case the SNCF réseau TSS power drawn from RTE network exceeds this value penalties will be paid in the form of CMDPS components. Table 4.1 shows the summary of the specification of the supervision system.

*Table 4.1 System specification of the supervision tool for both levels (day-ahead and real time)*

| Objectives | Constraints | Means of action |
|---|---|---|
| **Day ahead supervision (long term)** | | |
| • **TSS energy costs minimization**<br>Following the TURPE 6 HTB1 tariffication for TOU and CMDPS<br>Maximizing the use of PV for minimizing the electricity consumption costs | • SOC limits ($SOC_{min} \leq SOC \leq SOC_{max}$)<br>• Nb of ESS cycles<br>• End of day SOC of the ESS<br>• Unidirectional TSS<br>• Errors in the forecast | $P_{ref\_lt}$ |
| **Real time supervision (short term)** | | |
| • **To maintain the SOC within min and max limits**<br>• **To keep the DC voltage within an authorized range**<br>• **To maximize PV self-consumption**<br>• **To limit subscribed power overruns** | • ESS constraints:<br>o SOC limits ($SOC_{min} \leq SOC \leq SOC_{max}$)<br>o ESS power < $P_{sto\_max}$<br>o Nb of cycles per day<br>• Voltage at the DC bus<br>o $V_{crit} < V_{DC} < V_0$<br>• Availability of PV production<br>• Subscribed power $P_{sub}$ | $P_{ref\_st}$ |

#### 4.2.2.2 Supervisor structure

Once the objectives of the real-time supervision have been identified, it becomes necessary to structure the supervisor in order to translate these objectives into actionable control signals. The real time supervisor is developed using fuzzy logic, which dynamically adjusts the power setpoint of the energy storage system (ESS) based on a set of representative input variables. These variables are derived from real-time measurements available in the railway network and are normalized to ensure consistent processing within the fuzzy inference system.

Each input is therefore directly associated with one or more supervision objectives or constraints: SOC for the respect of storage limits, $\Delta V_{DC}$ (deviation of the DC bus voltage from the nominal voltage) for voltage stability and supports PV self-consumption purposes, $\Delta P_{ovr}$ (overrun of the subscribed power) for the reduction of subscribed power overruns, $P_{ref\_lt}$ for maintaining consistency with the day-ahead schedule, and $\Delta SOC$ improves tracking of end-of-day SOC and cycle constraints. In this way, the structure of the supervisor directly reflects inputs and output used to serve achieving the objectives behind the real time supervision.

The real-time supervisor is built around five input variables and one output variable:

- State of charge (SOC): The SOC provides the supervisor with a direct measurement of the available storage level. This information is essential for the supervisor to generate control actions that keep the ESS within operational limits, thereby avoiding saturation and ensuring long-term reliability
- Voltage deviation $\Delta V_{DC}$: This input reflects the deviation of the DC bus voltage from its nominal value:

$$\Delta V_{DC} = V_{DC} - V_n \tag{4.2}$$

  Where $V_{DC}$ is the measured voltage at the DC bus, and $V_n$ is the nominal voltage value, identified as a middle value between the maximum and minimum voltage levels.
  The supervisor uses this signal to address two complementary objectives:
  - Maintain the DC bus voltage within acceptable limits: When $V_{DC}$ approaches the no-load voltage $V_0$ (while the TSS demand exist), local generation exceeds demand, creating overvoltage risk. And when $V_{DC}$ approaches a critical minimum voltage level $V_{crit}$, supply is insufficient and corrective action is required.
  - Maximize PV self-consumption: A DC bus voltage close to $V_0$ also implies that the local power ($P_{PV}$ + $P_{sto}$) already covers the TSS demand, with nearly surplus energy available, in which case the ESS is charged to absorb excess PV and avoid curtailment

Since real-time measurements of TSS load are not available, the voltage deviation serves as an indirect indicator of the balance between local generation and consumption. If load data were accessible, the supervisor could instead rely directly on the comparison between $P_{load}$ and $P_{local}$ [101] . Where $P_{local}$ is the sum of ESS power and PV power.

Therefore, if real-time measurements of $P_{load}$ were available, it would be possible to directly compare them with the PV production and calculate the surplus of local power $\Delta P_{surplus}$. In that case, the supervisor could use an additional input defined as:

$$\Delta P_{surplus} = P_{PV} - P_{load} \tag{4.3}$$

A positive value of $\Delta P_{surplus}$ would indicate that PV generation exceeds the TSS demand, thus signalling an opportunity to store surplus energy and maximize self-consumption.

In our case, however, since real-time measurements of $P_{load}$ are not available, it is not possible to establish this direct comparison. For this reason, the real-time supervision does not use the PV power measurement as an explicit input. Instead, the supervisor relies on the DC bus voltage deviation $\Delta V_{DC}$, which indirectly reflects the balance between local generation and consumption and can therefore be used to guide the objective of maximizing PV self-consumption.

Fig. 4.2 Example of maximum and minimum voltage threshold with respect to the no-load voltage displays the important voltage levels that will impact on the real time supervisor's decision. First, the input variable is noted $\Delta V_{DC}$ and it will state whether the voltage is between $V_0$ and $V_{max}$, $V_{min}$ and $V_{crit}$, and when it is around the nominal voltage $V_n$ (between $V_{min}$ and $V_{max}$). In the latest, the voltage is considered within acceptable limits, unlike when it goes above

$V_{max}$ defined as a high threshold, the real time supervisor must change its behavior to deal with a potential high voltage. When the voltage is considered low when it goes below $V_{min}$.

$\Delta V_{DC}$ therefore, is considered a variable that varies from the $V_0 - V_n$ to $V_{crit} - V_n$ and it can be easily normalized with respect to its range of variation. The voltage cannot go over the no load voltage $V_0$ and not below the critical voltage $V_{crit}$. In this case $\Delta V_{DC}$ can vary from 0 (when $V_{DC} = V_n$) to 100V (when $V_{DC} = V_0$), and from 0 to -100V when (when $V_{DC} = V_{crit}$). For any value of $\Delta V_{DC}$ between -90 V and 90 V, the voltage is considered within normal operation range. Above 90 V, it is considered close to the no voltage (risk of excess of local production), and below -90 V, it is considered at minimum critical level.

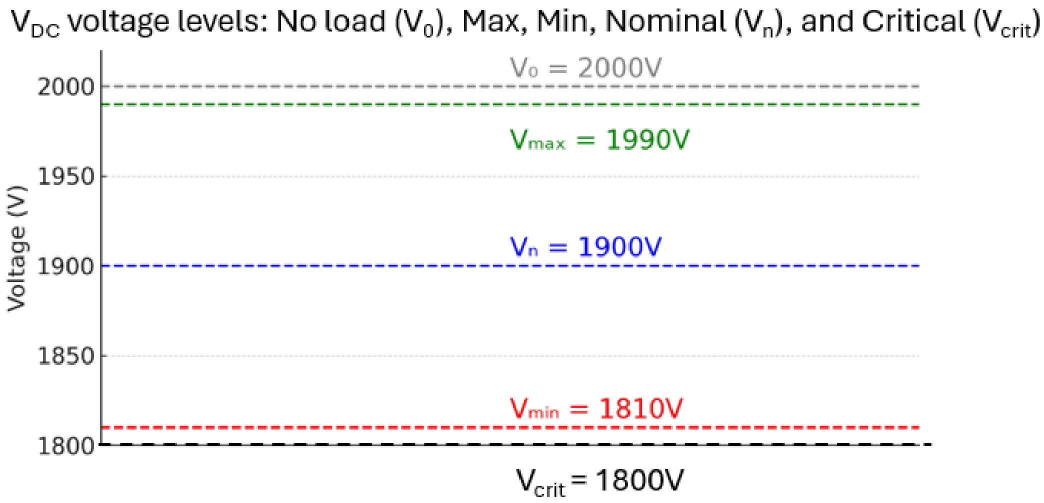


*Fig. 4.2 Example of maximum and minimum voltage threshold with respect to the no-load voltage*

- Subscribed power overrun ($\Delta P_{ovr}$): This input is critical for limiting excessive grid power usage that could trigger economic penalties. It is defined by:

$$\Delta P_{ovr} = P_{grid} - P_{sub} \tag{4.4}$$

where $P_{grid}$ is the total power drawn from the grid and $P_{sub}$ is the subscribed maximum power. When this value becomes positive, it signals a threshold breach, prompting the real-time supervisor to reduce grid dependency.

- Day-ahead ESS reference setpoints ($P_{ref\_lt}$): This input carries the pre-scheduled storage profile derived from day-ahead optimization, often based on predicted consumption and tariff signals. It ensures that the system remains aligned with economic objectives such as minimizing energy costs through time-of-use strategies.

- SOC deviation ($\Delta SOC$): Introduced to enhance the supervisor's ability to track the day-ahead plan by comparing the real-time SOC ($SOC_{st}$) with the estimated SOC derived from the day-ahead planning ($SOC_{lt}$). This input helps align real-time actions with long-term objectives, ensuring that end-of-day SOC and cycle counts remain close to the planned values. Formally, it is defined as:

$$\Delta SOC = SOC_{st} - SOC_{lt} \tag{4.5}$$

However, $\Delta SOC$ is only considered in the real-time supervisor's decision-making under normal operating conditions; it is disregarded when critical events occur, such as high DC voltage, subscribed power overruns, or SOC levels approaching their minimum or maximum limits.

The FL supervisor output variable is $P_{ref\_st}$, serves as the real-time reference power setpoint for the ESS. It integrates both long-term economic planning and short-term technical adjustments, ensuring robust operation under varying grid conditions, and responding to real time measurement, while optimizing for both performance and cost. $P_{sto}$ is the output of the energy storage considering the dynamics of the ESS in the Simulink simulation model. It will represent the actual power exchanged with the DC bus.

Fig. 4.3 Structure of the real time FL supervisor shows the real time supervisor structure. Each input is normalized with its proper normalization gain (K). The normalization gains are critical for the fuzzy logic supervisor's performance as they ensure that all input variables operate within comparable numerical ranges, typically [0,1] or [-1,1], preventing any single variable from dominating the decision-making process due to scale differences. This normalization enables proper weighting of each objective and ensures consistent fuzzy rule evaluation across all operating conditions. The output gain K6 then scales the fuzzy logic supervisor's decision back to the appropriate power reference range for the ESS, generating $P_{ref\_st}$ as the real-time setpoint that balances all operational constraints and objectives simultaneously.

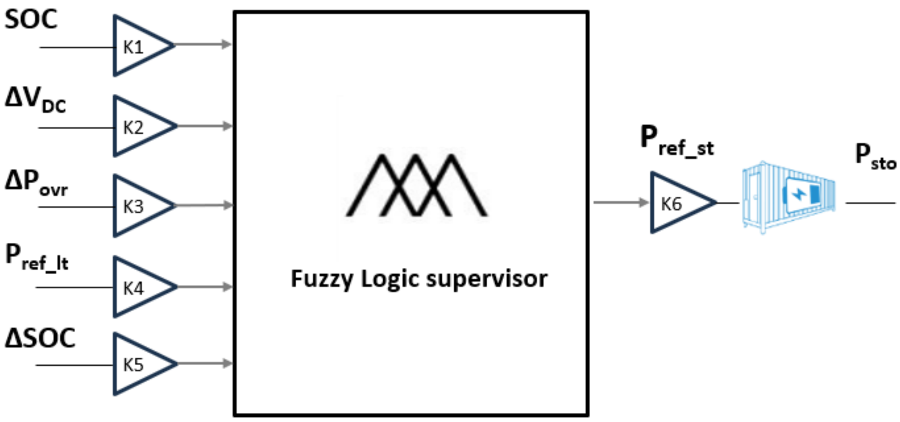


*Fig. 4.3 Structure of the real time FL supervisor*

#### 4.2.2.3 Graphical representation of the functional modes of the FL supervisor

The functional graphs provide a graphical representation of the intended behaviour of the real-time supervisor. They illustrate how the supervision strategy is designed to operate under different conditions and define the rules that govern transitions between operating modes.

Fig. 4.4 gives an overall view of the supervision logic: the supervisor changes its mode according to the SOC value. Mode M1 is activated when the SOC value is considered Medium. In this case, the storage system operates within an intermediate SOC band, typically centred around 50%, with the exact range determined by the membership functions. Within this band, the supervisor can either charge or discharge the ESS depending on the real-time conditions. The objectives in this mode are to follow the day-ahead reference setpoints under normal operation, while performing peak shaving when required and maintaining the DC bus voltage within acceptable limits.

Switching for modes M2 and M3, the same objectives are considered, however these modes additionally treat an important objective which is preventing the saturation of the ESS at high or low levels.

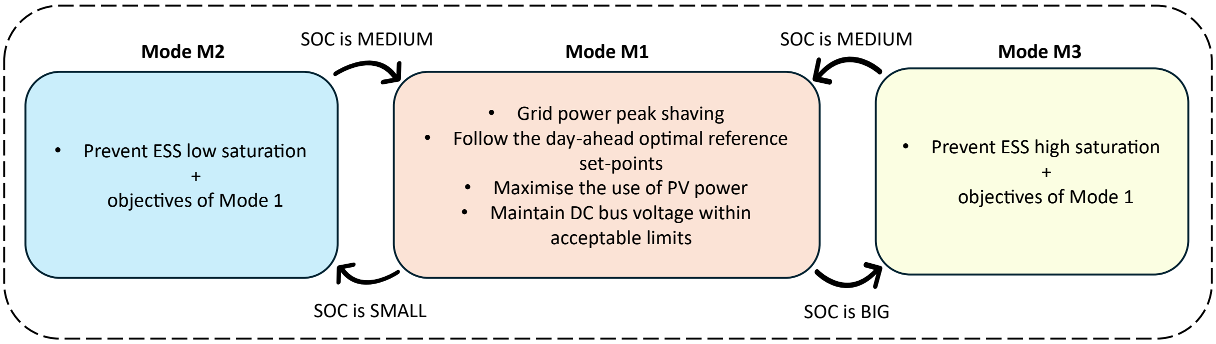


*Fig. 4.4 Global representation of the functional modes*

Fig. 4.5 shows the expanded graphical representation of mode M1 where the SOC is MEDIUM. The decision-making logic adapts based on three main real-time conditions: the DC bus voltage $V_{DC}$, the grid power $P_{grid}$, and the day-ahead reference setpoint $P_{ref\_lt}$, where a negative $P_{ref\_lt}$ implies a charging request, and a positive value corresponds to a discharging request. Through its inference mechanism, the real time supervisor decides whether soliciting the ESS in charging or discharging, and whether not soliciting the ESS. In addition to level of power used for charging or discharging. In the Fig. 4.5, 5 actions are identified:

- ESS not solicited: means that the supervisor decides to not use the ESS and no power is therefore exchanged with the DC bus.
- Medium charge: means that the supervisor will put the charge of the ESS in favour, but not with maximum power.
- High charge: means that the supervisor will ask to charge the ESS with maximum power.
- Medium discharge: means that the supervisor will put the discharge in favour with moderate power, without using maximum discharge power.
- High discharge: means that the supervisor will ask the ESS to discharge with maximum power.

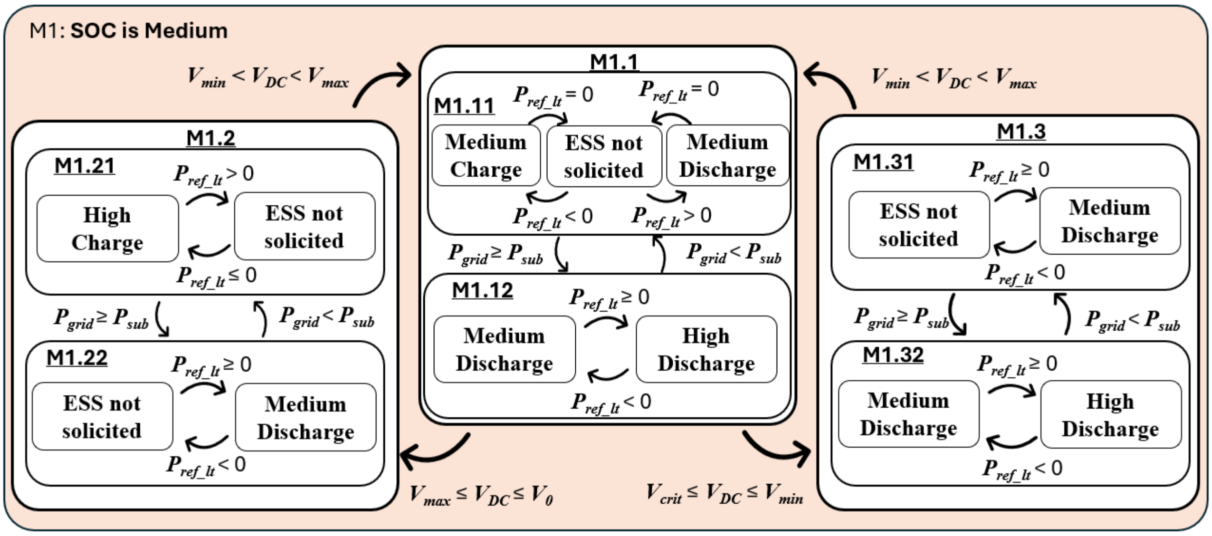


*Fig. 4.5 Functional graph for Mode M1*

In mode M1.1 the DC bus voltage is within its limits (between $V_{min}$ and $V_{max}$). If the power drawn from the grid is less than $P_{sub}$ (M1.11), the system follows the day ahead schedule without using the maximum power in charging and discharging since no event requires the use of high power. The real time supervisor is following the day ahead reference setpoints to ensure the economical objective that reduces the cost of the use of the electricity transport network. Allowing moderate charging and discharging depending on the day-ahead setpoint $P_{ref\_lt}$.

- $P_{ref\_lt}$ = 0, the real time supervisor will neither charge nor discharge.
- $P_{ref\_lt}$ > 0, the real time supervisor will discharge with moderate power.
- $P_{ref\_lt}$ < 0, the real time supervisor will charge with moderate power.

Mode M1.11 is expanded to cover the variation of $\Delta SOC$ as shown in Fig. 4.6. Addressing the objective of following the day ahead schedule as much as possible to ensure acceptable ESS cycling and end of day SOC. $\Delta SOC$ related rules exist only in mode M1.11 since this mode is where everything is considered normal at the substation. No SOC extreme values, normal voltage level, and no overrun of the subscribed power. This mode therefore enhances the follow of the day ahead. By acting as follow:

- When the day ahead reference setpoint is equal to zero (M.1.11.2), indicating that the ESS should not be solicited, the supervisor looks for the value of $\Delta SOC$.
  - If $\Delta SOC$ is equal to zero, $SOC_{st}$ is equal to $SOC_{lt}$ so the real time supervisor will decide to not solicit the ESS.
  - If $\Delta SOC$ > 0, $SOC_{st}$ is bigger than $SOC_{lt}$, the real time supervisor decides in this case to discharge the ESS with medium power (Medium discharge).
  - If $\Delta SOC$ < 0, $SOC_{st}$ is less than $SOC_{lt}$, so the supervisor decision is to charge the ESS with medium power
- When the day ahead reference setpoint is negative (charging), the real time supervisor in Mode M1.11.1 reacts as follow:
  - If $\Delta SOC \geq 0$, the supervision in real time will promote the charging of the ESS with medium power, following the day ahead reference setpoint
  - If $\Delta SOC$ < 0, the $SOC_{st}$ is smaller than $SOC_{lt}$, the supervisor decision here is to charge the ESS with high power instead of medium power.
- When the day ahead reference setpoint is positive (discharging), the real time supervisor in Mode M1.11.3 reacts as follow:
  - If $\Delta SOC$ > 0, the supervision in real time will discharge with high power instead of medium until $SOC_{st}$ becomes near or equal $SOC_{lt}$.
  - If $\Delta SOC \leq 0$, the $SOC_{st}$ is smaller than $SOC_{lt}$, the supervisor decision here is to discharge the ESS with medium power.

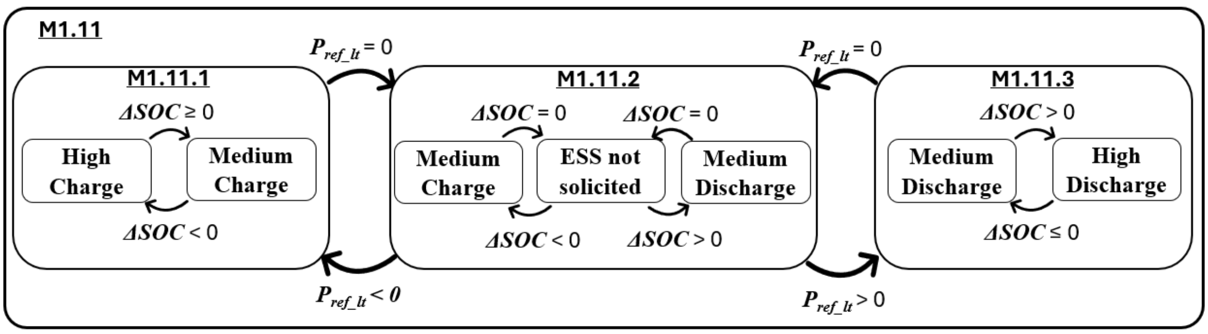


*Fig. 4.6 Extended graphical representation of mode M1.11*

In mode M1.12, the power drawn from the grid is equal or higher than the subscribed power $P_{sub}$, the priority for the supervisor is to discharge the ESS. For this reason, only two actions can be seen no matter what the value of the day ahead setpoint: either discharging with medium power or discharging with high power.

- $P_{ref\_lt}$ < 0, the real time supervisor will discharge the ESS with medium power (Medium Discharge)
- $P_{ref\_lt}$ ≥ 0, the real time supervisor will discharge the ESS with high power (High Discharge).

The medium discharge is proposed when the M1.12 occurs and $P_{ref\_lt}$ is negative, responding to two objectives at the same time: to limit the overrun of the subscribed power, so ESS must discharge with high power. To prevent the ESS to be far from the day ahead plan, discharging with medium power only when the day ahead is indicating negative values.

Mode M1.2 is activated when the DC bus voltage is higher than the upper voltage threshold $V_{max}$. In this situation, the supervisor will prioritize battery charging to absorb excess PV generation and prevent overvoltage conditions. If the power drawn from the grid is less than the subscribed power, the sub-mode M1.21 is active, and the supervisor decides between medium and high charging depending on the $P_{ref\_lt}$ value.

- $P_{ref\_lt}$ < 0, the real time supervisor will charge the ESS with high power.
- $P_{ref\_lt}$ ≥ 0, the real time supervisor will not follow the day-ahead one in discharging and it will not solicit the ESS if the day ahead decision was zero.

However, in sub-mode M1.22 the power drawn from the grid is higher or near the subscribed power. The storage must discharge to limit the peak grid consumption preventing any increase in the power drawn from the grid. At the same time, the supervisor decision cannot violate the voltage threshold $V_{max}$. For this reason, unlike in mode M1.12, when the voltage was between $V_{min}$ and $V_{max}$, and the supervisor forces the discharge regardless of what $P_{ref\_lt}$ indicates. M1.22 has two possible actions:

- ESS not solicited if $P_{ref\_lt}$ < 0 (charging).
- Medium discharge if $P_{ref\_lt}$ is ≥ 0 to limit the peak grid consumption.

Mode M1.3 is activated when the DC bus voltage $V_{DC}$ is lower than the low voltage threshold $V_{min}$. The real time supervisor will prioritize the discharge of the ESS, by injecting the DC with ESS power to maintain the voltage level within acceptable range between $V_{min}$ and $V_{max}$. The charging of the ESS is not possible in this case. The supervisor decision is between three possible actions: ESS not solicited, ESS discharge with medium power, ESS discharge with high power.

When the power drawn from the grid is less than the subscribed power $P_{grid} < P_{sub}$, Mode M1.31 controls the supervisor's output:

- ESS is not solicited if $P_{ref\_lt}$ < 0. The supervisor will not follow the day ahead reference setpoint in this case.
- ESS discharge with medium power (Medium Discharge) when $P_{ref\_lt}$ ≥ 0. The real time supervisor follows the day ahead setpoint if is positive. If $P_{ref\_lt}$ is zero, the real time supervisor proposes a medium discharge deviating from the day ahead reference setpoints to respond to the voltage objective.

Mode M1.32 is active when $P_{grid} \geq P_{sub}$, the only decision for the supervisor to make is to discharge the ESS in order to reduce the power drawn from the grid and limit the overrun of the subscribed power. Therefore, its decision is between medium discharge and high discharge depending on $P_{ref\_lt}$.

Fig. 4.7 shows the fuzzy logic supervision strategy under Mode M2, which is activated when the SOC of the energy storage system is SMALL. In this context, the supervisor prioritizes charging actions and restricts discharging operations to protect the battery and ensure energy availability for future demand peaks.

In Mode M2.1, which is active when $V_{min} < V_{DC} < V_{max}$, the supervisor seeks to follow the day-ahead plan while respecting the low SOC constraint. Two sub-modes are distinguished depending on the grid power relative to the subscribed power.

Sub-mode M2.11 is active when $P_{grid} \leq P_{sub}$:

- If $P_{ref\_lt} > 0$, the supervisor does not solicit the ESS. This decision differs from the day-ahead plan, which would suggest discharging the ESS.
- If $P_{ref\_lt} = 0$, the supervisor favours charging the ESS with medium power, deviating from the day-ahead setpoint.
- When $P_{ref\_lt} < 0$, the supervisor aligns with the day-ahead plan and proposes charging the ESS at high power.

Sub-mode M2.12 when $P_{grid} > P_{sub}$ leads to a conflict of objectives: the supervisor must both limit the subscribed power overrun by discharging the ESS and ensure that the SOC remains above its minimum permitted level.

- If $P_{ref\_lt} > 0$, the supervisor proposes discharging the ESS with medium power. This mitigates the power overrun while avoiding excessive discharge that could reduce the SOC below the allowed minimum.
- If $P_{ref\_lt} \leq 0$, the supervisor prohibits ESS charging. Unlike in M2.11, charging is prevented here because it would further increase the grid power overrun by adding to the demand.

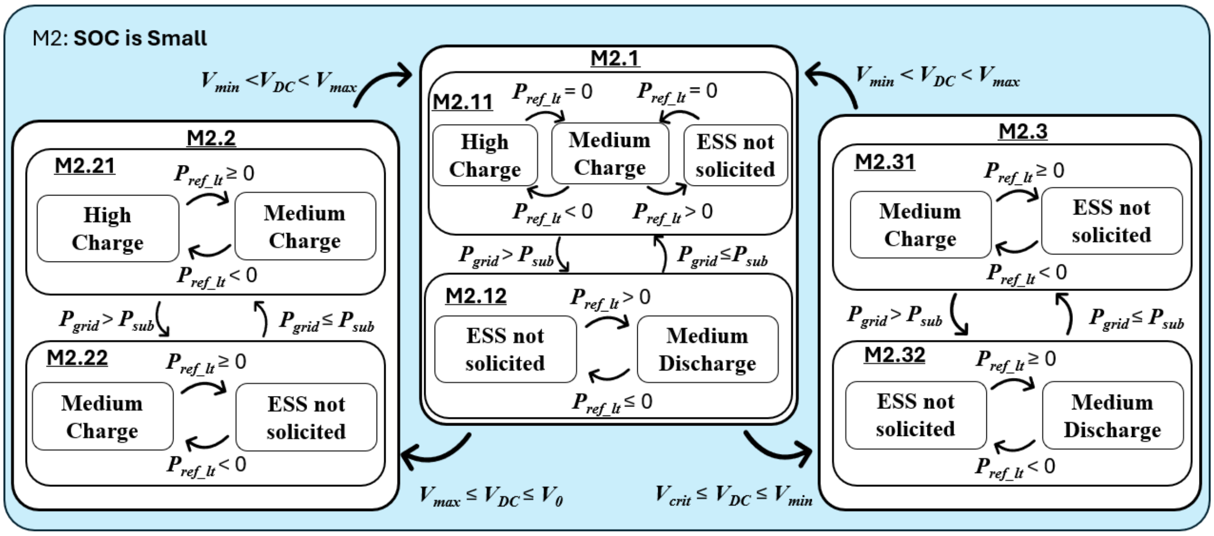


*Fig. 4.7 Functional graph for Mode M2*

Mode M2.2 is triggered when $V_{max} \leq V_{DC} \leq V_0$, favouring charging operations. In M2.21, if $P_{grid} \leq P_{sub}$, the system performs high or medium charging depending on the value of $P_{ref\_lt}$.

- $P_{ref\_lt}$ < 0, the real time supervisor will charge the ESS with high power.
- $P_{ref\_lt}$ ≥ 0, the real time supervisor will not follow the day-ahead, it will force the charge of the ESS instead with medium power.

When the power drawn from the grid overruns the subscribed power $P_{grid} > P_{sub}$, M2.22 limits charging to medium or suspends it entirely.

- $P_{ref\_lt}$ < 0, the real time supervisor will charge the ESS with medium power responding to the low SOC and high voltage levels.
- $P_{ref\_lt}$ ≥ 0, the real time supervisor will not solicite the ESS.

On the other hand, Mode M2.3 applies when the $V_{crit} \leq V_{DC} \leq V_{min}$, typically a condition where charging could worsen the situation of $V_{DC}$. In M2.31, if the grid is not overloaded, the system may perform medium charging or remain idle depending on $P_{ref\_lt}$.

- $P_{ref\_lt}$ < 0, the real time supervisor will charge the ESS with medium power. Favouring the charge of the battery with intermediate power respecting the low voltage level.
- $P_{ref\_lt}$ ≥ 0, the real time supervisor will not discharge in response to the limited stored energy at small SOC and absence of overrun of the subscribed power grid condition.

However, in M2.32, which deals with grid subscribed power overrun $P_{grid} \geq P_{sub}$, no charging is permitted regardless of the day-ahead setpoint, thus enforcing a decision between not soliciting the ESS or medium discharge to reduce the power drawn from the grid.

- $P_{ref\_lt}$ < 0, the real time supervisor will not charge the ESS in order to prevent any further power withdrawal from the grid.
- $P_{ref\_lt}$ ≥ 0, the real time supervisor will discharge the ESS with medium power, limiting grid power overrun.

This structured supervisory logic ensures that the storage system behaves conservatively under small SOC conditions, favouring recovery of energy in the ESS and preventing its saturation at low levels, while still adapting to grid and voltage constraints in real-time. While taking into consideration to a certain level the day ahead planning.

Mode M3, activated when the SOC of the storage system is high, is shown in Fig. 4.8. In this mode, the supervisor prioritizes discharging to avoid battery saturation and to keep capacity available for future surplus energy.

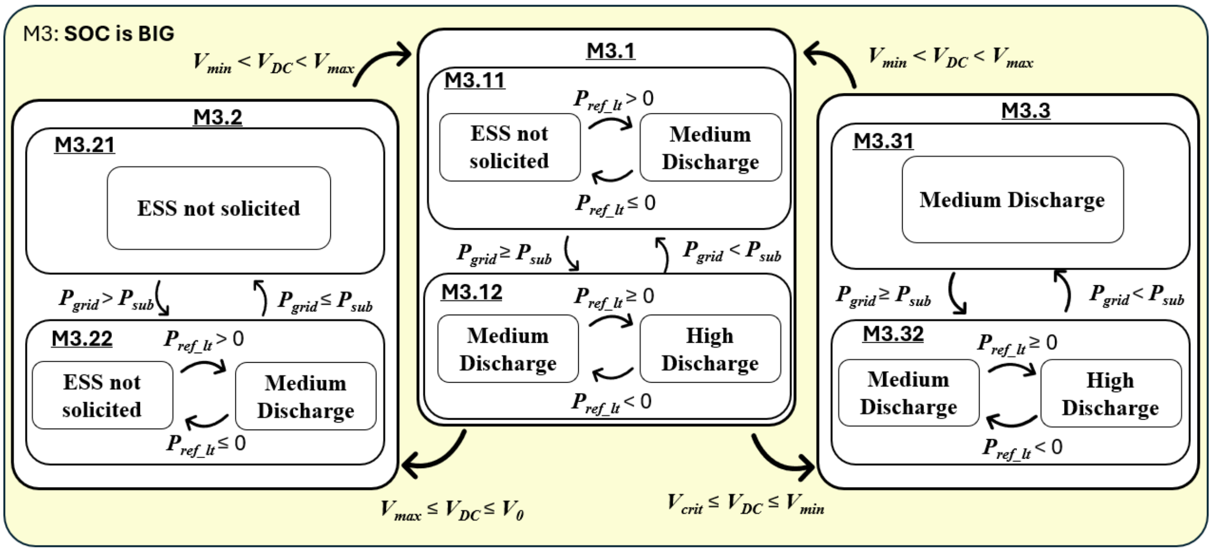


*Fig. 4.8 Functional graph of mode M3*

- M3.1 (Normal voltage, $V_{min} < V_{DC} < V_{max}$) :
  - If $P_{grid} < P_{sub}$,: the ESS discharges at medium power when $P_{ref-lt} > 0$,, otherwise it remains idle.
  - If $P_{grid} \geq P_{sub}$: the ESS discharges at high power when $P_{ref-lt} \geq 0$, and at medium power when $P_{ref-lt} < 0$.
- M3.2 (High voltage, $V_{max} \leq V_{DC} \leq V_0$):
  - If $P_{grid} \leq P_{sub}$: the ESS is not solicited.
  - If $P_{grid} > P_{sub}$: the ESS provides medium discharge when $P_{ref-lt} \geq 0$; otherwise, it remains idle.
- M3.3 (Low voltage, $V_{crit} \leq V_{DC} \leq V_{min}$):
  - If $P_{grid} < P_{sub}$: the ESS provides medium discharge regardless of $P_{ref-lt}$.
  - If $P_{grid} \geq P_{sub}$: the ESS discharges at medium power when $P_{ref-lt} < 0$, and at high power when $P_{ref-lt} \geq 0$.

#### 4.2.2.4 Membership Functions

In the proposed fuzzy logic supervisor, membership functions provide the interface between crisp (precise numerical value) input measurements and the fuzzy inference system. Each input variable of the supervisor, $SOC$, $\Delta V_{DC}$, $\Delta P_{ovr}$, $\Delta SOC$, and $P_{ref\_lt}$, is normalized and associated with fuzzy sets defined by membership functions. These fuzzy sets translate quantitative input values into qualitative, linguistic categories (SMALL, MEDIUM, BIG; NEGATIVE, ZERO, POSITIVE…), thereby enabling the supervisor to interpret system states in terms that align with expert knowledge and operational priorities.

Fig. 4.9 illustrates the membership functions for both input and output variables of the supervisor. On the y-axis, each label denotes the degree of membership (μ) corresponding to a specific variable.

The linguistic categories are carefully designed to reflect the operational ranges and critical thresholds of the system. For example, the SOC is divided into three fuzzy sets: S, M, and B

(SMALL, MEDIUM, BIG) respectively. Each function is linked with one of the three modes explained earlier in the functional graphs M1, M2, and M3.

- The fuzzy sets ‹‹ S ›› and ‹‹ B ›› are set to ensure the SOC level between minimum and maximum limits. Where the supervisor aims to prevent the saturation of the ESS at high and low levels.
- The fuzzy set ‹‹ M ›› is used to limit the subscribed power overrun, follow the day-ahead planning when needed, store the excess of PV production in the ESS.

$P_{ref\_lt}$ is categorized into three fuzzy sets defined by three membership functions as shown in Fig. 4.9 in $\mu P_{ref\_lt}$ graph. $P_{ref\_lt}$ belongs to the negative set ‹‹ N ›› when the ESS is in charging phase based on the day ahead planning ($P_{ref\_lt} < 0$). It belongs to the positive set ‹‹ P ›› when the day ahead setpoint $P_{ref\_lt} > 0$, indicating a discharge of the ESS. Finally, it belongs to zero set ‹‹ Z ›› when the day ahead decision is to not solicit the ESS and has zero power exchanged with the railway TSS ($P_{ref\_lt} = 0$).

The input variable $\Delta V_{DC}$ is mapped into three fuzzy sets. Negative ‹‹ N ››, Zero ‹‹ Z ››, and Positive ‹‹ P ›› which correspond to undervoltage, normal operation, and risk of overvoltage conditions, respectively. $\Delta V_{DC}$ is considered positive when there is a big positive deviation and negative when there is a big negative deviation, otherwise it belongs to the zero set that represent the acceptable voltage operation bounds.

The partitioning of $\Delta V_{DC}$ into these three fuzzy sets enables the supervisor to detect critical operating points overvoltage near $V_0$ or undervoltage near $V_{crit}$ while maintaining normal operation within the Zero set.

Similarly, for $\Delta P_{ovr}$ and $\Delta SOC$, the membership functions are divided into three sets Negative ‹‹ N ››, Zero ‹‹ Z ››, and Positive ‹‹ P ›› with membership functions $\mu\Delta P_{ovr}$ and $\mu\Delta SOC$:

- The negative set indicates that the power drawn from the grid is less than the subscribed power for $\Delta P_{ovr}$ ($P_{grid} < P_{sub}$). And for the $\Delta SOC$, it means indicates that the actual SOC in real time is below the planned trajectory ($SOC_{st} < SOC_{lt}$).
- Zero set indicates that the power drawn from the grid is around the subscribed power, for $\Delta P_{ovr}$ ($P_{grid} \approx P_{sub}$). And for $\Delta SOC$, Zero indicates good alignment between the actual and planned SOC, confirming that the battery trajectory is being followed as expected.
- The positive set indicates that the power drawn exceeds the subscribed power for $\Delta P_{ovr}$ ($P_{grid} > P_{sub}$). And that the actual SOC is higher than the planned trajectory ($SOC_{st} > SOC_{lt}$), suggesting an advance in the charging profile that may require corrective discharge or reduced charging.

The output variable $P_{ref\_st}$, is also represented by membership functions, which translate the supervisor's functional actions into linguistic variables. The five output categories of the functional graphs: High Discharge, Medium Discharge, ESS not Solicited, Medium Charge, and High Charge are mapped to the corresponding membership functions. Negative-Big (NB) for high charge, Negative-Medium (NM) for medium charge, Zero (Z) for ESS not solicited, Positive-Medium (PM) for medium discharge, and Positive-Big (PB) for high discharge.

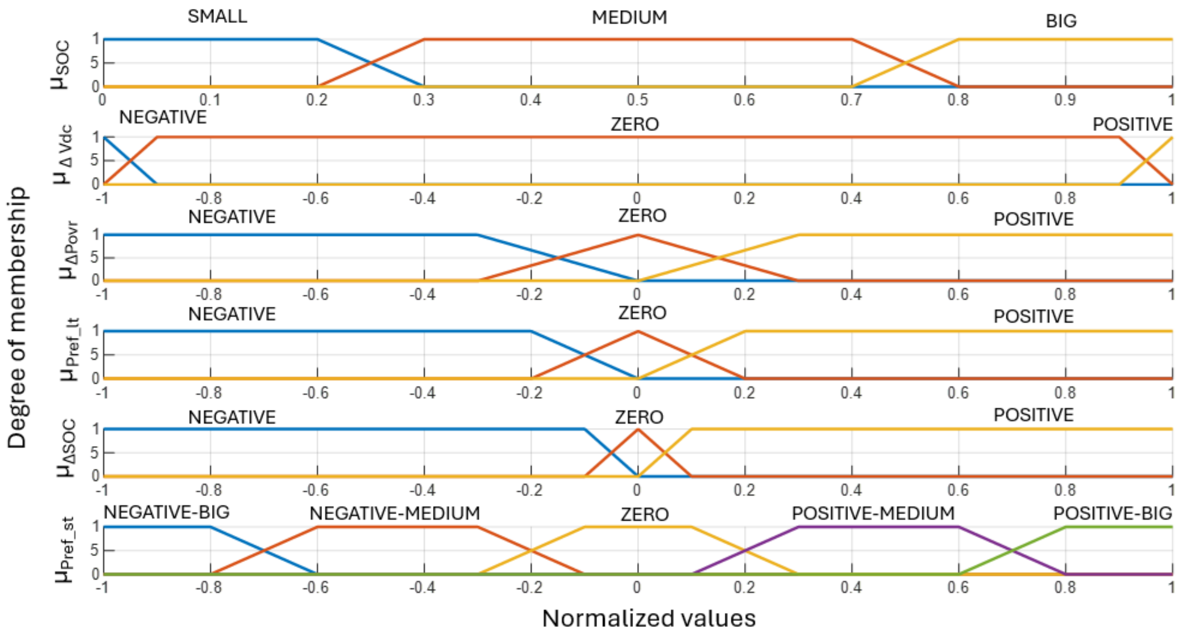


*Fig. 4.9 Membership functions of the fuzzy logic supervisor*

By mapping inputs into these fuzzy sets through trapezoidal or triangular membership functions, the system achieves smooth transitions between different operating regions, and real-time interpretability of complex system dynamics. During fuzzification, each normalized physical value of an input is assigned a degree of membership in one or more fuzzy sets, which directly determines the activation strength of the fuzzy rules in the inference engine. In this way, the membership functions form the foundation for consistent, adaptive for multiple objectives, and computationally efficient supervision of the RACCOR-D railway smart grid.

#### 4.2.2.5 Operational graphs

The operational graphs represent the transition from the functional description of the system to its concrete fuzzy logic implementation. By applying the membership functions defined earlier, the functional graphs are translated into operational graphs, which formally describe how the supervisor acts under different conditions. Each operational mode M1, M2, and M3 (with their sub-modes) corresponds to a specific regime of storage management, where the fuzzy sets of the input variables determine the system's state and trigger the corresponding control actions. In this way, the operational graphs embody the rule base of the fuzzy supervisor, ensuring that qualitative objectives such as SOC management, voltage regulation, and power overrun limitation are transformed into precise and adaptive decision rules. Fig. 4.10 – Fig. 4.13 illustrate these operational graphs for the three modes, showing the structured mapping from fuzzy sets to operational actions.

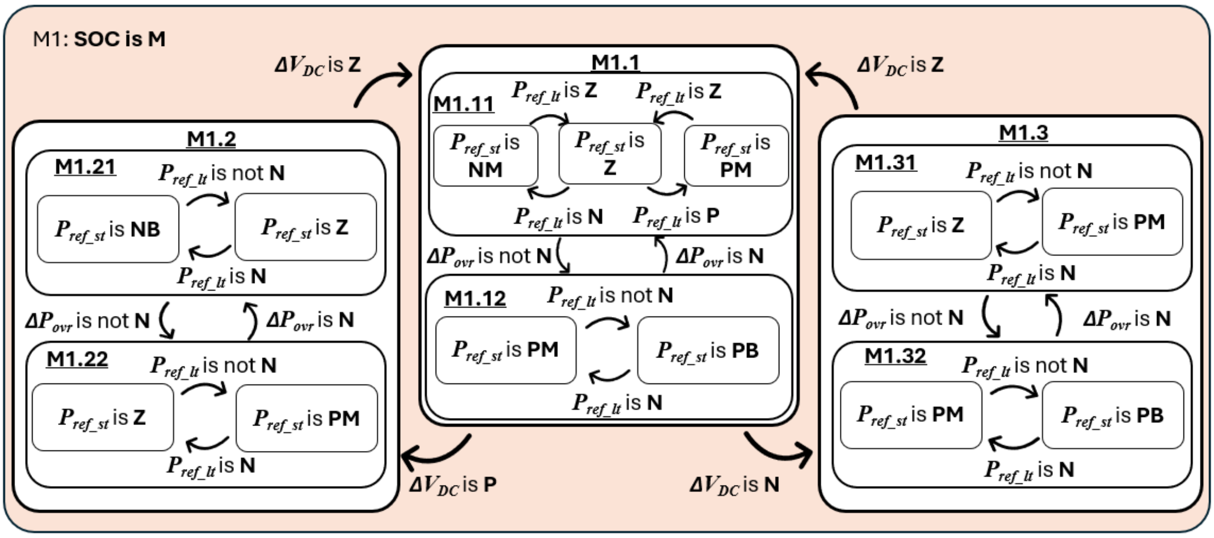


*Fig. 4.10 Operational graph for Mode M1*

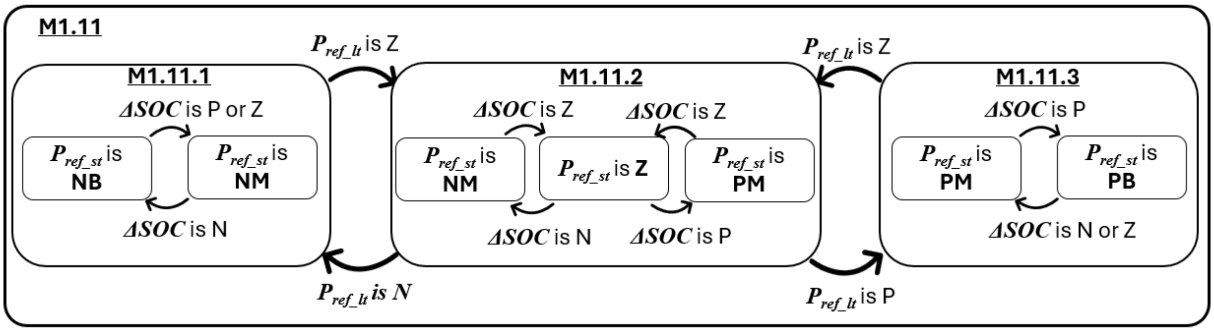


*Fig. 4.11 Extended graphical representation of operation mode M1.11*

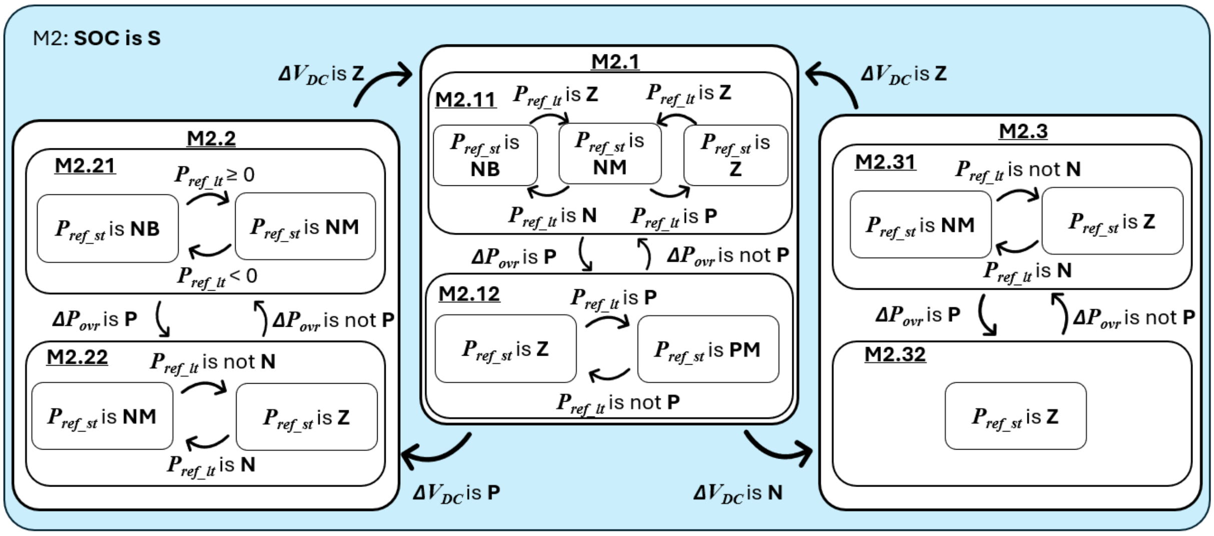


*Fig. 4.12 Operational graph for Mode M2*

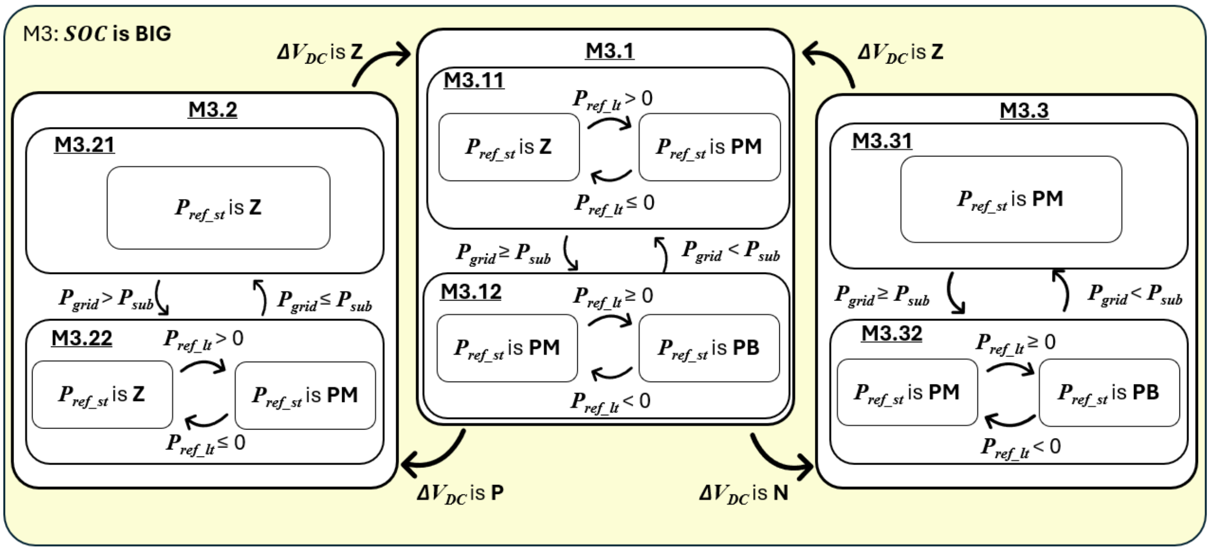


*Fig. 4.13 Operational graph for Mode M3*

#### 4.2.2.6 Fuzzy Rules

Based on the operational graphs defined for Modes M1, M2, and M3, the corresponding fuzzy rules have been systematically extracted to constitute the core of the inference engine. These rules are expressed in the standard *if–then* form, mapping combinations of fuzzy input variables: SOC (S, M, B), $\Delta V_{DC}$ (N, Z, P), $\Delta P_{ovr}$ (N, Z, P), $\Delta SOC$ (N, Z, P) $P_{ref\_lt}$ (N, Z, P) to the supervised output $P_{ref\_st}$. In doing so, the rule base formalizes the supervisor's decision logic, ensuring that real-time control actions remain consistent with both technical constraints (voltage stability, SOC limits, subscribed power) and economic objectives (PV self-consumption, penalty reduction). The resulting output fuzzy sets (NB, NM, Z, PM, PB) capture the supervisor's operational responses, ranging from strong charging (NB) to strong discharging (PB), with intermediate or idle states in between. Mode M3 generally promotes discharging at high SOC to prevent saturation, Mode M2 emphasizes charging when SOC is low to preserve storage availability, while Mode M1 balances both actions according to system needs. Table 4.2 summarizes the complete rule base, providing a transparent and interpretable foundation for the fuzzy logic supervisor to adapt dynamically under variable grid and load conditions.

*Table 4.2 Table of FL rules*

| | | | Conditions of Fuzzy Inputs | | | | | Output |
|---|---|---|---|---|---|---|---|---|
| | | Mode | SOC | $\Delta V_{DC}$ | $\Delta P_{ovr}$ | $P_{ref\_lt}$ | $\Delta SOC$ | $P_{ref\_st}$ |
| **M1** | **M1.1** | **M1.11.1** | M | Z | N | Z | Z | **Z** |
| | | | M | Z | N | Z | N | **NM** |
| | | | M | Z | N | Z | P | **PM** |
| | | **M1.11.2** | M | Z | N | N | N | **NB** |
| | | | M | Z | N | N | not N | **NM** |
| | | **M1.11.3** | M | Z | N | P | P | **PB** |
| | | | M | Z | N | P | not P | **PM** |
| | | **M1.12** | M | Z | not N | N | - | **PM** |
| | | | M | Z | not N | not N | - | **PG** |
| | **M1.2** | **M1.21** | M | P | N | not P | - | **NM** |
| | | | M | P | N | P | - | **Z** |
| | | **M1.21** | M | P | N | N | - | **Z** |
| | | | M | P | not N | not N | - | **PM** |
| | **M1.3** | **M1.31** | M | N | N | N | - | **Z** |
| | | | M | N | N | not N | - | **PM** |
| | | **M1.32** | M | N | not N | N | - | **PM** |
| | | | M | N | not N | not N | - | **PG** |
| **M2** | **M2.1** | **M2.11** | S | Z | not P | Z | - | **NM** |
| | | | S | Z | not P | N | - | **NB** |
| | | | S | Z | not P | P | - | **Z** |
| | | **M2.12** | S | Z | P | not P | - | **Z** |
| | | | S | Z | P | P | - | **PM** |
| | **M2.2** | **M2.21** | S | P | not P | N | - | **NB** |
| | | | S | P | not P | not N | - | **NM** |
| | | **M2.22** | S | P | P | N | - | **NM** |
| | | | S | P | P | not N | - | **Z** |
| | **M2.3** | **M2.31** | S | N | not P | N | - | **NM** |
| | | | S | N | not P | not N | - | **Z** |
| | | **M2.32** | S | N | P | - | - | **Z** |
| **M3** | **M3.1** | **M3.11** | B | Z | N | not P | - | **Z** |
| | | | B | Z | N | P | - | **PM** |
| | | **M3.12** | B | Z | not N | N | - | **PM** |
| | | | B | Z | not N | not N | - | **PG** |
| | **M3.2** | **M3.21** | B | P | not P | - | - | **Z** |
| | | **M3.22** | B | P | P | not P | - | **Z** |
| | | | B | P | P | P | - | **PM** |
| | **M3.3** | **M3.31** | B | N | N | - | - | **PM** |
| | | **M3.32** | B | N | not N | N | - | **PM** |
| | | | B | N | not N | not N | - | **PG** |

#### 4.2.2.7 Performance indicators

To evaluate the effectiveness of the proposed real-time supervision strategy, a set of quantitative performance indicators is introduced. These indicators aim to measure the system's economic and operational performance under the different supervision cases. The assessment includes:

- Excess local production
- ESS constraints (end of day SOC, number of cycles per day)
- CMDPS (Composante Mensuelle de Dépassement de Puissance Souscrite)
- Time of use of transport network cost
- Total energy cost

Excess local production occurs when the combined power from PV and ESS exceeds the TSS demand but cannot be exported to the grid due to the unidirectional configuration of the system. In such cases, surplus renewable energy is curtailed unless it can be absorbed by the ESS. At each time step $i$, the local production is given by:

$$P_{\mathrm{local}}(i) = P_{\mathrm{pv}}(i) + \mathrm{P}_{\mathrm{sto}}(i) \tag{4.6}$$

The excess is computed only when this local production exceeds the TSS load demand $P_{load}$:

$$P_{\mathrm{excess}}(i) = \max(P_{\mathrm{local}}(i) - P_{\mathrm{load}}(i),\ 0) \tag{4.7}$$

and the total excess energy $E_{\mathrm{excess}}$ is calculated over the whole simulation period (one day with 10-min steps):

$$E_{\mathrm{excess}} = \sum_{i=1}^{144} \frac{P_{\mathrm{excess}}(i)}{6} \quad [\mathrm{kWh}] \tag{4.8}$$

This indicator measures how effectively the system can utilize locally produced renewable energy and highlights situations where a PV curtailment occurs due to insufficient demand or storage capacity.

The energy used by the ESS is calculated via Equation (4.9), it is essential to evaluate at the end of the day the number of cycles of the ESS. When the ESS is subjected to real time supervision, the energy used by the ESS throughout the day must be kept within logical values, avoiding extensive charge and discharge.

$$E_{battery} = \sum_{t=1}^{144} \frac{|P_{\mathrm{sto}}(t)|}{6} \tag{4.9}$$

Where $P_{\mathrm{sto}}(t)$ is the average power of the ESS over 10minutes, represent as an absolute value to consider the charged and the discharged power. The division by 6 transforms the average from 10 minutes to 1 hour to obtain $E_{battery}$ in kWh.

The end of day SOC is calculated in Equation (3.10) to measure if the SOC level at the end of the day ensures certain availability of energy in the ESS.

$$SOC(end) = SOC_0 - \frac{1}{E_{sto}} \sum_{t=1}^{144} \frac{P_{sto}(t)}{6} \tag{4.10}$$

Where $E_{sto}$ is the ESS capacity expressed in kWh, $SOC_0$ is the initial SOC at the beginning of the day, and $P_{sto}$ is the power of the ESS, divided by 6 to transform the 10 minutes average.

Next, the total energy cost is evaluated using a function that aggregates three components:

- The electricity cost ($Electricity\_cost$)

$$Electricity\_cost = 0.2\sum_{i=1}^{144}\frac{P_{\text{grid}}(i)}{6} \tag{4.11}$$

Where 0.2 is the cost coefficient fixed throughout the day & $P_{\text{grid}}$ is the power drawn from the grid expressed in €/kWh.

- Time-of-use of public grid cost $TOU\_cost$ derived from $TURPE6$

$$TOU\_cost = \sum_{i=1}^{144} c_i \cdot \frac{P_{\text{grid}}(i)}{6} \tag{4.12}$$

Where $c_i$ is the variable coefficient of the tariff fir the usage of the electricity transport operator.

- The CMDPS (penalty for exceeding subscribed power) ($CMDPS\_cost$)

$$CMDPS\_cost = \sum_{i=1}^{144} 0.04 \cdot b_i \cdot \sqrt{\sum\left(P_{grid}(i) - P_{sub}\right)^2} \quad for \quad P_{grid} > P_{sub} \tag{4.13}$$

Where $0.04 \cdot bi$ represents the penalty rate defined by TURPE regulation.

The energy bill for one day is therefore calculated as

$$Energy\_bill = TOU\_cost + Electricity\_cost + CMDPS\_cost \tag{4.14}$$

Together, these indicators provide a comprehensive framework to evaluate the performance of the real-time supervision tool. They capture both the technical aspects of ESS operation such as cycling and capacity utilization. And the effective integration of PV production, by quantifying curtailed energy and self-consumption efficiency. At the same time, they reflect the achievement of economic objectives through the assessment of energy costs and subscribed power penalties, thereby linking operational performance to financial outcomes.

## 4.3 Results and analysis

The proposed supervision strategy is designed for real-time operation; therefore, the analysis must demonstrate the robustness and dynamic response of the fuzzy logic supervisor under the diverse and rapidly changing conditions of a DC railway network. The evaluation considers multiple operating states that may occur in real time, including variations in TSS demand and PV generation.

As shown in Chapter 3 through the historical data analysis, TSS consumption fluctuates significantly between weekdays and weekends, with some days exceeding the subscribed power limit while others remain below it. Consequently, the supervision tool must continuously adapt to these variations. Similarly, PV production depends strongly on meteorological conditions ranging from high and stable generation on sunny days to irregular and reduced output on cloudy days.

The simulation setup includes the definition of key parameters, the tested supervision cases, and the representative scenarios of PV generation and TSS consumption. The RACCOR-D railway architecture (Architecture 1) is modelled in MATLAB/Simulink to emulate the dynamic operation of the DC traction substation. Real-time measurements from the electrical model are used as inputs to the supervision layer, ensuring a realistic evaluation of system behaviour.

The analysis of the results thus focuses on assessing how effectively the real-time supervisor maintains system objectives, limiting CMDPS penalties, keeping the ESS state of charge (SOC) within bounds, maintain acceptable variation of DC bus voltage, and maximizing PV self-consumption, across all these conditions. The performance is evaluated using both behavioural analysis (via power flow curves) and key performance indicators (KPIs) derived from simulation results.

## 4.3.1 Representative scenarios for real-time supervision

### 4.3.1.1 TSS Load Demand Scenarios

To ensure robust and adaptive supervision strategies, it is essential to consider the variability of TSS load profiles across different types of days. The analysis of historical data reveals a clear distinction between weekdays and weekends as explained in Chapter 3, with weekdays generally exhibiting higher consumption levels. To represent this variability, three representative daily profiles have been selected:

- Day 1 (no exceedance): A weekend day with no exceedance of the subscribed power $P_{sub}$. In this case, the entire profile remains below the contractual limit.
- Day 2 (moderate exceedances): A typical weekday with occasional peaks above $P_{sub}$. These overruns are limited in magnitude and duration, illustrating moderate exceedance of the TSS subscribed power.
- Day 3 (significant exceedances): A critical weekday scenario with multiple peaks well above $P_{sub}$, reflecting strong demand and sustained overruns.

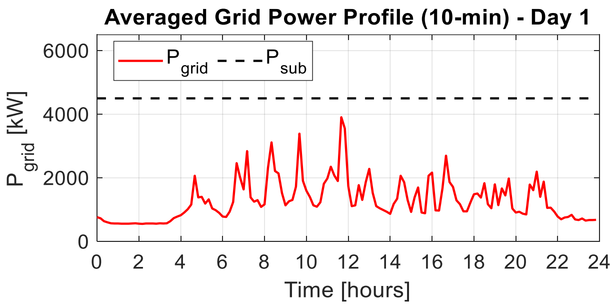


*Fig. 4.14 Power drawn from the grid in Day 1 scenario*

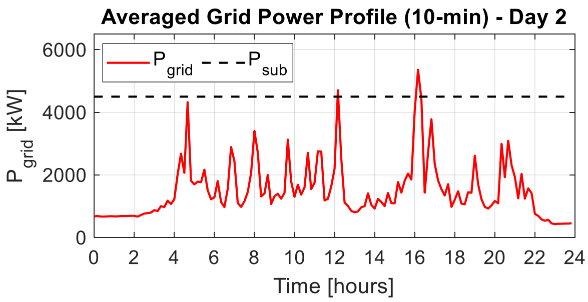


*Fig. 4.15 Power drawn from the grid in Day 2 scenario*

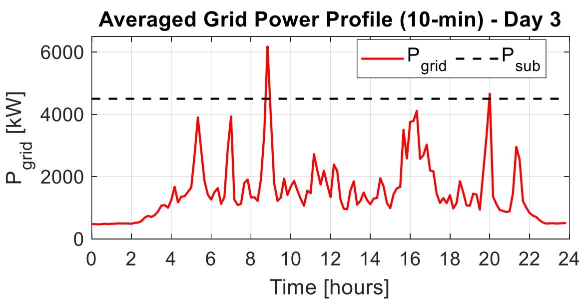


*Fig. 4.16 Power drawn from the grid in Day 3 scenario*

These three profiles allow us to simulate and assess the supervisor's behavior under no subscribed overrun, moderate overrun of the subscribed power, and significant overrun of the subscribed power conditions. By including diverse situations, the study ensures that the proposed fuzzy logic supervisor is tested under a wide range of realistic operating scenarios. This diversity in load profiles is essential for validating the supervisor's ability to limit subscribed power exceedance, improve self-consumption, and maintain DC bus voltage within acceptable limits, while respecting ESS SOC limits under dynamic consumption profiles.

#### 4.3.1.2 PV Generation Scenarios

On the generation side, PV output is highly sensitive to weather variability, which directly affects the balance between local production and TSS demand. To represent this uncertainty, two contrasting scenarios are considered and presented in Fig. 4.17 and Fig. 4.18:

- Sunny day: Characterized by high irradiance and a smooth PV output curve, closely following the predicted generation profile with minimal fluctuations. This scenario offers ideal conditions for PV integration and maximizes the potential for ESS charging during midday hours.
- Cloudy day: Marked by intermittent and unpredictable solar generation, and a maximum power at the middle of the day less than in sunny days by around 50%, leading to frequent mismatches between predicted and actual PV output. This scenario tests the supervisor's responsiveness to volatile renewable energy inputs and its capacity to adapt charging behaviour in real time.

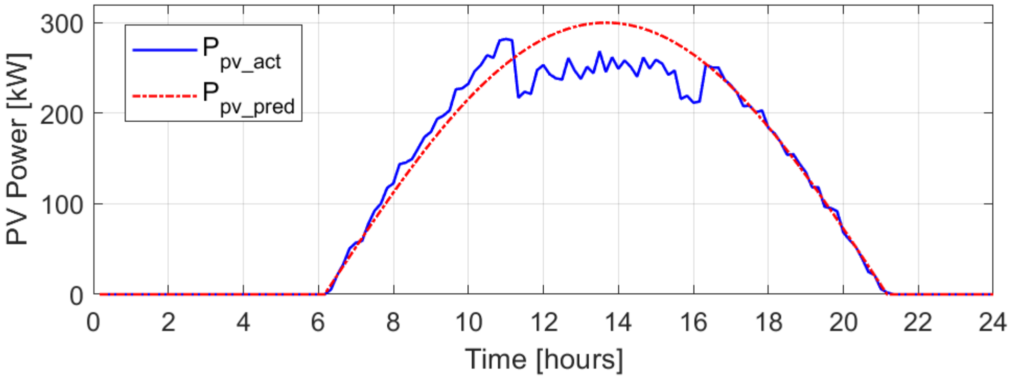


*Fig. 4.17 Actual and predicted PV generation profile (sunny day)*

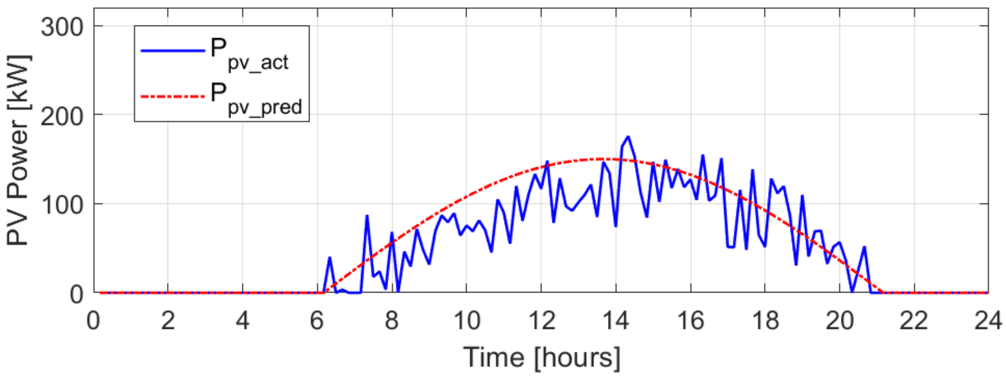


*Fig. 4.18 Actual and predicted PV generation profile (cloudy day)*

The PV profiles for both scenarios are shown in Fig. 4.17 and Fig. 4.18, where actual PV production $P_{PV\_act}$ is compared with day-ahead predictions $P_{PV\_pred}$. These scenarios will be used in conjunction with the selected TSS load profiles to assess the effectiveness of the fuzzy logic supervisor under realistic and challenging smart grid conditions.

### 4.3.2 Modelling parameters and supervision cases

To simulate the proposed real-time energy supervisor under realistic operating conditions, it is essential to define the parameters of the model used in the simulation. This section provides an overview of the input data, including the rated parameters of the PV system, the ESS, the TSS subscribed power, and the DC bus voltage. These parameters reflect the actual sizing of the ESS and the PV systems, and the configuration of important parameters in the railway TSS, such as the DC bus no load voltage, and the actual subscribed power.

*Table 4.3 Modelling parameters*

| ESS | PV | Subscribed power | DC bus voltage (no load) |
|---|---|---|---|
| $P_{max\_sto}$ = 1200 kW (charge and discharge)<br>$E_{sto}$ = 2400 kWh | $P_{PV\_max}$ = 300 kW | $P_{sub}$= 4500 kW | $V_0$ = 2000 V |

As shown in Table 4.3, the ESS has a nominal capacity of 2400 kWh. However, project constraints limit its charging and discharging power to 1200 kW (corresponding to 0.5 C). The PV system can deliver up to 300 kW, while the subscribed power of the TSS is set to 4500 kW. The DC bus no-load voltage is fixed at 2000 V.

For the assessment of performance of the real time supervision strategy, two cases of supervision are identified:

- Developed real time supervision explained in this chapter that takes into consideration the day ahead EMS (LT+ST)
- Long term supervision explained in chapter 3 without real time supervision (LT)

Under three scenarios represented with three consecutive days, characterized with different TSS load profile (Fig. 4.14 Power drawn from the grid in Day 1 scenario, Fig. 4.15, Fig. 4.16).

*Table 4.4 Scenarios and supervision strategies*

| Load Profile Scenario | PV Scenario | Strategy | Assessment Focus |
|---|---|---|---|
| **Day 1 (Low, no exceedance)** | Sunny | LT, LT+ST | Behavioural + Economic indicators + KPIs |
| **Day 2 (Moderate exceedance)** | Sunny | LT, LT+ST | |
| **Day 3 (Significant exceedance)** | Sunny | LT, LT+ST | |
| **Day 1 (Low, no exceedance)** | Cloudy | LT, LT+ST | Economic indicators only |
| **Day 2 (Moderate exceedance)** | Cloudy | LT, LT+ST | |
| **Day 3 (Significant exceedance)** | Cloudy | LT, LT+ST | |

In the sunny-day scenarios, detailed analyses of power flow dynamics, SOC evolution, and grid interactions are conducted to assess the supervisor’s behavioural performance and corresponding KPIs. In contrast, the cloudy-day scenarios focus solely on economic performance, including energy costs and CMDPS penalties. This comparative approach highlights the ability of the proposed supervision strategy to maintain economic efficiency even when renewable generation is limited.

### 4.3.3 Analysis of the real time supervision behaviour

To test the real time supervision, the actual profile of the TSS consumption is used in the simulation. This profile describes the real TSS power consumption measured on site and available in the historical data. Unlike the in the day ahead supervision level where the optimization relies on the predictions of the TSS power consumption. Fig. 4.19 shows the predicted and actual TSS load for the three consecutive days. It is seen that the prediction cannot detect high peak points. The day ahead supervision will struggle therefore with these peaks, as explained earlier in Chapter 3. Through the analysis of the results of the different simulations based on graphs interpretations and key performance indicators, the real time supervisor is evaluated by how much it can deal with the errors of the predictions and uncertainty of TSS load consumption and how it can improve and adjust the reference storage setpoints from the day ahead schedule.

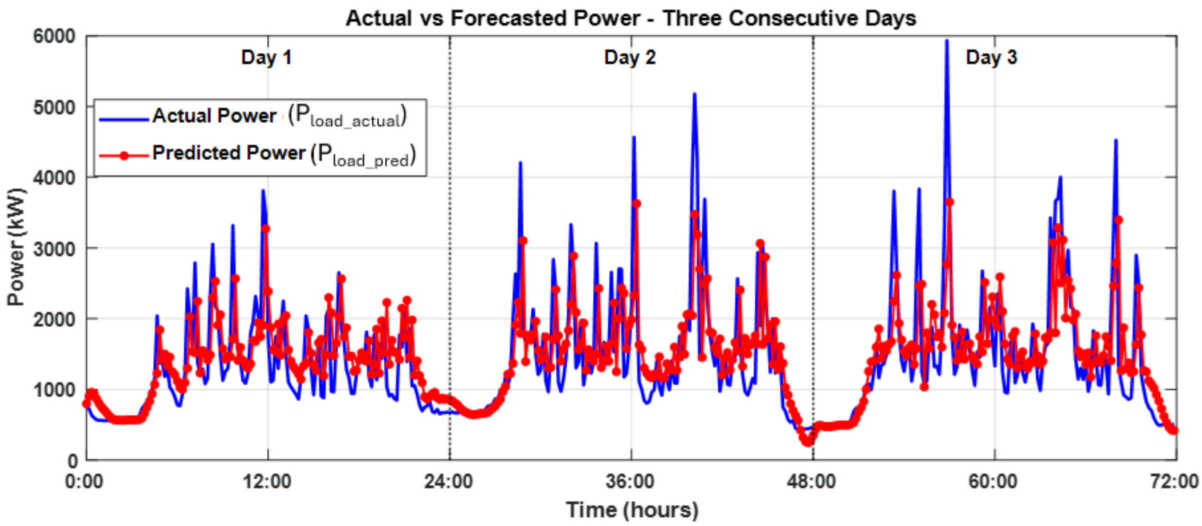


*Fig. 4.19 Predicted and actual TSS load*

The developed Simulink model explained in Chapter 2, require a controlled current source to represent the load consumption of the TSS. The actual power $P_{load}$ seen in Fig. 4.19 is used as the data source for the current source (after the division by the DC bus voltage value). By that, the simulation can be performed, and the real time supervisor starts reading the necessary measurement and perform required actions.

#### 4.3.3.1 Case LT+ST compared with LT for Day 1 (sunny day scenario)

This section presents the analysis of the real time supervisor (short term supervision) behaviour compared with the day ahead EMS (long term supervision) through graphs interpretation. For each simulated day, the output of the day ahead supervision $P_{ref-lt}$ is plotted along with output of the real time supervision $P_{ref-st}$ that incorporates the day ahead reference setpoints as input. Also, the power drawn from the grid, $P_{grid}$, in each case (long term supervision 'LT' alone and short-term supervision with long term schedule input 'LT+ST') is plotted to understand the direct impact of the ESS reference setpoints on the power drawn from the grid.

Fig. 4.20 presents the behaviour of the supervisor on Day 1, comparing the performance of the day-ahead only supervision (LT) with the combined day-ahead and real-time supervision

(LT+ST). The upper plot is for the TSS load consumption showing the forecast profile vs the actual profile. The middle plot illustrates the power drawn from the grid, while the lower plot shows the battery power setpoints and the evolution of the SOC.

Between 00:00 and 09:00, the real time supervisor follows the day-ahead setpoints in general with minor deviations that keep the real time schedule very close to the day ahead planning, as the load demand aligns closely with the forecasts, resulting in a charging phase fully consistent with the day ahead plan.

After 09:00, the day ahead reference indicating a high discharge near the maximum storage power (1000 kW), this has led the power drawn from the grid to set to zero and the substation load is entirely fed by the ESS and the PV without the need to draw power from the grid. The risk of excess of local production rises in this case with a fixed ESS schedule that cannot be changed in LT supervision. The real-time supervisor adjusts the battery setpoint accordingly, applying a lower discharge power than scheduled under LT supervision to avoid excess of local production that led to PV curtailment, underachieving the objective that aims to maximize the use of the PV generation. The DC voltage at 09:00 indicates exceedance of the maximum voltage threshold $V_{max}$ as shown in Fig. 4.21, which led the real time supervisor to discharge the ESS with moderate power not the maximum as planned in day-ahead to prevent any potential excess of local production.

Around 12:00, the power drawn from the grid increases and approaches the subscribed power threshold. To prevent a potential overrun, the real time supervisor initiates a small discharge of the storage. This anticipatory action ensures that any sudden overrun of the subscribed power by the power drawn from the grid is reduced by the power discharged from the ESS. This behaviour contrasts with the LT scenario, which lacks the flexibility to adapt in real time to peaks not detected by the forecast.

Moments before 20:00, the discharge power of the real time supervision remains below the day-ahead setpoint, again reflecting the supervisor's capacity to decrease the discharge power based on the voltage level indicator in this period that operates near the maximum threshold $V_{max}$. This is how real time supervision achieves the objective of maximizing the use of PV production. And after 20:00, the discharge of the ESS happens in real time case, in contrast to the day ahead plan that doesn't solicit the ESS. This is influenced by the SOC level in real time that is bigger than the day ahead ($SOC_{st} > SOC_{lt}$), the supervisor in this case aims to follow better the day ahead SOC so it favors the discharge of the ESS to get close to the day ahead SOC.

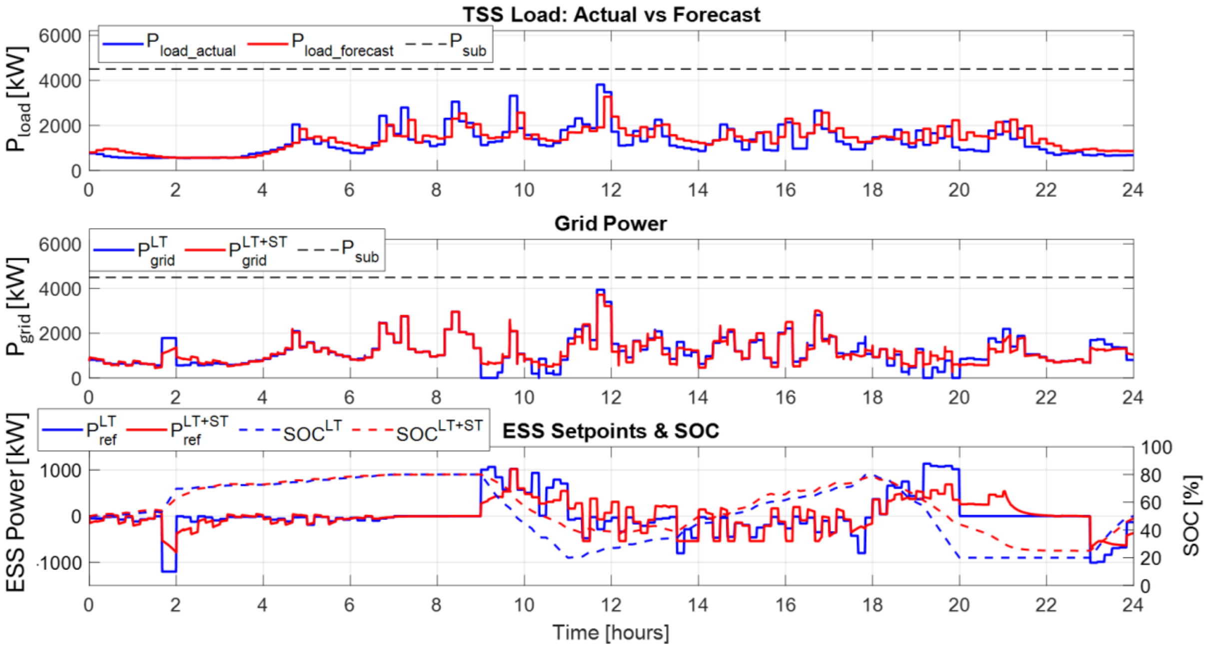


*Fig. 4.20 Simulation results for Day1*

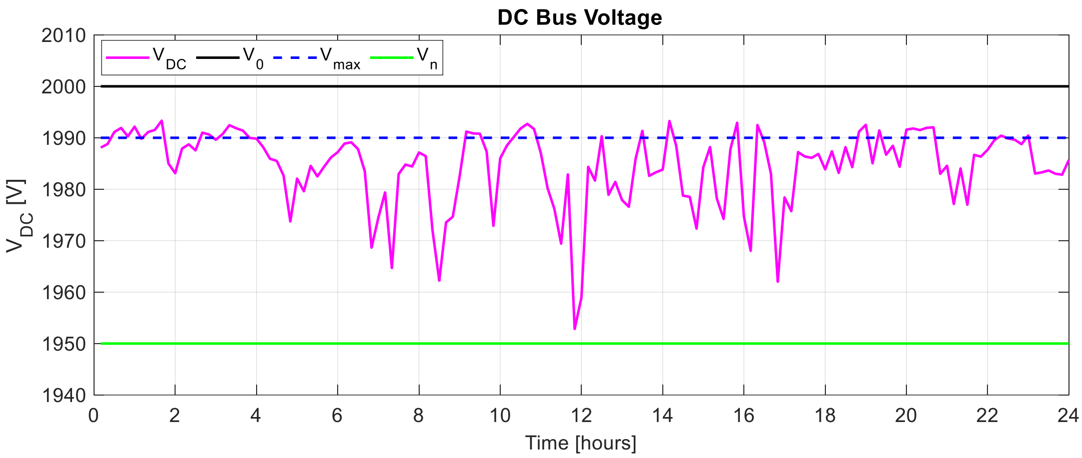


*Fig. 4.21 DC bus voltage variation in RT for Day 1 scenario*

#### 4.3.3.2 Case LT+ST compared with LT for Day 2 moderate TSS consumption

Fig. 4.22 illustrates the supervisor's behaviour on Day 2. At the beginning of the day the $P_{ref\_st}$ follows the day ahead schedule $P_{ref\_lt}$. At approximately 5:00, a noticeable increase in power drawn from the grid is observed, although the subscribed power limit is not exceeded. In response, the real-time supervisor triggers a preventive discharge from the ESS to anticipate the risk of overrunning the subscribed power, thereby anticipating a potential peak. The same phenomenon occurs around 12:00 and again at 16:00, when the power drawn from the grid reaches or exceeds the subscribed power. The real-time reference setpoint then deviates from the LT schedule by initiating discharges in periods where charging was originally planned. During these intervals, the TSS consumption forecast in the $P_{load}$ plot fails to capture the actual demand peaks, causing the day-ahead strategy not to solicit the ESS in discharge.

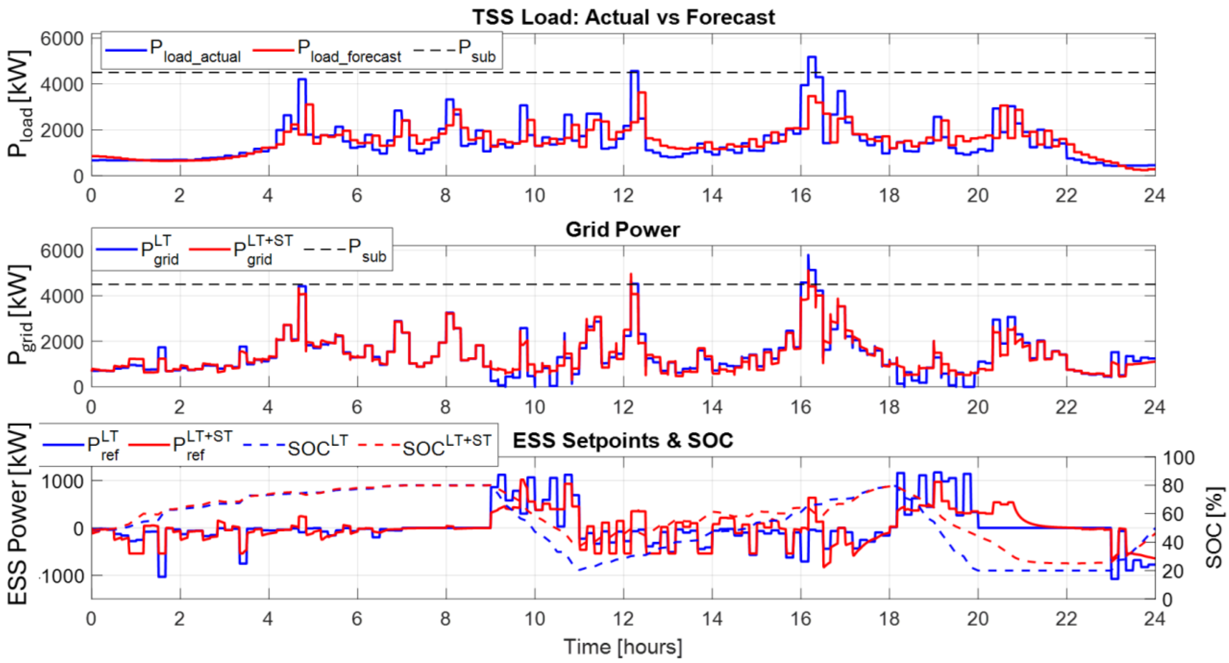


*Fig. 4.22 Simulation results for Day2*

Between 18:00 and 20:00, a different situation occurs. The discharge power remains below the LT reference due to high voltage detected on the DC bus as shown in Fig. 4.23. In this case, the real-time supervisor acts conservatively to prevent operating at no load voltage to avoid risking PV curtailment.

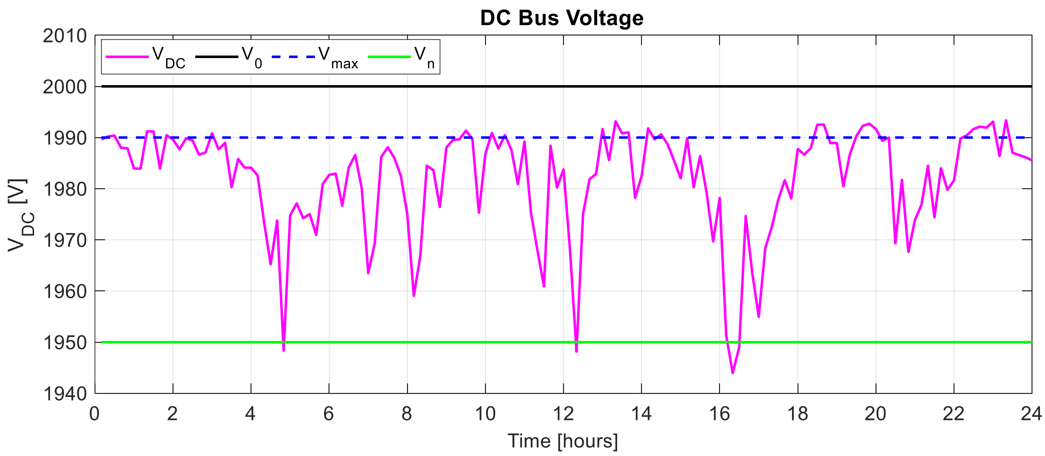


*Fig. 4.23 DC bus voltage variation in RT for Day 2 scenario*

#### 4.3.3.3 Cas LT+ST compared to LT only for Day 3

Fig. 4.24 illustrates the simulation results of Day 3 scenario. Two grid power overruns are observed outside the peak hour periods for the use of the transport network operator: one shortly before 9:00 and another just after 20:00. The day-ahead supervision fails to address these overruns because it relies on the forecasted $P_{load}$ profile, where the prediction model did not capture the actual consumption peaks. Consequently, the day-ahead plan schedules ESS discharging only during peak-hour periods for the use of the transport network operator (defined in TURPE 6). In contrast, the real-time supervisor detects the unexpected rise in demand and discharges the ESS at maximum power before 09:00, anticipating the overrun that occurs prior to the peak-hour window defined by the transport network operator. This action effectively reduces the grid power drawn, although not completely, due to the ESS's maximum discharge power limit and operational constraints. At 20:00, the storage system continues to discharge beyond the peak hour period due to a minor overrun of the subscribed power.

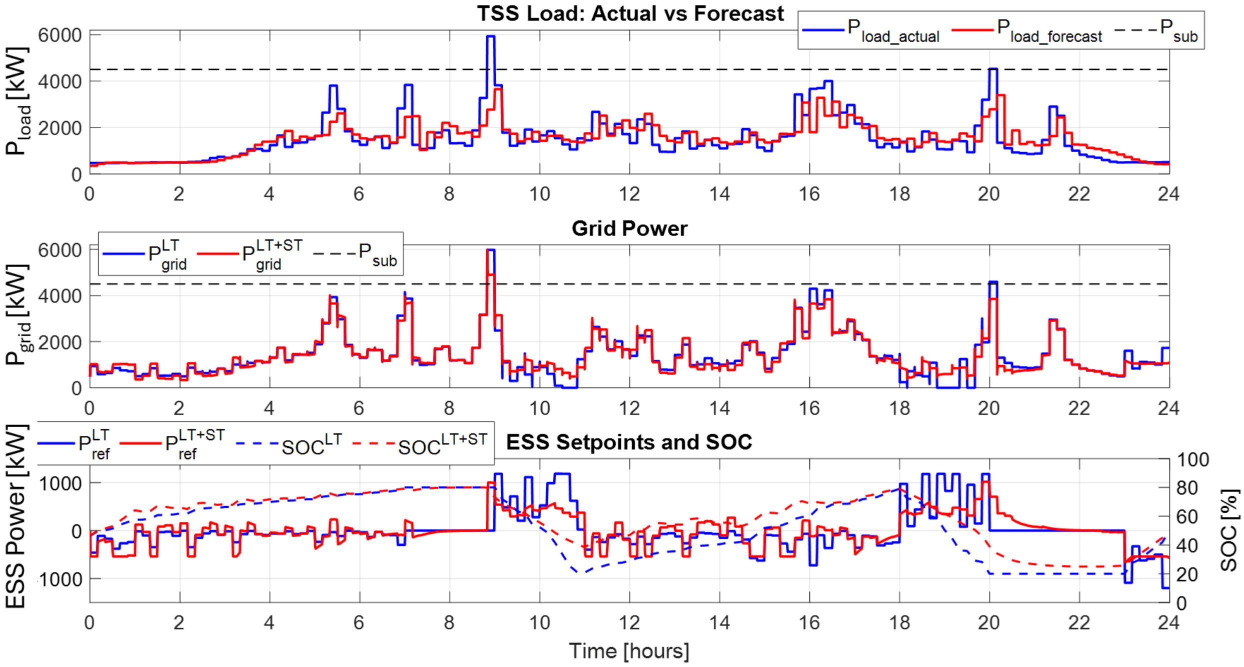


*Fig. 4.24 Simulation results for Day3*

Additionally, at 7:00 and 16:00, the grid power increases without exceeding the subscribed power. In these periods, the storage system preventively discharges with small power, demonstrating the supervisor's ability to anticipate potential peaks in TSS demand.

Between 18:00 and 20:00, the discharged power in the supervision case LT+ST is less than the LT case even though this period is considered peak hours for the use of the electricity transport network. This is back to the voltage level measured at the DC bus during this period, the voltage exceeds the maximum voltage threshold $V_{max}$ in three consecutive occasions as illustrated in Fig. 4.25.

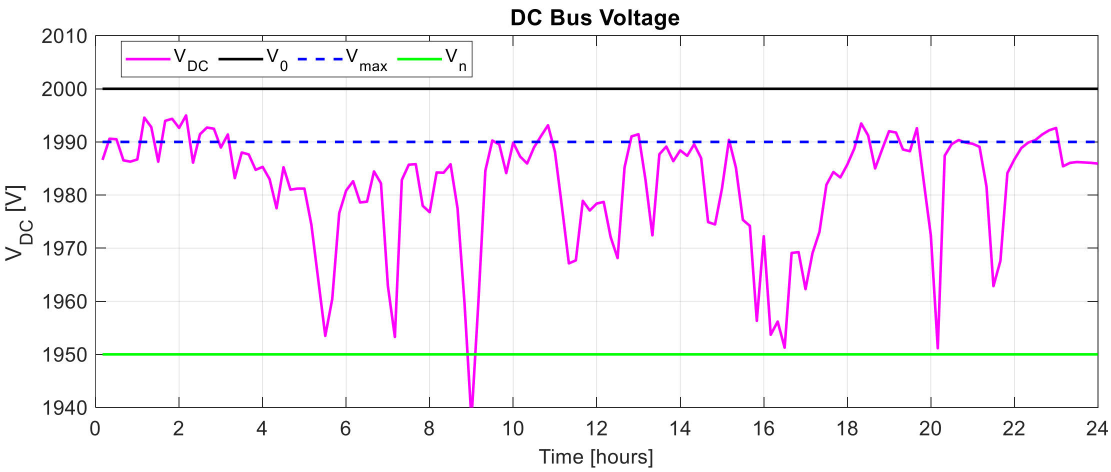


*Fig. 4.25 DC bus voltage variation in RT for Day 3 scenario*

### 4.3.4 Analysis of the key performance indicators

This section focuses on the evaluation of key performance indicators (KPIs), which are divided into two main categories. Technical indicators assess how effectively the system manages energy flows and technical resources, such as ESS operation and PV utilization. Economic indicators, on the other hand, capture the system's financial performance, including penalties related to subscribed power exceedance, time-of-use costs, and the total energy bill.

#### 4.3.4.1 Key performance indicators

The analysis of the technical indicators focuses on how effectively the proposed real-time supervisor ('LT+ST') improves energy management compared to the day-ahead-only strategy ('LT'). Table 4.4 summarizes the key indicators related to the use of the energy storage system (ESS) and photovoltaic (PV) power under the three representative load scenarios (Day 1, Day 2, and Day 3).

In terms of battery operation, In the day-ahead case ('LT'), the ESS follows a pre-established schedule designed to maintain optimal end-of-day conditions. This strategy consistently achieves the target 50% SOC and two complete charge–discharge cycles per day, confirming that the long-term planning ensures balanced operation and effective storage utilization under predicted conditions.

When real-time supervision is introduced ('LT+ST'), the ESS operation becomes more dynamic. The supervisor reacts to unexpected deviations in TSS demand such as unpredicted consumption peaks, or to variations in DC voltage not accounted for at the day-ahead level. These adaptations cause the ESS to deviate from the planned schedule. However,

The final state of charge (SOC) remains within acceptable limits for both cases, with only marginal differences between 'LT' and 'LT+ST' (e.g., 48.3% vs. 50%). This confirms that the real-time layer preserves the long-term balance of storage energy while improving short-term responsiveness

*Table 4.5 Performance indicators related to the ESS and the use of PV power*

| Scenario | Day 1 | | Day 2 | | Day 3 | |
|---|---|---|---|---|---|---|
| Indicator \ Case | LT | LT + ST | LT | LT + ST | LT | LT + ST |
| $\boldsymbol{E_{excess}}$ | 40 kWh | 0 | 52 kWh | 0 | 87 kWh | 0 |
| $\boldsymbol{SOC_{(end)}}$ | 50% | 48.3% | 50% | 46.3% | 50% | 49% |
| $\boldsymbol{E_{batt}}$ (nb of cycles) | 5.76 MWh (2) | 5.49 MWh (2) | 5.76 MWh (2) | 5.72 MWh (2) | 5.76 MWh (2) | 5.66 MWh (2) |

In summary, the 'LT+ST' strategy effectively preserves the technical consistency of the ESS operation established by the day-ahead plan while improving responsiveness to real-time variations in demand and voltage. The inclusion of $\Delta SOC$ as an input to the fuzzy logic supervisor enables intelligent correction mechanisms that maintain an acceptable end-of-day SOC. This confirms the robustness and adaptability of the real-time supervision layer in complementing the predictive LT strategy under uncertain operating conditions.

### 4.3.5 Economic indicators

The economic indicators evaluate the financial performance of the supervision strategies under different operating conditions. Table 4.6 and Table 4.7 present the results for sunny and cloudy day scenarios, respectively, comparing three cases: No RACC (no PV or ESS integration), 'LT' (day-ahead supervision), and 'LT+ST' (combined day-ahead and real-time supervision). The comparison highlights the RACCOR-D system's contribution to reducing energy costs through improved PV self-consumption, peak shaving, and efficient use of time-of-use tariffs.

As shown in Table 4.6 and Table 4.7, integrating real-time supervision (LT+ST) significantly enhances economic performance compared to LT and No RACC. The most notable benefit is the reduction of CMDPS costs, showing the supervisor's effectiveness in limiting subscribed power overruns. Meanwhile, $TOU\_cost$ values remain close to 'LT' results, confirming that the 'LT+ST' approach maintains day-ahead economic gain. By the incorporation of the day ahead planning as an input to the fuzzy logic supervisor, the real time supervision maintains the gain obtained with the day ahead optimal planning based on time-of-use of electricity transport network tariffs.

The small improvement of the $Electricity\_cost$ passing from 'LT' to 'LT + ST' case is back to the ability of the real time supervision tool to maximize the use of PV production avoiding PV curtailment.

Together, these results confirm that the economic gain stems from both reduced energy costs via PV self-consumption and penalty avoidance through intelligent peak management. The LT+ST supervision thus offers a cost-effective and resilient solution tailored to the operational and economic needs of railway substations.

*Table 4.6 Economic indicators under LT and LT+ST supervision cases for sunny day scenario*

| Scenarios & cases / Indicator | Sunny Day Scenario (Peak PV production at mid-day) | | | | | | | | |
|---|---|---|---|---|---|---|---|---|---|
| | Day 1 | | | Day 2 | | | Day 3 | | |
| | **No RACC** | **LT** | **LT+ST** | **No RACC** | **LT** | **LT+ST** | **No RACC** | **LT** | **LT+ST** |
| $TOU\_cost$ (€) | 588 | 516 | 520 | 676 | 605 | 607 | 687 | 616 | 620 |
| $CMDPS\_cost$ (€) | 0 | 0 | 0 | 137 | 99 | 0 | 260 | 229 | 66 |
| $Electricity\_cost$ (€) | 6 212 | 5 661 | 5 651 | 7 220 | 6 677 | 6 653 | 7 293 | 6 758 | 6 745 |

*Table 4.7 Economic indicators under LT and LT+ST supervision cases for cloudy day scenario*

| Scenarios & cases / Indicator | Cloudy Day Scenario (Peak PV production at mid-day) | | | | | | | | |
|---|---|---|---|---|---|---|---|---|---|
| | Day 1 | | | Day 2 | | | Day 3 | | |
| | **No RACC** | **LT** | **LT+ST** | **No RACC** | **LT** | **LT+ST** | **No RACC** | **LT** | **LT+ST** |
| $TOU\_cost$ (€) | 588 | 548 | 548 | 676 | 635 | 635 | 687 | 646 | 647 |
| $CMDPS\_cost$ (€) | 0 | 0 | 0 | 137 | 119 | 0 | 260 | 254 | 95 |
| $Electricity\_cost$ (€) | 6 212 | 5 970 | 5 941 | 7 220 | 6 981 | 6 951 | 7 293 | 7 051 | 7 033 |

#### 4.3.5.1 Total energy bill

The total daily energy bill is calculated as the sum of $TOU\_cost$, $CMDPS\_cost$, and $Electricity\_cost$ as explained in Equations (4.11, 4.12, 4.13, 4.14). For Day1 scenario, where there is no overrun of the subscribed power (in predictions and in real consumption), the economic gain is maintained by the real time supervision tool. The economic gain stays almost the same in both supervision cases LT and LT+ST. This validate that under normal operation, when no important events happen the developed real time supervision tool can guarantee the economic gain in the total energy bill obtained by the day ahead supervision.

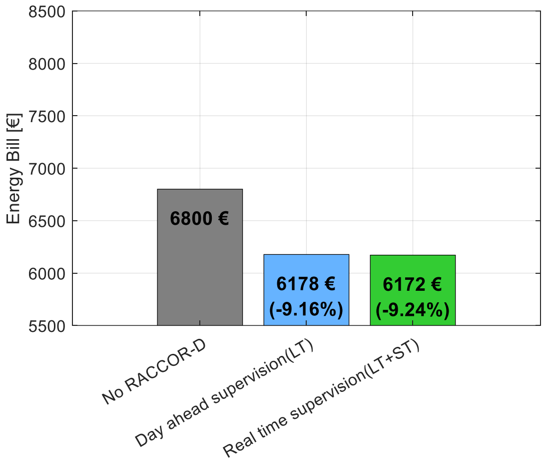


*Fig. 4.26 Daily energy for each supervision LT and LT+ST 'Day1' (sunny day scenario)*

For 'Day2' & 'Day3' as shown in Fig. 4.27 and Fig. 4.28, a substantial reduction in the energy bill is observed when applying LT supervision compared to the baseline (no RACCOR-D). However, the introduction of real-time supervision (LT+ST) brings further gains, with reductions reaching up to 10% relative to the no-supervision case. This improvement is directly linked to the increased local self-consumption of PV energy and the precise peak shaving actions executed by the real-time supervisor.

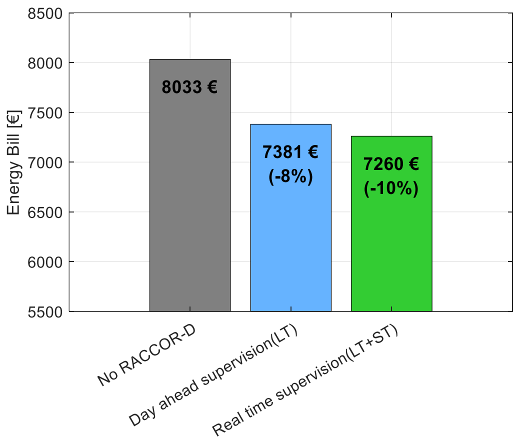


*Fig. 4.27 Daily energy bill for each supervision case 'Day2' (sunny day scenario)*

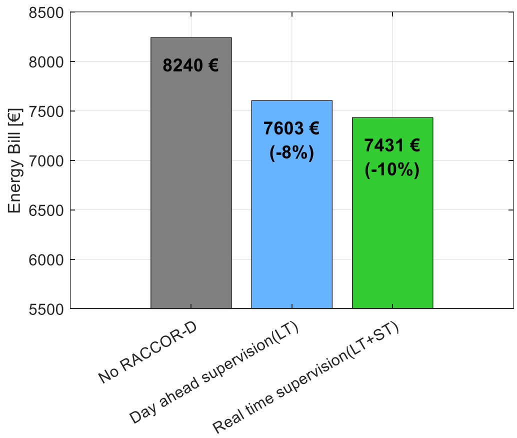


*Fig. 4.28 Daily energy bill for each supervision case 'Day3' (sunny day scenario)*

The evaluation of the energy bill is done also for the cloudy days. Where the PV production profile is the one described in Fig. 4.18. As shown in Fig. 4.29, the economic gain in the cloudy days simulation result in less gain regarding the energy bill compared to sunny days. Which is normal since there is less PV production. Although, it is important to mention the small improvement apported by the real time supervision in the case (LT + ST).

The 2% decrease of the total energy bill passing from day-ahead supervision to real time supervision can be very limited. Back to the fact that the PV sizing is very low compared to the TSS power consumption. This sizing reflects the 1st vision of what will be installed at first. Under such conditions, the day-ahead optimization already exploits most of the available flexibility offered by the ESS, leaving only a narrow scope for additional real-time adjustments.

With bigger or optimal sizing of the PV, more struggles will face the day-ahead supervision adding a new decision variable related to the curtailment of the PV power. With the forecast errors it is expected to cause higher power imbalance that cause higher PV curtailment in real time.

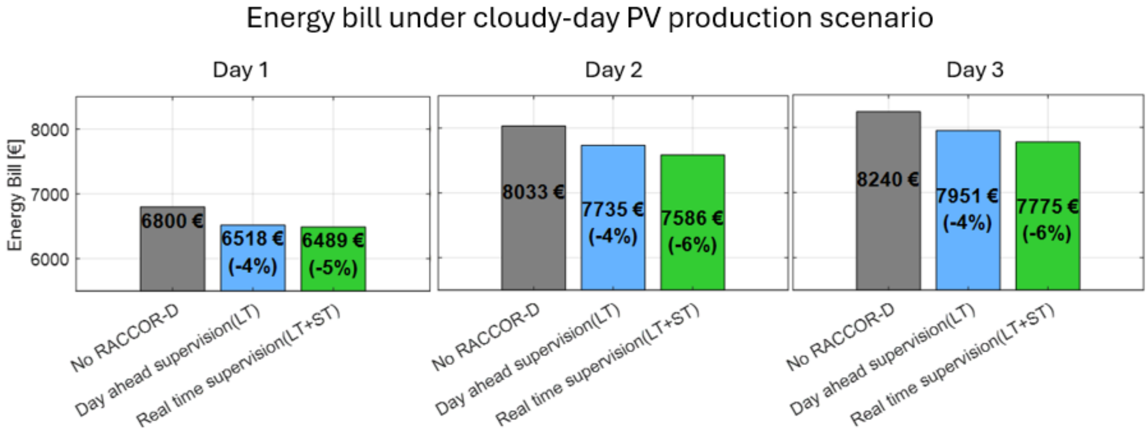


*Fig. 4.29 Economic gain of the total energy bill for 'Day1' 'Day2' 'Day3' under cloudy day scenario*

#### 4.3.5.2 CMDPS penalties costs

Regarding the CMDPS, the results reveal a more differentiated behaviour. On Day 2, the 'LT' supervision alone achieves a modest 28% reduction compared to the baseline. This occurs because the forecast-based supervision (LT) did not anticipate the peak demand accurately. Consequently, the storage system failed to discharge with sufficient power at the exact moment of consumption peaks, preventing CMDPS from being minimized effectively. In contrast, the 'LT+ST' supervision corrects this day ahead mismatch in CMDPS cost by detecting the real-time peak and discharging the ESS at high value to reduce undetected peaks, reducing CMDPS by 100% as shown in Fig. 4.30 CMDPS cost under sunny day scenario.

A similar pattern is observed on Day 3 where the overrun of the subscribed power is more remarkable. While the LT supervision alone results in a modest reduction in CMDPS of 12% (from 260 € to 229 €), it remains suboptimal due to its inability to predict and mitigate actual peak events. By contrast, the 'LT+ST' strategy achieves a drastic reduction of CMDPS by 75% lowering the penalty to just 66 €. This result clearly demonstrates the ability of the real-time supervisor to react promptly to unforeseen consumption peaks and adapt the ESS behaviour accordingly.

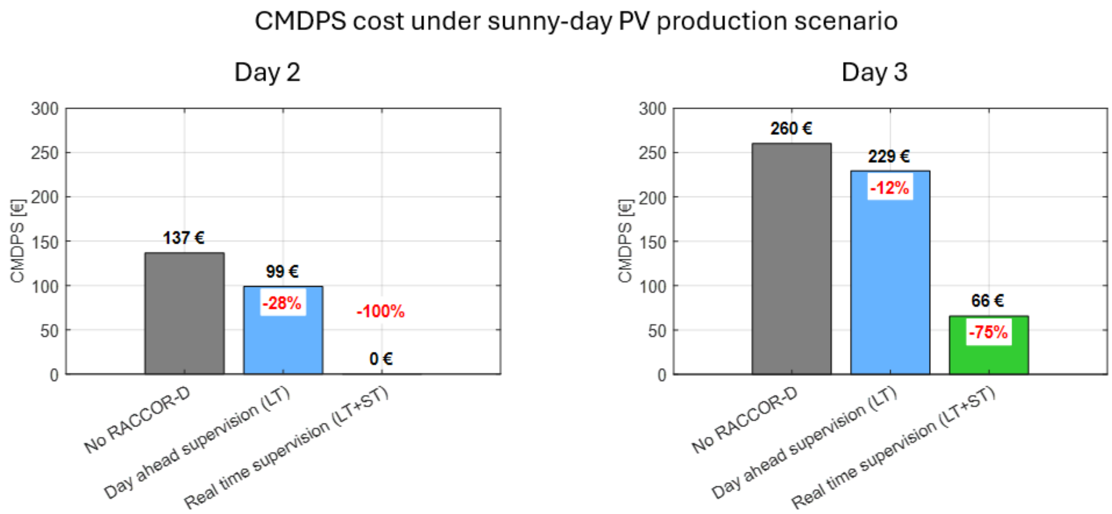


*Fig. 4.30 CMDPS cost under sunny day scenario*

Fig. 4.31 displays the CMDPS gains under the cloudy day scenario of PV generation, for Day 2 and Day 3 where the overrun of the subscribed exist. What is particularly noteworthy is the significant reduction in CMDPS costs achieved under the 'LT+ST' supervision strategy. Even under unfavourable meteorological conditions, where PV generation and economic gains are limited, the ESS when managed with the proposed real time supervision tool effectively mitigate peak demand penalties. This demonstrates the robustness of the proposed supervision approach, which ensures consistent performance and effective reduction of subscribed power exceedances under both favourable and constrained production conditions.

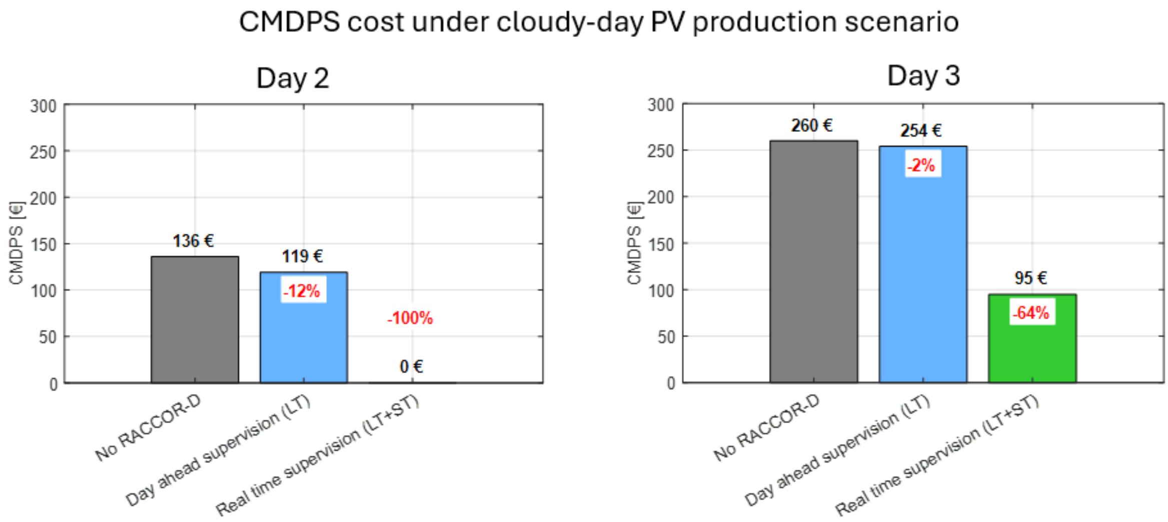


*Fig. 4.31 CMDPS cost under cloudy day scenario*

The reduction in CMDPS is more remarkable compared to the reduction of the total energy bill. With enough capacity of the ESS to limit the subscribed power overruns. The TURPE 6 period tested in the results takes place at the beginning of this tariffication scheme. Today the penalty coefficient has increased with the evolution of TURPE 6 and further increase is expected when passing into TURPE 7. When the new tariffication is applied to the simulated case, the economic gain will be more remarkable, and the relevance of the real time supervision can be better highlighted.

## 4.4 Design of real time fuzzy logic supervisor for Architecture 2

### 4.4.1 Reminder of the architecture 2

Architecture 2 of the RACCOR-D corresponds to a configuration in which both the photovoltaic (PV) system and the energy storage system (ESS) are connected directly to the catenary at the midpoint between two traction substations (TSS1 and TSS2), known as the (PMP: poste de mise en parallèle). The distance separating the two adjacent DC traction substations (TSS) is 20 km, with the PMP positioned at the midpoint, 10 km from each substation. TSS1, located at 0 km, serves as the origin point for trains on Track 1 and the destination point for trains on Track 2. In the contrary, TSS2 situated at 20 km, marks the endpoint for trains departing from TSS1 on Track 1 and the starting point for trains returning on Track 2. Fig. 4.32 provides the architecture reminder of the developed model to test the real-time supervision designed for the specific objectives of architecture 2 of RACCOR-D. A consistent power flow convention is adopted throughout the study: positive values correspond to elements injecting power into the DC network (buses, catenary, PMP…), whereas negative values indicate components absorbing power. According to this convention:

- $P_{TSS1}$, $P_{TSS2}$ represent the TSS power drawn from each traction substation including traction unit losses $P_{TSS} \geq 0$
- $P_{grid1}$, $P_{grid2}$ represent the power drawn from the transmission electricity network
- $P_{PV}$ is the power generated by the PV system $P_{PV} \geq 0$
- $P_{train1}$ & $P_{train2}$ are the power drawn by circulating trains $P_{train} \leq 0$
- $P_{sto}$ is the storage system power with convention: $P_{sto} > 0$ while discharging (power injected into the PMP). $P_{sto} < 0$ while charging (power absorbed by the storage)
- The voltage of the catenary at PMP is denoted $V_{cat}$
- The train pantograph voltage represents the measured voltage at the connection point between the train and the catenary and denoted $V_{pant}$

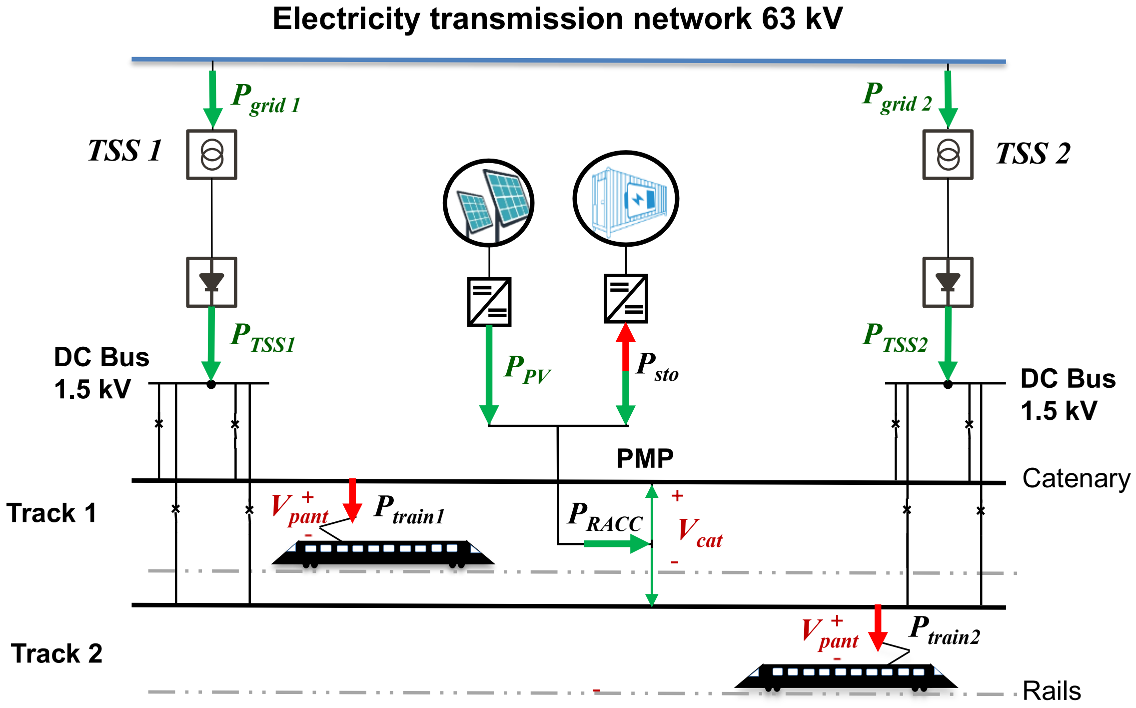


Fig. 4.32 Representation of the 2nd architecture of RACCORD

Unlike architecture 1, this architecture requires full knowledge of train dynamic. This architecture takes into consideration the detailed model of the TSS with catenary resistance variation. The 1st architecture was more global and treated like a classical smart grid. Where the TSS consumption profile is considered available and covers its whole demand. The TSS consumption profile covers without quantification the necessary power consumed by trains, losses, and auxiliary loads.

To enable the use of Architecture 2 as a test bench for the real-time fuzzy logic supervisor, several simplifying assumptions were introduced during the development of the model. These assumptions ensure a realistic yet computationally efficient representation of the railway DC system, allowing the supervisor to be evaluated under representative operating conditions while maintaining model stability and interpretability. The main assumptions are as follows:

- The TSSs consumption is caused by the supply of the moving trains along the tracks (Track 1 & Track 2) between two adjacent TSS (TSS1 & TSS2). Without influence from the train position between theme and the next neighbouring TSS.
- The train moves with constant speed among the tracks. No identification of the phenomenon of accelerations, deceleration and braking.
- The speed and the power consumption of every train is known.

Under these assumptions, the model offers a simplified yet sufficiently accurate representation of the electrical and dynamic behaviour of the railway system. It is therefore well suited for testing the real-time fuzzy logic supervisor under various operating scenarios and for analyzing its performance in managing multiple interacting dynamics within the traction network.

In terms of sizing of the smart grid components and TSS information, this architecture considers different sizing and specification of the ESS rather than the sizing considered in architecture one, that reflect the first vision of what will be established at the demonstrator site of the DC TSS. For architecture 2 the specification of the PV size and ESS capacity are taken from the results of the optimal sizing study that considers the 2nd architecture of RACCOR-D. The maximum power of the ESS is set to $P_{sto\_max}$ = 2 971 kW, corresponding to a 1C discharge rate. This means that the storage system can deliver its nominal energy capacity $E_{sto}$ = 2 971 kWh) in one hour of full-power discharge, which represents a balance between high-power capability and reasonable energy autonomy. $R_{rail}$ and $R_{cat}$ are the linear resistances of catenary and rails.

*Table 4.8 Architecture 2 specifications and components sizing*

| Component | Value |
|---|---|
| **Resistances** | $R_{rail} = 0.015\Omega/km$<br>$R_{cat} = 0.037\Omega/km$ |
| **ESS** | $E_{sto} =$ 2971 kWh<br>$P_{sto\_max} =$ 2971 kW |
| **Catenary** | $V_{cat\_max} = 1750\ V$<br>$V_{cat\_min} = 1350\ V$ |

### 4.4.2 Design of the real time supervision strategy specific for architecture 2

The proposed supervision strategy aims to treat the catenary voltage drop and show potential perspectives on how the PV and ESS can be integrated at mid-point PMP of two DC TSS and bring improvement to the performance of the railway network.

Since one of the main problems of the DC TSS is the limited voltage level and the high voltage drop that block certain train operation at a certain speed, the proposed real time supervision for architecture 2 aims to solicit the ESS in a way that reduce the voltage drop so the TSS can handle heavier trains in terms of speed and power consumption and to permit traffic increase while keeping the catenary voltage at a level that accept such increase.

Similar to the steps followed before in developed the FL real time supervision, the system specifications covering the objectives, constraints and means of actions are identified. Then the supervisor structure is explained. The necessary membership functions graphical representation of operation modes and the fuzzy rules are explained in a direct way. It explains how the energy supervision work and how it decides to manage the ESS.

Then fuzzy logic inference can be explained in the case of architecture 2 via surface area representation. Because the energy supervision in architecture 2 doesn't consider a day ahead supervision level, and treat less objectives compared to architecture 1. This is why the supervisor structure is simpler in terms of input variable which permits to understand the mechanism of the supervision through surface are analysis.

#### 4.4.2.1 System specification and supervisor structure of real time supervision for architecture 2

The main objective behind the real time supervision is to keep the ESS SOC within limits like architecture 1, and to keep the catenary voltage within operational bounds that guarantee safe and scheduled operation of the rolling stocks supplied by the TSS. Table 4.8 summarize the system specifications of the proposed real time supervision tool.

*Table 4.9 System specification for the developed real time supervision for architecture 2*

| Objectives | Constraints | Mean of action |
|---|---|---|
| **Real time supervision (short term 'ST')** | | |
| • **Keep the SOC within limits**<br>• **Minimize catenary voltage drop** | • $SOC_{min} \leq SOC \leq SOC_{max}$<br>• $V_{cat\_min} \leq V_{cat} \leq V_{cat\_max}$ | $\boldsymbol{P_{ref\_st}}$ |

The catenary voltage must remain within an acceptable range to ensure correct train circulation. In practice, maintaining this voltage level guarantees that the pantograph voltage, the effective supply seen by the rolling stock, stays above the minimum threshold required for rated operation. Heavier trains, with higher power demands and speeds, require higher minimum pantograph voltages to sustain normal performance.

In this study, it is assumed that the minimum catenary voltage at the PMP for all trains is $V_{cat\_min} = 1350\ V$, with a TSS rated at $V_{cat\_max} = 1750\ V$ reflecting the no-load voltage level observed at the RACCOR-D site and representing (no load voltage $V_0$). For SOC limits, the SOC must stay within 20% to 70%.

The supervisor structure incorporates two input variables, the SOC of the ESS and the catenary voltage deviation $\Delta V_{cat}$ calculated in Equation (4.15). It measures the deviation from the minimum permitted catenary voltage level.

$$\Delta V_{cat} = V_{cat} - V_{cat\_min} \tag{4.15}$$

Like in the first architecture, the output is the real term reference setpoint $P_{ref-st}$ that represent the decision of the short-term supervision. The fuzzy logic method is applied for the real time application, and each input is normalized through gains K1 and K2, and the output is returned to its real value through gain K3. The fuzzy logic treats two objectives at the same time, deciding the required action by the ESS after finding the best compromise of both objectives related to SOC and catenary voltage $V_{cat}$. The supervisor structure specific for architecture 2 is presented in Fig. 4.33.

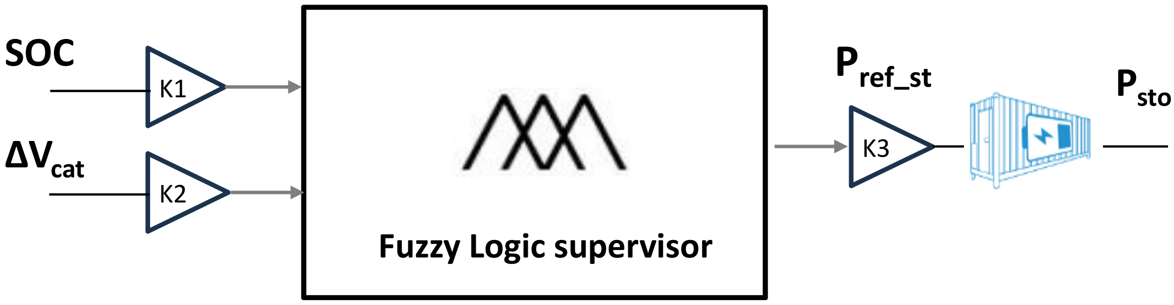


*Fig. 4.33 Architecture 2 fuzzy logic supervisor structure*

#### 4.4.2.2 Operational graphs and fuzzy rules

Following the explained methodology presented at first in a general way in Chapter 2 and in details in Chapter 4 for the first architecture of RACCOR-D. For the 2nd architecture, the membership functions are illustrated at first for the inputs and the output of the fuzzy logic supervisor. Then the operational graphs are shown to detail the different operations that the supervisor performs depending on the states of the input variables. The fuzzy rules are extracted from the operational graphs and listed in a table.

For the membership functions of the input variables of Fig. 4.34, the SOC MFs correspond to three linguistic variables, BIG (B), SMALL (S), and MEDIUM (M). Similarly, for the $\Delta V_{cat}$, BIG (B), SMALL (S), and MEDIUM (M) are used to indicate if the actual measured catenary voltage is far from the minimum and near no load catenary voltage level (B), or if it is near the minimum catenary voltage indicating a low deviation from this minimum (S), or if it is within a moderate level (M).

For the output $P_{ref\_st}$ presented in Fig. 4.35, five membership functions are available:

- Z: ZERO - ESS is not solicited
- NM: NEGATIVE-MEDIUM – ESS charging with medium power
- NB: NEGATIVE-BIG – ESS charging with high power
- PM: POSITIVE-MEDIUM – ESS discharging with medium power
- PB: POSITIVE-BIG – ESS discharging with high power

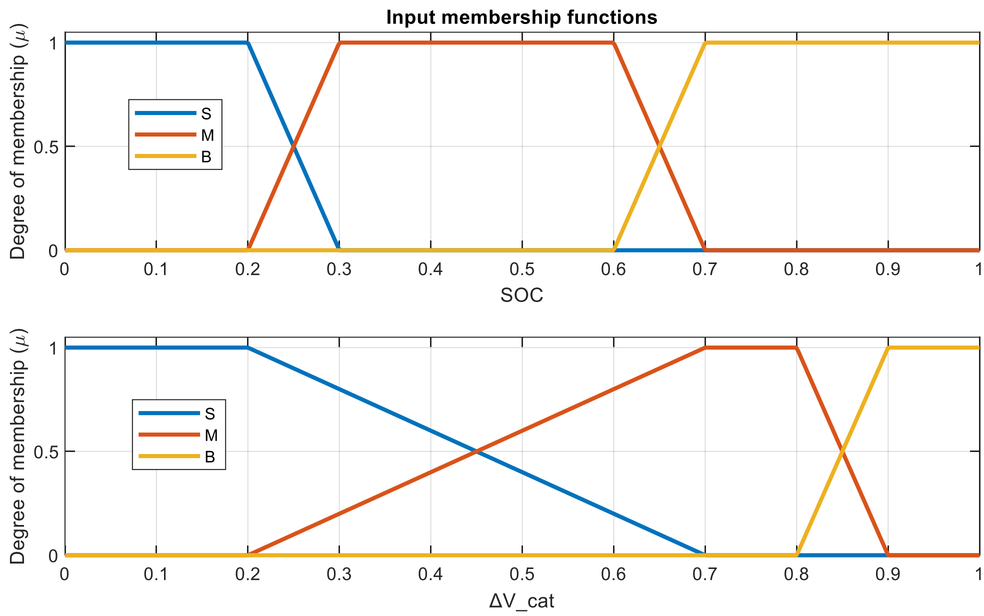


*Fig. 4.34 Membership functions for the input variables*

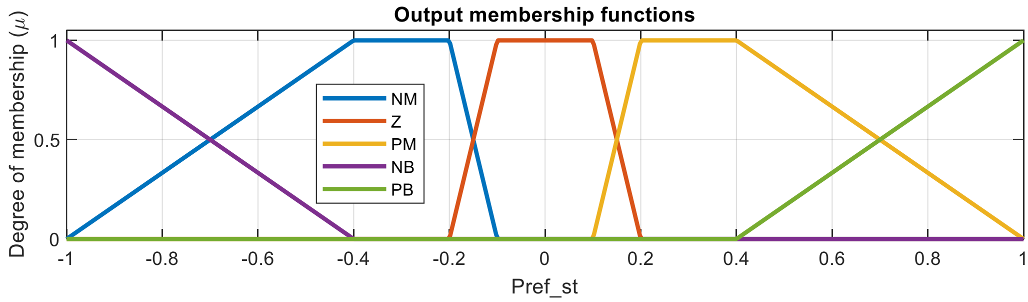


*Fig. 4.35 Membership functions for the output variable*

The operational graphs are illustrated in Fig. 4.36, when the SOC is M, the possible outcomes can be either charging the ESS with medium power if the catenary voltage variation from the minimum voltage is BIG, or not soliciting the ESS if this variation is MEDIUM, and to discharge with high power when this voltage deviation is SMALL indicating a voltage near the minimum value.

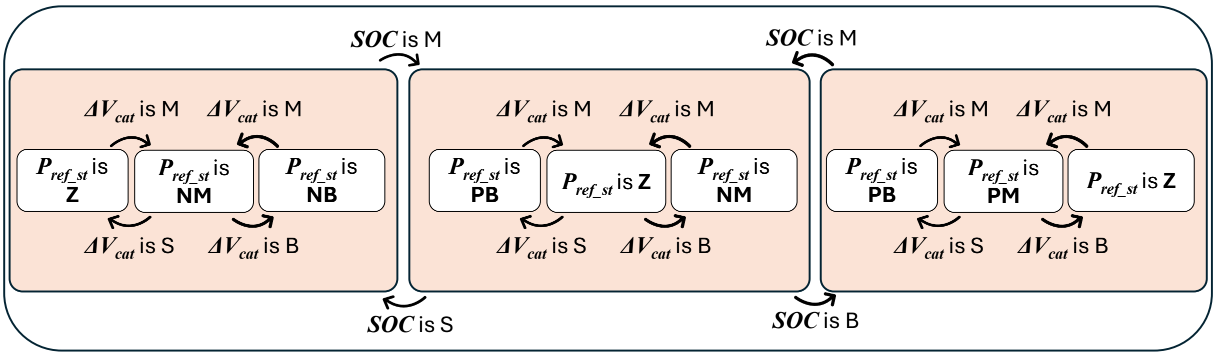


*Fig. 4.36 Operational graph of the FL supervisor (architecture 2)*

The rules are extracted from the operational graphs and listed in Table 4.10. A total number of 9 rules with similar weights are assigned to give both objectives regarding SOC and catenary voltage the same priority, the rules integrate all possible decisions of the FL supervisor with respect to the total combination of the states of the input variables.

*Table 4.10 Developed rules of the FL supervisor for architecture 2*

| Rule | Weight | Name |
|---|---|---|
| If $SOC$ is M and $\Delta V\_cat$ is B then $P_{ref\_st}$ is Z | 1 | rule1 |
| If $SOC$ is M and $\Delta V\_cat$ is M then $P_{ref\_st}$ is Z | 1 | rule2 |
| If $SOC$ is M and $\Delta V\_cat$ is S then $P_{ref\_st}$ is PB | 1 | rule3 |
| If $SOC$ is B and $\Delta V\_cat$ is S then $P_{ref\_st}$ is PB | 1 | rule4 |
| If $SOC$ is B and $\Delta V\_cat$ is M then $P_{ref\_st}$ is PM | 1 | rule5 |
| If $SOC$ is B and $\Delta V\_cat$ is B then $P_{ref\_st}$ is Z | 1 | rule6 |
| If $SOC$ is S and $\Delta V\_cat$ is B then $P_{ref\_st}$ is NB | 1 | rule7 |
| If $SOC$ is S and $\Delta V\_cat$ is M then $P_{ref\_st}$ is NM | 1 | rule8 |
| If $SOC$ is S and $\Delta V\_cat$ is S then $P_{ref\_st}$ is Z | 1 | rule9 |

#### 4.4.2.3 Fuzzy inference surface for real-time supervision

In Architecture 2, the operation of the real-time supervisor can be understood directly through the surface representation of the fuzzy inference system, which maps the normalized inputs (SOC and catenary voltage deviation) to the normalized output ($P_{ref\_st}$).

The surface as shown in Fig. 4.37, embodies the combined effect of all fuzzy rules, showing how the supervisor generates smooth transitions between charging, discharging, or idle states of the ESS depending on inputs conditions.

At low SOC (values near 0), the surface tends toward negative normalized outputs, reflecting rules that prioritize charging to guarantee storage availability. At high SOC (values towards 1), the output shifts positive, activating discharging rules to prevent saturation and free capacity. Along the voltage axis, when the normalized value of $\Delta V_{cat}$ is close to zero meaning important voltage drop, the surface rises toward positive values, meaning the fuzzy supervisor solicits ESS discharge to support the catenary voltage. Conversely, when the normalized value of $V_{cat}$ is approaches 1 (risk of overvoltage), the surface dips negative, favouring ESS charging.

This continuous and gradual evolution across the surface highlights the advantage of fuzzy logic: instead of abrupt mode changes, the system smoothly interpolates between rule-based actions, ensuring adaptive and stable real-time supervision. In this way, the surface provides a compact visualization of how the fuzzy rule base integrates SOC management and catenary voltage regulation into a single, normalized ESS reference setpoint output for architecture 2.

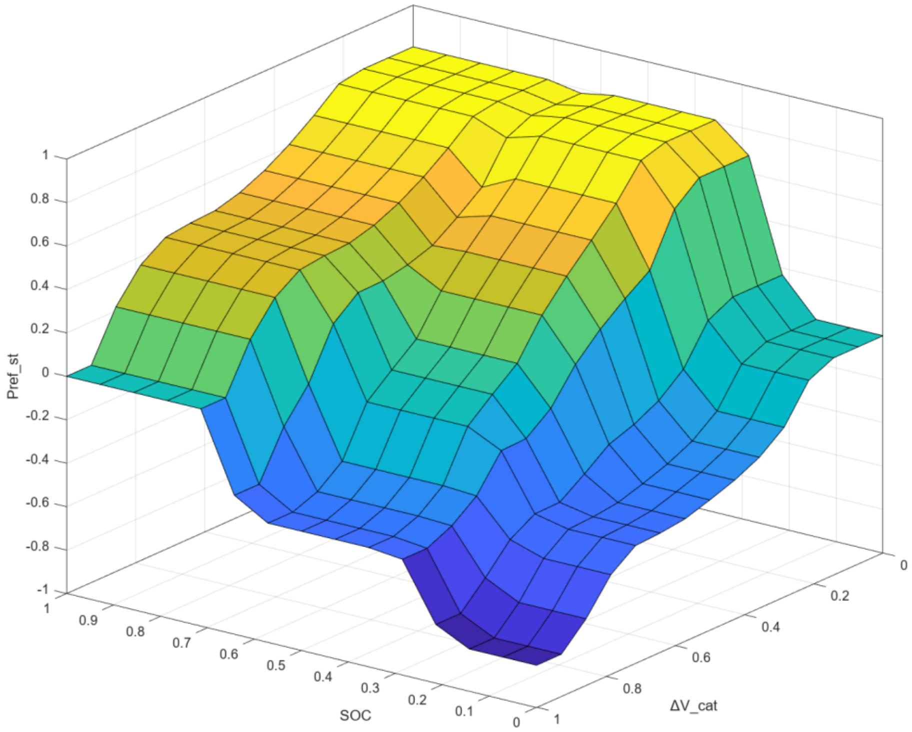


*Fig. 4.37 Surface representation of the fuzzy inference system in Architecture 2*

### 4.4.3 Results of the tested scenarios

This section presents the proposed scenarios to simulate the dedicated model built in Chapter 2 for the 2$^{nd}$ architecture. The scenarios are developed in a way that demonstrate the capabilities of the real time supervisor to manage the ESS in a way that achieves the objectives described earlier. The 2$^{nd}$ architecture is highly dynamic compared to the 1$^{st}$ architecture, a representation of the circulating train is proposed with dynamic circuit that requires the train position, speed and power consumption, to dynamically adjust the equivalent resistance of the catenary and the rails based on the position. For the tested results, only the ESS is connected at the PMP, without the PV. The supervisor doesn't take into consideration the PV, as there is no solution to curtail the necessary PV production to maintain a balance of the voltage at the catenary level.

#### 4.4.3.1 Unidirectional trains circulation (low traffic)

In this simulated scenario, the timetable schedules four trains within a one-hour circulation period, each entering the 20 km track at different times and with distinct operating speeds. The first train enters the track at minute 00:06 with a speed of 120 km/h, followed by a second train at minute 00:36 circulating with 180 km/h speed. Fig 4.38 shows trains trajectories on track 1, where the trains start travelling from TSS1 substation at 0 km towards TSS2 at 20 km. The travelled distance of every train is increased linearly due to the constant speed of the trains. As illustrated in Fig. 4.38, trains operating on Track 1 (TSS1 → TSS2) begin their journey at 0 km, travel towards the midpoint (PMP), and exit the section upon reaching 20 km at TSS2. In contrast, trains on Track 2 (TSS2 → TSS1) start at 20 km and move in the opposite direction toward TSS1 (0 km).

This scenario is characterized with low traffic, only trains that circulates on the first track from TSS1 to TSS2 exist without the opposite circulation in track 2. The single track cannot have two trains at the same time connected to it. A train must leave the track in order to allow a new train to enter the track.

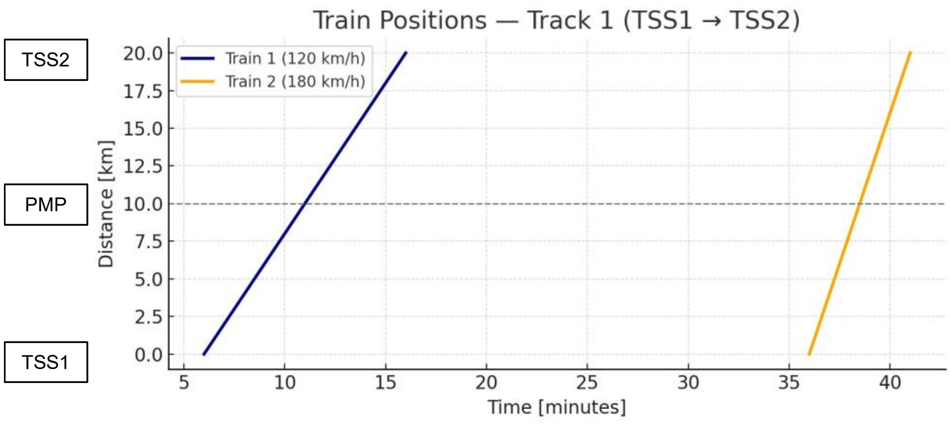


*Fig. 4.38 Trains position along the tracks represented by their kilometric distance from the TSS and the PMP*

The traction demand is expressed in terms of train power consumption at its rated speed. For each speed range, a specific power consumption value is assigned, the higher the speed, the greater the power demand. This timetable therefore produces a dynamic load profile on the railway lines, with multiple trains overlapping in time and position, enabling the evaluation of catenary resistance variations, current distribution along different track sections, and the overall aggregated electrical demand on the DC railway supply system. Table 4.11 summarizes the entry times (in minutes), speeds, and the power consumption of the trains that circulates at track 1.

*Table 4.11 Train timetable used for simulation*

| Track | Direction | Entry Time (min) | Speed (km/h) | Power (kW) |
|---|---|---|---|---|
| 1 | TSS1 → TSS2 | 6 | 120 | 2560 |
| 1 | TSS1 → TSS2 | 36 | 180 | 4000 |

The evaluation of the performance of the energy supervision system applied to the connected ESS and PV is done by comparing the results of the catenary voltage variation and the pantograph voltage variation with two other cases, a case where there is a parallel connection post PMP but without the ESS and the PV, and one case where there is no PMP connection at all. Therefore, the importance of the PMP can be highlighted, and the impact of the supervised ESS

The measured catenary voltage is shown in Fig. 4.39 (the catenary voltage graph). Comparing the catenary voltage in the case of PMP connecting the TSS without RACCOR-D ($V_{cat\_PMP}$) and the catenary voltage in the case of RACCOR-D system connected to the PMP ($V_{cat_{RACCOR-D}}$). The voltage drop is reduced in the case of ESS connected to the PMP. The ESS is managed by the FL supervisor to be solicited in discharge when the voltage of the catenary starts decreasing as shown in Fig. 4.39 in the ESS setpoints and SOC graph. The injected power from the ESS helps in reducing the catenary voltage drop at the mid-point between two TSS.

The fuzzy logic supervisor decides to discharge with higher levels in the 2$^{nd}$ train circulation that has the highest power and highest speed and causes the highest voltage drop. For the 1$^{st}$ train, the power consumption is lower than the 2$^{nd}$ one, the supervisor in this case proposes to discharge with lower power than in the 2$^{nd}$ circulation that consists of a heavier train in terms of speed and power. This validates that the supervisor model is adaptable to the different voltage drop levels.

The initial SOC level is set at 50% corresponding to the MEDIUM membership function, after the discharge of the ESS the SOC stays above 20%, for and it doesn't charge in between circulations. The charging of the ESS in the absence of PV is difficult to be optimized. The developed supervisor via its rules, can only propose the charging of the ESS when the SOC is very low.

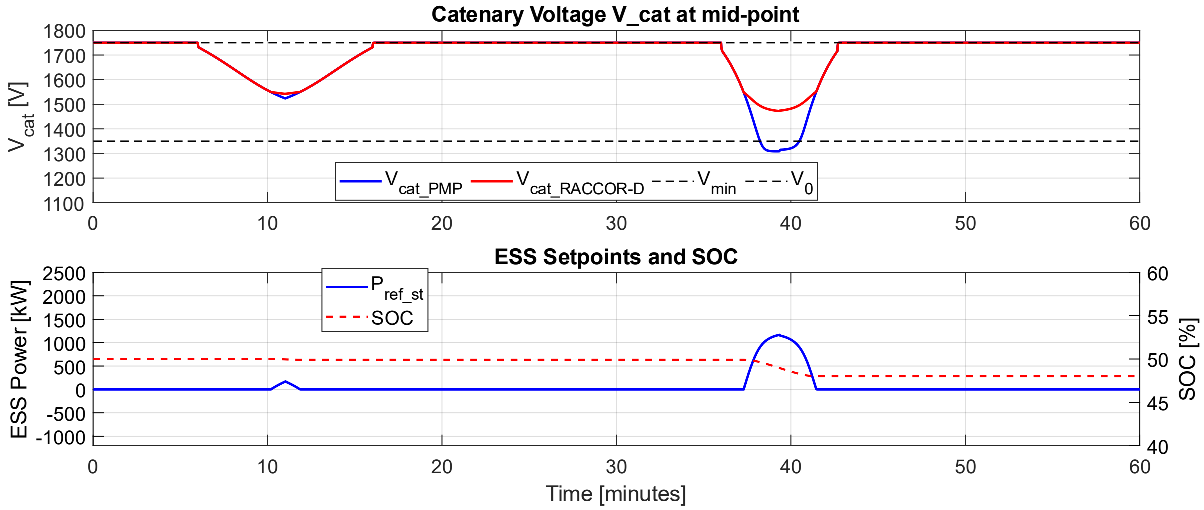


*Fig. 4.39 Catenary voltage variation and ESS reference setpoints for low traffic scenario*

The ESS and the PV connected at the PMP can be solicited in a way that reduce the voltage drop at midpoint between two TSS. Leading to a direct effect on the voltage levels at the train's pantograph. For every train that circulates along the tracks, depending on its rated power consumption it requires a minimum voltage level to operate at its rated speed. The voltage measured at the connection point between trains and catenary is plotted in Fig. 4.41 for the both cases (PMP, RACCOR-D). For the first circulation, where the ESS discharges with low power, the pantograph voltage in the case of RACCOR-D is very close to the case of PMP without RACCOR-D. The 2$^{nd}$ circulation with heavier train shows the importance of having an ESS to guarantee a higher voltage at the pantograph along the train's journey. Connecting ESS to the PMP improves the voltage level at the train pantograph, offering additional possibilities to circulate heavy trains in terms of power and speed to the classical PMP without additional energy sources.

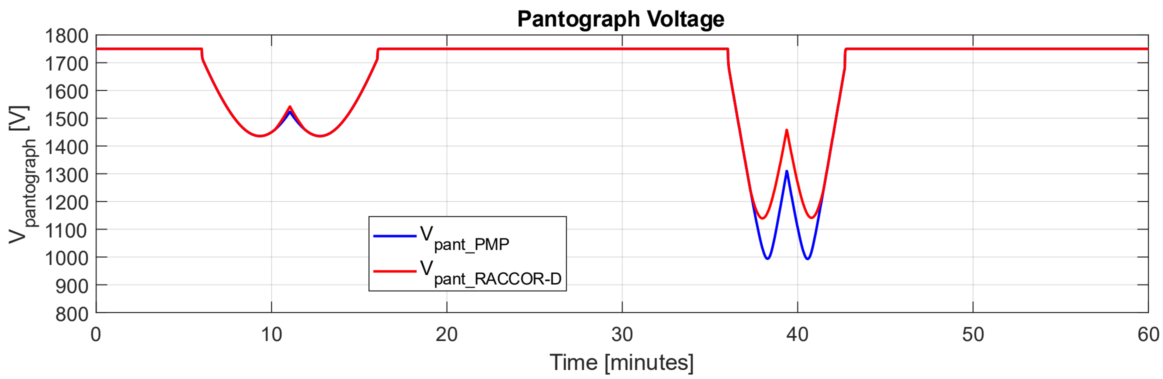


*Fig. 4.40 Pantograph voltage in the low traffic scenario*

#### 4.4.3.2 Bidirectional trains circulation (high traffic)

To represent a high traffic scenario, both of the tracks are occupied with trains, the moment a train enters Track 1 at TSS 1, another train enters Track 2 enters in the opposite direction. This represents a critical case, in general, the track cannot support the existence of two trains in the same direction due to safety regulation. So, to present a high traffic density, track 2 must be occupied with trains. To test this high traffic scenario, the 2nd circulation is kept as it is from scenario 1, and for the 1st circulation, a train in the opposite direction circulates in track. So, during the first circulation, both tracks are occupied in the high traffic scenario. Table 4.12 Train timetable for the high traffic scenario represents the trains information used for this one-hour simulation, the circulation of track 1 is kept the same as the scenario before.

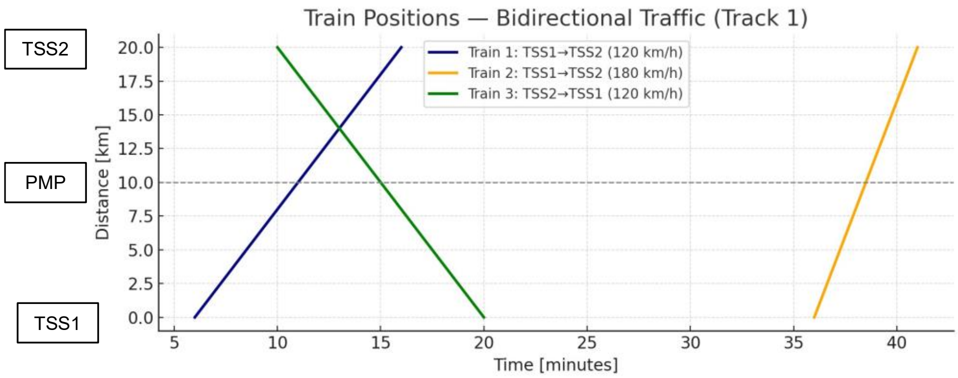


*Fig. 4.41 Trains position along the tracks represented by their kilometric distance from the TSS and the PMP*

*Table 4.12 Train timetable for the high traffic scenario*

| Track | Direction | Entry Time (min) | Speed (km/h) | Power (kW) |
|---|---|---|---|---|
| 1 | TSS1 → TSS2 | 6 | 120 | 2560 |
| 1 | TSS1 → TSS2 | 36 | 180 | 4000 |
| 1 | TSS2 → TSS1 | 9 | 120 | 2560 |

Fig. 4.43 shows the catenary voltage and the ESS reference setpoints. In this scenario the voltage drop of the catenary is more remarkable, going lower than the minimum catenary voltage level in the cases PMP without RACCOR-D. For the first circulation of trains that has two 120 km/h trains, in case of classical PMP, the catenary voltage at mid-point falls under the minimum operational level 1350V due to high traffic caused by the train that circulates now on track 2.

The discharge power of the ESS is higher than the discharge occurring in the low traffic scenario. Reaching around 1000 kW value instead of 165 kW in the low traffic scenario. The higher discharge occurs to compensate the greater voltage drop that arrives at the catenary level due to the circulation of two trains at each track unlike before. For less voltage drop occurring during the 2nd circulation, the ESS discharges with less power than during the first circulation. Demonstrating the capability of smart discharging repartition depending on the catenary voltage level.

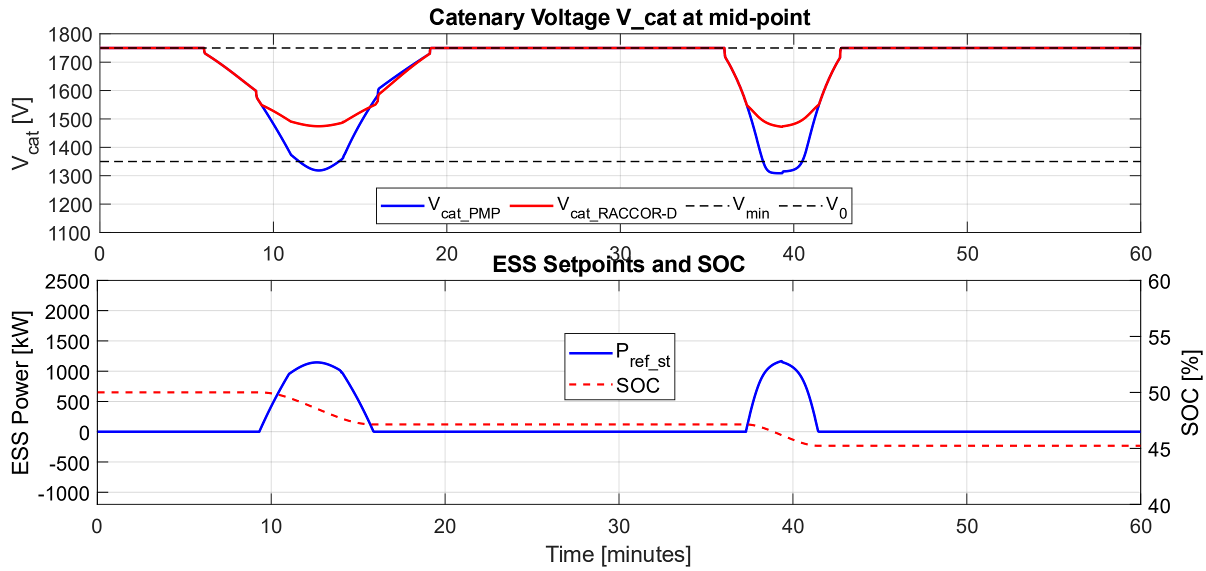


*Fig. 4.42 Catenary voltage variation and ESS reference setpoints for low traffic scenario*

For the pantograph, the RACCOR-D case maintains higher voltage at the pantograph terminals of the circulating trains as shown in Fig. 4.43  Pantograph voltage in the different cases of PMP in the high traffic scenarioeven though both tracks are occupied, and the consumption is higher. The ESS contributes effectively to the reduction of the voltage at the pantograph.

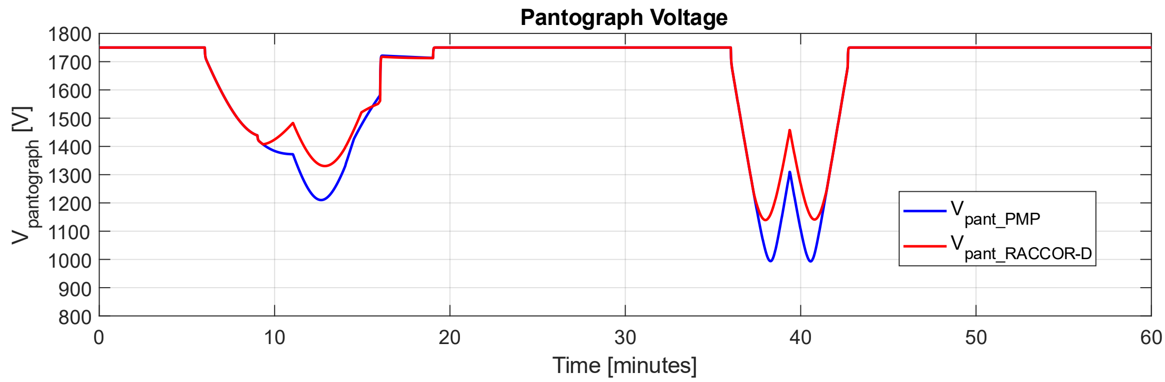


*Fig. 4.43  Pantograph voltage in the different cases of PMP in the high traffic scenario*

## 4.4.4 Assessment and potential

The voltage deviation is calculated for both scenarios and for the different cases, the lowest voltage levels recorded for the pantograph and the catenary are presented in the table below. Considering the first circulation of trains occurring in the 6$^{th}$ minute of the simulation. With the pantograph voltage measured at the born of the train1 of track 1. The catenary voltage is always measured at the mid-point PMP. For both scenarios, the case of RACCOR-D system connected to PMP reduce the voltage drop compared to the other cases. Achieving higher voltage at the catenary and pantograph levels as shown in Table 4.13.

*Table 4.13 Pantograph and catenary minimum measured voltage*

| **Scenario** | **Voltage** | **Cases** PMP | PMP_RACCOR-D | |
|---|---|---|---|---|
| Low traffic | Pantograph | 1 435 V | 1 435 V | Train 1<br>Track 1 |
| High traffic | | 1 210 V | 1 341 V | |
| Low traffic | Catenary | 1 523 V | 1 542 V | |
| High traffic | | 1 318 V | 1 474 V | |

The calculation of the catenary voltage deviations for each circulation of trains in the high and low traffic scenarios can tell the percentage of improvement of the voltage drop when the ESS is connected to the PMP as shown in Table 4.14. To evaluate improvement, the relative gain in catenary voltage for each circulation as in Equation (4.16).

$$Improvement\ (\%) = \frac{\left(\Delta V_{cat,\,PMP\ with\ RACCOR-D} - \Delta V_{cat,\,PMP\ no\ RACCOR-D}\right)}{\left|\Delta V_{cat,\,PMP\ no\ RACCOR-D}\right|} \times 100 \quad (4.16)$$

*Table 4.14 Catenary voltage deviation*

| **Scenario** | **Circulation** | **Cases** $\Delta V_{cat}$ PMP no RACCOR-D | $\Delta V_{cat}$ PMP with RACCOR-D | Improvement (%) |
|---|---|---|---|---|
| Low traffic | 1st | +173 V | +192 V | + 11 % |
| | 2nd | - 42 V | +124 V | + 395 % |
| High traffic | 1st | -32 V | +124 V | + 487.5 % |
| | 2nd | - 42 V | +124 V | + 395 % |

The comparative results presented in Table 4.14 clearly demonstrate the positive impact of the RACCOR-D supervision allowing the ESS to contribute to maintaining higher catenary voltage levels. Under low-traffic conditions in the first circulation, the voltage improvement at the PMP is around 11% since the catenary voltage drop is not very remarkable.

The improvement reaches up to +300% and 400% during the second circulation with the fastest train and the first circulation in the high traffic scenario, indicating that the proposed real-time supervision is particularly effective under heavily loaded conditions. This demonstrates the capability of the supervised ESS to dynamically support the catenary and significantly mitigate voltage drops, even when the network experiences maximum stress.

On average, the RACCOR-D configuration enhances the catenary voltage by approximately 300 - 400 % compared to the unsupervised PMP case, effectively mitigating voltage drops and ensuring that the minimum operational threshold (1350 V) is consistently respected even during heavy traffic. This demonstrates that the proposed real-time supervision successfully increases network robustness and enables higher train density without compromising traction performance.

These results highlight the potential benefits of applying the RACCOR-D system within the context of the 2nd architecture of RACCOR-D, positioned at the midpoint between two adjacent substations. The main objective of this configuration is to reduce catenary voltage drops occurring during periods of intense railway traffic and high train speeds. The real-time supervision tool, developed using fuzzy logic, has demonstrated its capability to dynamically regulate the ESS operation to maintain the catenary voltage within acceptable limits, even under rapid load variations caused by successive train passages.

The enhancement in the catenary voltage at mid-point, aligns with perspective of SNCF réseau, that tries to increase the distance between DC substations. The voltage drop depends on the catenary resistance, over long distances the resistivity increases, and the risk of higher voltage drop exists. Integrating energy sources at the PMP can mitigate this voltage drop

At this stage, the study of this architecture should be considered as a perspective rather than a fully validated large-scale evaluation. The simulations cover a one-hour time window, focusing primarily on the dynamic response of the real-time supervisor to catenary voltage fluctuations. Performance or economic indicators have not been assessed, since the simplified catenary and train circulation models do not allow accurate day-long operation or cost estimation.

Nevertheless, this work provides a solid basis for further developments. Integrating additional inputs related to PV production and consumption would enable more efficient management of the ESS charging process. In the current setup, the ESS is charged only when there is no train circulation and when the SOC level reaches medium or low values. A more advanced supervisory logic could optimize the use of surplus PV generation and recover regenerative braking energy during train deceleration phases. Achieving this, however, requires a more detailed dynamic train model that explicitly accounts for acceleration and braking profiles.

## 4.5 Chapter conclusion

This chapter represented the core of the proposed real time supervision strategy for the ESS of the railway smart grid. Under two architectures, the methods followed to develop the real time supervision strategy is validated through result analysis.

For architecture 1, the fuzzy logic supervisor proved capable of managing multiple objectives of different natures (economic, technical, and operational) while acting through a single control variable, the ESS power reference. Designed as a real-time supervision layer operating over the short term (ST) and complementing the day-ahead EMS functioning as a long-term supervisory level, it effectively ensures dynamic correction of forecast deviations and real-time constraint satisfaction. Despite the limited set of measurements available from the railway substation, the supervisor demonstrated robustness and adaptability, maintaining optimal operation under diverse scenarios. The combined operation of the day-ahead EMS and the real-time supervisor showed superior overall performance, achieving economic objectives while ensuring compliance with technical constraints and improving the global efficiency of the railway smart grid. It should be noted that these conclusions remain valid within the modelling framework and assumptions adopted in this chapter. Any extrapolation to different system configurations or operational contexts would require additional investigation.

The analysis of architecture 2 explored a different context, where the real-time supervisor operates without a preceding day-ahead EMS. In this case, the supervision strategy relies solely on fuzzy logic to manage the ESS and mitigate catenary voltage drop along a railway section composed of two adjacent traction substations.

Due to the absence of detailed train power consumption data and dynamic circulation profiles, a simplified equivalent electrical model was developed to represent the midpoint (PMP) section of the line. Economic indicators were not assessed in this case, as the study focuses mainly on demonstrating technical feasibility. The absence of train power consumption cannot allow to have two load profiles of two substations caused by the specific trains' dynamics.

This architecture stays as a solid perspective for the future, where the railway network operator aims with a proper sizing of PV and ESS can cover up the TSS and can maintain operation without the need of the conventional TSS with transformer and rectifier. This has an impact on future projection to remove a TSS and replacing it with green friendly sources responding to ecological regulation and to reduce the energetic bills and improve the performance of the railway lines operating in DC. As the spacing problem is back to the voltage level that the railway network operator must maintain.

Although the current model is limited to a one-hour simulation window, it provides a solid perspective for future research. With proper sizing of PV and ESS systems, the proposed configuration could eventually replace conventional traction substations, allowing local renewable generation and storage to sustain train operation independently. In the present DC railway networks, substation spacing remains a limiting factor for system expansion. Integrating PV and ESS installations between substations can play a crucial role in increasing the allowable distance between two substations. With adequate real-time supervision, these resources could be coordinated to compensate for voltage drops and maintain catenary voltage within acceptable limits that guarantee the train circulations, thereby overcoming one of the main technical barriers to wider deployment of renewable-powered DC railway systems.

# Chapter 5. Experimental validation and industrial transfer

## 5.1 Introduction

The experimental validation stage aims to verify the effectiveness and robustness of the developed energy management and real-time supervision strategies before any field deployment on an actual railway TSS. For this purpose, a Software-in-the-Loop (SiL) is implemented using OPAL-RT real time simulator and a definition of the Hardware-in-the-Loop (HiL) environment is presented to prepare the supervisor for industrial integration. This environment allows the complete model of the traction substation, integrating TSS load, PV generation, and energy storage, to be executed in real time while interacting with external supervisory algorithms through industrial communication protocols.

The objective is to reproduce in a controlled laboratory setting, the dynamic behavior of the RACCOR-D system under realistic operating conditions and communication delays, thus bridging the gap between offline simulations and on-site implementation.

The experimental validation is carried out with OPAL-RT. The developed Simulink model used for simulation is compiled to OPAL-RT simulator. Unlike the results of Chapter 4, in this chapter the results are obtained with 1 second dynamic. It represents a good opportunity to analyses the response of the supervisor with 1s time step measurement and explore more precise dynamic of the TSS load profile.

The industrial transfer consists of developing the suitable architecture that prepares the implementation of the real time supervision tool in TSS demonstrator. This chapter covers the definition of the global architecture proposed for the industrialization of the supervisor, in addition to the different technologies that enters in this development.

The experimental validation with OPAL-RT is done at first, to verify the possibility of creating a real time environment from the Simulink model. Then the results obtained through MATLAB/Simulink simulation are compared with the results obtained when OPAL-RT has adapted the developed Simulink file called experimental results. The real time simulation architecture is explained in detail. Then the industrial transfer is explained, with a global SCADA information system architecture and choices of strategies. For the moment, it serves as a perspective since it requires adaptation and transformation of the real time supervisor to Python programming language.

## 5.2 Experimental validation environment with OPAL-RT

### 5.2.1 Overview of OPAL-RT platform

The OPAL-RT platform is a high-performance real-time simulator designed for power system and power electronics applications. It combines multicore CPUs and field-programmable gate arrays (FPGAs) to execute detailed electrical models with time steps down to a few microseconds, ensuring accurate representation of fast-switching converter dynamics and grid transients.

One of the key features of justifying its use in RACCOR-D to test the real time supervision is its ability to execute models developed in MATLAB/Simulink directly within the RT-LAB environment, ensuring deterministic and real-time performance.

Another essential aspect of OPAL-RT is its hardware-in-the-loop (HIL) capability. Real industrial controllers such as PCs or programmable logic controllers (PLCs) can be interfaced with the simulator through analogue or digital inputs and outputs or via standard communication protocols such as Modbus-TCP, CAN, or IEC-61850. This enables closed loop testing under realistic operating conditions without risking damage to actual equipment.

The platform also offers significant scalability and modularity. Different subsystems of the railway power network, including TSS load, ESS and PV systems, and the grid, can be executed on separate computational cores. This configuration allows for parallel execution and fine adjustment of individual sampling times, ensuring that each component operates under optimal computational conditions.

In addition, OPAL-RT provides high-fidelity time synchronization, which is fundamental for validating real-time supervisory algorithms and verifying the temporal coherence of fuzzy-logic-based decision systems.

In the context of this thesis, OPAL-RT serves as the environment simulator of the railway smart grid, hosting the complete Simulink model of the traction substation, including the electrical network, the ESS and PV connected as in architecture 1.

### 5.2.2 Real-time simulation architecture

Fig. 5.1 presents the overall architecture of the implemented platform. The OPAL-RT simulator executes, in real time, the detailed model of the DC railway smart grid with the PV system, the energy storage system (ESS), the traction substation load consumption (TSS Load), and the grid model. Electrical variables such as the DC-bus voltage $V_{DC}$, the power drawn from the grid $P_{grid}$, and the state of charge ($SOC$) are transmitted through a Modbus-TCP communication link to an industrial PC hosting the global energy supervision tool. This interface reproduces the communication infrastructure that would be deployed on site between sensors, converters, and the supervisory control unit.

Within this framework, the OPAL-RT platform emulates the physical system operating in real time, while the industrial PC performs the decision-making and supervisory functions. It implements the two-level control architecture proposed in this work. The first level corresponds to the day-ahead energy management system (EMS), which optimizes the 24-hour scheduling of storage charge and discharge operations based on consumption forecasts obtained from LSTM models and photovoltaic production forecasts provided by the SteadySun API. The second level is the real-time fuzzy logic supervisor, responsible for continuously adjusting the ESS power reference $P_{ref\_st}$ considering the actual measurement of the SOC, the DC-bus voltage $V_{DC}$, and the instantaneous grid power. The industrial PC also manages data acquisition and hosts Dockerized services dedicated to forecasting, optimization, and data exchange tasks.

A Modbus emulator ensures the deterministic synchronization of data flows between the OPAL-RT simulator and the supervisory PC, whereas the PcVue environment provides a human–machine interface enabling real-time visualization and demonstration of the system's operation.

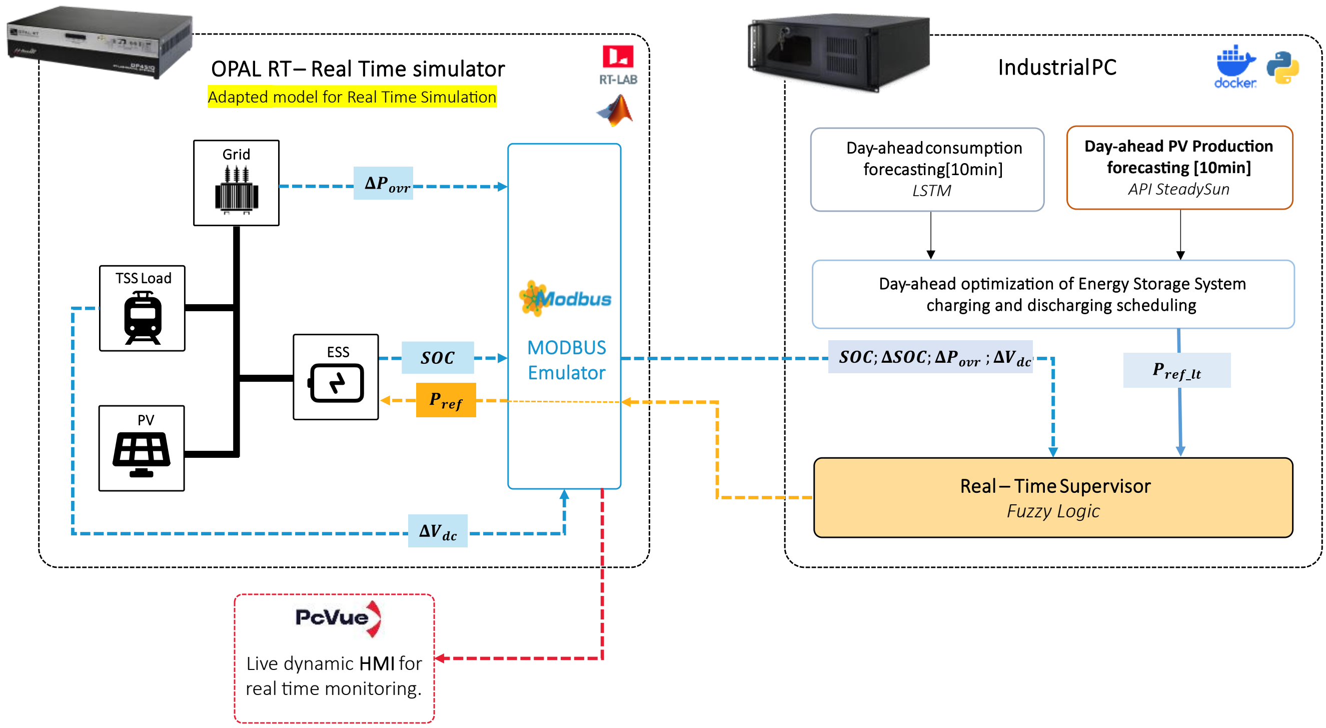


*Fig. 5.1 Representation of the interconnection between OPAL-RT simulation environment and industrial PC*

### 5.2.3 Role of the industrial PC

Although the OPAL-RT simulator is used for laboratory validation, the final deployment of the RACCOR-D supervision framework will rely on an industrial PC installed at the substation. This computer is designed to host:

- The day-ahead energy management system (EMS).
- The real-time fuzzy supervisor.
- The forecasting and data acquisition modules (TSS consumption, PV production, SOC, $V_{dc}$).
- All required communication interfaces with sensors and converters.

Hence, during the OPAL-RT experiments, the industrial PC serves as a real time supervisor interacting with the simulated system. In the industrial transfer phase, the same configuration will be reused, but the PC will communicate directly with the real substation equipment instead of the OPAL-RT model. This approach ensures full software portability between the laboratory environment and the field installation.

### 5.2.4 Software-in-the-loop validation process

The software-in-the-loop (SIL) validation was conducted to assess the interaction between the supervisor algorithms and the simulated railway power system before proceeding to hardware implementation. The process involved several successive stages designed to ensure real-time compatibility and communication consistency between the OPAL-RT model and the supervisory software.

The detailed Simulink model of Architecture 1, representing the PV and ESS integration at the traction substation, was first adapted to meet real-time execution constraints. This step involved simplifying non-essential dynamic elements and verifying the numerical stability of the fixed time-step solver. The adapted model was then compiled under the RT-LAB environment and partitioned into subsystems allocated to the OPAL-RT computational cores, enabling parallel execution and deterministic simulation performance.

Subsequently, the communication layer was configured by replacing physical input–output channels with Modbus-TCP variables corresponding to the measurement signals and control commands exchanged with the supervisory application. This setup established a closed-loop interaction in which the industrial PC transmitted the ESS power reference $P_{ref}$ to the simulated plant, while OPAL-RT continuously returned the state of charge (SOC), the DC-bus voltage $V_{dc}$, and the grid power $P_{grid}$to the supervisor at each sampling interval.

Throughout the simulation, all quantities were monitored in real time using the PcVue interface, which also ensured systematic data logging for subsequent performance evaluation. The recorded datasets were analyzed to assess response time, numerical stability, cost reduction, and improvement of PV self-consumption.

Overall, this SIL configuration enabled comprehensive testing of real time energy supervision, under realistic dynamic conditions, prior to deployment on the physical hardware platform.

## 5.3 Experimental validation results

### 5.3.1 Tested scenario

The proposed 1st architecture of RACCOR-D is considered for the experiment, where available historical data are extracted with a sampling time of 1s covering the TSS load consumption. As shown in Fig. 5.2, the dynamic load is characterized with multiple overruns that occur for small duration, the subscribed power overrun can be instantaneously overpassed.

Unlike in Chapter 4 where the TSS power consumption is with 10-minutes average, the numerous instantaneous overruns do not exist. Although, it was necessary to analyze the behaviour of the real time supervisor with graphs plotted with 10-minutes average, especially for the calculation of the CMDPS. The experimental validation chapter is a good place to investigate the dynamic behaviour of the energy supervision tool with available TSS load measurement with 1s time step.

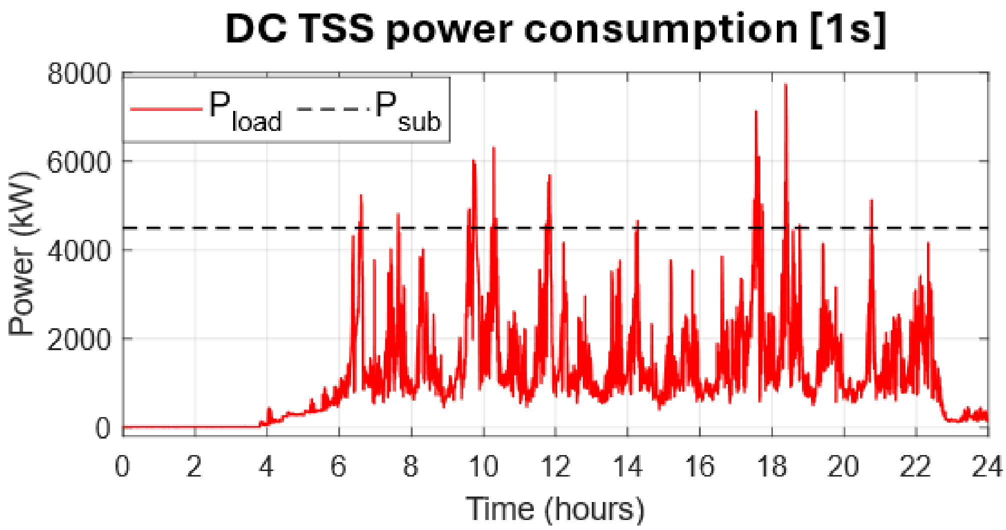


*Fig. 5.2 TSS consumption profile used in the experimental validation*

For the PV generation, Fig. *5.3* shows the PV production profile of a sunny day scenario where maximum PV power is achieved at mid-day.

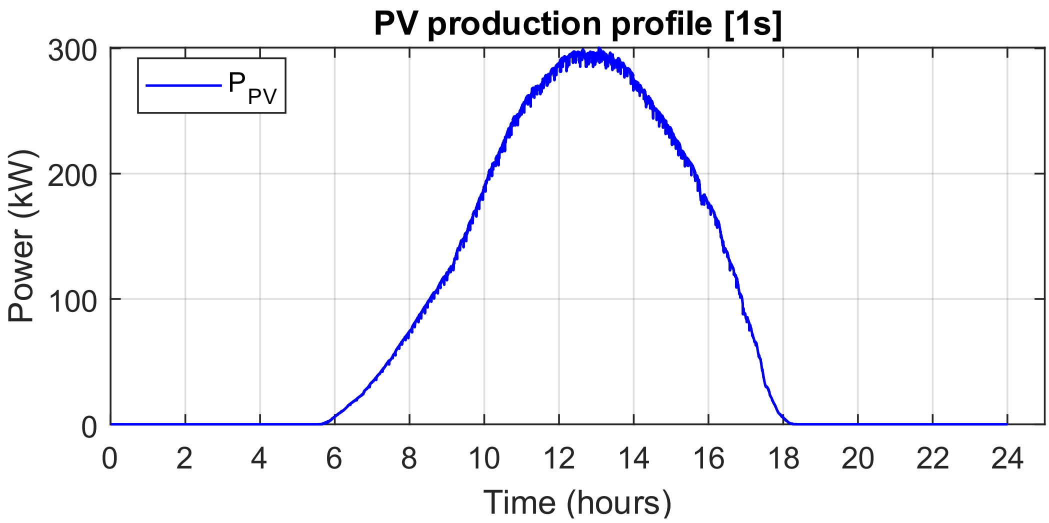


*Fig. 5.3 PV production profile for the tested scenario*

The day ahead reference setpoints $P_{ref\_lt}$ is obtained through the day ahead optimization, with 10 minutes average. The historical data of power consumption is resampled into 10 minutes average, and a forecast profile with errors and deviations from the actual TSS consumption is used as input to the optimization algorithm. For the day ahead planning, the use of 10 minutes average is compatible with the nature of the optimization algorithm, reducing the time step will lead to a higher number of decision variables. Causing negative impact on the capability of the optimization algorithm to converge into feasible solution.

### 5.3.2 Simulation results

The simulation results of 1 day are shown in Fig. 5.4, where the power drawn from the grid is plotted in two supervision modes, the day ahead (LT) and the real time (ST). Also, the ESS reference setpoints provided by the real time energy supervision tool is compared to the reference setpoints of the day ahead supervision alone without real time level with 10 minutes average.

The real time reference setpoints $P_{ref\_st}$ shows better dynamics suitable for the 1s time step of the TSS load. The real time supervisor adjusts the reference set point of the ESS every 1 second, in response to the variation of input variables (DC voltage, grid power overrun, SOC …).

The instantaneous subscribed power overruns happening between 6:00 and 9:00 caused the real time supervisor to solicit the ESS in discharge to limit this overrun avoiding penalties CMDPS. This behaviour is the contrary of the day ahead planning that doesn't capture these overruns due to 10 minutes average that leads to an average less than the subscribed power.

The real time supervisor exerted similar behaviour to the results explained in Chapter 4, while showing more dynamic response for a smaller time step. The main purpose behind presenting simulation results is to compare it with OPAL-RT experimental results to validate that OPAL-RT environment provides similar and accurate behaviour of the energy supervision tool. Also, to show that the proposed energy supervision tool is compatible with high dynamics and responsive in a small time step, which suits well the dynamic nature of the railway TSS load. For this reason, the analysis of the KPI's and economic gains is not performed like in Chapter

4 to avoid repetitions and to prevent adding information and explanations already described in the results of Chapter 4.

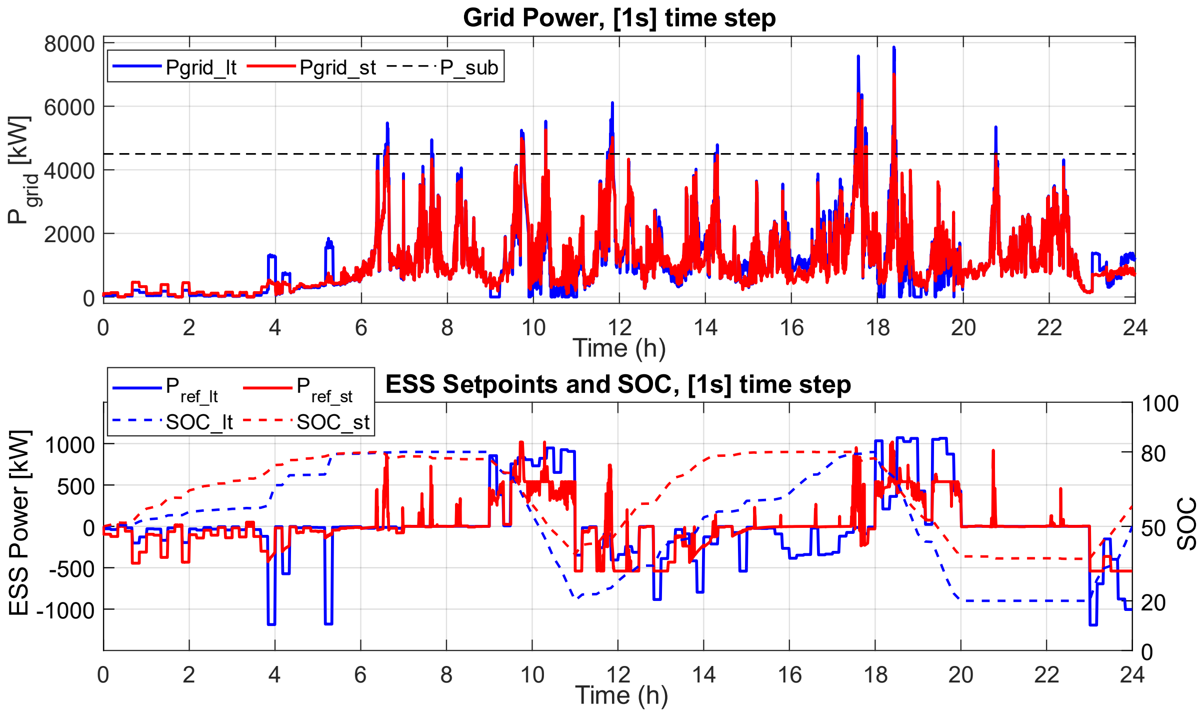


*Fig. 5.4 ESS reference setpoints, and power drawn from the grid for day ahead 'LT' and real time 'ST' supervision cases*

The obtained profile of ESS setpoints from simulation will be compared to the experimental results with OPAL-RT. After adapting the Simulink model to OPAL-RT configuration so the model can run in real time.

### 5.3.3 Experimental results

To obtain the experimental results, the developed MATLAB/Simulink model is transferred to OPAL-RT. The Simulink model covers the supervisor built with fuzzy logic toolbox, and the railway smart grid model. With the necessary measurement and the data obtained by the day ahead schedule of the day ahead supervision, the model runs in OPAL-RT in real time. The objective is to validate the real time simulation with OPAL-RT to see whether it aligns with the expected results obtained through MATLAB/Simulink simulation.

Fig. 5.5 displays these results. The power drawn from the gid is plotted with the ESS reference setpoints in real time $P_{ref\_st}$.

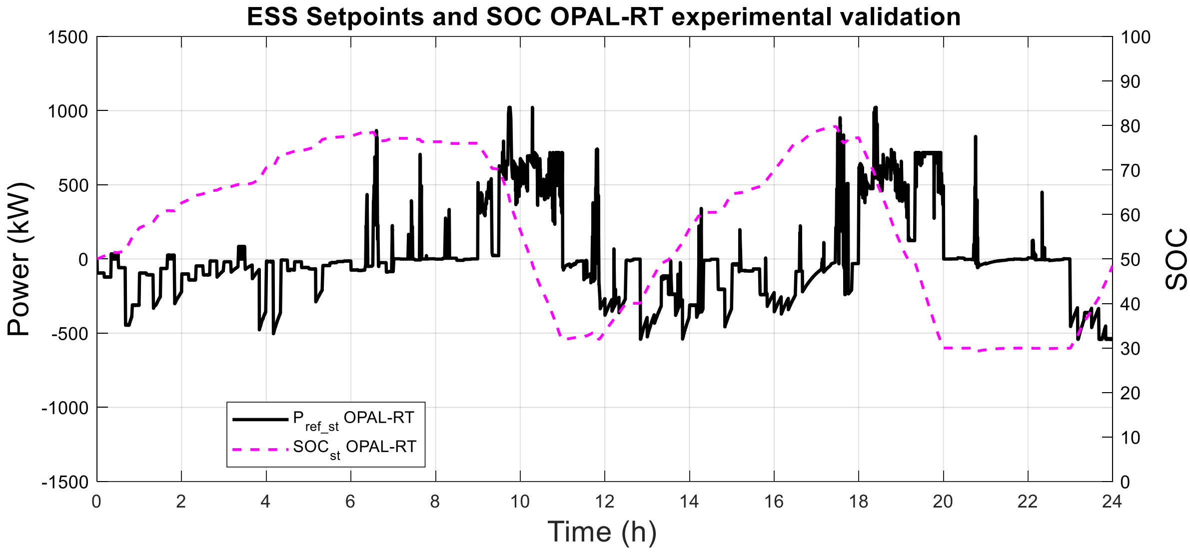


*Fig. 5.5 ESS reference setpoints obtained through OPAL-RT simulation*

### 5.3.4 Comparison between simulation and experiment

The ESS setpoints obtained through simulation and through OPAL-RT experiment are plotted in Fig. 5.6 Comparison between ESS setpoints obtained through MATLAB/Simulink and OPAL-RT simulations. The errors are calculated to see if there any deviation between what is simulated in Simulink and what is simulated in real time.

The error between the simulation and experimental simulation results is negligible from graph interpretation of Fig. 5.6. The experimental results align perfectly as expected with simulation of MATLAB/Simulink model. It demonstrates OPAL-RT capabilities to achieve an important part of the proposed architecture in Fig. 5.1. By that OPAL-RT can be prepared to be the real time simulator of the railway grid model while the supervisor can be implemented on the industrial PC in the future.

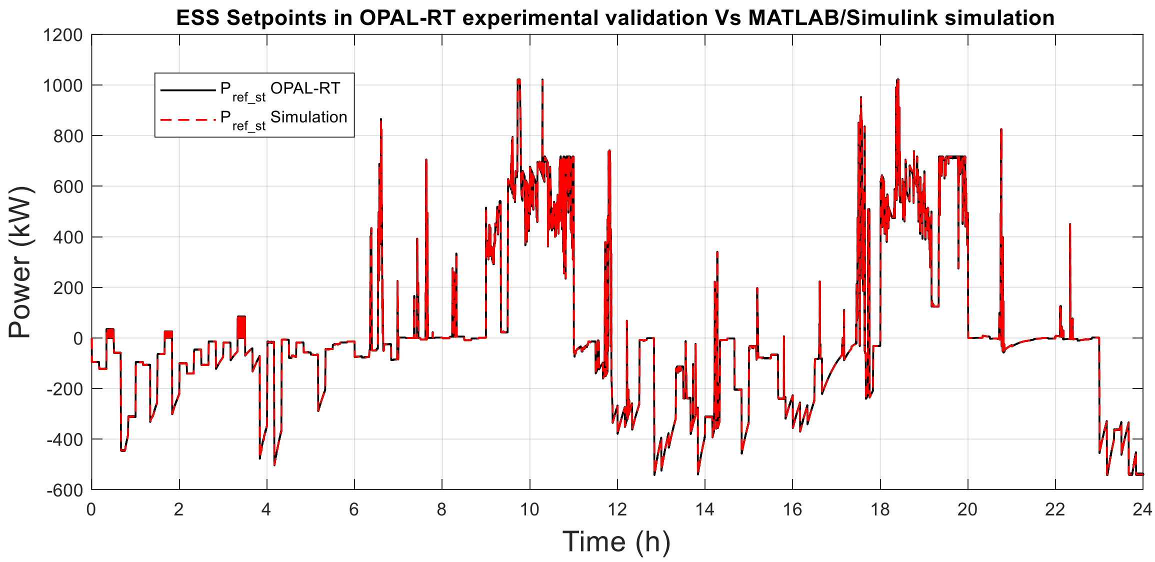


*Fig. 5.6 Comparison between ESS setpoints obtained through MATLAB/Simulink and OPAL-RT simulations*

## 5.4 Industrial transfer

### 5.4.1 Introduction and objectives

After the successful real-time validation of the proposed energy management system using the OPAL-RT simulator, the next essential phase involves the industrial transfer of the developed supervision strategies. The objective of this phase is to move from a laboratory-based, simulation-driven environment to a robust industrial setup capable of continuous operation under real constraints. This transition represents the final step toward demonstrating the operational feasibility of the proposed architecture within an actual DC traction substation integrating photovoltaic generation and energy storage systems.

In this stage, the day-ahead energy management system (EMS) and the real-time fuzzy supervisor, initially validated through Software-in-the-Loop (SiL) must be deployed on an industrial PC that will interact directly with the physical subsystems of the railway network. Unlike the OPAL-RT platform, which emulates the physical system, the industrial PC serves as the decision-making and supervisory unit within the real installation. It executes the predictive algorithms for forecast, performs day ahead optimization and real time supervision, and communicates continuously with the smart grid elements (traction substation, the PV system, and the storage system).

This section introduces the industrial information system architecture that supports this deployment. It provides an overview of the technological framework that enables the integration of the developed algorithms into a modular, scalable, and maintainable industrial platform. The implementation relies on a micro-services architecture, where each functional block (data acquisition, forecasting, optimization, control, and visualization) operates independently within a Docker container. These services communicate through the Kafka distributed messaging system, which ensures efficient, low-latency, and asynchronous data exchange between modules.

The main objectives of this section are threefold:

- To describe the structure of the industrial information system that hosts and coordinates the execution of the energy management algorithms, ensuring reliable communication between supervisory layers and field equipment.
- To detail the communication infrastructure and technological choices including the use of Modbus TCP/IP, Kafka, and Docker. That guarantee the robustness, flexibility, and real-time performance required for industrial operation.
- To clarify the role of the industrial PC, which replaces the OPAL-RT simulator in the final deployment, acting as the central intelligence of the system by managing forecasting, decision-making, and supervision in real time.

Through this industrial implementation, the developed supervisory architecture evolves from a research prototype to a fully operational SCADA-based energy management system, capable of real-time control, data acquisition, and autonomous decision-making in a railway substation environment. The following subsections detail the composition, communication flow, and technological foundations of this architecture, preparing for its validation and on-site integration.

### 5.4.2 Overview of the industrial system architecture

The industrial architecture proposed within the RACCOR-D project aims to ensure that all algorithms (initially designed and validated in MATLAB/Simulink) can be executed autonomously on an industrial PC using a robust and scalable SCADA-based architecture. This configuration, shown in Fig. 5.7, enables real-time monitoring, decision-making, and communication with field equipment, thus bridging the gap between research-grade validation and industrial implementation.

The overall system of Fig. 5.7 relies on three hierarchical layers:

- Decision layer: implemented on an industrial PC/SCADA server, responsible for executing the day-ahead optimization, forecasting models, and real-time fuzzy logic supervisor. This layer also manages the communication with external services (e.g., weather forecast API, SFTP data servers) and supervises data acquisition, storage, and visualization.
- Execution layer: composed of Programmable Logic Controllers (PLCs) denoted as PLC gateway associated with each physical subsystem of the smart grid (TSS, PV, ESS). The PLCs act as gateways between the field devices and the SCADA server, executing low-level control loops while exchanging set-points and measurements with the supervisory layer.
- Physical layer: includes the electrical infrastructure (transformer–rectifier unit, PV installation, batteries, and catenary) as well as sensors (current, voltage, SOC) that provide continuous feedback to the higher layers.

The communication between the supervisory system and the field-level controllers is achieved through a Modbus TCP/IP backbone, ensuring reliable, low-latency data exchange between the industrial PC and the programmable logic controllers (PLCs) associated with the traction substation, photovoltaic generator, and energy storage system. The SCADA layer manages all information flows required for supervision, including the acquisition of real-time measurements, data preprocessing and storage, forecasting, day-ahead optimization, and short-term control. These operations are organized as modular software services running on the industrial PC, each responsible for a specific task and communicating through standardized interfaces. The same configuration enables continuous data monitoring, execution of the fuzzy supervisor, and graphical visualization via PcVue.

All modules are deployed in an integrated and scalable environment that supports real-time execution, data synchronization, and continuous operation. This industrial setup thus ensures full portability of the algorithms initially validated under OPAL-RT, providing a seamless transition between simulation and operational implementation.

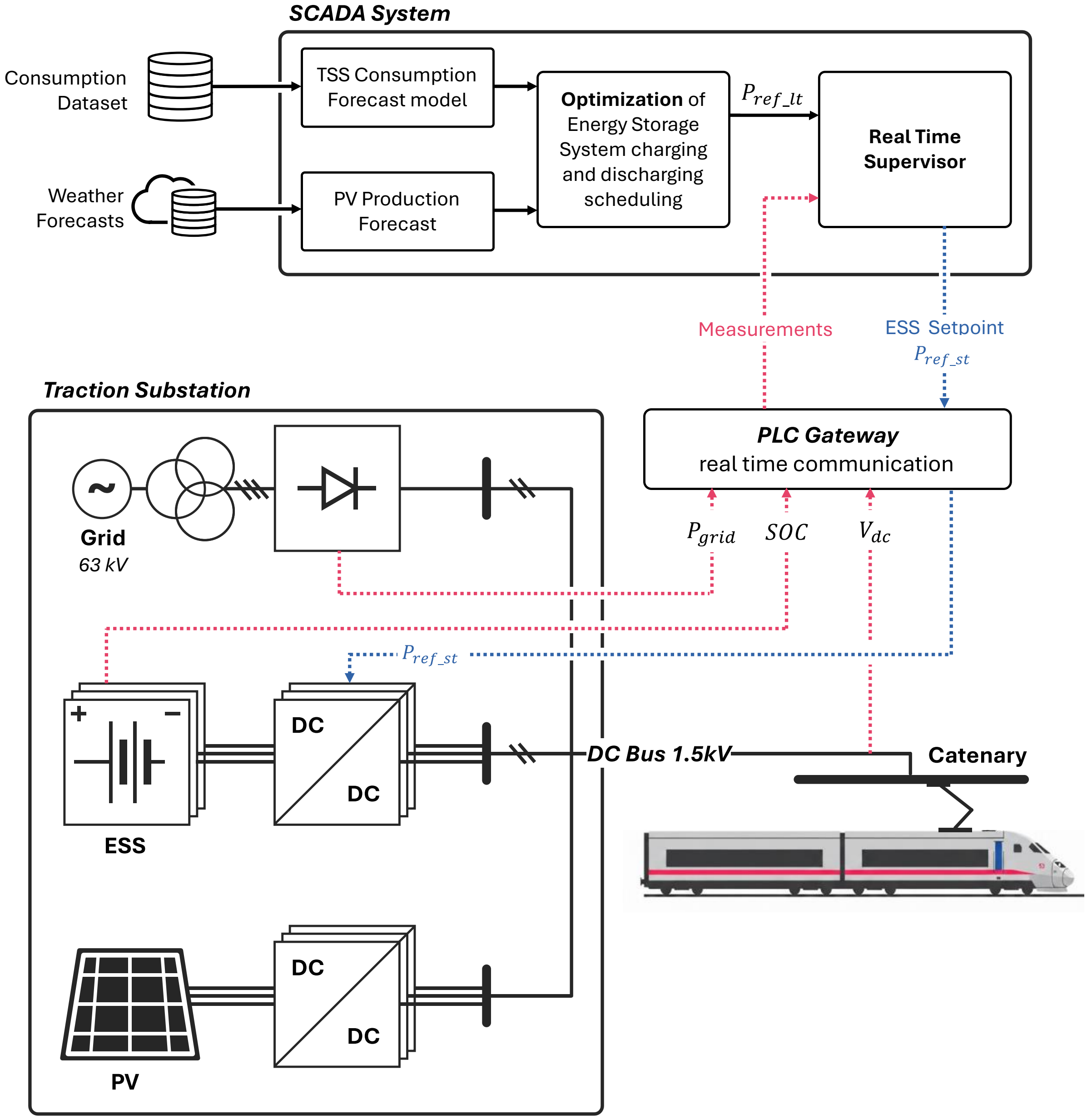


*Fig. 5.7 Diagram of TSS with local PV and ESS with simplified operational schema of SCADA*

As illustrated in Fig. 5.7, the proposed SCADA-based architecture establishes a continuous information loop between forecasting, optimization, and real-time control, ensuring coherent decision-making across all operational horizons. The industrial PC acts as the central intelligence of the system, coordinating both long-term and short-term supervision through a unified data flow. Measurements from the PLC gateway such as $P_{grid}$, $V_{dc}$, and SOC are periodically transmitted to the SCADA layer, where they are processed to update forecasts and adjust the ESS power reference in real time. This bidirectional exchange guarantees a consistent synchronization between physical and supervisory layers, allowing the controller to react within industrial-grade time constraints. The architecture therefore not only replicates the logical structure validated on the OPAL-RT platform but also provides a scalable and interoperable foundation for on-site deployment, where additional functionalities can be integrated without altering the existing control logic.

### 5.4.3 Technological choices and implementation framework

The transition from a research-oriented environment to an industrial deployment requires careful selection of software and system technologies that guarantee robustness, maintainability, scalability, and reliability. The proposed SCADA system has therefore been designed according to three main technological pillars:

- A micro-services software architecture
- A Kafka-based distributed data streaming platform
- Docker containerization for deployment and encapsulation used separate microservices.

Together, these technologies ensure modularity, real-time performance, and ease of industrial transfer.

#### 5.4.3.1 Micro-services architecture

To meet industrial standards for flexibility and maintainability, the SCADA software is structured according to a micro-services architecture. Instead of building a single large application, the system is divided into small, independent services, each responsible for a specific task such as:

- Data acquisition through Modbus TCP/IP
- Data cleaning and averaging
- Consumption and production forecasting
- Day-ahead optimization
- Real-time supervision
- Data visualization through the graphical user interface (GUI)

Each micro-service runs autonomously, communicating with other services through standardized interfaces. This design greatly simplifies integration, testing, and updates, since a modification in one module does not affect the others as long as input/output specifications are respected.

This modular design improves the system's ability to be updated and adapted over time, both key aspects of sustainable industrial operation and long-term product lifecycle. It also facilitates collaborative development among multiple contributors (engineers, researchers, or industrial partners), who can each develop and validate their specific service independently before integrating it into the global system.

From an industrial perspective, this approach brings the added advantage of allowing progressive upgrades: individual services such as improved forecasting or optimization algorithms can be replaced or updated without halting the overall SCADA operation. This ensures the continuity of supervision and reinforces the long-term sustainability of the control system.

#### 5.4.3.2 Kafka data streaming platform

Communication between the micro-services is coordinated through the Apache Kafka, a distributed data streaming platform that serves as the central communication hub. Kafka was selected for its ability to handle large, continuous data flows between producers (services that generate data) and consumers (services that process or use it) with high reliability and scalability.

Within the SCADA system, Kafka supports three key functions:

- Publishing and subscribing to real-time data streams (measurements, forecasts, optimization outputs, control set-points).
- Long-term storage of event streams to preserve and track all communications
- Real-time data processing, while still allowing historical analysis when needed.

Each micro-service writes its output to a specific Kafka topic as a producer. Other services that depend on this data subscribe to the same topic as consumers and are automatically updated when new information becomes available. For example, the real-time controller consumes data produced by the forecasting and optimization services, while the GUI consumes measurements and control outputs for visualization and diagnostics.

Kafka also ensures synchronized timing and data consistency between services, essential for maintaining the real-time responsiveness of the system. Its built-in monitoring and logging tools support continuous supervision and simplify troubleshooting. As a result, the architecture combines efficient data coordination with strong observability, ensuring dependable interaction between all micro-services.

Although Kafka introduces some challenges for achieving fully deterministic real-time behaviour in the most time-critical loops (e.g., 200 ms control cycles), it offers the scalability and reliability needed for future system expansion, such as coordinating multiple substations or integrating additional data-driven services.

#### 5.4.3.3 Docker containerization

Each micro-service is deployed within an isolated Docker container, which encapsulates the software environment, dependencies, and execution parameters specific to that service. Docker containerization provides several advantages for industrialization:

- Reproducibility and portability: Each container includes the exact version of libraries and configurations required, eliminating dependency conflicts and ensuring that the system behaves identically across development, test, and production environments.
- Simplified deployment and maintenance: The same containers can be transferred seamlessly from laboratory computers to industrial servers, enabling rapid installation or recovery in case of system updates or failures.
- Independence and resilience: Since services run in separate containers, the malfunction of one service does not compromise the others, ensuring partial operation continuity even under degraded conditions.

This container-based approach enables parallel development and deployment, as teams can work on independent containers and integrate them without version incompatibilities. It also facilitates automatic orchestration using tools such as Docker Compose or Kubernetes in future industrial implementations.

The integration of Kafka and Docker within this micro-services framework provides an industrial-grade orchestration layer for real-time data management, ensuring smooth coordination between forecasting, optimization, and control functions. These technological choices guarantee that the architecture can evolve over time, integrating new modules (e.g., cybersecurity, advanced analytics, or AI-based diagnostics) without requiring structural modifications.

#### 5.4.3.4 Summary of the whole architecture

The complete SCADA system architecture, showing the different Dockerized micro-services, is presented in Fig. 5.8. Communication between Kafka, operating as the internal data bus, and each micro-service is achieved through dedicated internal channels that ensure asynchronous yet synchronized data exchange across the entire supervision chain.

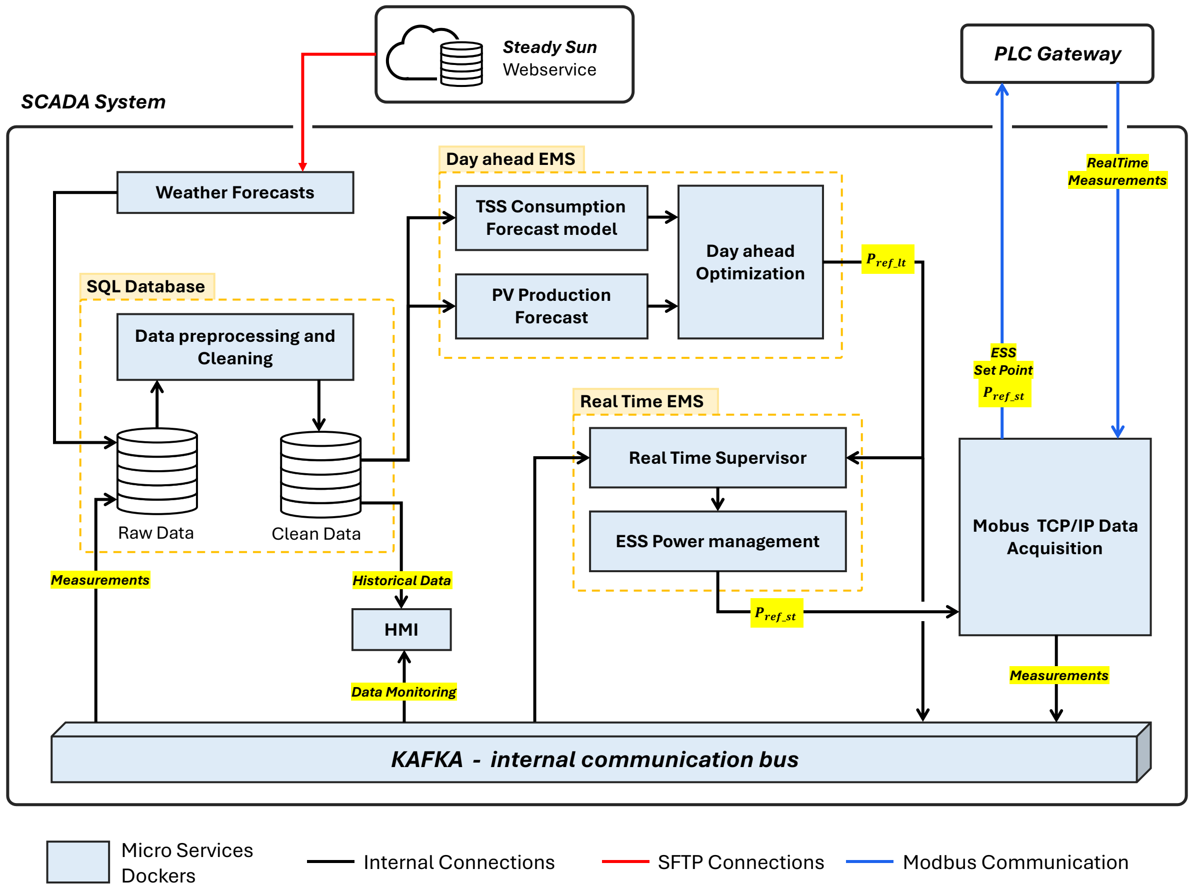


*Fig. 5.8 SCADA information system architecture*

The blue blocks represent the independent services running in Docker containers, each handling a specific task such as data acquisition, preprocessing, forecasting, optimization, or real-time control. Measurements collected from the field are transmitted through the Modbus TCP/IP interface to the PLC gateway, which performs real-time data acquisition and forwards the information to the SCADA system via Kafka. This mechanism guarantees deterministic updates of key variables such as $P_{grid}$, $V_{dc}$, and SOC, which are subsequently stored, filtered, and processed by the data-cleaning module before being made available to other services. External data, including weather forecasts from the Steady Sun web service, are integrated into the same communication flow and used by the forecasting modules to predict PV production and TSS consumption. These predictions feed the day-ahead optimization process, which generates reference setpoints $P_{ref,lt}$transmitted to the real-time supervisor. In turn, the real-time EMS refines these setpoints into short-term references $P_{ref,st}$ according to instantaneous system states received from the PLC gateway. All exchanges between services are coordinated through Kafka topics, ensuring both data consistency and operational scalability. The overall configuration thus provides a robust and modular architecture capable of supporting continuous operation and future functional extensions without altering the supervisory framework.

## 5.5 Chapter conclusion

This chapter presented the experimental validation and industrial transfer framework developed for the RACCOR-D energy supervision system. The real-time environment was first configured on the OPAL-RT platform, allowing the complete Simulink model of the traction substation to be executed in closed loop with the supervisory algorithms. This Software-in-the-Loop configuration confirmed the feasibility of running the proposed two-level control strategy under real-time constraints and demonstrated its stable and responsive behaviour with a one-second dynamic.

Beyond this experimental validation, the chapter also outlined the perspective for industrial deployment. The transition from OPAL-RT to an industrial PC has been prepared through the definition of a SCADA-based architecture integrating modular, Dockerized micro-services and a Kafka data exchange backbone. This environment establishes the foundation for future on-site implementation, where the same supervisor will operate autonomously within the demo site traction substation, enabling full validation of the industrial transfer.

# General Conclusion

This thesis has addressed the challenge of energy supervision in DC railway networks by proposing a global, multi-timescale supervision framework adapted to the strong technical and economic constraints of railway traction substations. The proposed approach goes beyond the development of isolated control tools by structuring energy management as a coordinated process combining anticipation, optimization, and real-time adaptation. In this framework, photovoltaic generation and energy storage systems are not treated as independent assets, but as integrated components of a railway smart grid whose operation must simultaneously ensure voltage stability, limit grid dependency, and reduce energy costs under regulated tariff schemes.

A key contribution of this work lies in the explicit coupling between a forecasting-based day-ahead energy management system and a real-time adaptive supervision layer. The day-ahead level exploits load and generation forecasts to plan the optimal use of the energy storage system with respect to tariff-driven economic objectives and operational constraints, while the real-time supervision compensates for forecasting errors and fast railway dynamics through a fuzzy logic-based corrective strategy. This hierarchical organization enables the system to reconcile long-term economic optimization with short-term robustness and safety requirements inherent to DC railway operation. By considering both substation-level integration and mid-point architectures between substations, the proposed supervision framework also demonstrates its adaptability to different infrastructure configurations envisioned within the RACCOR-D project. The results obtained show that coordinated multi-layer supervision constitutes an effective lever for improving the energy efficiency, economic performance, and operational resilience of existing DC railway substations, without requiring immediate large-scale infrastructure replacement.

The scientific contributions of this thesis can be summarized along four complementary axes. First, a methodological contribution is made through the design of a hierarchical energy supervision strategy explicitly tailored to DC railway smart grids. By combining forecasting-based day-ahead optimization with a real-time fuzzy logic supervisor, the proposed framework reconciles long-term economic objectives with short-term operational constraints, an aspect that is rarely addressed jointly in existing railway energy management approaches.

Second, this work provides a railway-specific contribution by embedding the technical and economic constraints of DC traction substations directly into the supervision logic. In particular, voltage limits, fast load dynamics induced by train circulation, and tariff-driven penalties related to subscribed power exceedance are explicitly considered, leading to supervision strategies that are both technically safe and economically relevant for railway operators.

Third, an architectural contribution is achieved through the analysis and supervision of two complementary integration schemes for photovoltaic generation and energy storage systems. The first focuses on substation-level integration, while the second investigates mid-point installation between two substations to mitigate catenary voltage drops. The proposed real-time supervision strategies demonstrate the capacity of energy storage to support both energy optimization and voltage regulation objectives.

Finally, this thesis contributes at the experimental and pre-industrial level by validating the proposed supervision framework in a real-time simulation environment with high temporal resolution, and by developing an industrially compatible implementation architecture. This step bridges the gap between academic development and practical deployment and constitutes a necessary foundation for future large-scale implementation within DC railway substations.

Despite the encouraging results obtained, the scope of this thesis is subject to several limitations that define clear directions for further research. First, the energy storage system and photovoltaic installation are considered with fixed sizing parameters, and their dimensioning is not jointly optimized with the supervision strategy. While this assumption is consistent with the RACCOR-D demonstrator context, it limits the ability to fully assess the interactions between infrastructure sizing, subscribed power selection, and operational performance. This justifies the low gains obtained in the total energetic bill in the day-ahead and the real time supervision cases. Also, the proposed supervision framework is primarily evaluated at the level of a single traction substation or a limited number of interacting substations. Although this approach is suitable for validating control principles and real-time behaviour, it does not yet capture the full complexity of large-scale, network-wide coordination that may arise in future railway smart grids.

Building on these results, several short- and medium-term research perspectives can be identified. In the short term, a natural extension of this work consists in coupling the proposed multi-layer supervision strategy with a joint sizing and planning approach, integrating the dimensioning of energy storage, photovoltaic capacity, and subscribed power directly into the optimization process. Such a strategy would enable globally optimal solutions that better reflect long-term economic and technical trade-offs. Further short-term developments include the integration of probabilistic forecasting and robust or stochastic optimization techniques, combined with adaptive real-time supervision, to enhance resilience under highly variable traffic and renewable generation conditions.

In the medium term, the proposed supervision architecture could be generalized to coordinated multi-substation and network-level management. Such an extension would allow energy storage systems distributed across several traction substations or parallel posts to be coordinated, enabling system-wide peak smoothing, voltage support, and improved use of regenerative and renewable energy. This perspective is particularly relevant in the context of progressive transitions toward medium-voltage DC railway networks. Plus, the results obtained in the second architecture offers a solid perspective responding to the improvement of DC traction substations. The problem of short distances between DC TSS can be tackled with the integration of the ESS between two TSS at midpoint. Short distances exist to maintain a certain voltage level and to limit the voltage drop that doesn’t support high traffic and higher speed of trains. With smart energy supervision for the ESS, the voltage drop is limited in a way that offers higher distance between the TSS while maintaining acceptable values of catenary voltage level. This is the cornerstone in expanding the work in larger scale studying the impact of integrating ESS between multiple TSS not just 2 and therefore assessing the possibility to increase the distances between the DC substations and therefore reduce the numbers of TSS in each railway line.

# Publications

**Journal article:**

- M. Shmaysani, K. Almaksour, H. Caron, B. Robyns, and C. Saudemont, “Energy management system for DC railway smart grid based on substation power forecast and energy storage system optimization,” *Mathematics and Computers in Simulation*, vol. 238, pp. 497–515, 2025, doi: 10.1016/j.matcom.2025.06.028.

**Conference papers:**

- M. Shmaysani, K. Almaksour, H. Caron, B. Robyns and C. Saudemont, "Real Time Energy Supervision for Battery Storage System in a Hybrid DC Railway Smart Grid," *2024 IEEE International Conference on Electrical Systems for Aircraft, Railway, Ship Propulsion and Road Vehicles & International Transportation Electrification Conference (ESARS-ITEC)*, Naples, Italy, 2024, pp. 1-6, doi: 10.1109/ESARS-ITEC60450.2024.10819796.
- K. Almaksour, M. Shmaysani, F. Gosselin, H. Caron, A. Ducrocq, *et al.*, “Information system architecture for supervision and control of railway smart grids,” in *Proc. 26th European Conf. on Power Electronics and Applications (EPE’25 ECCE Europe)*, Paris, France, Mar. 2025, doi: 10.34746/epe2025-0139.

# References


[1] 'Rail', IEA. Accessed: Jun. 28, 2025. [Online]. Available: https://www.iea.org/energy-system/transport/rail

[2] 'Final energy consumption in transport - detailed statistics'. [Online]. Available: https://ec.europa.eu/eurostat/statistics-explained/index.php?title=Final_energy_consumption_in_transport_-_detailed_statistics

[3] Eurostat. "Railway Transport Statistics." [Online]. Available: https://ec.europa.eu/eurostat/statistics-explained/index.php?title=Railway_transport_statistics

[4] European Commission. "Sustainable and Smart Mobility Strategy – putting European transport on track for the future," 2020. [Online]. Available: https://transport.ec.europa.eu

[5] Asuene. "Railway Transport and $CO_2$ Emissions." [Online]. Available: https://asuene.com/us/blog/decarbonizing-rail-how-eu-green-deals-mobility-strategy-is-driving-low-emission-transportation

[6] European Commission. "European Green Deal," 2019. [Online]. Available: https://ec.europa.eu/info/strategy/priorities-2019-2024/european-green-deal

[7] M. Lawrence and R. Bullock, *The Role of Rail in Decarbonizing Transport in Developing Countries*. Washington, DC : World Bank, 2022. doi: 10.1596/38214.

[8] 'Railways are the backbone of sustainable mobility & key to delivering EU climate objectives'. [Online]. Available: https://www.cer.be/cer-press-releases/railways-are-the-backbone-of-sustainable-mobility-key-to-delivering-eu-climate-objectives

[9] U.-I. union of railways, 'Sustainability', UIC - International union of railways. [Online]. Available: https://uic.org/sustainability/

[10] R. Štěrba, 'Development Strategy of Czech State Railway Infrastructure', *Transportation Research Procedia*, vol. 77, pp. 123–127, 2024, doi: 10.1016/j.trpro.2024.01.016.

[11] T. Shibayama and B. Laa, 'Sustainable Mobility Guarantee: Developing the concept from a transport planning perspective', *Transport Policy*, vol. 155, pp. 287–299, Sep. 2024, doi: 10.1016/j.tranpol.2024.07.003.

[12] E. M. Da Silveira Brito, P. Ladoux, J. Fabre, and B. Sonier, 'Reinforcement of DC Electrified Railways by a Modular Battery Energy Storage System', *Electronics*, vol. 13, no. 10, p. 1933, May 2024, doi: 10.3390/electronics13101933.

[13] 'Rly Power Supply in Europe'. Accessed: Jul. 06, 2025. [Online]. Available: https://www.lococarriage.org.uk/eurlypwrsply.html

[14] P. Simiyu and I. E. Davidson, 'MVDC Railway Traction Power Systems; State-of-the Art, Opportunities, and Challenges', *Energies*, vol. 14, no. 14, p. 4156, Jul. 2021, doi: 10.3390/en14144156.

[15] V. Sychenko, V. Kuznetsov, A. Rojek, P. Hubskyi, and Y. Kosariev, 'Energy Characteristics of the DC Distributed Power Supply Systems', *Komunikácie*, vol. 23, no. 2, pp. C37–C43, Apr. 2021, doi: 10.26552/com.C.2021.2.C37-C43.

[16] O. Bossi, 'Contribution au dimensionnement et à la gestion par optimisation de systèmes de stockage d'énergie pour les réseaux électriques ferroviaires', These de doctorat, Université Grenoble Alpes (ComUE), 2016. Accessed: Jul. 06, 2025. [Online]. Available: https://theses.fr/2016GREAT001

[17] K. Tournoux, A. Houari, M. F. Benkhoris, F. Terrien, and P.-L. Garmier, 'Investigation of a 25 kV–50 Hz Railway-Substation Power Supply Based on a Back-to-Back Modular Multilevel Converter Topology', *Energies*, vol. 17, no. 6, p. 1318, Mar. 2024, doi: 10.3390/en17061318.

[18] H. Alnuman, D. Gladwin, and M. Foster, 'Electrical Modelling of a DC Railway System with Multiple Trains', *Energies*, vol. 11, no. 11, p. 3211, Nov. 2018, doi: 10.3390/en11113211.
[19] H. Hu *et al.*, 'Traction power systems for electrified railways: evolution, state of the art, and future trends', *Rail. Eng. Science*, vol. 32, no. 1, pp. 1–19, Mar. 2024, doi: 10.1007/s40534-023-00320-6.
[20] I. Watson, A. Ali, and A. Bayyati, 'Energy Efficiency of High-Speed Railways', *Adv Environ Eng Res*, vol. 03, no. 04, pp. 1–22, Dec. 2022, doi: 10.21926/aeer.2204055.
[21] S. Sharifi *et al.*, "Medium-voltage DC electric railway systems: A review on feeding arrangements and power converter topologies," *IET Electrical Systems in Transportation*, vol. 12, no. 3, pp. 223–233, 2022pure-oai.bham.ac.ukpure-oai.bham.ac.uk.
[22] P. Arboleya *et al.*, "A review of railway feeding infrastructures: Mathematical models for planning and operation," *eTransportation*, vol. 5, Article 100063, 2020researchgate.net.
[23] D. Ramsey *et al.*, "Comparison of energy recovery solutions on a suburban DC railway system," *IEEE Trans. Transportation Electrification*, vol. 7, no. 3, pp. 1849–1857, 2021
[24] 'List of railway lines in France', *Wikipedia*. Apr. 16, 2025. Accessed: Oct. 08, 2025. [Online]. Available: https://en.wikipedia.org/w/index.php?title=List_of_railway_lines_in_France&oldid=1285912190
[25] 'Simulation Of Rail Voltage And Earth Current In A Pc-based Traction Power Simulator', Accessed: Oct. 09, 2025. [Online]. Available: https://www.witpress.com/elibrary/wit-transactions-on-engineering-sciences/3/13284
[26] Y. C. R.J. Hil, 'Simulation Of Rail Voltage And Earth Current In A Pc-based Traction Power Simulator', Accessed: Oct. 09, 2025. [Online]. Available: https://www.witpress.com/elibrary/wit-transactions-on-engineering-sciences/3/13284
[27] SNCF Réseau, *Appendix 5.1.2 – Network Statement 2024: Principles for the charges related to the use of the railway infrastructure*, Feb. 2024. [Online]. Available: https://www.sncf-reseau.com/medias-publics/2024-02/ns2024m_appendix_5_1_2_eng.pdf
[28] 'Comprendre le tarif d'utilisation du réseau (TURPE) - RTE Portail Services', Portail Services RTE. Accessed: Jul. 10, 2025. [Online]. Available: https://www.services-rte.com/fr/decouvrez-nos-offres-de-service/comprendre-le-tarif-d-utilisation-du-reseau-turpe.html
[29] A. Verdicchio, P. Ladoux, H. Caron, and C. Courtois, 'New Medium-Voltage DC Railway Electrification System', *IEEE Trans. Transp. Electrific.*, vol. 4, no. 2, pp. 591–604, Jun. 2018, doi: 10.1109/TTE.2018.2826780.
[30] H. Shigeeda, H. Morimoto, K. Ito, T. Fujii, and N. Morishima, 'Feeding-loss Reduction by Higher-voltage DC Railway Feeding System with DC-to-DC Converter', in *2018 International Power Electronics Conference (IPEC-Niigata 2018 -ECCE Asia)*, Niigata: IEEE, May 2018, pp. 2540–2546. doi: 10.23919/IPEC.2018.8507567.
[31] 'Tarif d'utilisation des réseaux publics de transport d'électricité (TURPE 7 HTB)'. Accessed: Jul. 10, 2025. [Online]. Available: https://www.cre.fr/documents/deliberations/tarif-dutilisation-des-reseaux-publics-de-transport-delectricite-turpe-7-htb-1.html
[32] M. Brzeziński and D. Pyza, 'A Refined Model for Carbon Footprint Estimation in Electric Railway Transport', *Energies*, vol. 16, no. 18, Art. no. 18, Jan. 2023, doi: 10.3390/en16186567.
[33] European Union Agency for Railways, *Energy Consumption and Power Supply Systems in the Rail Sector*, ERA Report No. 20242052, TR0924239ENN, 2024. [Online]. Available: https://www.era.europa.eu/system/files/2024-07/20242052_PDF_TR0924239ENN_002.pdf

[34] Ministère de la Transition Écologique, *National Low-Carbon Strategy – Draft Version (SNBC)*. [Online]. Available: https://www.ecologie.gouv.fr/sites/default/files/documents/Projet%20SNBC%20EN.pdf

[35] A. Verdicchio, P. Ladoux, H. Caron, and S. Sanchez, 'Future DC Railway Electrification System - Go for 9 kV', in *2018 IEEE International Conference on Electrical Systems for Aircraft, Railway, Ship Propulsion and Road Vehicles & International Transportation Electrification Conference (ESARS-ITEC)*, Nottingham: IEEE, Nov. 2018, pp. 1–5. doi: 10.1109/ESARS-ITEC.2018.8607304.

[36] Andrea Verdicchio. Nouvelle électrification en courant continu moyenne tension pour réseau ferroviaire. Energie électrique. Institut National Polytechnique de Toulouse - INPT, 2019. Français. ⟨NNT : 2019INPT0093⟩. ⟨tel-04169712⟩

[37] J. Fabre *et al.*, 'Characterization and Implementation of Resonant Isolated DC/DC Converters for Future MVDC Railway Electrification Systems', *IEEE Trans. Transp. Electrific.*, vol. 7, no. 2, pp. 854–869, Jun. 2021, doi: 10.1109/tte.2020.3033659.

[38] A. Gomez-Exposito, J. M. Mauricio, and J. M. Maza-Ortega, 'VSC-Based MVDC Railway Electrification System', *IEEE Trans. Power Delivery*, vol. 29, no. 1, pp. 422–431, Feb. 2014, doi: 10.1109/TPWRD.2013.2268692.

[39] I. Ferencz, D. Petreus, and P. Tricoli, 'Converter Topologies for MVDC Traction Transformers', in *2020 IEEE 26th International Symposium for Design and Technology in Electronic Packaging (SIITME)*, Pitesti, Romania: IEEE, Oct. 2020, pp. 362–367. doi: 10.1109/SIITME50350.2020.9292214.

[40] F. Cascetta *et al.*, 'Impact of a reversible substation on energy recovery experienced on-board a train', *Measurement*, vol. 183, p. 109793, Oct. 2021, doi: 10.1016/j.measurement.2021.109793.

[41] V. Gelman, 'Energy Savings With Reversible Thyristor Controlled Rectifier', in *2009 Joint Rail Conference*, Pueblo, Colorado, USA: ASMEDC, Jan. 2009, pp. 41–46. doi: 10.1115/jrc2009-63013.

[42] 'Enviline™ ESS Energy Storage System'. Accessed: Jul. 10, 2025. [Online]. Available: https://search-ext.abb.com/library/Download.aspx?DocumentID=4116PL860-W1-en.&LanguageCode=en&DocumentPartId=&Action=Launch

[43] M. Popescu and A. Bitoleanu, 'A Review of the Energy Efficiency Improvement in DC Railway Systems', *Energies*, vol. 12, no. 6, Art. no. 6, Jan. 2019, doi: 10.3390/en12061092.

[44] 'Rail charging converter', Siemens Mobility Global. Accessed: Oct. 09, 2025. [Online]. Available: https://www.mobility.siemens.com/global/en/portfolio/rail-infrastructure/electrification/ac-traction-power-supply/rail-charging-converter.html

[45] 'Recording of webinar: Save energy costs and CO2 emissions with Sitras® PCI', Siemens Mobility Global. [Online]. Available: https://www.mobility.siemens.com/global/en/company/fairs-events/webinars/safe-energy-costs-with-sitras-pci.html

[46] S. Sharifi and P. Tricoli, "Medium voltage DC (MVDC) railway electrification systems: Assessment of performance," in *Proc. World Congress on Railway Research (WCRR)*, Birmingham, United Kingdom, 2022.

[47] J. Araúz and S. Martinez, 'Methodology for assessing the impact of regenerative braking energy injection of a direct current railway system on the distribution grid', *Electric Power Systems Research*, vol. 220, p. 109368, Jul. 2023, doi: 10.1016/j.epsr.2023.109368.

[48] Z. Sheng, A. Iovine, G. Damm, and L. Galai-Dol, 'Power Management for a DC MicroGrid in a Smart Railway Station including Recovery Braking', in *2019 18th European Control Conference (ECC)*, Naples, Italy: IEEE, Jun. 2019, pp. 1418–1423. doi: 10.23919/ECC.2019.8795676.

[49] S. Sekijima, H. Sato, and H. Hayashiya, ‘Application of Smart Grid Technology to Railway Power Supply’, p. 6.
[50] S. V. Mitrofanov, N. G. Kiryanova, and A. M. Gorlova, ‘Stationary Hybrid Renewable Energy Systems for Railway Electrification: A Review’, *Energies*, vol. 14, no. 18, p. 5946, Sep. 2021, doi: 10.3390/en14185946.
[51] M. Brenna, F. Foiadelli, and H. J. Kaleybar, ‘The Evolution of Railway Power Supply Systems Toward Smart Microgrids: The concept of the energy hub and integration of distributed energy resources’, *IEEE Electrific. Mag.*, vol. 8, no. 1, pp. 12–23, Mar. 2020, doi: 10.1109/MELE.2019.2962886.
[52] S. Aatif, X. Yang, H. Hu, S. Kumar Maharjan, and Z. He, ‘Integration of PV and Battery Storage for Catenary Voltage Regulation and Stray Current Mitigation in MVDC Railways’, *Journal of Modern Power Systems and Clean Energy*, vol. 9, no. 3, pp. 585–594, 2021, doi: 10.35833/MPCE.2019.000155.
[53] S. Nasr, M. Iordache, and M. Petit, ‘Smart micro-grid integration in DC railway systems’, in *IEEE PES Innovative Smart Grid Technologies, Europe*, Istanbul, Turkey: IEEE, Oct. 2014, pp. 1–6. doi: 10.1109/ISGTEurope.2014.7028913.
[54] L. Alfieri, L. Battistelli, and M. Pagano, ‘Impact on railway infrastructure of wayside energy storage systems for regenerative braking management: a case study on a real Italian railway infrastructure’, *IET Electrical Systems in Transportation*, vol. 9, no. 3, pp. 140–149, Sep. 2019, doi: 10.1049/iet-est.2019.0005.
[55] Szeląg, A., et al. (2025). *Hybrid Energy Storage System for Regenerative Braking Utilization and Peak Power Decrease in 3 kV DC Railway Electrification System*. Electronics.
[56] ABB. (2017). *DC Rail Transit – Wayside Energy Storage Systems*. ABB White Paper.
[57] F. Meishner and D. U. Sauer, ‘Wayside energy recovery systems in DC urban railway grids’, *eTransportation*, vol. 1, p. 100001, Aug. 2019, doi: 10.1016/j.etran.2019.04.001.
[58] F. Meishner, C. Ünlübayir, and D. U. Sauer, ‘Model-based investigation of an uncontrolled LTO wayside energy storage system in a 750 V tram grid’, *Applied Energy*, vol. 331, p. 120337, Feb. 2023, doi: 10.1016/j.apenergy.2022.120337.
[59] C. Feng, Z. Gao, Y. Sun, and P. Chen, ‘Electric railway smart microgrid system with integration of multiple energy systems and power-quality improvement’, *Electric Power Systems Research*, vol. 199, p. 107459, Oct. 2021, doi: 10.1016/j.epsr.2021.107459.
[60] P. Obrycki, K. Perlicki, and M. Stawowy, ‘Peak Shaving Strategy in the Context of the Charging Process of a Battery Energy Storage System in the Railway Microgrid’, *Energies*, vol. 18, no. 11, Art. no. 11, Jan. 2025, doi: 10.3390/en18112674.
[61] ‘Overcoming capacity constraints with BESS through peak shaving | Aggreko UK’. Accessed: Jul. 10, 2025. [Online]. Available: https://www.aggreko.com/en-gb/resources/gu-blog---overcoming-capacity-constraints-with-bess-through-peak-shaving
[62] F. Zhou, Z. Tang, X. Zhang, L. Chou, and D. Tan, ‘An Energy Storage System for Regulating the Maximum Demand of Traction Substations’, *Energies*, vol. 18, no. 1, Art. no. 1, Jan. 2025, doi: 10.3390/en18010131.
[63] J. Yuan, L. Peng, H. Zhou, D. Gan, and K. Qu, ‘Recent research progress and application of energy storage system in electrified railway’, *Electric Power Systems Research*, vol. 226, p. 109893, Jan. 2024, doi: 10.1016/j.epsr.2023.109893.
[64] Z. Zhong, J. Mi, Y. Zhao, Z. Yang, and F. Lin, ‘Coordinated Control of the Onboard and Wayside Energy Storage System of an Urban Rail Train Based on Rule Mining’, *Urban Rail Transit*, vol. 10, no. 3, pp. 232–247, Sep. 2024, doi: 10.1007/s40864-024-00223-7.
[65] P. V. Radu, M. Lewandowski, and A. Szelag, ‘On-Board and Wayside Energy Storage Devices Applications in Urban Transport Systems—Case Study Analysis for Power Applications’, *Energies*, vol. 13, no. 8, p. 2013, Apr. 2020, doi: 10.3390/en13082013.

[66] S. Akbari, S. Saeed Fazel, and H. Hashemi-Dezaki, ‘Energy Management of Networked Smart Railway Stations Considering Regenerative Braking, Energy Storage System, and Photovoltaic Units’, *Energy Engineering*, vol. 120, no. 1, pp. 69–86, 2023, doi: 10.32604/ee.2022.024121.
[67] S. Akbari and S. S. Fazel, ‘Multistage Multiobjective Optimization for Optimal Energy Management of the Connected Cophase Traction Power System’, *International Transactions on Electrical Energy Systems*, vol. 2022, pp. 1–14, Jan. 2022, doi: 10.1155/2022/7217478.
[68] H. H. Alnuman, D. T. Gladwin, M. P. Foster, and E. M. Ahmed, ‘Enhancing energy management of a stationary energy storage system in a DC electric railway using fuzzy logic control’, *International Journal of Electrical Power & Energy Systems*, vol. 142, p. 108345, Nov. 2022, doi: 10.1016/j.ijepes.2022.108345.
[69] A. Pam, Q. Levy-Abegnoli, T. Letrouvé, M. H. Kharrat, and H. Caron, ‘Environmental and Techno-economic Life Cycle Assessment of Energy Storage Systems in Railway supply system’, *Transportation Research Procedia*, vol. 72, pp. 1372–1379, 2023, doi: 10.1016/j.trpro.2023.11.600.
[70] ‘Directive - 96/92 - EN - EUR-Lex’. [Online]. Available: https://eur-lex.europa.eu/eli/dir/1996/92/oj/eng
[71] CRE (Commision de Régulation d’Energie) website, http://www.cre.fr/
[72] ‘Understanding the public transmission system access tariff (TURPE) - RTE Services Portal’, Portail Services RTE. Accessed: Oct. 10, 2025. [Online]. Available: https://www.services-rte.com/en/learn-more-about-our-services/understanding-the-public-transmission-system-access-tariff-turpe.html
[73] SNCF Group, *SNCF Group Full-Year Financial and Sustainability Report 2024*, SNCF, Paris, France, Mar. 2025. Available: https://www.groupe-sncf.com/medias-publics/2025-03/full-year-financial-report-2024-sncf-group.pdf
[74] ‘A rail-based solar setup that turns our tracks into clean energy sources’, SNCF Group. Accessed: Oct. 10, 2025. [Online]. Available: https://www.groupe-sncf.com/en/innovation/solveig-rail-based-solar-prototype
[75] J. T. Jacobo, ‘French railway company SNCF to build 1GW of solar PV by 2030’, PV Tech. Accessed: Oct. 10, 2025. [Online]. Available: https://www.pv-tech.org/french-railway-company-sncf-to-build-1gw-of-solar-pv-by-2030/
[76] C. Starbuck, ‘Linear Regression’, in *The Fundamentals of People Analytics*, Cham: Springer International Publishing, 2023, pp. 181–206. doi: 10.1007/978-3-031-28674-2_10.
[77] M. R. Saouthi, S. Brisset, C. Saudemont, and T. Letrouve, ‘Sizing and Energy Management System of Hybrid Dc Railway Substation’, in *2024 IEEE International Conference on Electrical Systems for Aircraft, Railway, Ship Propulsion and Road Vehicles & International Transportation Electrification Conference (ESARS-ITEC)*, Naples, Italy: IEEE, Nov. 2024, pp. 1–7. doi: 10.1109/ESARS-ITEC60450.2024.10819788.
[78] J. Nocedal and S. J. Wright, *Numerical optimization*, Second edition. in Springer series in operations research and financial engineering. New York, NY: Springer, 2006.
[79] A. Aouad, K. Almaksour, and D. Abbes, ‘Storage management optimization based on electrical consumption and production forecast in a photovoltaic system’, *Mathematics and Computers in Simulation*, vol. 224, pp. 128–147, Oct. 2024, doi: 10.1016/j.matcom.2023.10.007.
[80] J. Yuan, K. Cheng, and K. Qu, ‘Optimal dispatching of high-speed railway power system based on hybrid energy storage system’, *Energy Reports*, vol. 8, pp. 433–442, Nov. 2022, doi: 10.1016/j.egyr.2022.08.039.

[81] J. A. Aguado, A. J. Sanchez Racero, and S. De La Torre, ‘Optimal Operation of Electric Railways With Renewable Energy and Electric Storage Systems’, *IEEE Trans. Smart Grid*, vol. 9, no. 2, pp. 993–1001, Mar. 2018, doi: 10.1109/TSG.2016.2574200.
[82] A. Akter *et al.*, ‘A review on microgrid optimization with meta-heuristic techniques: Scopes, trends and recommendation’, *Energy Strategy Reviews*, vol. 51, p. 101298, Jan. 2024, doi: 10.1016/j.esr.2024.101298.
[83] A. Zhadan, A. Martemyanov, A. Allahverdyan, O. Petrosian, and H. Gao, ‘Linearization method for MINLP energy optimization problems’, *Sci Rep*, vol. 15, no. 1, p. 27853, Jul. 2025, doi: 10.1038/s41598-025-11380-5.
[84] S. Park and S. R. Salkuti, ‘Optimal Energy Management of Railroad Electrical Systems with Renewable Energy and Energy Storage Systems’, *Sustainability*, vol. 11, no. 22, p. 6293, Nov. 2019, doi: 10.3390/su11226293.
[85] S. Akbari, H. Hashemi-Dezaki, and S. S. Fazel, ‘Optimal clustering-based operation of smart railway stations considering uncertainties of renewable energy sources and regenerative braking energies’, *Electric Power Systems Research*, vol. 213, p. 108744, Dec. 2022, doi: 10.1016/j.epsr.2022.108744.
[86] I. Sengor, H. C. Kilickiran, H. Akdemir, B. Kekezoglu, O. Erdinc, and J. P. S. Catalao, ‘Energy Management of a Smart Railway Station Considering Regenerative Braking and Stochastic Behaviour of ESS and PV Generation’, *IEEE Trans. Sustain. Energy*, vol. 9, no. 3, pp. 1041–1050, Jul. 2018, doi: 10.1109/TSTE.2017.2759105.
[87] Y. Ji, Q. Xu, J. Zhao, Y. Yang, and L. Sun, ‘Day-ahead and intra-day optimization for energy and reserve scheduling under wind uncertainty and generation outages’, *Electric Power Systems Research*, vol. 195, p. 107133, Jun. 2021, doi: 10.1016/j.epsr.2021.107133.
[88] M. Chen, Z. Cheng, Y. Liu, Y. Cheng, and Z. Tian, ‘Multitime-Scale Optimal Dispatch of Railway FTPSS Based on Model Predictive Control’, *IEEE Trans. Transp. Electrific.*, vol. 6, no. 2, pp. 808–820, Jun. 2020, doi: 10.1109/TTE.2020.2992693.
[89] Z. Cheng, M. Chen, Y. Liu, and Y. Cheng, ‘A Two-level Energy Management Model for Railway Substation with POC and Energy Storage’, in *2020 15th IEEE Conference on Industrial Electronics and Applications (ICIEA)*, Kristiansand, Norway: IEEE, Nov. 2020, pp. 397–401. doi: 10.1109/ICIEA48937.2020.9248285.
[90] Z. Sheng, A. Iovine, G. Damm, and L. Galai-Dol, ‘Power Management for a DC MicroGrid in a Smart Railway Station including Recovery Braking’, in *2019 18th European Control Conference (ECC)*, Naples, Italy: IEEE, Jun. 2019, pp. 1418–1423. doi: 10.23919/ECC.2019.8795676.
[91] S. Ghorbani, R. Unland, H. Shokouhandeh, and R. Kowalczyk, ‘An Innovative Stochastic Multi-Agent-Based Energy Management Approach for Microgrids Considering Uncertainties’, *Inventions*, vol. 4, no. 3, p. 37, Jul. 2019, doi: 10.3390/inventions4030037.
[92] D. M. Glavic, ‘Agents and Multi-Agent Systems: A Short Introduction for Power Engineers’.
[93] S. Boudoudouh, ‘Multi agent system solution to microgrid implementation’, *Sustainable Cities and Society*, 2018.
[94] A. Anvari-Moghaddam, A. Rahimi-Kian, M. S. Mirian, and J. M. Guerrero, ‘A multi-agent based energy management solution for integrated buildings and microgrid system’, *Applied Energy*, vol. 203, pp. 41–56, Oct. 2017, doi: 10.1016/j.apenergy.2017.06.007.
[95] M. K. C. Paniah, J. Gil-Quijano, and D. Mercier, ‘Systèmes multi-agents pour la gestion de sources d’énergie renouvelable et de stockage de masse’.
[96] H. Priyadarshana, M. Kalhan Sandaru, K. Hemapala, W. Wijayapala, and Department of Electrical Engineering, University of Moratuwa, Colombo, Sri Lanka, ‘A review on Multi-Agent system based energy management systems for micro grids’, AIMS Energy, vol. 7, no. 6, pp. 924–943, 2019, doi: 10.3934/energy.2019.6.924.

[97] D. El Hafiane, A. El Magri, H. E. Chakir, R. Lajouad, and S. Boudoudouh, ‘A multi-agent system approach for real-time energy management and control in hybrid low-voltage microgrids’, *Results in Engineering*, vol. 24, p. 103035, Dec. 2024, doi: 10.1016/j.rineng.2024.103035.
[98] L. Razik, N. Berr, S. Khayyam, F. Ponci, and A. Monti, ‘REM-S–Railway Energy Management in Real Rail Operation’, *IEEE Trans. Veh. Technol.*, vol. 68, no. 2, pp. 1266–1277, Feb. 2019, doi: 10.1109/TVT.2018.2885007.
[99] M. Davoodi, H. Jafari Kaleybar, M. Brenna, and D. Zaninelli, ‘Energy Management Systems for Smart Electric Railway Networks: A Methodological Review’, *Sustainability*, vol. 15, no. 16, p. 12204, Aug. 2023, doi: 10.3390/su151612204.
[100] M. S. Soliman *et al.*, ‘Supervisory energy management of a hybrid battery/PV/tidal/wind sources integrated in DC-microgrid energy storage system’, *Energy Reports*, vol. 7, pp. 7728–7740, Nov. 2021, doi: 10.1016/j.egyr.2021.11.056.
[101] P. Pankovits, D. Abbes, C. Saudemont, S. Brisset, J. Pouget, and B. Robyns, ‘Multi-criteria fuzzy-logic optimized supervision for hybrid railway power substations’, *Mathematics and Computers in Simulation*, vol. 130, pp. 236–250, Dec. 2016, doi: 10.1016/j.matcom.2016.05.002.
[102] A. Fathollahi, ‘Machine Learning and Artificial Intelligence Techniques in Smart Grids Stability Analysis: A Review’, *Energies*, vol. 18, no. 13, p. 3431, Jun. 2025, doi: 10.3390/en18133431.
[103] A. R. Singh, M. S. Sujatha, A. D. Kadu, M. Bajaj, H. K. Addis, and K. Sarada, ‘A deep learning and IoT-driven framework for real-time adaptive resource allocation and grid optimization in smart energy systems’, *Sci Rep*, vol. 15, no. 1, p. 19309, Jun. 2025, doi: 10.1038/s41598-025-02649-w.
[104] A. J. Bidgoli, ‘AI-Driven Framework to Optimize Smart Grid Operations, Enhance Energy Efficiency, and Facilitate Seamless Integration Using Hybrid (LSTM-CNN) Models’, *Journal of Information Systems Engineering and Management*, vol. 10, no. 35s, pp. 173–182, Apr. 2025, doi: 10.52783/jisem.v10i35s.5947.
[105] R. Tang *et al.*, ‘A literature review of Artificial Intelligence applications in railway systems’, *Transportation Research Part C: Emerging Technologies*, vol. 140, p. 103679, Jul. 2022, doi: 10.1016/j.trc.2022.103679.
[106] T. A. Rajaperumal and C. C. Columbus, ‘Transforming the electrical grid: the role of AI in advancing smart, sustainable, and secure energy systems’, *Energy Inform*, vol. 8, no. 1, p. 51, Apr. 2025, doi: 10.1186/s42162-024-00461-w.
[107] H. Javed, F. Eid, S. El-Sappagh, and T. Abuhmed, ‘Sustainable energy management in the AI era: a comprehensive analysis of ML and DL approaches’, *Computing*, vol. 107, no. 6, p. 132, Jun. 2025, doi: 10.1007/s00607-025-01485-0.
[108] A. Ji, W. L. Woo, E. W. L. Wong, and Y. T. Quek, ‘Rail track condition monitoring: a review on deep learning approaches’, *IR*, 2021, doi: 10.20517/ir.2021.14.
[109] B. Mohajer K. and S. M. Mousavi G., ‘Energy management optimization in smart railway stations with the ability to charge plug-in hybrid electric vehicles’, *Journal of Energy Storage*, vol. 70, p. 107867, Oct. 2023, doi: 10.1016/j.est.2023.107867.
[110] ‘Solar forecast | Accurate solar power generation forecasts’, Steadysun. Accessed: Oct. 07, 2025. [Online]. Available: https://steady-sun.com/solar-energy-forecasts/
[111] ‘Steadymet | Day-ahead solar & wind power forecasts’, Steadysun. Accessed: Oct. 07, 2025. [Online]. Available: https://steady-sun.com/steadymet-day-ahead-forecasts/
[112] B. Robyns, B. François, G. Delille, C. Saudemont, Energy storage in electric power grids, ISTE Editions, 2015.

[113] C. Saudemont, « Méthodologie de développement de stratégies de supervision énergétique en temps réel dans les systèmes électriques de puissance », HDR, Université Lille1, 2013.
[114] S. Aatif, H. Hu, F. Rafiq, and Z. He, 'Analysis of rail potential and stray current in MVDC railway electrification system', *Rail. Eng. Science*, vol. 29, no. 4, pp. 394–407, Dec. 2021, doi: 10.1007/s40534-021-00243-0.
[115] A. Salam and A. El Hibaoui, 'Energy consumption prediction model with deep inception residual network inspiration and LSTM', *Mathematics and Computers in Simulation*, vol. 190, pp. 97–109, Dec. 2021, doi: 10.1016/j.matcom.2021.05.006.
[116] N. Shirzadi, A. Nizami, M. Khazen, and M. Nik-Bakht, 'Medium-Term Regional Electricity Load Forecasting through Machine Learning and Deep Learning', *Designs*, vol. 5, no. 2, p. 27, Apr. 2021, doi: 10.3390/designs5020027.
[117] A. Nespoli, E. Ogliari, S. Pretto, M. Gavazzeni, S. Vigani, and F. Paccanelli, 'Data quality analysis in day-ahead load forecast by means of LSTM', in *2020 IEEE International Conference on Environment and Electrical Engineering and 2020 IEEE Industrial and Commercial Power Systems Europe (EEEIC / I&CPS Europe)*, Madrid, Spain: IEEE, Jun. 2020, pp. 1–5. doi: 10.1109/EEEIC/ICPSEurope49358.2020.9160840.
[118] MathWorks. fmincon. https://www.mathworks.com/help/optim/ug/fmincon.html, 2025.
[119] A. F. Agarap, 'Deep Learning using Rectified Linear Units (ReLU)', Feb. 07, 2019, *arXiv*: arXiv:1803.08375. doi: 10.48550/arXiv.1803.08375.
[120] P. Pankovits, *Gestion énergétique optimale des installations fixes de traction électrique ferroviaire hybrides*, Ph.D. dissertation, Univ. Lille 1, Lille, France, 2015.
[121] K. Almaksour et al., 'Comparison of dynamic models for a DC railway electrical network including an AC/DC bi-directional power station', Mathematics and Computers in Simulation, vol. 184, pp. 244–266, Jun. 2021, doi: 10.1016/j.matcom.2020.05.027.
[122] J. Segarra-Tamarit, E. Pérez, E. Moya, P. Ayuso, and H. Beltran, "Deep learning-based forecasting of aggregated CSP production," *Mathematics and Computers in Simulation*, vol. 184, pp. 306–318, Jun. 2021, doi: 10.1016/j.matcom.2020.02.007.

# Abstract

As railway traffic and energy costs continue to rise, SNCF Réseau wants to improve the performance of its traction substations while meeting European $CO_2$ reduction targets. Although the main railway lines use AC electrification, a large part of the French network still operates with DC systems. The latter is characterized by relatively low voltage and limited traffic density. The RACCOR-D project aims to address these issues by preparing the move toward higher-voltage DC networks (above 1500 V). As part of this effort, SNCF Réseau plans to upgrade its substations and turn them into smart, modern facilities. These new substations will include photovoltaic (PV) panels and energy storage systems (ESS). Their goal is to reduce dependence on the national electricity grid, lower operating costs, and avoid financial penalties for exceeding contracted power limits. Integrating both ESS and PV into a railway substation creates several challenges. To fully benefit from these technologies, a smart energy management system is essential. It must operate the ESS in a way that maximizes the use of local PV production while helping SNCF Réseau achieve its goals of reducing energy consumption and avoiding penalty charges. In this context, the objective of this PhD thesis is to design an energy supervision system specifically for DC railway networks. The goal is to optimize how the ESS is used in two RACCOR-D possible architectures, where the PV system and the storage are connected directly to the DC bus of the substation and when connected between two traction substations. The supervisor aims to improve both the energy performance and the operating costs of the traction substation, while respecting the technical constraints of DC systems. The supervision strategy is developed with two temporal levels, the long term (day ahead) and the short term (real time). The supervision framework was validated through real-time simulations using OPAL-RT. And to support industrial deployment, a SCADA-based architecture was designed to ensure reliable communication with all smart grid components. This industrial setup enables the supervisor to operate on an industrial PC and to be integrated into the railway substation demonstrator, paving the way for large-scale implementation of intelligent DC substations. This thesis is done within RACCOR-D project, funded by the French government as part of France 2020.



**Keywords:** **Energy management, Real time energy supervision, DC railway network, smart grid, Energy optimization, Electric power forecast, Day-ahead EMS, Wayside ESS.**



# Résumé

Face à l'augmentation continue du trafic ferroviaire et des coûts énergétiques, SNCF Réseau souhaite améliorer les performances de ses sous-stations de traction tout en respectant les objectifs européens de réduction des émissions de $CO_2$. Bien que les principales lignes ferroviaires utilisent l'électrification en courant alternatif, une grande partie du réseau français fonctionne encore avec des systèmes à courant continu. Ces derniers se caractérisent par une tension relativement faible et une densité de trafic limitée. Le projet RACCOR-D vise à résoudre ces problèmes en préparant le passage à des réseaux à courant continu à plus haute tension (supérieure à 1 500 V). Dans le cadre de cette initiative, SNCF Réseau prévoit de moderniser ses sous-stations et de les transformer en installations intelligentes et modernes. Ces nouvelles sous-stations comprennent des panneaux photovoltaïques (PV) et des systèmes de stockage d'énergie (ESS). L'objectif est de réduire la dépendance au réseau électrique national, de diminuer les coûts d'exploitation et d'éviter les pénalités financières liées au dépassement des limites de puissance contractuelles. L'intégration des ESS et des PV dans une sous-station ferroviaire pose plusieurs défis. Pour tirer pleinement parti de ces technologies, un système de gestion intelligente de l'énergie est essentiel. Il doit exploiter les ESS de manière à maximiser l'utilisation de la production PV locale tout en aidant SNCF Réseau à atteindre ses objectifs de réduction de la consommation d'énergie et d'évitement des pénalités financières. Dans ce contexte, l'objectif de cette thèse de doctorat est de concevoir un système de supervision énergétique spécifiquement destiné aux réseaux ferroviaires à courant continu. L'objectif est d'optimiser l'utilisation du système ESS dans deux architectures RACCOR-D possibles, où le système photovoltaïque et le stockage sont connectés directement au bus CC de la sous-station et lorsqu'ils sont connectés entre deux sous-stations de traction. Le superviseur vise à améliorer à la fois la performance énergétique et les coûts d'exploitation de la sous-station de traction, tout en respectant les contraintes techniques des systèmes CC. La stratégie de supervision est développée avec deux niveaux temporels, le long terme (jour à l'avance) et le court terme (temps réel). Le cadre de supervision a été validé par des simulations en temps réel à l'aide d'OPAL-RT. Et pour soutenir le déploiement industriel, une architecture basée sur SCADA a été conçue pour assurer une communication fiable avec tous les composants du réseau intelligent. Cette configuration industrielle permet au superviseur de fonctionner sur un PC industriel et d'être intégré dans le démonstrateur de sous-station ferroviaire, ouvrant la voie à la mise en œuvre à grande échelle de sous-stations CC intelligentes. Cette thèse est réalisée dans le cadre du projet RACCOR-D, financé par le gouvernement dans le cadre de France 2030.

**Mots clés: Gestion de l'énergie, Supervision énergétique en temps réel, Réseau ferroviaire à courant continu (CC), Réseau électrique intelligent, Optimisation énergétique, Prévision de la puissance électrique, day-ahead EMS, Système de stockage d'énergie en bord de voie.**